

Ductility in timber structures - possibilities and requirements with regard to dowel type fasteners

Frank Brühl

Mitteilungen

Ductility in timber structures – possibilities and requirements with regard to dowel type fasteners

Von der Fakultät Bau- und Umweltingenieurwissenschaften der Universität Stuttgart
zur Erlangung der Würde eines Doktor-Ingenieurs (Dr.-Ing.)
genehmigte Abhandlung

Vorgelegt von

Frank Brühl

aus Göppingen

Hauptberichter:

Prof. Dr.-Ing. Ulrike Kuhlmann

Mitberichter:

Prof. Dr. Ir André Jorissen

Prof. Dr.-Ing. habil. Jörg Schänzlin

Tag der mündlichen Prüfung:

27. Januar 2020

Institut für Konstruktion und Entwurf der Universität Stuttgart

2020

Mitteilung des Instituts für Konstruktion und Entwurf Nr. 2020-1

Frank Brühl Ductility in timber structures –
possibilities and requirements with regard
to dowel type fasteners

Herausgeber Prof. Dr.-Ing. Ulrike Kuhlmann
Pfaffenwaldring 7
70569 Stuttgart
Deutschland
Telefon: 0711/685-66245
Telefax: 0711/685-66236

Redaktion Simon Mönch

D93

© Institut für Konstruktion und Entwurf, Stuttgart 2020

Alle Rechte vorbehalten

ISSN: 1439-3751

Never give up on a dream just because of the time
it will take to accomplish it. The time will pass
anyway.

- Earl Nightingale -

Acknowledgements

This research work has been carried out to a large extent during my professional activity as a research member of the Institute of Structural Design at the Universität Stuttgart.

First and foremost I would like to express my sincere gratitude to Prof. Dr.-Ing. Ulrike Kuhlmann for giving me the opportunity and the confidence to work as a scientific fellow at the Institute of Structural Design. The continuous support, the guiding discussions and taking over the supervision have to be especially emphasized.

In this context I would also like to express my deep gratitude to Prof. Dr. Ir. A.J.M. André Jorissen for taking over the co-supervision. Especially for providing me with the opportunity to stay at the Technische Universiteit Eindhoven for a short term scientific mission within the COST E55 'Modelling of the performance of timber structures' program. Despite the short time we had numerous fruitful discussions which are especially acknowledged.

A special gratitude is given to Prof. Dr.-Ing. habil. Jörg Schänzlin who always gave me support and motivation to bridge the most challenging periods of the PhD project, even after the time at the institute.

I want to express my gratitude to my colleagues of the Institute of Structural Design for the pleasant working atmosphere and the highly diversified discussions, especially to the timber fellows Pietro Aldi, Reiner Hofmann and Katrin Kudla (née Stephan) who have always had an open door for discussions.

The theoretical elaborations are supported by experiments. It was a pleasure to conduct the experiments with the technician Oliver Schneider, who always gave great input into the performance of the experiments.

Related to that, I would like to thank the companies for their support in conducting the experiments. WIEHAG GmbH for the glulam members, HMR Jacob - Haslinger GmbH for the flitch plates and ordinary dowels, SFS intec AG for providing the self-drilling dowels and SPAX International GmbH & Co. KG for their contribution of the self-drilling fully threaded screws.

Furthermore I would like to thank all of the supervised students for their curiosity and discussions, which also contributed to the finalization of this work.

Finally, I would like to express my cordial gratitude to my parents and my wife Christina. I thank my love for your untiring patience, your continuous understanding, your motivation to finalize this work, to support and join me in the new job and finally for listening to me when I got stuck or when I was filled with verve reported on my work.

A special thanks is given to my parents for their patience in showing me how to walk on the right side, and giving me the wind beneath my wings to walk my way with an unreserved confidence.

To my parents

Abstract

The main objective of this research work is to clarify the possibility of an orderly use of the ductile behavior of dowel type fasteners in the design of timber structures. The investigations are focusing on requirements and possibilities to introduce the ductile behavior to timber structures. For other structural materials, such as steel or reinforced concrete as well as composite structures, guidelines describing the ductile behavior of structural parts are already defined. Thus it is possible for these materials to apply design methods with respect to the ductility. The necessity to describe the ductile behavior in a reliable manner is given in the currently valid codes. To design preferable ductile structures, with the ability to announce a collapse, is one of the key elements in the design of structures. The timber code EN 1995-1-1:2004 allows the application of the ductile behavior of joints to redistribute internal actions, but no indications are given about the behavior of fasteners.

A first study has been conducted within this work to evaluate different types of fasteners with respect to the ductile behavior to gain a first database of the inherent ductility of different fasteners. The study is based on experiments obtained from literature. Different methods have been applied and discussed to evaluate the ductility. The study underlines the large variation of the ductile behavior. Non-reinforced doweled type connections show a rather brittle behavior, whereas the reinforcement of dowel type connections significantly increases the ductile behavior of a joint.

Several known experiments were only performed according to EN 26891:1991-07 up to a displacement of 15 mm was reached. Prerequisites for a substantive assessment of the ductile behavior are results which are performed up to defined maximum displacement is reached. Hence, further experiments on reinforced dowel connections have been performed with a variation of the number of dowels and the dowel arrangement. The experiments were mainly divided into two test setups. Connection test loaded in tension and experiments on joints loaded with a pure bending moment. It is shown, that the connections behave in a ductile manner in both test setups. For a dowel diameter of 7 mm a solidification could be observed due to the reinforcement screws.

To describe the moment-rotation behavior of joints an analytical model based on the component method is developed and verified against the conducted experiments. The model shows reliable results, reliable not only with the view on the bearing resistance but also in capturing the ductile behavior. A simplified procedure is presented to introduce a practical application.

Regardless of the application of ductility in timber structures, it is necessary to avoid a

brittle failure of the timber elements before the ductile element is in the stage of yielding. An over-strength factor is introduced to consider the required clearance of the load bearing resistances of the beam element to the introduced bending moment initiated by the load carrying capacity of the fasteners. Hence, a Monte-Carlo simulation has been conducted to focus particularly on the scattering of the material properties to determine a reliability index of a joint loaded in bending. Since the reliability index depends highly on the consequences of failure, an equation is developed to determine certain over-strength factors for different reliability indices.

The thesis concludes with the consideration of multi-span beams in order to activate the ductile behavior of joints to redistribute internal actions. An analytical approach is proposed to determine the minimum stiffness of the joint with respect to the load-carrying capacity of the joint and the bearing resistance of the timber member, in order to redistribute internal actions. It appears that the consideration of the stiffness is unavoidable, since a lesser stiffness leads to a brittle failure at mid-span. Corresponding formulas have been developed and indicated for chosen cases.

Thus it is possible to formulate the plastic behavior of joints in accordance with the currently valid timber code EN 1995-1-1:2004 and make the behavior accessible to optimization of timber structures.

Kurzdarstellung

Die vorliegende Arbeit befasst sich mit der planmäßigen Berücksichtigung des duktilen Verhaltens von stiftförmigen Verbindungsmitteln in der Berechnung von Holztragwerken, mit dem Ziel plastische Gelenke im Holzbau planmäßig ausbilden zu können. Andere Werkstoffgruppen, wie beispielsweise der Stahlbau oder der Stahlbetonbau sowie der Verbundbau, haben bereits Regelwerke entwickelt, um die Vorteile des plastischen Verhalten planmäßig zu nutzen. Die Notwendigkeit, das duktile Verhalten zuverlässig zu beschreiben und die Anwendbarkeit von Fließgelenken in Holzbau zu ermöglichen, ergibt sich direkt aus der derzeit gültigen Bemessungsnorm im Holzbau EN 1995-1-1:2004. Diese lässt Berechnungsmethoden unter dem Ansatz der Duktilität zu. Im Hinblick auf die Umsetzung der Berücksichtigung der Duktilität sind jedoch keine ausreichenden Angaben vorhanden.

Im Rahmen dieser Arbeit wurde anhand der Sichtung von Versuchsergebnissen aus der Literatur eine Auswertung von verschiedenen Verbindungsmitteln hinsichtlich ihres duktilen Verhaltens durchgeführt, um eine erste Datenbasis zur Einstufung der einzelnen Verbindungsmittel zu schaffen. Dabei wurden unterschiedliche Bewertungsverfahren herangezogen, um das duktile Verhalten einzuordnen. Diese wurden im Rahmen dieser Arbeit hinsichtlich ihrer Anwendbarkeit beurteilt. Die Auswertung der Daten zeigt eine große Varianz der einzelnen Verbindungsmittel. Stabdübelverbindungen ohne jegliche Verstärkungsmaßnahmen können eher als spröde eingestuft werden. Verstärkte Stabdübelverbindungen zeigen hingegen ein ausgeprägtes duktilen Verhalten.

Innerhalb der Auswertung der bereits durchgeführten Versuche aus der Literatur konnte festgestellt werden, dass einige Versuche nur bis zu einer Verschiebung von 15 mm entsprechend DIN EN 26891:1991-07 durchgeführt wurden. Dies führt zu einem Informationsverlust hinsichtlich der Bestimmung der Duktilität der Verbindung, da über das Verhalten nach 15 mm in diesen Fällen keine Aussagen getroffen werden können. Im Rahmen dieser Arbeit wurden daher gezielt Versuche an verstärkten Stabdübelverbindungen durchgeführt. Dabei wurde sowohl die Anzahl der Stabdübel als auch ihre Anordnung variiert. Um die Duktilität und damit die Möglichkeit der Bildung von plastischen Gelenken zu untersuchen, wurden sowohl Komponentenversuche in Form von Zugversuchen als auch gesamte Trägerstöße untersucht. Es konnte gezeigt werden, dass beide Versuchsserien über ein ausgeprägtes duktilen Verhalten verfügen. Versuche an Stabdübeln mit einem Durchmesser von 7 mm zeigen aufgrund der Verstärkungsmaßnahme durch selbstbohrende Holzschrauben eine Wiederverfestigung.

Um das Momenten-Rotations Verhalten von Anschlüssen mit stiftförmigen Verbindungsmitteln

teln zu erfassen, wurde eine analytische Betrachtung durchgeführt. Diese beruht auf dem Komponentenmodell, das einzelne Traganteile eines Anschlusses als Federn abbildet. Die Ergebnisse des entwickelten Modells sind mit den Versuchsergebnissen verglichen worden. Nicht nur die maximale Tragfähigkeit sondern auch die Anschlussverformung wird durch das Modell verlässlich abgebildet. Um das Modell der Praxis zugänglich zu machen, wurde ein vereinfachtes Verfahren zur Ermittlung des Momenten-Rotations Verhalten vorgestellt.

Eine der wichtigsten Forderungen beim Einsatz von plastischen Gelenken im Holzbau ist, dass kein sprödes Holzversagen eintritt, bevor sich ein Fließen des Gelenkes eingestellt hat. Um dies zu gewährleisten, wurde ein Überfestigkeitsfaktor mit Hilfe einer Monte-Carlo-Simulation ermittelt, der eine Mindesttragfähigkeit des spröden Holzelements in Anlehnung an das einwirkende Biegemoment durch den Anschluss bestimmt. Dieser Überfestigkeitsfaktor wurde dabei in Abhängigkeit der Versagenskonsequenz ermittelt, so dass dieser Überfestigkeitsfaktor der jeweiligen Anwendung angepasst werden kann.

Damit Schnittgrößen durch duktile Elemente innerhalb eines Tragwerks umgelagert werden können, wurden abschließend analytische Untersuchungen zu Mindestanforderungen an die Anfangssteifigkeit von duktilen Elementen an Mehrfeldträgern durchgeführt. Der Ansatz zeigt, dass es unumgänglich ist, eine Mindeststeifigkeit des Anschlusses zu fordern, da bei einer zu geringen Steifigkeit ein Holzversagen außerhalb des Anschlussbereichs, z.B. in Feldmitte eintreten kann, bevor es zu einem Fließen des plastischen Gelenkes kommt. Die Mindeststeifigkeiten wurden dabei für ausgewählte Fälle bestimmt.

Damit ist es möglich, das plastische Verhalten von Anschlüssen in Anlehnung an die Forderungen der derzeit gültigen Bemessungsnorm EN 1995-1-1:2004 zu formulieren, so dass plastische Gelenke im Holzbau und damit deren Vorteile im Hinblick auf Tragfähigkeit und Robustheit genutzt werden können.

Contents

1	Introduction	1
1.1	Background	1
1.2	Objectives and limitations	2
1.3	Content of this study	3
2	Current design methods	5
2.1	General	5
2.2	Determination of the maximum load-bearing capacity	6
2.2.1	Elastic-elastic design method	6
2.2.2	Elastic-plastic design method	6
2.2.3	Plastic-plastic design method	7
2.3	Discussion of the different design methods	8
2.4	Application of the plastic design methods	10
2.4.1	Steel structures	10
2.4.2	Reinforced concrete structures	13
2.4.3	Composite structures	14
2.4.4	Plastic design of joints	15
2.5	Design situation in timber structures	15
2.5.1	General	15
2.5.2	Design of cross-sections	16
2.5.3	Design of dowel-type fasteners	17
2.5.4	Consideration of the stiffness	18
3	Connections in timber structures - review and former investigations	21
3.1	General	21
3.2	Dowel type fasteners	21
3.2.1	Introduction	21
3.2.2	K. W. Johansen (1949)	22
3.2.3	A. Meyer (1957)	24
3.2.4	J. Ehlbeck and H. Werner (1988)	24

3.2.5	H.J. Blaß (1990)	26
3.2.6	A. Mischler (1998)	28
3.2.7	A. Jorissen (1998)	33
3.2.8	I. Bejtka (2005)	35
3.3	Tube connections	37
3.3.1	Introduction	37
3.3.2	A.J.M. Leijten (1998)	37
3.4	Split rings	39
3.4.1	Introduction	39
3.4.2	Investigations at the Universität Karlsruhe (1997)	40
3.4.3	Investigations at the Ruhr-Universität Bochum	42
3.5	Nail plates	43
3.5.1	Introduction	43
3.5.2	Kevarinmaki	43
3.6	Summary	44
4	Ductile behavior of fasteners in timber structures	47
4.1	General	47
4.2	Evaluation of the ductility	48
4.2.1	Parameters	48
4.2.2	Appraisal of the ductility	52
4.3	Evaluation of different types of fasteners	57
4.3.1	General	57
4.3.2	Investigations on dowel type connections	58
4.3.3	Miscellaneous connections	70
4.4	Discussion and conclusion	76
5	Experimental research	79
5.1	Introduction	79
5.2	Description of the specimens	80
5.2.1	Overview	80
5.2.2	Fabrication	82
5.2.3	Material properties	83
5.3	Experiments on connections in tension	93
5.3.1	Test setup	93
5.3.2	Results of the experiments on connections in tension	95
5.3.3	Ductility evaluation	100
5.3.4	Summary and conclusions	102

5.4	Experiments on joints in bending	107
5.4.1	Test setup	107
5.4.2	Results of the experiments on joints in bending	109
5.4.3	Ductility evaluation	114
5.5	Miscellaneous experimental research	116
5.5.1	Introduction	116
5.5.2	Experiments in tension perpendicular to the grain	116
5.5.3	Cyclic testing	119
5.6	Summary	128
6	Analytical determination of the rotation capacity	131
6.1	General	131
6.2	Identification of the different components	133
6.2.1	Introduction of the single components	133
6.2.2	Components acting in compression	134
6.2.3	Components acting in tension	136
6.2.4	Rotation of a group of dowels	142
6.3	Verification of the model	146
6.3.1	Comparison of the measurement results of the experiments on joints in bending	146
6.3.2	Validation based on individual components	147
6.3.3	General	147
6.3.4	Discussion of the parameters	147
6.3.5	Geometrical conditions	149
6.3.6	Summary	151
6.4	Simplification - proposal of a practical application	151
6.4.1	Introduction	151
6.4.2	Discussion of the initial stiffness	152
6.4.3	Simplification of the load-deflection behavior	154
6.5	Application and justification of the simplified model	156
6.5.1	General	156
6.5.2	Load-displacement behavior	156
6.5.3	Moment-rotation behavior	157
6.6	Summary	160
7	Effects of the material scattering	161
7.1	General	161
7.2	Introduction of an over-strength factor	162

7.2.1	General	162
7.2.2	Representation of the failure probability	163
7.2.3	Determination of the structural reliability	167
7.2.4	Reliability based investigations to determine the over-strength factor .	174
7.2.5	Results of the Monte-Carlo Simulation	185
7.3	Influence on the beam end-rotation	188
7.3.1	General	188
7.3.2	Determination of the material impact factor k_{mat}	189
7.3.3	Parametrical study and results	193
7.4	Summary and conclusion	195
8	Requirements on the joint stiffness	197
8.1	Introduction	197
8.2	Consideration of the joint stiffness on a two span beam	198
8.2.1	General	198
8.2.2	Required joint stiffness	198
8.3	Further Investigations	200
8.3.1	General	200
8.3.2	Required joint stiffness	201
8.4	Summary	202
9	Conclusions and Outlook	205
9.1	General remarks	205
9.2	Conclusions	205
9.3	Limitation	208
9.4	Recommendations for future research	208
	Appendix	223
A	Example of the application of the findings on the ductile behavior	223
A.1	General	223
A.2	Introduction of the structure	224
A.2.1	General	224
A.2.2	Elastic beam design	224
A.3	Design considering the plastic behavior	226
A.3.1	General	226
A.3.2	Design of the joint	226

A.3.3	Determination of the internal actions under the consideration of a plastic hinge	230
A.4	Summary & scheduling of the process steps	232
B	Load-deflection graphs	235
B.1	Nailed connections	235
B.2	Timber-steel-timber doweled connections	237
B.2.1	Experiments on BSB-connections performed by Mischler [88]	237
B.2.2	Experiments on self-drilling dowels performed by Mischler [56]	239
B.2.3	Experiments on ordinary dowels performed by Sandhaas [90]	242
B.3	Timber-timber doweled connections	244
B.4	Reinforced timber-steel-timber connections	247
B.5	Miscellaneous connections	250
B.5.1	Experiments on tube connections performed by Leijten [87]	250
B.5.2	Experiments on split rings performed by Blaß et al. [11]	251
B.5.3	Experiments on split rings performed by Reyer et al. [64]	253
B.5.4	Experiments on nail plates performed by Kevarinmaki [84]	255
C	Material properties	257
C.1	Timber properties	257
C.1.1	Overview of all lamellae	257
C.1.2	Density of the tension specimens	259
C.1.3	Density of the joints of the bending specimens	260
D	Experimental results	267
D.1	Experiments on connections in tension	267
D.2	Experiments on joints in bending	271
D.3	Miscellaneous experiments	275
E	X-ray scans	277
E.1	Introduction	277
E.2	Tension specimens	278
E.3	Bending specimens	284
F	Drawings	291
F.1	Experiments on connections in tension	291
F.1.1	Connecting device	291
F.1.2	Steel Elements	292
F.1.3	Timber Elements	295

F.2 Experiments on joints in bending	298
F.2.1 Steel Parts	298
F.2.2 Timber Parts	301

1 Introduction

1.1 Background

Timber as a natural material has been valued and processed for many centuries as a building material. It is characterized by a warm and friendly nature combined with a brilliant behavior in the view of sustainability compared with other building materials.

The traditional carpenter joints transferred the load mainly via compression (common halving, backfill, tenons, etc.). The tenon joints were reinforced with wooden dowels in order to transfer tension forces as well. Dowel-type fasteners became more and more of interest with the application of nails. A characteristic connection with dowel-type fasteners is nowadays frequently used in combination with flitch plates and fully threaded screws in timber engineering.

Structural elements and fasteners in timber structures are mainly designed using the elastic-elastic design method. This means that elastically determined stresses are combined with the elastic resistance of structural elements. Hence only the elastic connection behavior is considered, whereas the plastic behavior is currently neglected (see Fig. 1.1). The elastic-elastic design method is in general not limited in the applicability. Hence only a cross-section

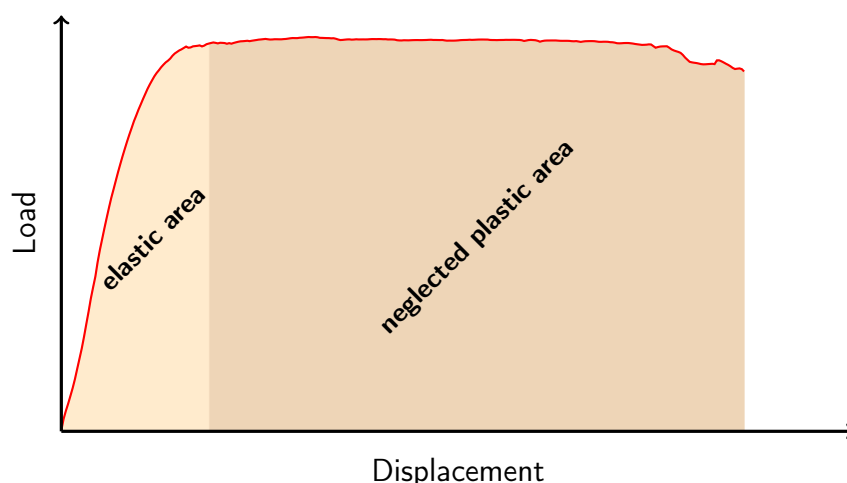


Figure 1.1: Typical load displacement behavior of a reinforced dowel connection showing the neglected plastic area

with a maximum utilization mainly governs the dimensions of the structural element. The major premise in order to introduce the elastic-plastic design method is the activation of the currently unused ductility within the joint with its inherent ductile behavior. If it is possible to form ductile elements in a structure, the utilization is not limited to a certain area within a statically indeterminate structure (comp. Fig. 2.3 on p. 8). The elastic-plastic design method allows a redistribution of internal actions to lesser utilized structural elements. Therefore economical solutions can be achieved. Since timber is in general a brittle material, the current design code EN 1995-1-1 [109] allows as a resultant mainly the elastic-elastic design method, but it gives the opportunity to use the elastic-plastic design method if ductile joints are introduced into structures.

—
 |
 | *For structures able to redistribute the internal forces via connections of adequate ductility, elastic-plastic methods may be used for the calculation of the internal forces in the members.*

EN 1995-1-1 [109, 5.1(3)]
 —
 |

Therefore a redistribution of internal actions is in general possible, but the standard does not give guidelines which describe clearly the ductility of connections and the application. The neglect of the ductile behavior can also be seen in the family of standards. The relevant standard [110] to perform tests on mechanical fasteners does not focus on the ductility of fasteners. It defines the maximum load as the maximum load as soon as a displacement of 15 mm is reached. Due to this principle the necessary ultimate displacement is not implicitly recorded within the conducted experiments. However, the ultimate displacement is a key element to evaluate fasteners with the attention on the ductility.

Besides the unknowns and restrictions of the standards it is necessary to clarify these undefined parameters to introduce the ductile behavior of selected types of fasteners.

1.2 Objectives and limitations

The objective of this work is to bridge the gap in the code and give a first design approach to introduce the ductile behavior of dowel-type fasteners in timber structures. The study develops requirements to enable the elastic-plastic design method and show possibilities in the application.

Since timber is a rather brittle material, only a slight ductility in compression can be assumed. However, the deformability is too small to form plastic hinges. Therefore attention is given to the possibility of the formation of plastic hinges at the joint. If it succeeds in introducing plastic hinges to timber structures, such structures gain access to the advantageous elastic-plastic or plastic-plastic design method.

A general overview of the ductile behavior of different types of fasteners is given to gain a comprehensive insight. Therefore split rings, tube connections and nail plates are examined besides dowel type fasteners. However, this research work mainly focuses on connections with dowel-type fasteners. To avoid a brittle failure all of the experiments were reinforced with fully threaded screws, which is currently state of the art [12].

This study is related to glue-laminated timber produced by coniferous wood, which represents the majority of manufactured lumber in Europe. No attention is given to deciduous wood.

In order to introduce plastic hinges to timber structures, a mechanical model has been developed, to describe the semi-rigid behavior of joints in a reliable way, reliable not only with the focus on the load capacity, but also on the rotational capacity. This model is simplified to give a first practical approach.

Regardless of the application of the ductility in timber structures it is important to define guidelines to activate the ductility. More strictly spoken, if the ductility is used to dissipate energy in the case of an earthquake or to redistribute internal actions, also with the view on robustness, it is absolutely essential to consider guidelines.

The natural material scattering of timber has a direct influence on the bearing resistance of joints and the deformation of load-bearing elements within a structure. In order to apply the elastic-plastic design method within timber structures, it is indispensable to observe these influences on a structure. The influences are considered within a probabilistic framework and some statistical studies.

1.3 Content of this study

The currently used design methods are introduced and discussed in the first part. A brief outline of the history in the field of research of the plastic design method is mentioned, followed by the application for the different types of materials. Subsequently, a more detailed introduction of the consideration of the ductility in timber structures is given.

The second part comprises a limited number of earlier research work on fasteners in timber structures from literature. It gives the major focus of the different scientific treatises. The load-deflection behavior of the different fasteners is discussed and presented. In order to classify the behavior of the fasteners in timber structures, methods to evaluate the behavior of fasteners are also discussed in the second part. A classification was conducted on the previously introduced types of connections. Based on the application of the different methods, an extension of the ductility classification is given.

The experimental research is given in the third part. The experiments are generally divided

into two domains. On one hand pure tension experiments on dowel connections, on the other bending experiments on joints are realized. The joints were designed in such a way, that the previously tested connections create a joint component to transfer the tension force. In order to reflect the load-displacement behavior, respectively the moment-rotation behavior, a model was developed based on the component model. The third part concludes with a simplified model with regard to the practical application.

The fourth part considers the scattering of the material properties. It is indispensable to ensure, that a ductile behavior takes place before a brittle failure occurs next to the joint. Therefore, a Monte Carlo simulation was conducted to develop an over-strength factor. The investigations were extended in such a way, that a reliability line was developed, which gives an over-strength factor depending on the desired reliability index β of the structure. The material scattering has also an effect on the required rotation of the joint. A factor was developed which covers the influence on the required rotation.

The closure gives a summary with limitations and recommendations for upcoming research work.

An exemplarily design, considering the plastic behavior of a joint is given in the Appendix A.

2 Current design methods

2.1 General

The guarantee of a sufficient load bearing capacity of structural elements is an indispensable demand on a structure. An adequate bearing capacity is given, if the effect of actions is not greater or equal than the resistance of structural members, described as sections and joints (comp. Eq. (2.1)).

$$E_d \leq R_d \quad (2.1)$$

where

E_d : effect of actions

R_d : ultimate load bearing capacity

There are in general three different design methods to achieve this requirement. They differ substantially by the determination of the effects of actions and the determination of the bearing resistance of structural members.

Table 2.1 gives an overview of the current different design methods in order to determine the maximum load-bearing capacity of a structure.

Table 2.1: Overview of the different design methods

Method	Determination of	
	effects of actions	bearing resistance
Elastic-elastic	Theory of elasticity	Theory of elasticity
Elastic-plastic	Theory of elasticity	Theory of plasticity
Plastic-plastic	Theory of plasticity	Theory of plasticity

However, the load bearing capacity of a complete structure differs within the different design methods. On the other hand, the different design methods also demand different requirements of cross-sections and joints. The different methods are presented in the following.

2.2 Determination of the maximum load-bearing capacity

2.2.1 Elastic-elastic design method

The elastic-elastic design method is generally used in combination with brittle or slightly ductile materials (e.g masonry and timber). It also may be applied in steel structures. It is characterized by elastically determined stresses, given by the structure, and the elastic resistance of the cross-section. Within this design method Equation (2.1) turns into

$$\sigma_{E,d} \leq \sigma_{R,d} \quad (2.2)$$

where

$\sigma_{E,d}$: stresses caused by actions

$\sigma_{R,d}$: ultimate elastic stresses

The advantage of this method is the linear correlation of the determined stresses and the loading on the structure. Therefore the principle of superposition is valid. Stresses of different load cases may be superimposed.

The disadvantage of this method is the underestimation of the load-carrying capacity of structures of ductile materials. In order to increase the economic efficiency of such materials the elastic-plastic design method has been developed.

2.2.2 Elastic-plastic design method

The elastic-plastic design method takes advantage of the ductile material behavior. This method is used in steel, steel-concrete composite and reinforced concrete structures. Within the elastic-elastic design method only the fibers at the edges of the cross-section are at the point of yielding, whereas the main cross-section is still in the elastic stage (see Fig. 2.1(a)). A further load increase is possible until the entire cross-section is plasticized (see Fig. 2.1(c)). This state is known as a plastic hinge.

Since the design method is based on an entire plasticized cross-section it is not possible to refer directly to Equation (2.2). The proof of the load bearing capacity is in this case based on the plastic bearing resistance of the cross-section, for instance $M_{pl,Rd}$, $N_{pl,Rd}$ etc. (comp. Eq. (2.3)).

$$X_{E,d} \leq X_{pl,R,d} \quad (2.3)$$

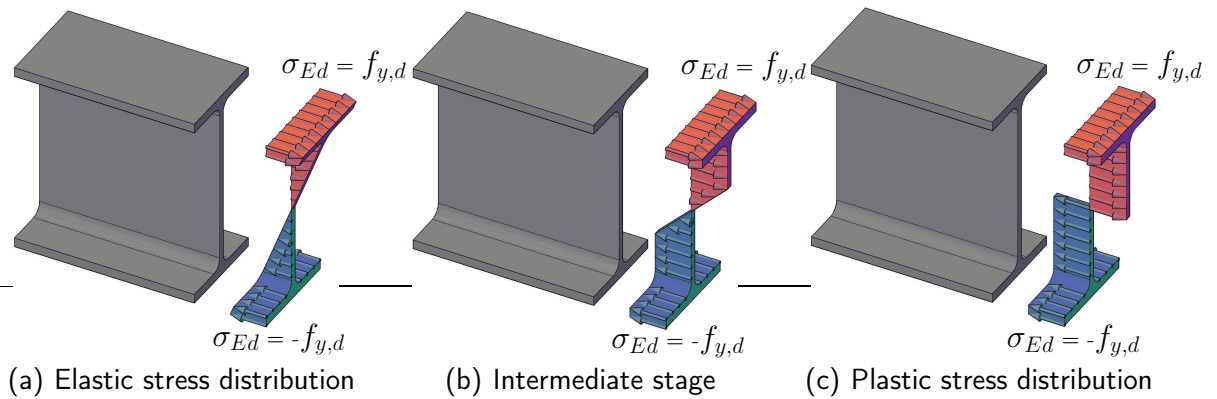


Figure 2.1: Different stress distributions of an IPE beam

where

$X_{E,d}$: internal forces caused by actions, e.g. bending moment $M_{E,d}$

$X_{pl,Rd}$: ultimate plastic resistance, e.g. moment resistance $M_{pl,Rd}$

2.2.3 Plastic-plastic design method

The plastic-plastic design method allows a further load increase in statical indeterminate structures, using plastic system reserves, until the system transforms into a mechanism. This design method is particularly used in steel and steel-concrete composite structures. The maximum load on the structure is either given by the virtual-work or by the complex yield zone theory. Within these methods the location of the plastic hinges is determined in order to achieve the maximum possible load on the structural system. Therefore the general design equation (comp. Eq. (2.1)) is based on the maximum load (comp. Eq. (2.4)). Within this design method it is necessary that the plasticized cross-section has in addition a distinctive rotation capacity. In order to form all of the required plastic hinges (see Fig. 2.2), it is necessary that the single plastic hinges within the structure have a sufficient rotation

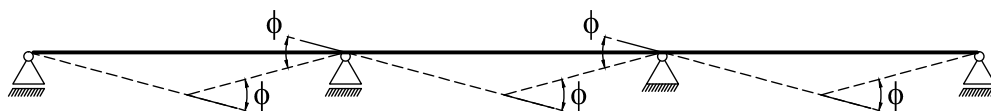


Figure 2.2: Definition of the rotation ϕ on a structural element

capacity (comp. Eq. (2.5)) to enable the formation of all plastic hinges.

$$q_{E,d} \leq q_{pl,R,d} \quad (2.4)$$

$$\phi_{req} \leq \phi_{ex,pl} \quad (2.5)$$

where

$q_{E,d}$: existing design load	ϕ_{req} : rotation caused by actions
$q_{pl,R,d}$: ultimate load	$\phi_{ex,pl}$: ultimate rotation capacity

A structure, designed with the plastic-plastic design method, has no more reserve of strength except the strain hardening in steel structures. The structure will collapse if any load greater than $q_{pl,R,d}$ is applied.

2.3 Discussion of the different design methods

Cost effective solutions can be achieved with the application of the elastic-plastic or plastic-plastic design method. Hence, materials allowing a plastic design method have an economical benefit due to the higher load carrying capacity compared with the elastic-elastic design method used with brittle materials. Figure 2.3 shows the differences in the design methods. Within the elastic design consideration the maximum load on a single span girder, clamped on one side, is achieved if the bearing resistance at the support is reached. In this case

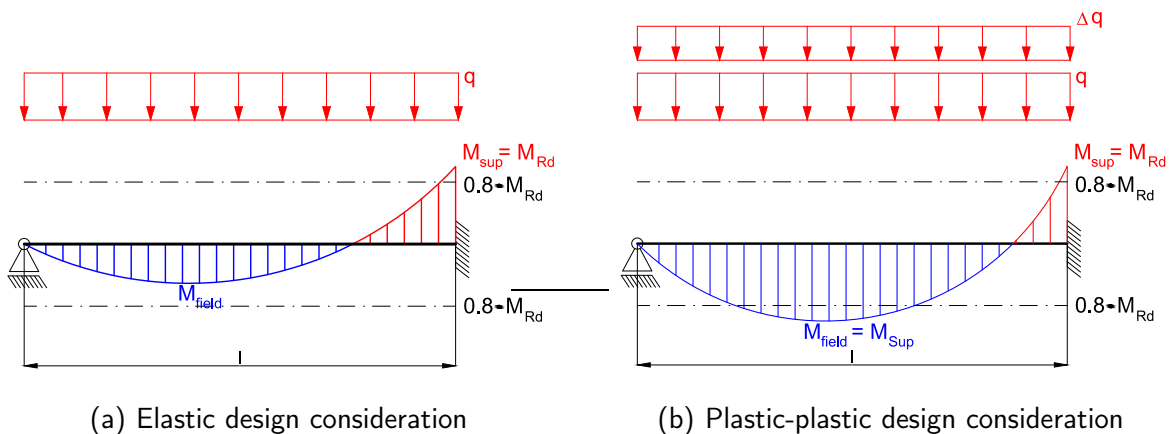


Figure 2.3: Load increase in statically indeterminate structures

the cross-section is only utilized with a target magnitude above 80 % at a certain area at the fixed support (see Fig. 2.3(a)). If the plastic design method is applied, an additional load (Δq) can be applied until the bearing resistance in the field is also reached. (see Fig. 2.3(b)).

Larger deformations are caused by higher loads which need to be checked in the serviceability limit state.

Besides the advantage of a possible redistribution of internal actions in indeterminate structures, the consideration of the plastic behavior has more benefits, especially with regard to robustness.

Robustness has become more important in recent time. A main requirement on robust structures is the claim that no sudden failure occurs at any time. Ductile elements announce a failure due to large deformations, rotations or cracks. Therefore, options are open to react carefully.

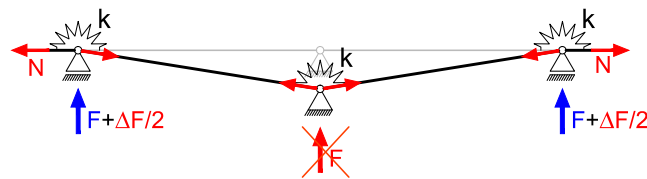


Figure 2.4: Development of membrane actions due to ductile elements

In case of an unforeseen impact (e.g. collision, explosion, etc.) it is important to ensure that the structure is not endangered due to collapsing. Therefore either the structural elements are oversized, or the plastic hinges are well selectively installed. Plastic hinges are able to redistribute the additional load either under large deformations or by developing membrane actions in the structure (see Fig. 2.4).

Within the seismic design, ductility is an integral demand on a structure or on structural elements under a seismic loading. The bearing resistance under a seismic loading mainly depends on the energy dissipating behavior of the structure. Brittle materials have only



Figure 2.5: Destroyed cathedral in Christchurch, NZ after the earthquake from the 22nd of February 2011

a little potential to dissipate energy. During the earthquake in 2011, the church tower of the cathedral in Christchurch, New Zealand collapsed in a brittle manner (see Fig. 2.5). Well designed details and mechanical fasteners exhibit a well dissipative behavior in timber structures [46]. The introduced energy in case of an earthquake is quashed due to friction within the mechanical joints and the deformability of the connections. Therefore, timber structures behave in general in a good manner in case of an earthquake.

The common design method is the elastic-elastic design. For materials allowing a

plastic design, the elastic-plastic method is generally used, followed by the plastic-plastic design method, which is rarely used [45]. Reasons for this is the complex determination of the location of the plastic hinges within a structural system and therefore of the ultimate possible load ($q_{pl,Rd}$ in equation 2.4).

2.4 Application of the plastic design methods

2.4.1 Steel structures

The first experimental approaches of the plastic design method in steel structures were already performed in the year 1914 by the Hungarian civil engineer *Gábor v. Kazinczy* (1889-1964) [50].

The experiments were focused on the load bearing capacity of a double-sided fixed profile (I 160) [44]. The general test setup is shown in Figure 2.6. Two different lengths were performed, a beam length of 5.60 m and a length of 6.0 m.

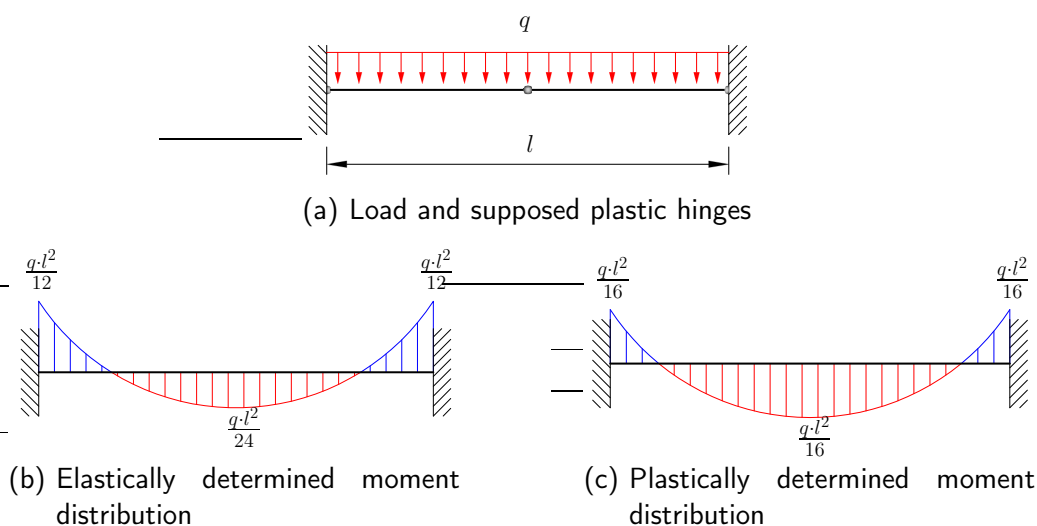
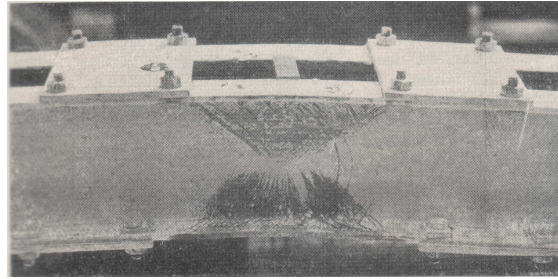


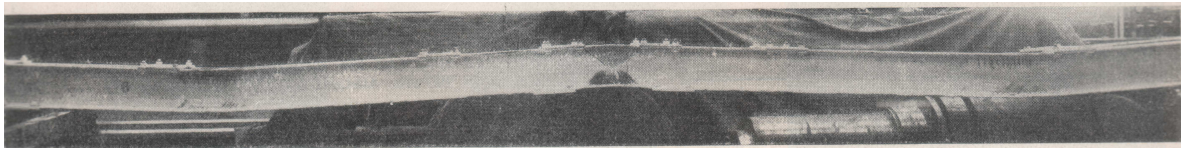
Figure 2.6: Experiments conducted by Kazinczy [44]

G. v. Kazinczy supposed that the beam forms three plastic hinges at failure (see Fig. 2.6(a)). The experiments confirmed his assumption; it has been shown, that the design for the fixed ends is based on a bending moment of $M = q \cdot l^2 / 16$ instead of $M = q \cdot l^2 / 12$ [50], therefore the supposed three plastic hinges have been developed.

Maier-Leibnitz [52] was another trailblazer of the theory of plasticity. The experiments were conducted in order to give a contribution to the question of the load bearing behavior of continuous beams which has been questioned by the building inspectors. The experiments confirmed the assumed theory of the plastic design. Figure 2.7 shows the formation of all plastic hinges occurred during the experiments.



(a) Plastic hinge



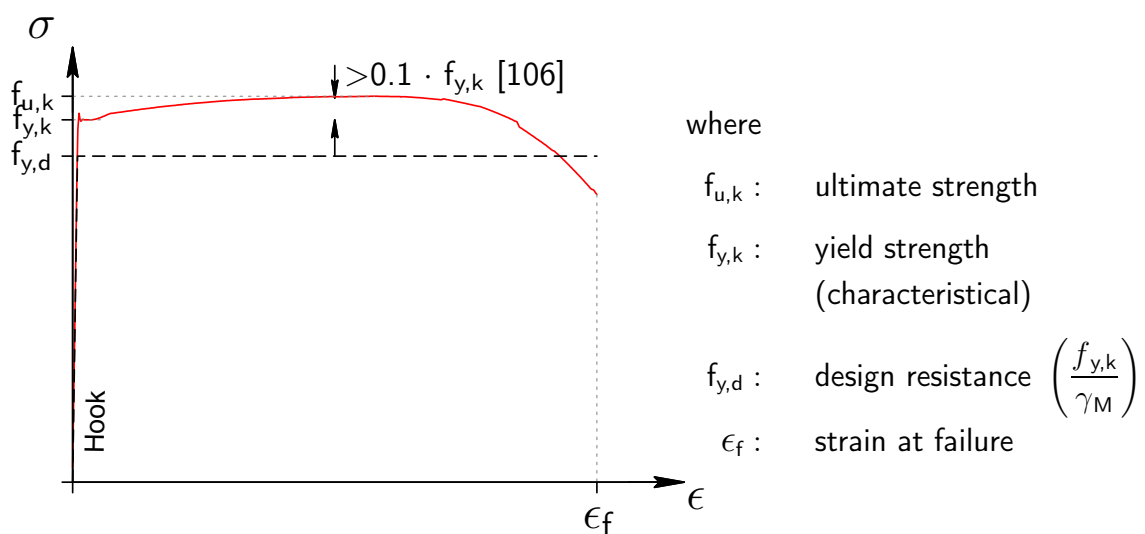
(b) Set up of a continuous beam, with the presence of all developed plastic hinges

Figure 2.7: Experiments on the bearing resistance of a two-span beam in steel [52]

Fritz Stussi and *Curt Fritz Kollbrunner* [75] conducted experiments in the mid thirties. The theoretical findings could not be confirmed with the experiments. A discussion followed in the subsequent years between proponents and opponents of the plastic design method [74]. The contradiction could be explained in the year 1952 by *P. S. Symonds* and *B. G. Neal* [76]. The rotation of the plastic hinges were unacceptably large for the used cross-section in the conducted experiments.

Further work on the plastic design was carried out. Therefore, the plastic design is nowadays implemented in the standard [106].

The material properties set the basic requirements for the application of the plastic design in

**Figure 2.8:** Parameters of the stress-strain relationship of steel

steel structures. Figure 2.8 shows the stress-strain relationship of steel in tension. It forms a clear linear elastic stiffness at the beginning (*Hooke's Line*), followed by an area of constant stresses with increasing strains. A strain hardening continues the steady stress-strain relation until the ultimate tensile strength is reached. After overstepping the ultimate strength local necking occurs, the material fails considerably later.

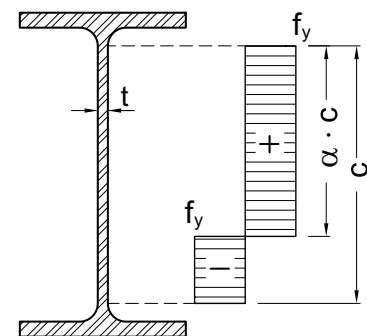
The elastic-plastic behavior of the material is approximated for the design as a bilinear approach. The constant yield plateau is given considering the partial safety factor γ_M (see Fig. 2.8).

However, the plastic design in steel structures claims some restrictions. The ultimate strength of the used steel grade has to be at least 10% greater than the adjusting yield strength [106]. Furthermore, the demand on the rotation capacity increases with the plastic-plastic design method (comp. Sec. 2.2.3). Hence the cross-sections are divided into different classes based on the ratio of (c/t) (see Tab. 2.2) and [106, Table 5.2]. The plastic resistance (see Fig. 2.1(c)) can be determined for profiles of class 1 or class 2, whereby the rotational capacity is limited for class 2 profiles. For class 3 and class 4 profiles the resistance has to be determined elastically (Figure 2.1(a) and [106]). For class 4 profiles a local buckling occurs before the yield stress is reached. Table 2.2 shows the requirements for class 1 and class 2 cross-sections.

In addition to the plastic design of cross-sections it is possible to design joints with the plastic design method [107].

Table 2.2: Classification of class 1 and class 2 steel I profiles

	loading		
	bending	compression	compression & bending
class 1	$c/t \leq 72 \cdot \varepsilon$	$c/t \leq 33 \cdot \varepsilon$	$\alpha > 0.5: c/t \leq \frac{396 \cdot \varepsilon}{13 \cdot \alpha - 1}$ $\alpha \leq 0.5: c/t \leq \frac{36 \cdot \varepsilon}{\alpha}$
class 2	$c/t \leq 83 \cdot \varepsilon$	$c/t \leq 38 \cdot \varepsilon$	$\alpha > 0.5: c/t \leq \frac{456 \cdot \varepsilon}{13 \cdot \alpha - 1}$ $\alpha \leq 0.5: c/t \leq \frac{41.5 \cdot \varepsilon}{\alpha}$



where

- | | | | |
|---|------------------------|---------|---|
| c | : height of the web | alpha | : proportional compressed stressed area [106] |
| t | : thickness of the web | epsilon | : $\sqrt{235/f_y}$ |

2.4.2 Reinforced concrete structures

Besides the linear elastic design method, the calculation method based on the plasticity may be used in reinforced concrete structures [105]. If the choice is set to the plastic design method, a reinforcing steel with a high ductile behavior (B500B) has to be chosen [98]. It is possible to redistribute internal forces, determined with the linear elastic design method (non-cracked condition), to lesser utilized structural elements. Special attention has to be given to the limits of the redistribution. The limits depend on the concrete grade and the ductility classification of the reinforcing steel. Therefore a better utilization of the structure and a better distribution of the reinforcement between the positive and negative bending moment [20] can be achieved.

In accordance with steel structures, the plastic design of reinforced concrete structures is also based on the formation of plastic hinges.

Figure 2.9 shows the simplified trilinear moment-curvature relationship for the nonlinear design approach. The initial stiffness undergoes a decrease of the stiffness before the point of yielding is reached. At this point the concrete turns from the non-cracked condition to

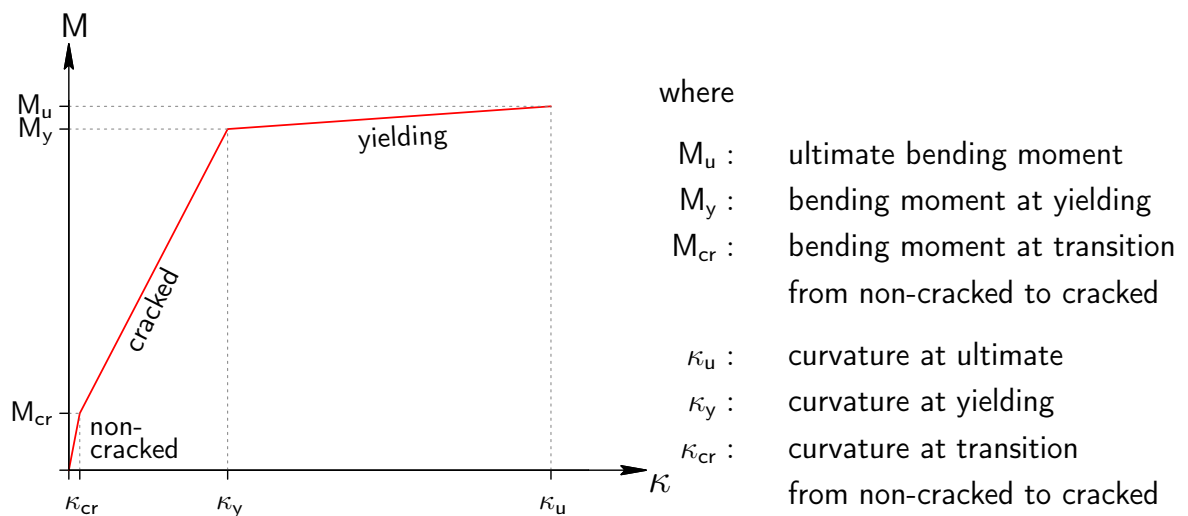


Figure 2.9: Simplified M - κ correlation

the cracked condition. A redistribution of internal forces to stiffer (non-cracked) areas takes place in indeterminate structures until a cracking occurs in the non-cracked areas as well. At this stage the moment distribution mainly depends on the ratio of the stiffness in cracked condition [81]. An additional load increase is possible, until all of the plastic hinges have formed.

2.4.3 Composite structures

Composite structures consist of different types of materials which are linked with shear connectors. The main idea is to connect materials according to the ideal material behavior in order to form an efficient hybrid section. Composite structures are not only used in bridge constructions but also in building constructions.

For composite structures consisting of steel and concrete a design method based on the theory of plasticity is in general possible. Figure 2.10 shows a typical composite section consisting of

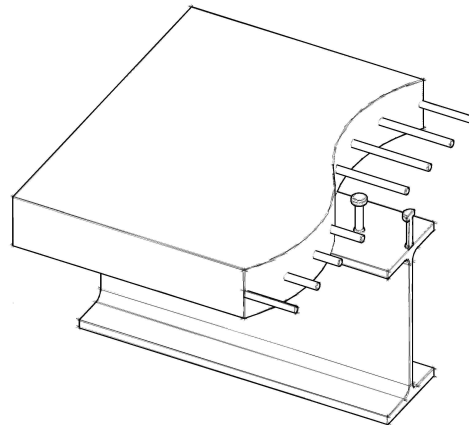


Figure 2.10: Sketch of a steel-concrete composite structure

steel and concrete. The shear stresses between the two materials are transferred by headed studs.

According to the classification in steel structures, the cross sections are divided into different classes (comp. Sec. 2.4.1). The limitation of the c/t value is based on [106], with the major difference that the concrete is taken into account (see Fig. 2.11(a)). Only cross-sections of

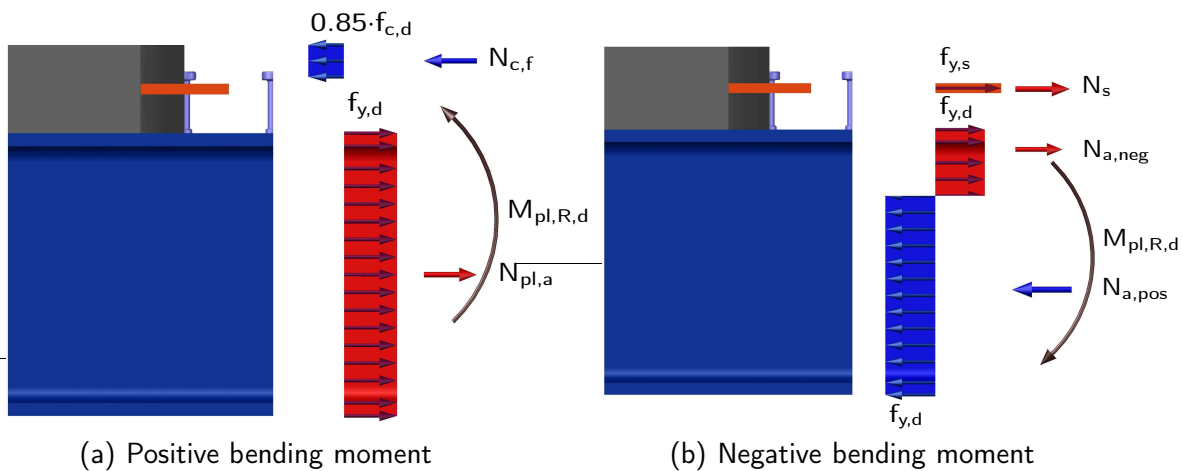


Figure 2.11: Stress distribution and internal forces acting on a composite cross-section

class 1 and 2 are permitted in the plastic design [108]. If the composite section is within a negative bending moment area (see Fig. 2.11(b)), the reinforcing steel has to have a minimum percentage of reinforcing of grade B or C in order to ensure a sufficient rotation capacity. Reinforcing steel of grade B is classified as highly ductile. Due to the application in the seismic design a grade C reinforcement with a higher strain capacity at ultimate load compared to a grade B reinforcement is required. Figure 2.11 displays the internal stresses with its resultants for a positive and negative bending moment acting on the cross-section.

2.4.4 Plastic design of joints

Besides the plastic design of sections, it is also possible to design joints with the theory of plasticity. The component method is used to describe the mechanical behavior of the joint. The general idea is to divide the joint in its different load-carrying elements, the so called components. The component method is used to assemble the different components with their particular structural behavior, which can be found in [48, 107, 108]. It is possible to illustrate the structural behavior of the joint based on the component model. Therefore, not only the load bearing capacity, but also the rotational capacity can be evaluated. The component method is described more precisely in Chapter 6.

It has been shown, that the experimentally examined joints have a large rotational capacity. This is not only desirable in the view of the load carrying capacity but also with regard to robustness [90].

2.5 Design situation in timber structures

2.5.1 General

Timber as a natural growing material behaves rather brittle, therefore the design of timber structures is inherently elastic-elastic.

Despite the brittle behavior of timber Maier-Leibnitz [53] conducted some experiments in view of the bearing resistance of a continuous beam. These experiments were performed parallel to the experiments on steel beams (comp. Sec. 2.4.1). A remarkable observation has been noticed. Following the bending moment distribution of a continuous beam, the experiments should have collapsed at mid support. In complete contrast to the expectations the beam failed at mid-span (see Fig. 2.12). The group of researchers attributed the surprising result to the large deformations at the mid-support (see Fig. 2.12(a)). The timber beam redistributed the internal forces to the lesser utilized cross-section in the span by the large deformations at the mid-support. Figure 2.12(b) shows the typical brittle failure at mid-span.

A further experiment with a significant displacement at the mid-support confirmed the pre-

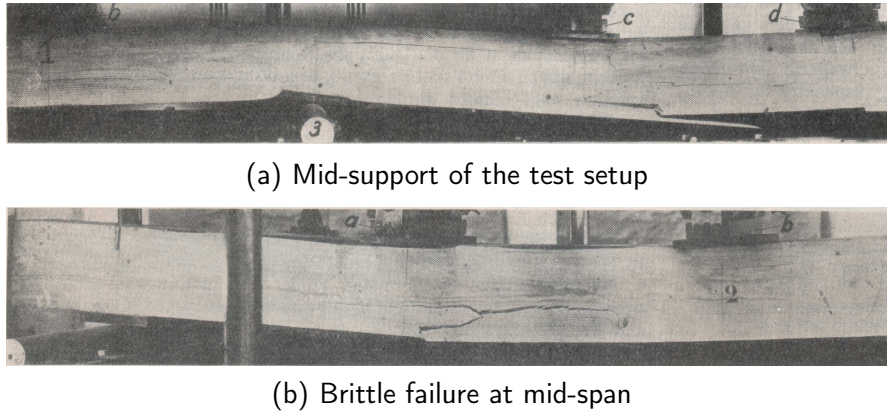


Figure 2.12: Experiments on the bearing resistance of a two-span beam in timber [53]

vious assumption. The researchers certified a self-healing system of continuous beams in timber structures [53].

An increase of the permissible stresses was admitted for continuous beams at an early stage of the German timber standard DIN 1052 [94]. The permissible stresses of [94] were also taken into the timber standard of the German Democratic Republic [61], therefore a stress redistribution of internal actions was implemented. An increase of the stresses in bending of 10% was still permitted in the last versions of the German timber standard [96, 5.1.8] [95, 8.1 (5-7)]. The increase of the stresses is attributed to the homogeneity of timber [26] and the ductile behavior of timber in compression.

A part consideration of ductility is already implemented in the standards [99, 109, 114] and described in the following.

2.5.2 Design of cross-sections

Despite the brittle behavior, timber shows a limited plastic behavior in compression [32]. Therefore the compression stresses are considered squared within the interaction design of normal stresses and stresses caused by bending (comp. Eq. 2.6 & Eq. 2.7).

$$\left(\frac{\sigma_{c,0,d}}{f_{c,0,d}}\right)^2 + \frac{\sigma_{m,y,d}}{f_{m,y,d}} + k_m \cdot \frac{\sigma_{m,z,d}}{f_{m,z,d}} \leq 1 \quad (2.6)$$

and

$$\left(\frac{\sigma_{c,0,d}}{f_{c,0,d}}\right)^2 + k_m \cdot \frac{\sigma_{m,y,d}}{f_{m,y,d}} + \frac{\sigma_{m,z,d}}{f_{m,z,d}} \leq 1 \quad (2.7)$$

Hence the stress redistribution of highly utilized fibers at the edges to lesser utilized adjacent fibers is considered with an increase of the deformations due to the non-linear behavior of timber in compression.

Since buckling is in general a brittle failure, it is not allowed to consider the compression stresses with the power of two [109, 6.3].

2.5.3 Design of dowel-type fasteners

The mechanical behavior of connections with dowel-type fasteners is attributed on the findings of Johansen [37] & Meyer [55] and nowadays state of the art [109, 114]. It is also well known as the European Yield Model (EYM). The theory was first published in the year 1949 and is based on the formation of plastic hinges within the steel dowel. The development of plastic hinges within the dowel-type fastener enables the possibility to keep the loading level with an increase of the deformations.

According to EN 1995-1-1 [109] and [99], there are three different failure modes for timber-steel-timber connections accomplished as fitch plates, where the smallest value is governing.

- Bearing stress

The consideration of the bearing stress follows the determination in steel structures. Thereby the stresses on the borehole are taken into account in order to determine the load bearing resistance (comp. Fig. 2.13(a) & Eq. 2.8)

$$F_{v,Rk} = f_{h,1,k} \cdot t_1 \cdot d \quad (2.8)$$

with

- $f_{h,1,k}$: bearing stress of the timber element
- t_1 : embedded length of the fastener
- d : diameter of the fastener

This type of failure mode is rather brittle since no plastic hinge is formed within the steel dowel. Only the partially ductile behavior of timber under compression may lead to a slight ductility. This type of failure is in general known as a brittle failure.

- Formation of one plastic hinge per shear plane

The embedded strength of the timber element is able to form a plastic hinge per shear plane in the dowel (comp. Fig. 2.13(b) & Equation (2.9)).

$$F_{v,Rk} = f_{h,1,k} \cdot t_1 \cdot d \cdot \left[\sqrt{2 + \frac{4 \cdot M_{y,k}}{f_{h,1,k} \cdot d \cdot t_1^2}} - 1 \right] \quad (2.9)$$

with

- $M_{y,k}$: yield moment of the dowel-type fastener

A ductile behavior of the connection is achieved due to the formation of a plastic hinge

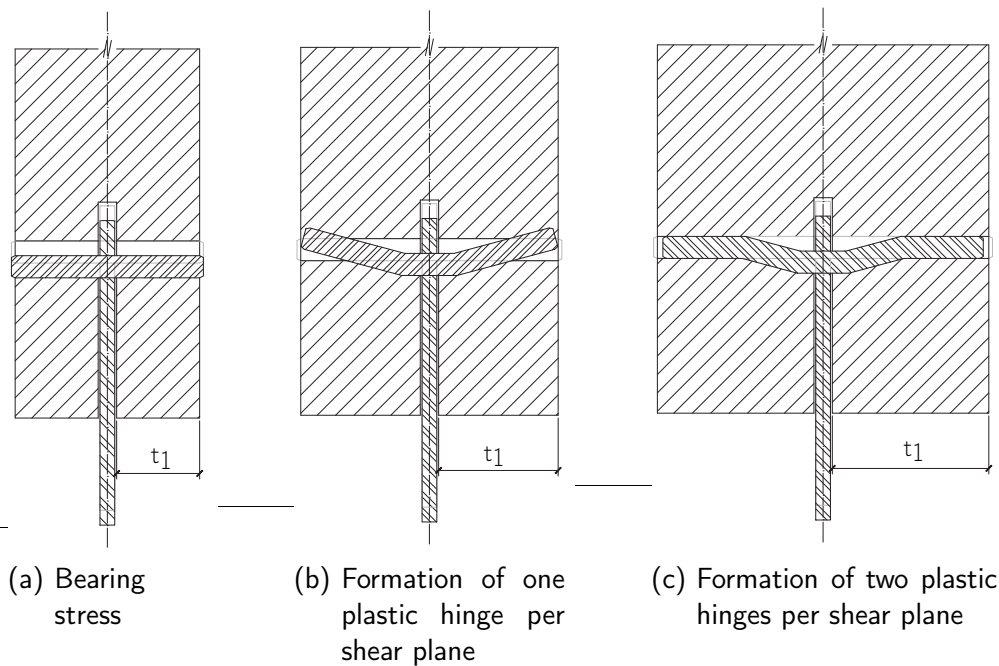


Figure 2.13: Failure modes according to [37]

of the dowel-type fastener.

- Formation of two plastic hinges per shear plane

According to the previous failure mode, the embedded strength is able to form two plastic hinges per shear plane in the dowel (comp. Fig. 2.13(c) & Equation (2.10)).

$$F_{v,Rk} = \sqrt{2} \cdot \sqrt{2 \cdot M_{y,k} \cdot f_{h,1,k} \cdot d} \quad (2.10)$$

The steel dowel has formed all plastic hinges, therefore this type of failure is also a ductile failure mode.

The effective number of fasteners parallel to the grain (n_{ef}) is equal to the existing number of fasteners, if the connection is reinforced with fully threaded screws [12] & [82]. The fully threaded screws prevent a splitting of the timber within the connection, therefore the compatibility of deformations within the connection is ensured. Thus all of the inserted fasteners participate in the bearing resistance of the connection. If a splitting is not prevented, local cracks occur and the load bearing resistance has to be reduced.

2.5.4 Consideration of the stiffness

As already mentioned, EN 1995-1-1 [109] allows an elastic-plastic design method if connections have an adequate ductility. This is a new point of view which amplifies a redistribution

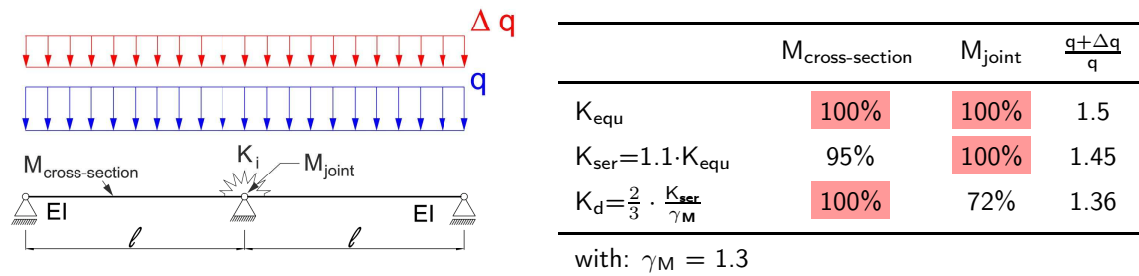


Figure 2.14: Influence of the joint stiffness on the bending moment distribution M_{joint} and $M_{\text{cross-section}}$

of internal forces and therefore a rise of the cost efficiency of timber structures.

The standard [109] is not giving any declaration about the ductile behavior of connections, therefore only the elastic behavior, represented by the slip modulus K_d , can be applied. Since the stiffness only accounts within the elastic range, the displacement is rather small. Therefore, it is hardly possible to achieve an optimized redistribution and thus a limited application.

First investigations on a two span beam showed [15], that the bending moment distribution strictly depends on the stiffness of the joint at the mid support [66]. Figure 2.14 shows preliminary results of the utilization of the support (M_{joint}) and the utilization within the field ($M_{\text{cross-section}}$), depending on the joint stiffness (K_i). Within this first approach the bearing resistance of the joint and the cross-section is considered to be equal. For a determined stiffness (K_{equ}) the load-bearing resistance at the joint and in the field is reached at the same time. The stiffness is given as:

$$K_{\text{equ}} = 3 \cdot \frac{EI}{l} \quad (2.11)$$

The stiffness K_{equ} is calculated based on the findings described in Chapter 8 (comp. page 198). However, if the stiffness is taken as the initial stiffness (K_{ser}), assumed as 110 % of K_{equ} , the structure collapses at the joint with a lower ultimate load compared to the stiffness K_{equ} . If the stiffness is determined according to the code [99], it is shown, that the structure fails brittle within the field at a lower ultimate load level compared to the consideration of K_{equ} .

Therefore, it is shown, that the stiffness of the joint is a driving parameter within the calculation approach. If the stiffness is underestimated it is shown, that a undesirable brittle collapse occurs within the field, whereas a failure at the support perhaps represents a desired, robust and ductile failure.

Furthermore, it remains an open question whether it is possible to develop plastic hinges within timber structures. First insights and initial solutions to clarify this topic are given within this scientific work.

3 Connections in timber structures - review and former investigations

3.1 General

The previous chapter has shown that the application of the ductility in timber structures is only possible by the activation of the ductile behavior of the inserted fasteners.

This chapter presents earlier investigations on the load-carrying and on the load-displacement behavior of fasteners which are reviewed and discussed. The results of the presented investigations are partially examined with regard to the ductile behavior in Chapter 4.3.

It should be noted, that a large number of experiments were conducted on dowel type fasteners compared to other types of fastenings. This may result from the fact that dowel type connections are mainly used in practical applications.

Additional information on the investigations of the various test series are given in Annex B.

3.2 Dowel type fasteners

3.2.1 Introduction

Dowel type fasteners are a commonly used type of connection in timber structures (see Fig. 3.1). The family of dowel type fasteners includes:

- nails
- bolts
- steel dowels
- screws
- staples

This type of fasteners mainly acts in shear, although screws, bolts, staples and special nails are also able to transfer tension forces to a certain extent. The design of this type of connection is based on the Theory of Johansen [37] (comp. Sec. 3.2.2).



Figure 3.1: Typical connections accomplished with dowel type fasteners (Source: WiEHAG)

3.2.2 K. W. Johansen (1949)

Johansen [37] contributed on the load carrying capacity of timber connections in the early forties. His focus was set, not only, but particularly to dowel type connections. Within the investigations it became obvious that the load bearing resistance of connections with dowel-type fasteners depend not only on the timber resistance but also on the bending resistance of the dowel itself. To gain more information Johansen [37] conducted experiments on the embedding strength of different species of timber. The achieved results showed a plastic behavior of the

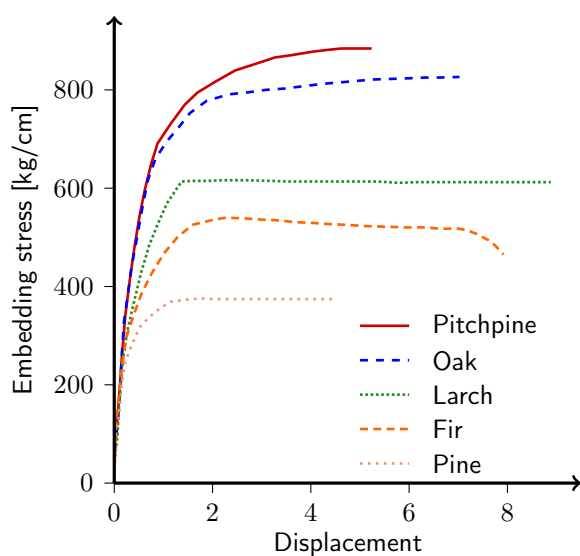


Figure 3.2: Embedding strength of different timber species [37]

embedding strength for different tested species (see Fig. 3.2).

On the basis of a plastic behavior of the embedment strength and of the dowel type connector, Johansen [37] developed equations to determine the load bearing resistance of such kind of fasteners (comp. Eq. (3.1) to Eq. (3.4)). The findings are displayed on a timber to timber connection whereby the timber is in the plastic stage and two plastic hinges are formed within the fastener (see Fig. 3.3). It is assumed that the stresses towards the ends from the plastic hinges are

equal (see Fig. 3.3(b)), thus these parts

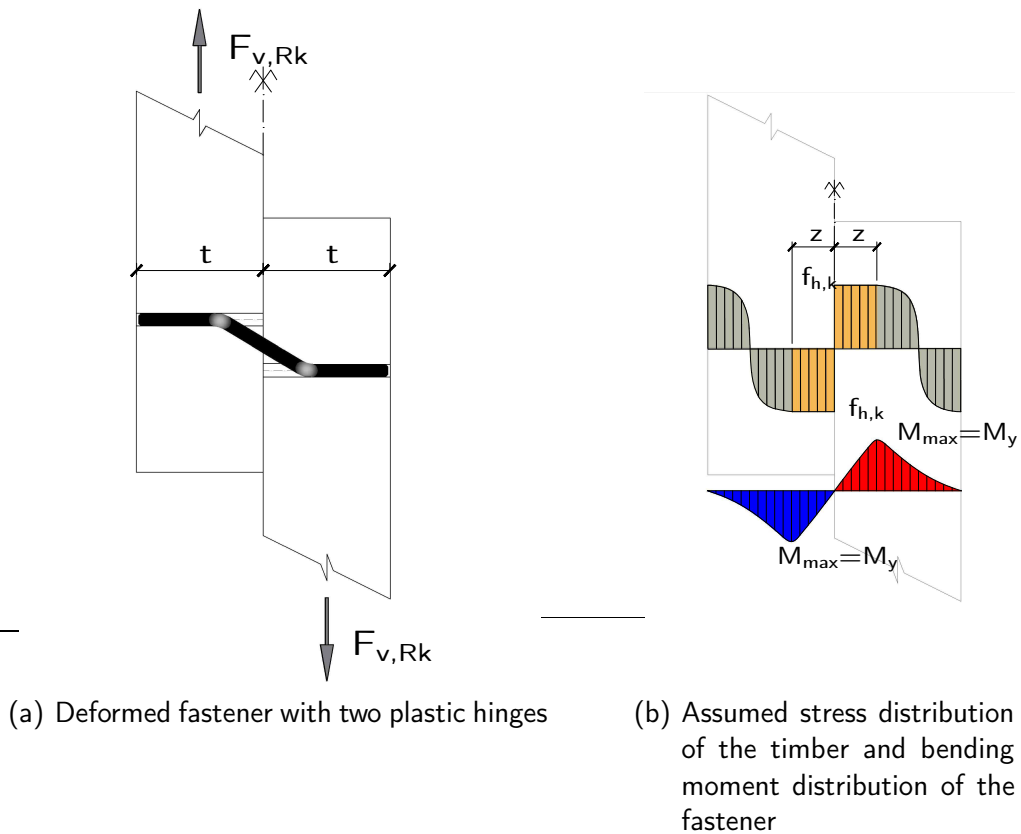


Figure 3.3: Investigations of Johansen [37] on dowel type connections

do not contribute to the load carrying capacity of the fastener. The equilibrium is given by:

$$F_{v,Rk} = f_{h,k} \cdot d \cdot z \quad (3.1)$$

Having a closer look on the bending moment distribution of the fastener, the maximum bending moment can be found as:

$$M_{max} = \frac{1}{2} \cdot F_{v,Rk} \cdot z = \frac{1}{2} \cdot \frac{F_{v,Rk}^2}{f_{h,k} \cdot d} \quad (3.2)$$

At that time, no investigation on the yield moment of the fasteners were conducted. Based on the mechanics, a yielding moment of $\frac{11}{32} \cdot f_y \cdot d^3$ was assumed for the fastener. Hence the load carrying capacity was given as:

$$F_{v,Rk} = 0.442 \cdot \sqrt{f_y \cdot f_{h,k} \cdot d^4} \quad (3.3)$$

The current basic valid equation of the European Yield Model (EYM) has been found for

certain yielding moments by applying Equation (3.2):

$$F_{v,Rk} = \sqrt{2 \cdot M_y \cdot f_{h,k} \cdot d} \quad (3.4)$$

The load carrying capacity of double shear connections for equal timber grades was also derived by Johansen [37], among others.

3.2.3 A. Meyer (1957)

Meyer [55] conducted experiments on nailed connections with the view on influencing parameters on the load carrying capacity. The focus was also set to a mathematical formulation to determine the load carrying capacity of nailed connections.

Following the findings of Johansen [37], Meyer [55] extended the derived formulations for connections of different timber grades and various thicknesses of wooden products. According to [55] & [109] the factor β describes the ratio of the different connected timber members. Considering different timber grades or timber products, Equation (3.2) turns to:

$$F_{v,Rk} = 2 \cdot \sqrt{\frac{M_y \cdot \beta}{f_{h,1,k} \cdot d \cdot (1 + \beta)}} \cdot f_{h,1,k} \cdot d \quad (3.5)$$

$$= \sqrt{\frac{2 \cdot \beta}{1 + \beta}} \cdot \sqrt{2 \cdot M_y \cdot f_{h,1,k} \cdot d} \quad (3.6)$$

with:

$$\beta = \frac{f_{h,2,k}}{f_{h,1,k}}$$

Thus it was possible to consider different timber properties for the different failure modes given by Johansen [37].

Attention was also given to the bending strength of nails. Two nails were tested together as simply supported beams loaded at mid-span. The distance of the supports was between 10d and 15d. Table 3.1 shows the test results of the conducted experiments. For steel grades with a non pronounced yielding the bending strength follows the elastic load bearing capacity. The capacity increased by about 70 % for elastic-plastic material properties compared to elastic materials.

As a result of the investigations it was concluded that the load carrying capacity of nails mainly depends on the timber width, the embedment strength and the bending capacity of the nails.

3.2.4 J. Ehlbeck and H. Werner (1988)

The investigations of Gehri and Fontana [30] led to further studies in Germany on dowel type connections. Attention was given to which extent a non-staggering alignment of fasteners

Table 3.1: Bending strength of different cross-sections and steel properties [55]

steel grade	cross-section	bending strength
elastic, no pronounced yielding	●	$0.10 \cdot d^3 \cdot f_y$
	■	$0.167 \cdot a^3 \cdot f_y$
	◆	$0.118 \cdot a^3 \cdot f_y$
elastic-plastic, pronounced yielding	●	$0.17 \cdot d^3 \cdot f_y$
	■	$0.25 \cdot a^3 \cdot f_y$
	◆	$0.235 \cdot a^3 \cdot f_y$

with:

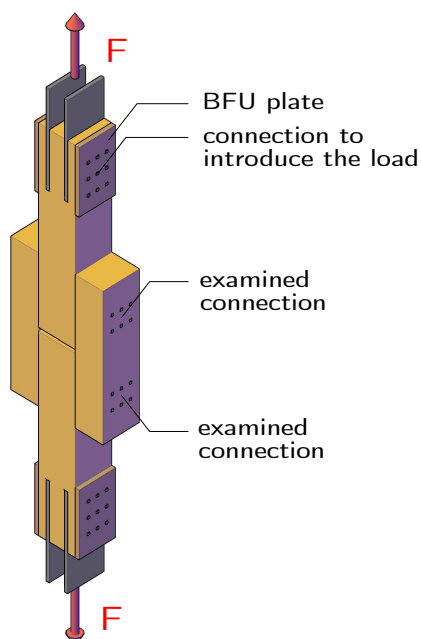
- d : diameter of the cross-section
a : edge length of the cross-section

parallel to the grain influences the load carrying capacity of a connection. Further parameters were observed to verify other possible causes.

Ehlbeck and Werner [24] conducted experiments with the focus on the following parameters

- dowel arrangement
- wood density
- timber species
- type of loading
- dowel diameter
- dowel slenderness
- dowel steel grade

The general test setup for tension experiments is displayed in Figure 3.4. All of the obtained

**Figure 3.4:** Tension specimen [24]

experiments were performed as double shear connections in grain direction. The load was introduced with a double flitch plate connection, where the side timber members were stiffened by BFU plates. Two identical connections were tested at once, but the load carrying capacity was always ascertained from the weaker connection [24]. The mean value of the density was 443 kg/m^3 and the 5 % quantile was determined to 380 kg/m^3 .

The experiments showed, that a staggered alignment hardly influences the load carrying capacity. The mean value of a staggered arrangement was about 3 % higher compared to a non-staggered alignment [24]. Based on the experiments it was observed, that the load carrying capacity and the stiffness increases linearly with the density.

The experiments confirmed the assumption that the embedded strength of the timber depends on the diameter of the fastener. The bearing resistance decreases with an increase of the dowel diameter. As a result a linear regression was developed to determine the embedded strength based on the dowel diameter and the timber density (comp. Eq. (3.7)).

$$f_h = 31.95 \cdot (1 - 0.012 \cdot d) \Rightarrow \begin{cases} = 0.072 \cdot (1 - 0.012 \cdot d) \cdot \rho_{mean} \\ = 0.083 \cdot (1 - 0.012 \cdot d) \cdot \rho_k \end{cases} \quad (3.7)$$

The experiments on other coniferous species confirmed Equation (3.7). No influence of the diameter could be ascertained for Bongossi wood. It was noted, that further experiments needed to be conducted on deciduous wood.

A database with experimental data was created and evaluated to gain more knowledge about the behavior of coniferous and deciduous wood [93]. For this purpose 119 experiments were available for deciduous timber and 360 for coniferous timber. Therefore, a regression could be found for deciduous timber as well (comp. Eq. (3.8)) [93]:

$$f_h = 0.102 \cdot (1 - 0.01 \cdot d) \cdot \rho_k \quad (3.8)$$

Equation (3.7) was revised within the consideration of the 360 experiments, resulting in the current valid equation to determine the embedded strength in grain direction (comp. Eq. (3.9)) [93] [109].

$$f_h = 0.082 \cdot (1 - 0.01 \cdot d) \cdot \rho_k \quad (3.9)$$

Moreover, it was found that the load carrying capacity of pure shear tests in compression is about 25 % higher compared to pure tension tests. The different load introduction was supposed as a possible cause [24].

The concerns about a load carrying decrease of non-staggered dowel arrangements could not be confirmed within these investigations. However, it was found that the reliability of the standard decreases with an increase of the dowel diameter.

3.2.5 H.J. Blaß (1990)

Blaß [6] performed 1088 experiments on 109 specimens with the focus on the variation of the single load-displacement behavior of non pre-drilled nailed connections within a group of fasteners in grain direction. The different load distribution of single fasteners in a multiple fastener connection is caused by different longitudinal expansions of the connected components. This fact is considered in steel structures by a reduction of a weld length larger than 150 times of the weld thickness by the factor β_{Lw} , and for multiple bolts in a row with a connection length larger than 15 times the diameter by the factor β_{Lf} [107].

The ascertained data forms the basis of a later developed model to simulate the load-displacement behavior of multiple connections parallel to grain [8].

All of the performed experiments were carried out in tension. A specimen was prepared for ten tests, but only a single connection was tested in each test cycle (see Fig. 3.5). After each cycle the specimen was removed and the nail rejected.

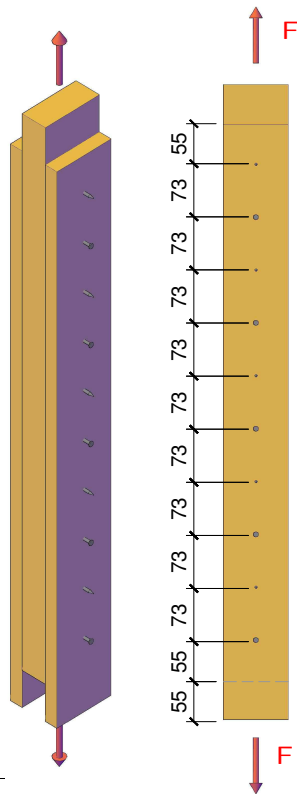


Figure 3.5: Experiments in grain direction [6]

The further nail was inserted from the opposite side as the previous one and tested. The distance of 20 times the diameter ensured that no test was influenced by a previous test. Thus the real load-displacement was recorded for every fastener position in the joint. The specimens were manufactured from solid spruce with a mean density of 407 kg/m^3 and a standard deviation of 44.6 kg/m^3 [6]. The end of the tests was defined as a rupture or if a displacement of approximately 20 mm was reached.

The experiments showed in general a consistent load-deflection behavior of the single tests within a specimen. However, in a few experiments the load-deflection behavior differ strongly from each other. This is caused to some extent by knots either in the side or in the middle member of the specimen. In these cases the load increased by about 20 % compared to the mean value of the consistent results.

An approximation function was developed within the

investigations to describe the load-displacement behavior of nailed connections (comp. Eq. (3.10)) [6].

$$f(x) = (K_2 + K_3 \cdot x) \cdot (1 - e^{-K_1 \cdot \frac{x}{K_2}}) \leq F_{max} \quad (3.10)$$

with:

f_x	= force at a certain displacement	K_1	= slope at the beginning
x	= displacement	K_2	= intercept of the end tangent
F_{max}	= maximum force according to ISO 6891 [113]	K_3	= slope at the end tangent

The approximation is shown in Figure 3.6 and shows the different input values.

Besides the study on the variation in grain direction, experiments were also conducted with the view on the variation perpendicular to the grain [7]. Thus 2438 mm long boards with a width of 235 mm were cut into three 810 mm long pieces. These were cut again in the longitudinal direction into four 56 mm wide pieces, the basic material of four specimens. The middle part of the original board forms the mid-section of the double shear connection with one nail. The pieces of the first and third part were cut again into 19 mm high members,

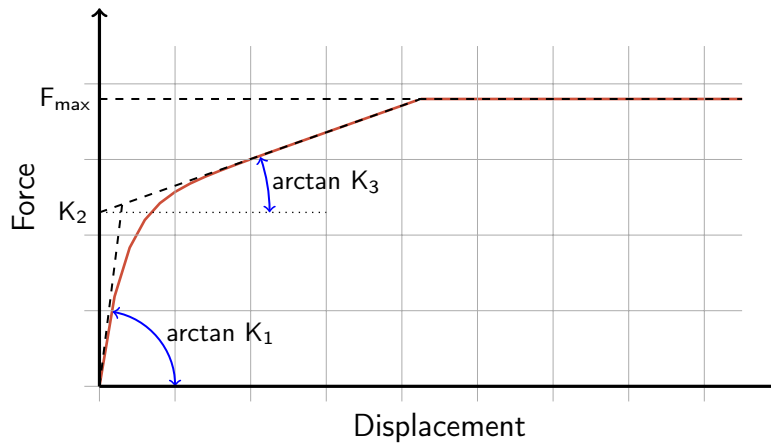


Figure 3.6: Approximation of the load-displacement behavior

which form the side components. Hence the dimensions of the investigations perpendicular to the grain are equal to the dimensions of the specimens on the investigations in grain direction. The test series was also performed as tension test in grain direction

The investigations on both variants, parallel and perpendicular to the grain, showed a decrease of the maximum load for the test setup perpendicular to the grain of about 10 - 14 %. This is to some extent due to the fact of a smaller density of about 4 % compared to the mean density of specimens on the experiments in grain direction.

All of the displayed experiments in [6] and [7] showed a distinctive plastic plateau.

3.2.6 A. Mischler (1998)

The aim of Mischler [89] was the optimization of the design of steel-timber connections. The main requirements within the investigations on connections were defined as:

- high effectiveness regarding the load-carrying capacity
- high stiffness
- ductile behavior

Mischler [89] describes the effectiveness of a connection as:

$$\text{efficiency factor } \eta = \frac{R_{U, \text{connection}}}{R_{U, \text{cross-section}}} \quad (3.11)$$

with:

- $R_{U, \text{connection}}$: load-carrying capacity of the connection
- $R_{U, \text{cross-section}}$: bearing resistance of the cross-section

Both the load-carrying capacity of the connection ($R_{U, \text{connection}}$) and the bearing resistance of the cross-section ($R_{U, \text{cross-section}}$) are depending on various material properties as already mentioned. A sufficient stiffness is a further main requirement and in general a major determining factor in view of the serviceability limited state, and therefore the driving parameter in the analysis of the deflection. Gehri [29] illustrated the stiffness of different building materials, as the ratio of the strength to the stiffness (f/E). Based on Table 3.2 it can be seen

Table 3.2: Relationship of the strength to the stiffness [29]

building material	ratio f/E [$\times 10^3$]
steel	1.2 - 2
reinforced concrete	0.5 - 1
timber	2 - 3

that timber is in general more susceptible in terms of the serviceability limit state.

The stiffness of connections has also a significant impact on the load distribution within a statically indeterminate system (comp. Chap. 8).

The third main requirement in optimizing connections is set to the ductility. Connections are usually a weak point within the structure, therefore it is important that the connections allow large deformation before a failure occurs. Due to ductile connections it is possible to

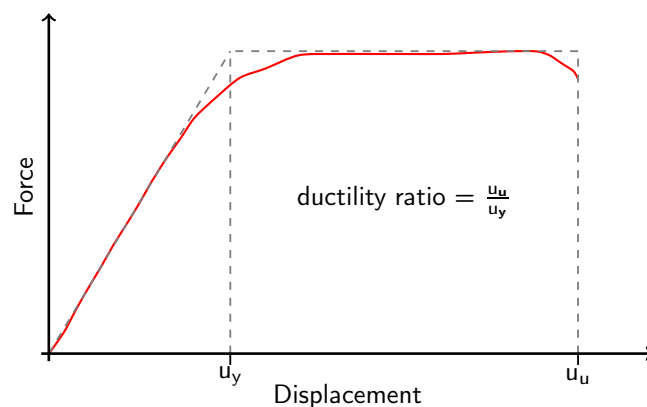


Figure 3.7: Definition of the ductility

compensate or even to increase the load capacity of a structure [89]. Mischler [89] describes the ductility as the ratio of the ultimate displacement (u_u) to the displacement at yielding (u_y see Figure 3.7). The definition of the ductility is an important parameter to consider the ductility of timber structures (comp. Sec. 4.2).

Gehri [28] characterized the ductility as the working ability. The working ability describes

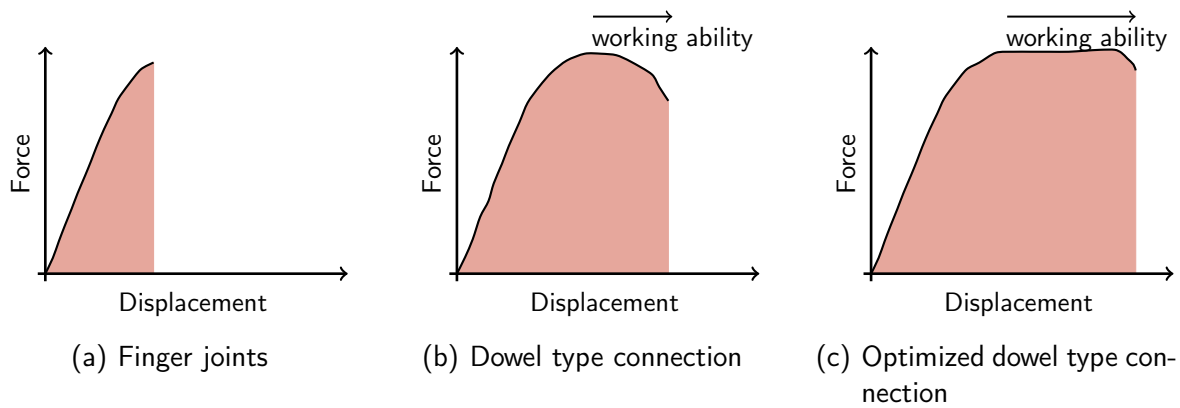


Figure 3.8: Working ability [28]

the capacity of a connection to redistribute internal actions if an indeterminate structure is overloaded. Figure 3.8 illustrates the different working abilities. Finger jointed connections hold almost no working ability (see Fig. 3.8(a)), whereas an optimized dowel type connection exhibits a high working ability (see Fig. 3.8(c)). Standard dowel type connections hold a regular working ability (see Fig. 3.8(b)).

Experiments were performed to optimize steel-timber connections with the focus on a ductile behavior with a high effectiveness. The test setup was split into two different test series. On the one hand experiments with the view on the design of connections, and on the other with the focus on the relevance of the timber properties.

The majority of the tested connections were accomplished as BSB-connections, developed by Herman Blumer, Swiss. The BSB-connection is a dowel type flitch plate connection, with three or four slotted plates. The diameter of the fastener is $6.3 \text{ mm} \pm 0.05 \text{ mm}$ with a minimum tensile strength of 550 N/mm^2 [89]. The mean tensile strength of the used dowels was 652 N/mm^2 . The width of the specimen was 200 mm with a height of also 200 mm. Therefore, it was possible to install the slotted plates in either directions, parallel

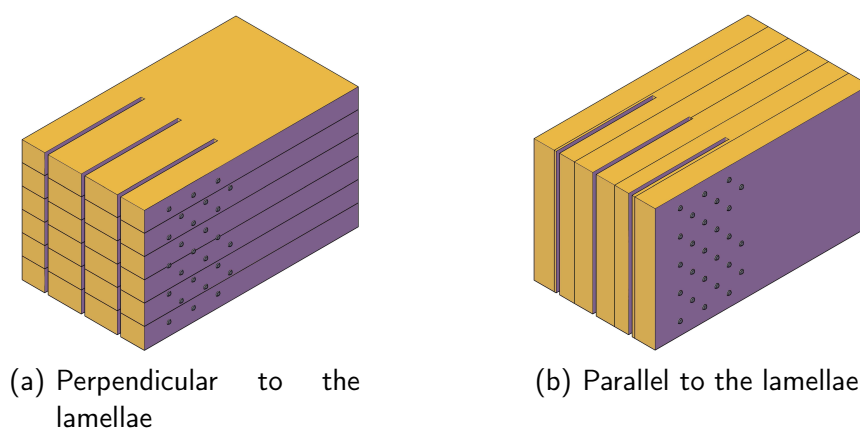


Figure 3.9: Orientation of the slotted plate [89]

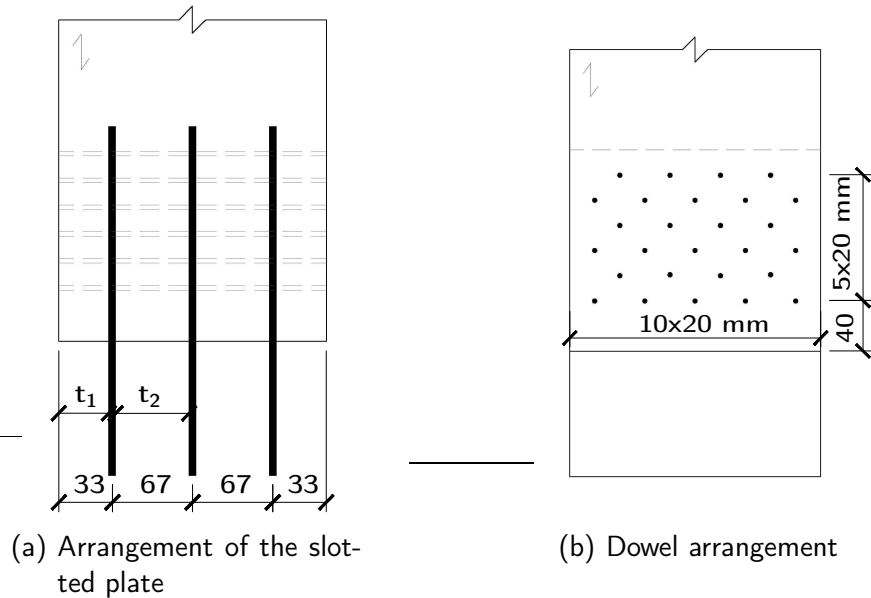


Figure 3.10: Regular BSB-connection with 3 slotted plates

and perpendicular to the lamellae (see Fig. 3.9).

The regular BSB-connection is displayed in Figure 3.10, it consists of 9 dowels in three rows. The regular connection got revised with different dowel arrangements and different distances of the slotted plates. Mischler [89] found out that the ratio of t_1/t_2 (see Fig. 3.10) should range between 1/2 to 2/3 for an optimized connection with two or more slotted plates. Furthermore an optimal slenderness is given for the thickness t_2 (see Fig. 3.10). The slenderness is defined as:

$$\lambda_{exist} = \frac{t_2}{d} \geq \lambda_{optimal} \quad (3.12)$$

with :

t_2 : embedding length of the dowel within the timber member 2 (see Fig. 3.10(a))

d : diameter of the bolt

Equation (3.12) is not given any attention to the steel grade of the dowel itself. Therefore a further equation is given to determine the optimal slenderness [89]:

$$\lambda_{optimal} \geq 1.4 \cdot \sqrt{\frac{8 \cdot M_{u,95}}{f_{h,05} \cdot d^3}} \quad (3.13)$$

with :

$M_{u,95}$: 95 % quantile of the yield moment

$f_{h,05}$: 5 % quantile of the embedded strength

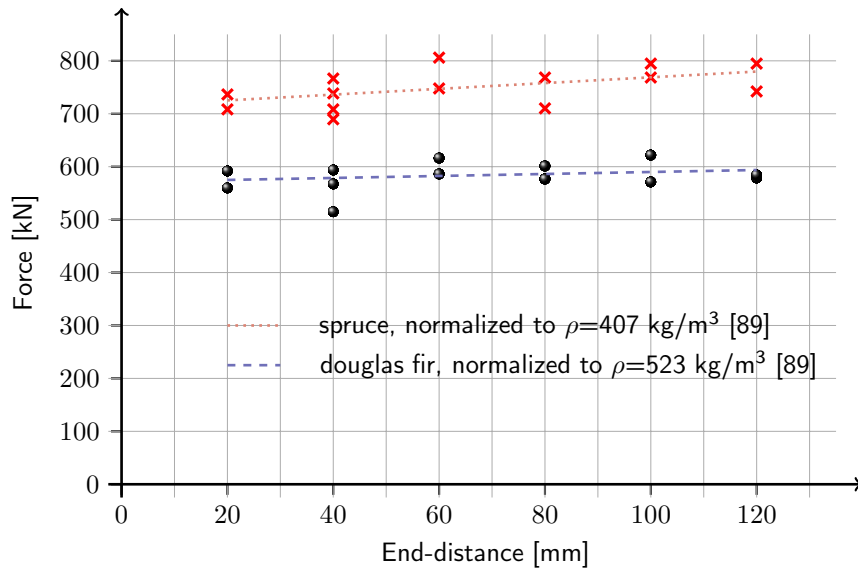


Figure 3.11: Influence of the end-distance ($a_{3,t}$) on the ultimate load [89]

Having the result from Equation (3.13) it is possible to determine the optimal cross-section with Equation (3.12).

It is shown that a connection likely fails if the slotted plate is perpendicular oriented to the lamellae (see Fig. 3.9). A dowel is embedded with the full length in a certain lamellae or in the intersection zone of two lamellae. Therefore the weakest lamellae are governing the failure [89]. The dowel permeates each lamella if the slotted plate is oriented parallel to the lamellae. Therefore it is possible that the lamination reduces the danger due to splitting. It has been shown that the load-carrying capacity decreases slightly for a rectangular orientation [89].

The investigation on the end-distance ($a_{3,t}$) showed no significant influence on the load-

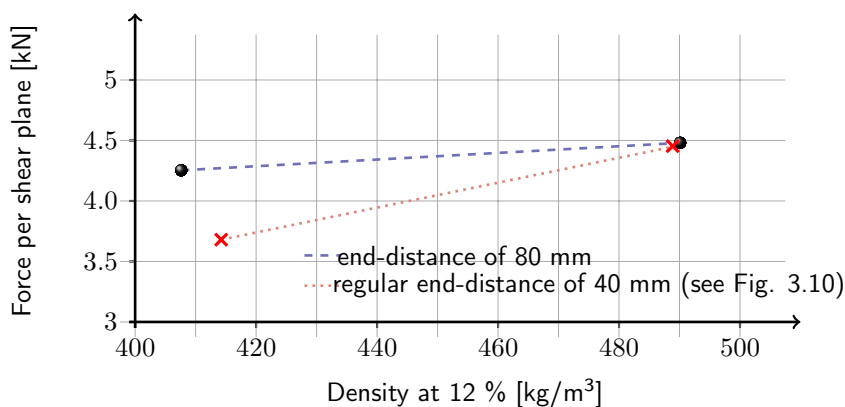


Figure 3.12: Influence of the density for certain end-distances [89]

carrying capacity of a BSB-connection (see Fig. 3.11). However, a difference has been observed with the perspective of the ductility. Since EN 1995-1-1 [109] stipulates a minimum end-distance $a_{3,t}$ of 80 mm, experiments were also performed with the claim to the end-distance. The risk of splitting was reduced by the rise of the end-distance, therefore the ductility was positively influenced (comp. Sec. 4.3.3).

BSB-connections accomplished in timber with a higher density have in general a higher load-carrying capacity at a certain displacement. It is assumed that timber consisting of a higher density has a higher resistance in shear and tension perpendicular to the grain [89]. The risk of splitting is reduced by a large end-distance of 80 mm ($12.7 \times d$), therefore the influence of a higher density is in this case less pronounced (see Fig. 3.12).

3.2.7 A. Jorissen (1998)

Jorissen [84] very intensively investigated unreinforced double shear timber to timber connections, accomplished with dowel type fasteners loaded parallel to the grain (see Fig. 3.13(b)). The focus was set to the strength of multiple fastener connections and consequently to resulting requirements of such alignments.

A load distribution model was developed for multiple fasteners connections to predict the load-carrying capacity and the related deformation characteristic. To gain knowledge about the influence of certain parameters within multiple fastener connections, experimental studies were conducted at the Delft University of Technology. The following parameters, among others were considered more closely.

- slenderness ratio
- end-distance
- hole clearance
- number of fasteners in a row
- density
- fastener diameter

Jorissen [84] developed λ -values based on Johansen's Yield Model to predict a ductile behavior of double shear timber to timber connections as well (comp. Eq. (3.14)). The minimum thickness for side (t_s) and middle members (t_m) (see Fig. 3.13(b)) can be found by:

$$\lambda = \frac{t_i}{d} > \begin{cases} 1,39 \cdot \sqrt{\frac{F_y}{f_h}}, & \text{for side members} \\ & \text{[84, table 2.3]} \\ 1,15 \cdot \sqrt{\frac{F_y}{f_h}}, & \text{for middle members} \\ & \text{[84, table 2.3]} \end{cases} \quad (3.14)$$

with :

f_y : yield strength of the dowel type fastener
in bending

f_h : embedment strength

With regard to the material properties of the specimens of the experiments, according to [84], a timber thickness for the side member of 59 mm and for the middle member of 48 mm are required in order to achieve a ductile behavior. Figure 3.13(a) shows the influence of the slenderness ratio λ for a multiple dowel connection of three dowels parallel to the grain. The connection with the largest widths reaches the highest strength and deformability. Furthermore the direct effect of the in-between distance a_1 is also evident with regard to the connection strength. The risk of splitting is reduced with a larger in-between distance. A regression analysis was conducted based on the experiments and the simulations of the load-carrying capacity. The simplified design rule given by Jorissen [84] is given by:

$$F_{multiple} = 0.52 \cdot n^{0.90} \cdot \left(\frac{a_1}{d}\right)^{0.25} \cdot F_{single} \approx n^{0.90} \cdot \sqrt[4]{\frac{a_1}{13 \cdot d}} \cdot F_{single} \quad (3.15)$$

This rule is given in the current design code for the effective number of fasteners in a row [109].

Investigations based on fracture mechanics showed, that tension perpendicular to the grain is the driving parameter for a failure. Although the experiments showed that an end-distance of $5 \times d$ compared to $7 \times d$ has almost no influence on the load-carrying capacity [84], the

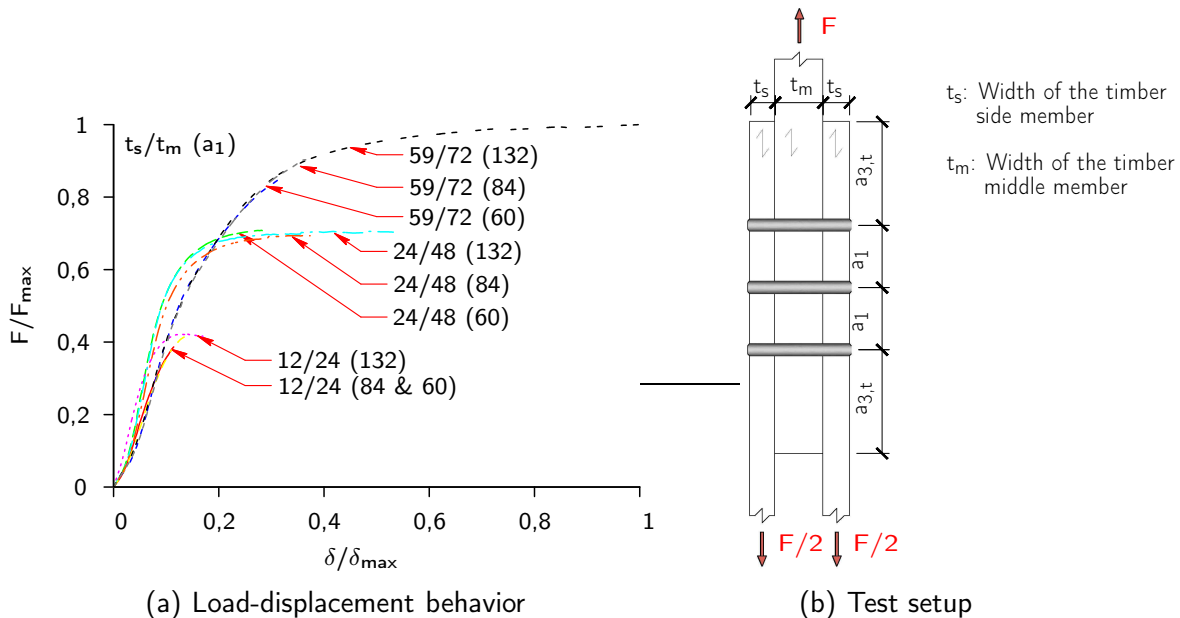


Figure 3.13: Load-slip behavior of 3 dowels depending on the distance a_1 and the thickness of the timber members

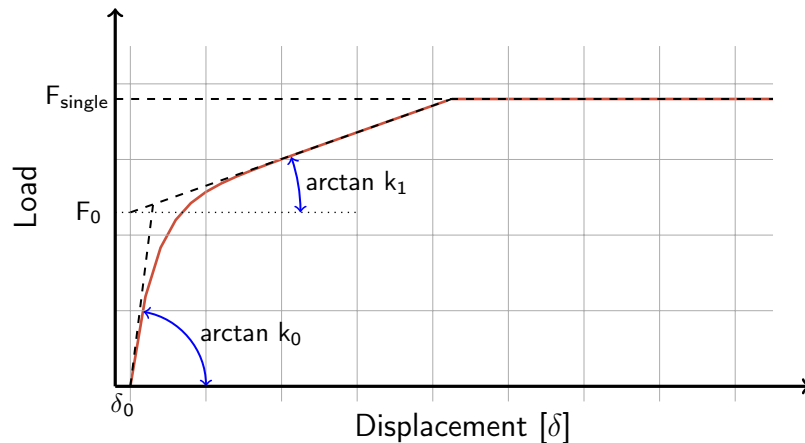


Figure 3.14: Approximation of the load-displacement behavior [84]

investigations based on fracture mechanics pointed to a possible failure, especially for long term loadings. The density is in general strongly correlated to the embedded strength and the fracture energy [84]. Thus connections accomplished in timber with a lower density have a lower fracture energy and tend therefore to splitting. This was not always the case in the performed experiments, which may be explained by the variation of the density within a full size structural element. Hence the used end-distance of $7 \times d$ in EN 1995-1-1 [109] is appropriate.

A slip can almost not be prevented within a connection due to the fabrication process. Jorissen [84] extended the load-displacement approximation given by Blaß [6] for nails by an initial slip (δ_0) (see Fig. 3.14). Considering the initial slip Equation (3.10) turns to:

$$F = (F_0 + k_1 \cdot (\delta - \delta_0)) \cdot \left(1 - e^{\frac{-k_0 \cdot (\delta - \delta_0)}{F_0}}\right) \leq F_{single} \quad (3.16)$$

Since all of the fasteners within a connection have a different initial slip, the load of each fastener is randomly distributed, whereas in connections with almost no slip (e.g. bolts in steel structures) the first and last connector transfers the maximum load. Jorissen [84] conducted simulations assuming different slips of each fastener within a connection accomplished with four fasteners. It was found that the hole tolerance has no influence on the load-carrying capacity if the displacement at failure is larger than 2,1 mm and smaller than 5,6 mm [84].

3.2.8 I. Bejtka (2005)

Bejtka [82] gathered knowledge in optimizing and in accomplishing connections with fully threaded screws. Fully threaded screws are a rather new product with increasing popularity. The application possibilities of this dowel type fastener are widely spread. Self tapping fully threaded screws are mainly used as a connector transferring normal forces. One possible

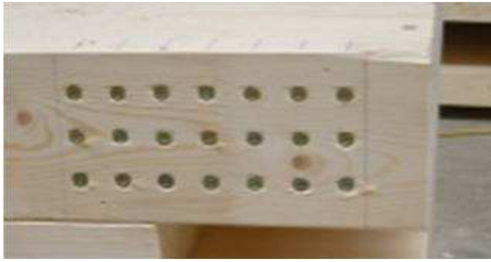


Figure 3.15: Strengthened support situation with fully threaded screws (©WIEHAG)

application is the strengthening of highly utilized support situations perpendicular to the grain (see Fig. 3.15). The connector is in this case loaded in compression embedded within the timber. Investigations have been conducted to obtain knowledge about the reinforcing method and the buckling behavior of the screws. The study has shown that a significant increase of the load-carrying capacity can be achieved with this type of reinforcing [82]. A common failure mode in connections accomplished with dowels or bolts is the splitting

of the timber in grain direction. A failure caused by splitting depends on the end and in-between distances and on the timber density as already mentioned. A splitting failure is due to the brittle connection behavior undesired, and has to be avoided. Bejtka [82] carried out experimental and numerical investigations of a targeted application of fully threaded screws to reduce the risk of splitting within a connection. The test series was divided into reinforced and unreinforced flitch plate connections. All of the specimens had a width of 200 mm with a 10 mm thick inserted steel plate. The used diameter of the used dowels were 16 mm and 24 mm with a tensile strength of 360 N/mm² and 800 N/mm². Several positionings of the reinforcing screws were tested.

Figure 3.16 shows the influence of the reinforcing method to the load-carrying capacity and

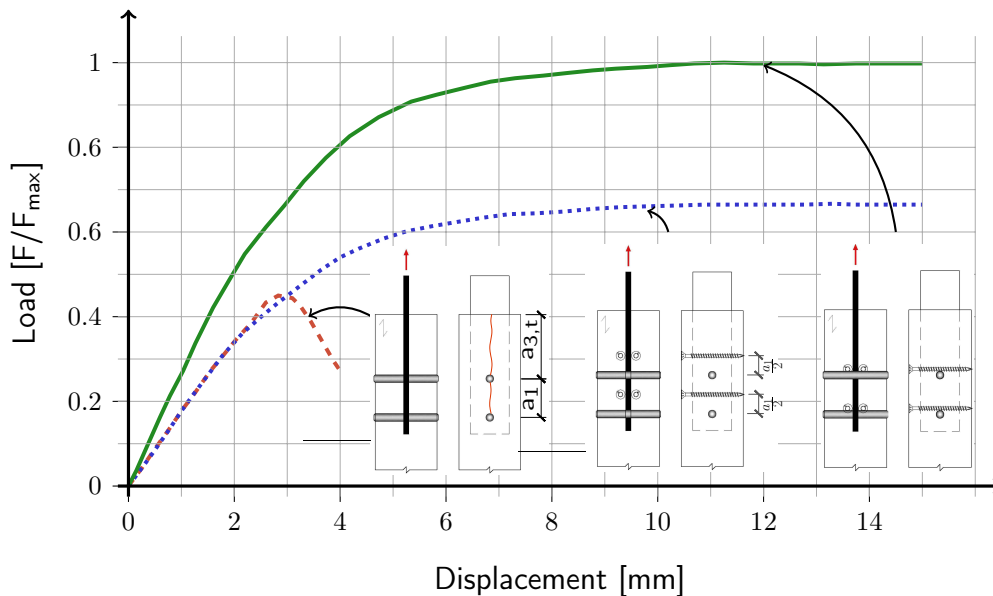


Figure 3.16: Various load-displacement behaviors of unreinforced and differently reinforced dowel type connections [9]

the deformability. The reinforcing has an influence on both parameters. The deformability and therefore the ductile behavior increases significantly due to reinforcing with full threaded screws (see Fig. 3.16). Furthermore, if the reinforcing is attached directly on the surface of the dowel, a considerable increase of the load-carrying capacity can be achieved. The screw is acting as a further support of the dowel and increases the load-carrying capacity in this case [82]. The experiments were carried out upto a deformation of 15 mm was achieved (comp. EN 26891 [110]).

The effective number of fasteners in grain direction may be set as the actual number of fasteners. This is only allowed if a suitable prevention of the risk of splitting is guaranteed.

3.3 Tube connections

3.3.1 Introduction

Connections accomplished with tubes are a rather new and unknown type of fastening. The timber members are pre-drilled with an oversized hole within the installing process. The pipe, manufactured from mild steel, is fitted in with two washers on each side. The tube is expanded in a further step, so that the tube fits with no clearance in the borehole.

The well known Het Bosch restaurant in Amsterdam is one of the first buildings designed and constructed with tube connections by Lignostone[®] (see Fig. 3.17).



Figure 3.17: Construction of the Het Bosch Restaurant, Amsterdam (©A.J.M. Leijten)

3.3.2 A.J.M. Leijten (1998)

Leijten [88] carried out research on this type of connection with various experiments. The shear planes are typically reinforced with densified veneer wood (dvw) to prevent premature splitting of the timber (see Fig. 3.18). The main focus was also set to the three major requirements in view of the limit state: strength, stiffness and ductility [88]; among others,

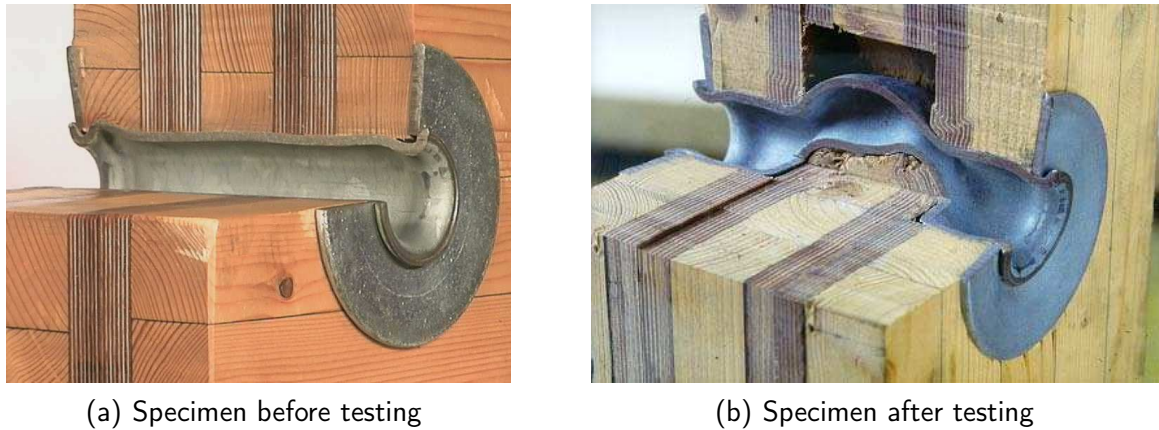


Figure 3.18: Reinforced tube connection (©A.J.M. Leijten)

the end- and in-between spacing of the fasteners are considered closer. Experiments were performed parallel to the grain in tension and four point bending tests. Furthermore, tests were obtained on knee joints, which describes a post-bar connection loaded in bending. In addition, cyclic loaded experiments were conducted.

The raw material of the tubes were ordinary galvanized butt-welded gas pipes with a diameter

of 18 mm or 35 mm. The driving parameter to select regular gas pipes was the appropriate ratio between the wall thickness and the diameter. The mean density of the used timber was 436 kg/m^3 with a standard deviation of 42.8 kg/m^3 . The size of the timber members for the experiments in tension parallel to the grain consisted of a width of 100 mm with a thickness of the side members of 30 mm and 50 mm for the middle section respectively (see Fig. 3.19). The thickness of the reinforcing dvw was 8 mm, 10 mm and 12 mm for the 18 mm diameter tubes, and 12 mm and 18 mm for the 35 mm diameter tube experiments. The end-distance in grain direction varied from $2 \times d$, $3.5 \times d$ to $5 \times d$.

The experiments were conducted following the test procedure given in EN 26891 [110]. Therefore, the experiments were terminated by a achieving a displacement of 15 mm, unfortunately (see. App. B.5.1).

Three timber members, with a width of 400 mm and a thickness of 70 mm for the middle member and 45 mm for the side members, were connected

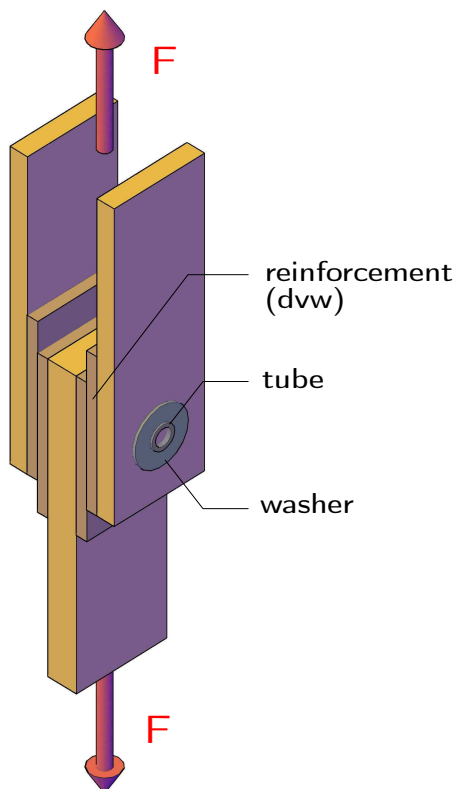


Figure 3.19: Specimen parallel to the grain [88]

with two tube connections for the four point bending experiments. The tubes were either placed on the center line parallel to the grain or diagonally displaced to transfer the applied bending moment.

The experiments in tension, the four point bending tests and the knee joint test showed, that the load-displacement behavior is almost independent of the loading angle to the direction of the grain.

Within the developed design guidelines Leijten [88] it assumed, that a displacement up to 25 mm can be achieved. Table 3.3 gives the suggested minimum for the design of tube connections ascertained within the test program.

Table 3.3: Minimum end and edge distances for tube connections [88]

Expanded tube \emptyset [mm]	loaded end $a_{3,t}$ [mm]	unloaded end $a_{3,c}$ [mm]	loaded edge $a_{4,t}$ [mm]	unloaded edge $a_{3,d}$ [mm]	dvw thickness [mm]
18	$3.5 \times d = 63$	$2.0 \times d = 36$	$3.5 \times d = 63$	$3.0 \times d = 54$	12
22	$3.5 \times d = 77$	$2.0 \times d = 44$	$3.5 \times d = 77$	$3.0 \times d = 66$	14
28	$3.5 \times d = 98$	$2.0 \times d = 56$	$3.5 \times d = 98$	$3.0 \times d = 84$	16
35	$3.5 \times d = 123$	$2.0 \times d = 70$	$3.5 \times d = 123$	$2.5 \times d = 88$	18

3.4 Split rings

3.4.1 Introduction

Connection accomplished with split rings are only able to transfer shear forces. All of the connectors need to be designed with an additional tension force carrying fastener, to take care of the moment due to the load transfer. This can be achieved by a bolt or nowadays with fully threaded screws as well. The additional fastener ensures, that no opening of the connection occurs under loading. The minimum tension force of the additional fastener should be at least 25 % of the bearing resistance of the split ring connection [99]. The classification of the different type of connector is based on the mounting of the fastener. There are in general three different types on the market (see Fig. 3.20):

- pressed-countersunk split rings (type C10 & Typ C11)
- countersunk split rings (type A1 & type B1)
- Pressed split rings (type C1 - type C5), also known as tooth plate

The countersunk dowels type A1 and B1 are placed in a matching prefabricated milling groove. The group of pressed split rings are pressed together. This can either be accom-

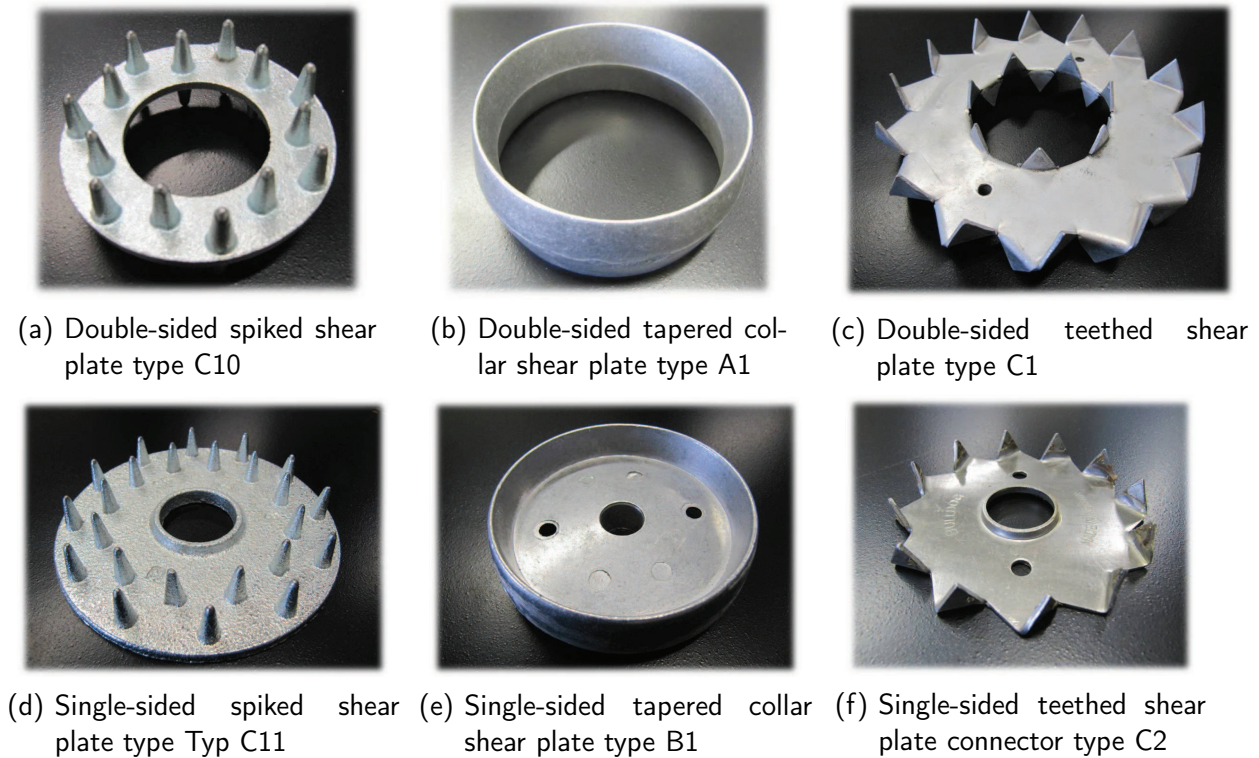


Figure 3.20: Different types of split ring connectors

plished with the inserted bolt, for small diameters, or with hydraulic presses. The third type of connector is a combination of both systems. A groove is prepared which fits to the ground plate of the connector. The spikes are then pressed into the timber to obtain a locking of both elements.

3.4.2 Investigations at the Universität Karlsruhe (1997)

Blaß et al. [11] conducted a large number of experiments with the focus on multiple connections with split rings and on the end- and in-between distances of split rings, further information is given in App. B.5.2. Two different types of split rings were examined. Double tapered collar shear plate connectors (type A1, see Fig. 3.20(b)) within the test series A, and double spike shear plate connectors (type C10, see Fig. 3.20(a)) within the test series D. Several different companies were charged to manufacture the test specimens in order to get information about the influence of the production accuracy.

Experiments loaded in compression were conducted to gain knowledge about the load-displacement behavior of a single fastener (see Fig. 3.21). Experiments with the view on the influence of two or more fasteners in grain direction were performed in tension. No information could be gained from the experiments loaded in tension since the test failed in an unforeseen manner. The design method at that time appeared as unsafe due to the insufficient attention to the net cross-section of the side members.

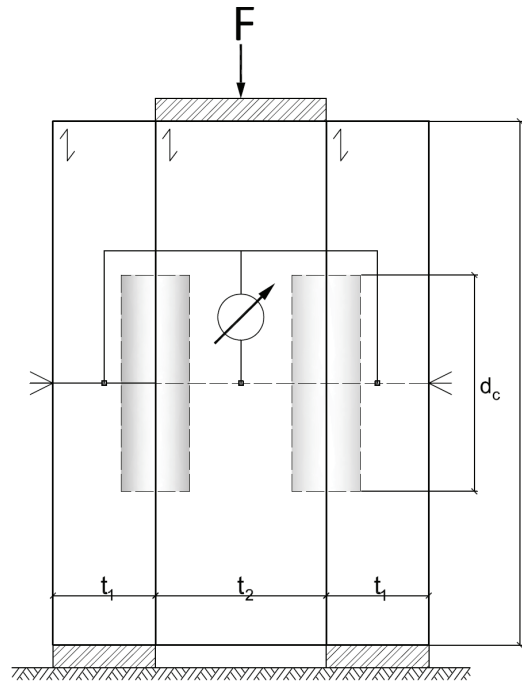


Figure 3.21: Test setup for the experiments loaded in compression [11]

The influence of the timber thickness was a further issue of the investigations on the experiments. Therefore, two different timber thicknesses were used. The series N was performed with a timber thickness according to the then valid standard DIN 1052:1988 [96]. The series M was accomplished with a reduced timber thickness.

The study has shown that the timber thickness has a direct influence on the load-carrying capacity. The mean value of the load-carrying capacity of the test series M was less compared to the test series N.

The developed design equations for the design of double spike shear plate connectors (type C10) is implemented at the current design standard [109].

$$F_{v,Rk} = 25 \cdot k_{\rho} \cdot k_{a_e} \cdot k_t \cdot d_c^{1,5} (N) \quad (3.17)$$

with :

d : diameter of the split ring

k_{ρ} : parameters to consider the timber density

k_{a_e} : parameters to consider the end distance

k_t : parameters to consider the embedded depth

In order to gain more information about multiple connections accomplished with split rings it was proposed to conduct further experiments.

3.4.3 Investigations at the Ruhr-Universität Bochum

Reyer et al. [64] conducted experiments with the view on the shear force transmission of the thread of a securing bolt or a threaded rod within a split ring connection. It has been established that the associated bolts or threaded rods have always a larger characteristic load-carrying capacity compared to the split ring connector [96]. Thus it was verified whether a uneconomic decrease of the load-carrying capacity of 50 % is necessary [64].

Experiments were conducted with single-sided split rings. Two types were examined, a shear plate connector with teeth (Typ C2, see Figure 3.20(f)) and with spikes (Typ C11, vgl. Figure 3.20(d)). All of the specimens met the requirements of the then valid standard [96] with different diameters. The experiments were performed either as timber to timber connections (see Fig. 3.22(a)) or steel to timber connections (see Fig. 3.22(b)).

The studies showed that there is in general no significant difference in the load-carrying capacity of connections accomplished with bolts compared to threaded rods, if those belong to the same steel grade. A maximum permitted load was defined by the authors as the minimum of one third of the maximum load achieved in the experiments or the load at a displacement of 1,5 mm. Indeed a decrease of the defined permitted load compared to the values given in [96] could be ascertained (see Tab. 3.4). The ratio of the permitted load to the load given in [96] decreases with an increase of the diameter of the split ring.

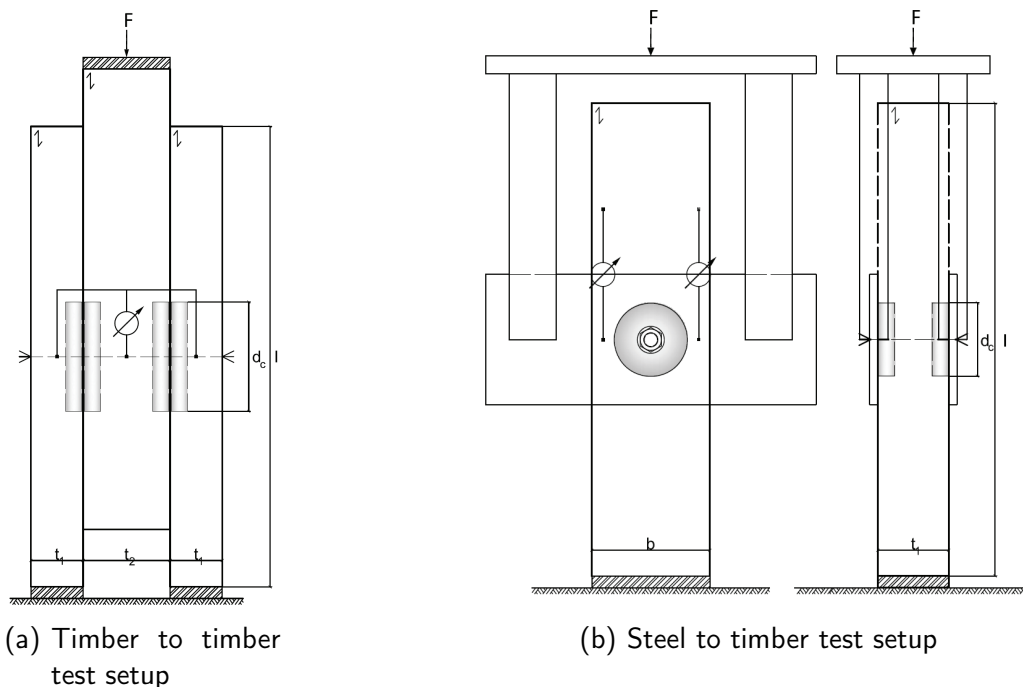


Figure 3.22: Test setups of the two different experiments conducted at the Ruhr-Universität Bochum [64]

Table 3.4: Decrease of the load given in [96] compared with the permitted load given in [64]

	type	
	C2	C11
timber to timber connection	59.5 %	44.6 %
steel to timber connection	94.5 %	64.5 %

3.5 Nail plates

3.5.1 Introduction

Nail plate connectors are mainly manufactured from a galvanized sheet with a thickness of about 0.9 mm to 2.5 mm. The nails are punched and bent under an angle of 90 degrees. The connectors are mainly used in prefabricated girders for the roofing of supermarkets, barns, hall structures and residential buildings (see Fig. 3.23). A further reasonable application method is as falsework of a concrete frame work.



(a) Nail plate connection



(b) Girder accomplished with nail plates

Figure 3.23: Typical structure accomplished with nail plates

3.5.2 Kevarinmaki

The experimental results were gained from investigations conducted by Kevarinmaki [85]. Nail plates were attached on the front and back of the two connected timber elements (see Fig. 3.24). Three different types of nail plates were provided by Mitek Finland Oy to perform experiments. The nail plates differed in the geometrical properties and thickness of the steel

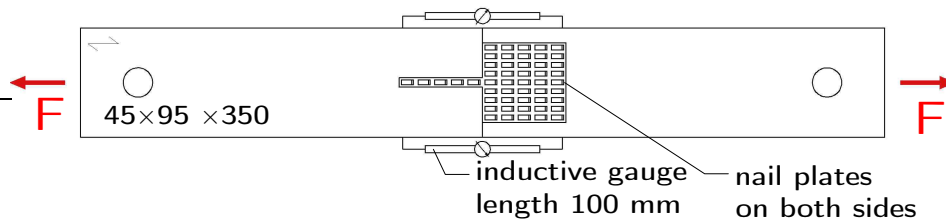


Figure 3.24: Specimen for the experiments on nail plates (horizontally displayed)

sheet (see Fig. 3.25).

Different dimensions of the nail plates were chosen to perform the experiments. Hence the size of the nail plate type Fix was chosen to 65 mm \times 200 mm, for type TOP to 91 mm \times 180 mm and for type W to 60 mm \times 150 mm.

Experiments were not only conducted in grain direction. Tests were also performed with different angles of the fastener to the grain direction to gain knowledge about the influence of the main fastener direction to the grain direction.

type	t_t [mm]	w_t [mm]	h_t [mm]	f_y [$\frac{N}{mm^2}$]	f_u [$\frac{N}{mm^2}$]
Fix	1,3	3,0	13	360	420
TOP 91	1,3	2,8	14	360	420
W	1,75	3,667	14,1	400	500

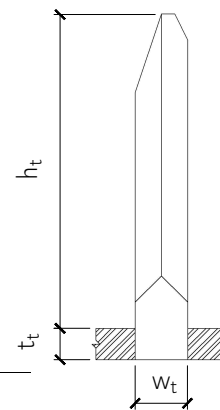


Figure 3.25: Different geometrical properties of the various nail plates

3.6 Summary

Studies on several different types of fasteners are introduced and discussed within this Chapter. Most of the presented fasteners show in general a ductile behavior with a pronounced behavior for different fasteners. For instance, if the risk of splitting is reduced within a doweled connection, which can be accomplished by either increasing the end- and in between distance or by reinforcing the single fasteners, the ductile behavior of dowel type fasteners is significantly increased.

To introduce plastic hinges within timber structures it is necessary to establish tangible indicators with view on ductility. Therefore investigations on a standardized evaluation of

ductility are given in Chapter 4. The introduced fasteners are evaluated based on the assessed criteria to classify the different types of fasteners.

4 Ductile behavior of fasteners in timber structures

4.1 General

The currently valid design standards (e.g. [109] and [114]) consider only the linear elastic behavior of fasteners in timber structures. The elastic stiffness for the serviceability limit state is given in the code as K_{ser} , whereas the elastic stiffness in the ultimate limit state (K_u) is given as two thirds of the value given for the serviceability limit state in EN 1995-1-1 [109, 7.1] (see Fig. 4.1). In order to introduce the consideration of the non-linear behavior [109, 5.1 (2)] it is indispensable to evaluate the different types of fasteners. Therefore, it is necessary to classify the different types of fasteners in view of their plastic behavior.

As a basis it is important to establish uniform rules which describe the procedure to evaluate fasteners in view of the non-linear behavior. Different methods to determine the plastic behavior are currently used to determine the plastic behavior. The available methods are described and discussed. Certain procedures are selected based on the consequences of the discussion to determine the ductile behavior.

The findings are fundamentals to evaluate and classify different types of fasteners in further steps.

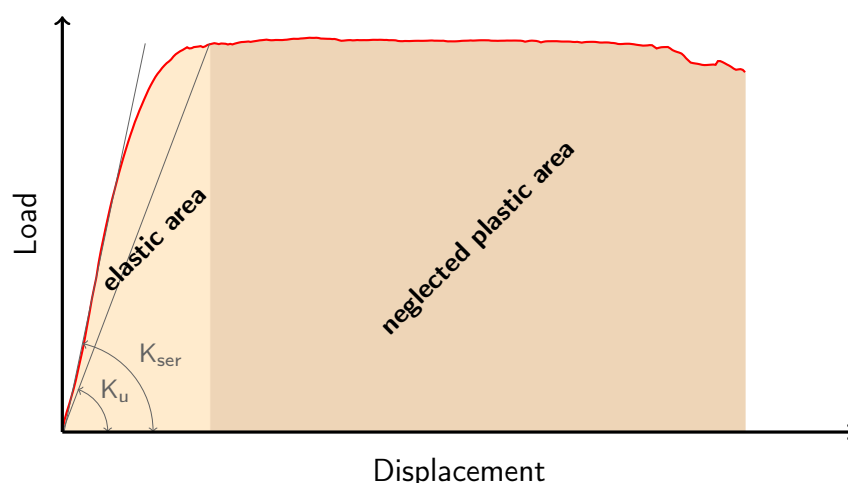


Figure 4.1: Typical load-displacement behavior of a reinforced dowel connection

4.2 Evaluation of the ductility

4.2.1 Parameters

4.2.1.1 Definitions

A uniform declaration is only possible, if certain parameters of the ductile behavior are clearly defined (see Fig. 4.2).

These are:

- u_y = displacement at yielding
- u_u = displacement at ultimate load
- u_f = displacement at failure
- K_0 = initial stiffness

The maximum possible displacement (u_f) is found by definition at failure of a connection. A failure is clearly defined in [102, 110, 114]. Hence, not only an obvious rupture is defined as a failure. Failure is also achieved, either at a load decrease to 80 % of the ultimate load or at a defined displacement. EN 26891 [110] suggests a maximum displacement of 15 mm to define a failure, whereas EN 12512 [102] proposes a maximum displacement of 30 mm. The displacement at yielding (u_y) with the corresponding load at yielding (F_y) describes the point where the elastic behavior passes into a plastic behavior. Irreversible deformations occur in the plastic range. These deformations increase to a higher degree with a slight increase of the load compared to the elastic deformation.

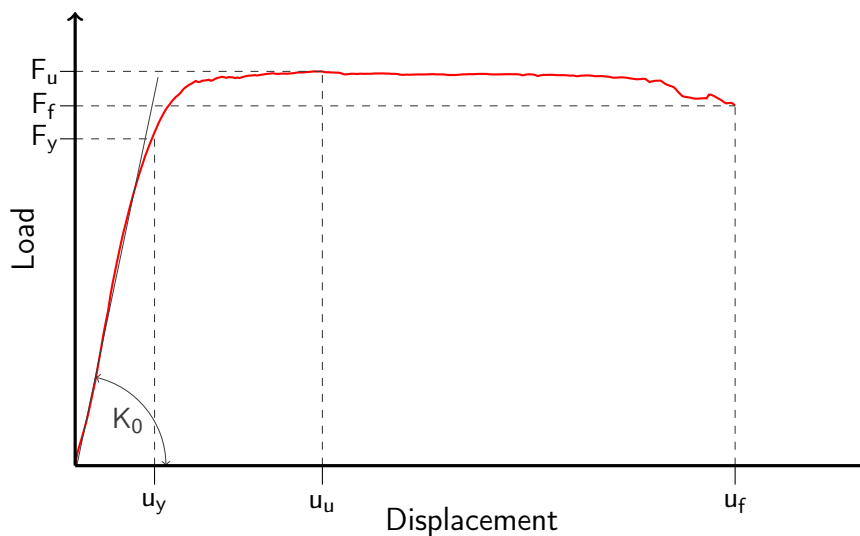
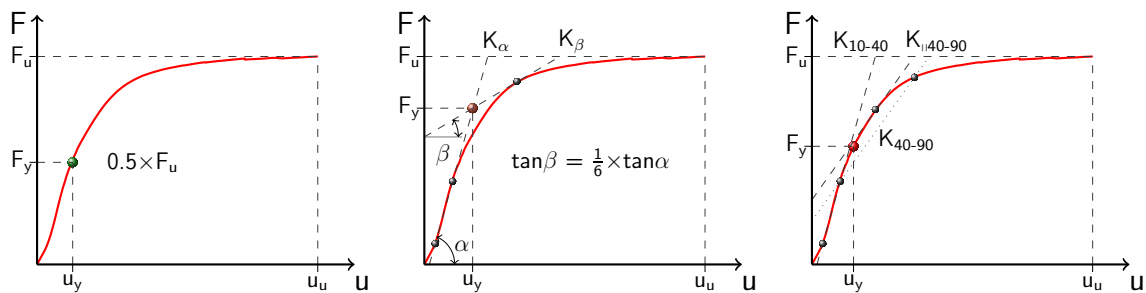


Figure 4.2: Definition of the parameters for characterizing a non-linear behavior

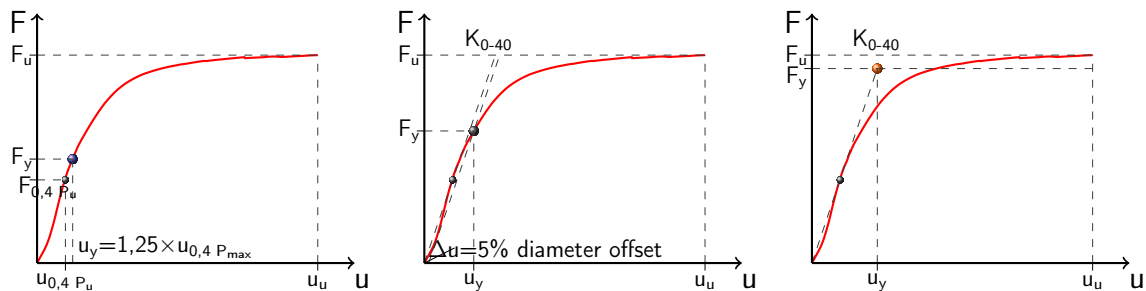
The ultimate load (F_u) describes the maximum load achieved within an experiment. The associated displacement is given as the displacement at ultimate load (u_u , see Fig. 4.2).

4.2.1.2 Displacement at yielding

The deformation at yielding is an important parameter within the consideration of the plasticity. It separates the elastic behavior and the plastic behavior. There are several different definitions available which are summarized in Muñoz et al. [57]. Figure 4.3 shows the dif-



(a) Karacabeyli and Ceccotti [43] (b) EN 12512 [102] & SIA 265:2012 [114] (c) Yasumura and Kawai [80]



(d) CSIRO [19] (e) 5% diameter offset AF & PA [1] (f) EEEP [14]

Figure 4.3: Most common definitions of the point of yielding, see [57]

ferent definitions to determine the point of yielding. According to Figure 4.3(a) Karacabeyli and Ceccotti [43] describe the point of yielding as the displacement at 50 % of the maximum load (F_u), whereas EN 12512 [102] and SIA 265:2012 [114] define the point of yielding as the intersection point of the initial stiffness, determined as the secant at 10 % and 40 % of the maximum load, and a tangent of one sixth of the initial stiffness explained (comp. Figure 4.3(b)). Yasumura and Kawai [80] assume the point of yielding following the method described by EN 12512 [102] & SIA 265:2012 [114]. The main difference lies in the second secant. Within this consideration the stiffness of the second secant is defined between 40 % and 90 % of the maximum load. The intersection point is horizontally projected to the

graph to gain a point on the actual load-displacement behavior (comp. Figure 4.3(c)). The Commonwealth Scientific and Industrial Research Organization (CSIRO) [19] assumes the point of yielding at a displacement of 1.25 times the displacement at 40 % of the ultimate load (comp. Figure 4.3(d)). A further definition is given by the American National Standards Institute as a 5 % offset by the fastener diameter of the initial stiffness [1], measured from zero to 40 % of the ultimate load (comp. Figure 4.3(e)). The equivalent energy elastic-plastic curve (EEEP) defines the point of yielding by an artificial graph. The quintessence of this method is to define a linear elastic-plastic graph with an initial stiffness, measured from the point of zero to 40 % of the maximum load, which inhabits the same area as the discussed graph. The point from the elastic behavior to the plastic range is defined as the point of yielding (comp. Figure 4.3(f)).

Discussion of the different methods

There are several requirements set on the point of yielding. First and foremost to separate rather brittle behaviors from ductile behaviors. Strictly spoken, a point of yielding should only be achieved for connections with a certain ductile behavior, but no point of yielding should be given for brittle behaviors.

Some of the methods give a point of yielding and therefore a displacement at yielding although the behavior is rather brittle. Since Karacabeyli and Ceccotti [43] set the point of yielding to 50% of the ultimate load and CSIRO to $1.2 \times u_{0.4 P_{max}}$ a displacement of yielding is

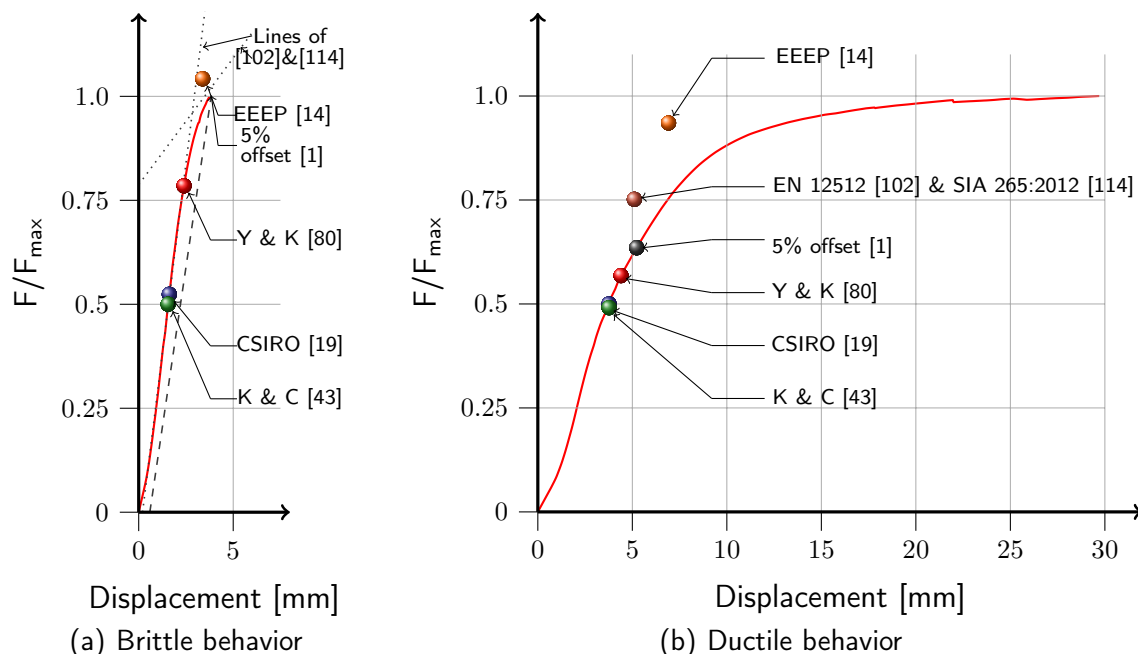


Figure 4.4: Illustration of the different methods to evaluate the point of yielding

found for every load displacement behavior regardless of the actual connection behavior (see Fig. 4.4(a)). Yasumura and Kawai [80] suggest to define the point of yielding as an intersection point of the initial slope and a tangent with a slope of a secant passing 40% and 90% of F_u .

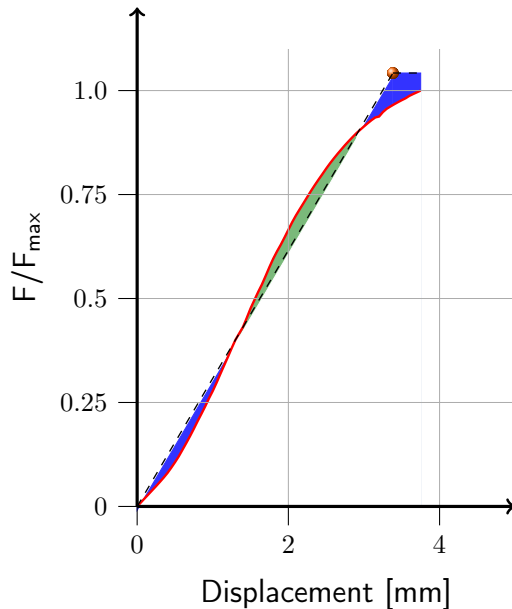


Figure 4.5: Increase of the ultimate load within the EEEP method

As shown in Figure 4.5, the areas above and underneath the actual graph to the EEEP graph need to be equal and therefore the plastic range rises to a higher value than the actual maximal load.

On the other hand, the method of a 5% offset achieves a displacement at yielding only if a certain, from the initial elastic stiffness differing, displacement occurs.

No yield displacement could be defined based on the method of EN 12512 [102] & SIA 265:2012 [114] since the tangent stiffness strictly depends on the initial stiffness of the connection itself (see Fig. 4.4). Therefore it was not possible to apply a tangent to connections with a rather brittle behavior (see Fig. 4.4(a)). A similar method to [102] & [114] is given by the European Convention for Constructional Steelwork [77]. The difference is in the determination of the second secant, which is defined as one tenth of the initial stiffness. This leads to a slightly higher force at yielding compared to EN 12512 [102] & SIA 265:2012 [114] with an associated larger displacement at yielding.

Given the previous discussion with a succeeding of some methods, it seems reasonable to use methods which find a displacement at yielding only for ductile connections. As a consequence the following methods are used to determine the point of yielding in the further investigations.

- EN 12512 [102] & SIA 265:2012 [114]
- 5% diameter offset [1]
- EEEP [14]

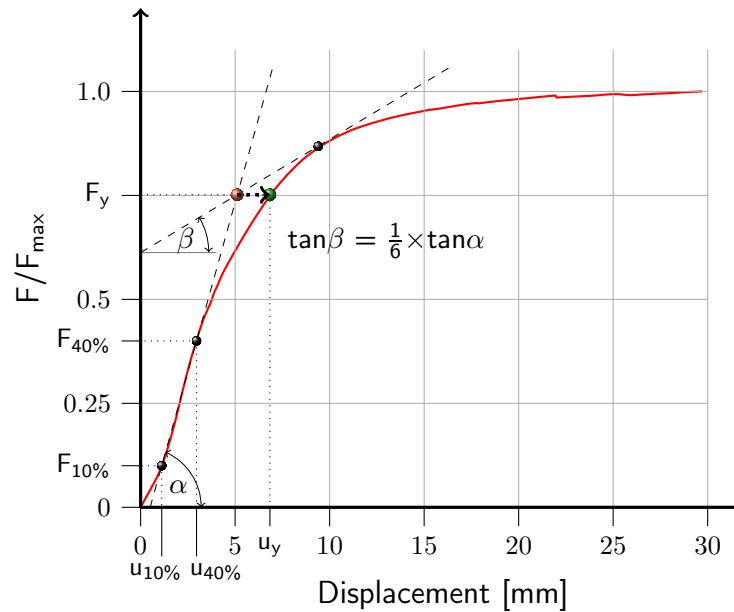


Figure 4.6: Modified method based on EN 12512 [102] to determine the displacement at yielding

However, the method based on EN 12512 [102] & SIA 265:2012 [114] was modified according to an approach given in Yasumura and Kawai [80]. Within the procedure, given by [102] & [114], the actual displacement at yielding is found at the intersection point of the initial stiffness and a tangent with a slope of one sixth of the initial stiffness as described previously. Hence, the displacement at yielding is not directly linked to the actual behavior, or in other words, it is given as the vertical transformation to the graph. Therefore, the given point does not truly reflect a point on the actual graph. The element introduced by Yasumura and Kawai [80] projects the point of yielding horizontally to the graph (see Fig. 4.3(c)). Thus the given point of yielding reflects an actual point on the examined behavior.

Therefore, a further method (EN 12512_{mod}) to describe the point of yielding is introduced for the ductility studies on connections in timber structures. Within this study the point of yielding is transformed horizontally to the actual graph to gain a point which is linked to the real behavior (see Fig. 4.6).

4.2.2 Appraisal of the ductility

Within the consideration of the ductility, it is indispensable to classify different types of fasteners in view of the ductile behavior. The reference value is in general set to the ductility ratio D_i . The ductility ratio is defined as the proportion of the displacement at failure (u_f) to the displacement at yielding (u_y) within EN 12512 [102] and SIA 265:2012 [114] (comp.

Eq. (4.1)).

$$D_f = \frac{u_f}{u_y} \quad (4.1)$$

This is one of the most common definitions of the ductility ratio.

Stehn and Björnfoot [72] introduce several other possibilities to evaluate the ductility ratio D_i . They are in general divided into two different groups. On one hand the relative values represented by Equation (4.1) to Equation (4.7)

$$D_u = \frac{u_u}{u_f} \quad (4.2) \quad D_{f/u} = \frac{u_f}{u_u} \quad (4.3) \quad C_f = \frac{u_f - u_y}{u_f} \quad (4.4)$$

$$C_u = \frac{u_u - u_y}{u_f} \quad (4.5) \quad D_{s/u} = \frac{K_0}{F_1} \cdot u_u \quad (4.6) \quad D_{s/f} = \frac{K_0}{F_1} \cdot u_f \quad (4.7)$$

$$F_1 = F_{max} \quad (0 \leq u \leq 5mm) \quad F_1 = F_{max} \quad (0 \leq u \leq 5mm)$$

and on the other hand the absolute values given by Equation (4.8) to Equation (4.10).

$$D_{uy} = u_u - u_y \quad (4.8) \quad D_{fy} = u_f - u_y \quad (4.9) \quad D_{fu} = u_f - u_u \quad (4.10)$$

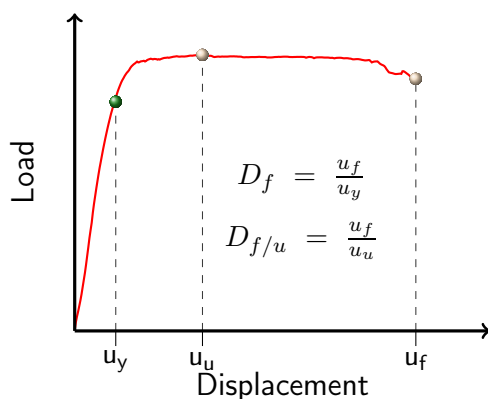
The certain variables are shown in Figure 4.2 on page 48.

Another possibility to determine the ductility ratio is based on energy. For this method the area underneath the load-displacement graph is calculated (comp. Eq. (4.11) and Eq. (4.12)).

$$E_u = \int_{u=0}^{u=u_u} f(F,u) du \quad (4.11) \quad E_f = \int_{u=0}^{u=u_f} f(F,u) du \quad (4.12)$$

Smith et al. [69] show an approach to classify fasteners in timber structures based on a ductility ratio D_i (see Fig. 4.7). The classification gives the possibility to group certain connections based on their load-displacement behavior.

A definition of the ductility ratios of different types of fasteners is already implemented in the Swiss timber code [114] (see Tab. 4.1). The partial factor may be reduced, if the duc-



Classification	Ductility ratio
Brittle	$D_i \leq 2$
Low ductility	$2 < D_i \leq 4$
Moderate ductility	$4 < D_i \leq 6$
High ductility	$D_i > 6$

with $i = u$ or f/u

Figure 4.7: Classification of fasteners with respect to the ductility ratio D_i by Smith et al. [69]

Table 4.1: Different ductility ratios of fasteners in timber structures according to SIA 265:2012 [114]

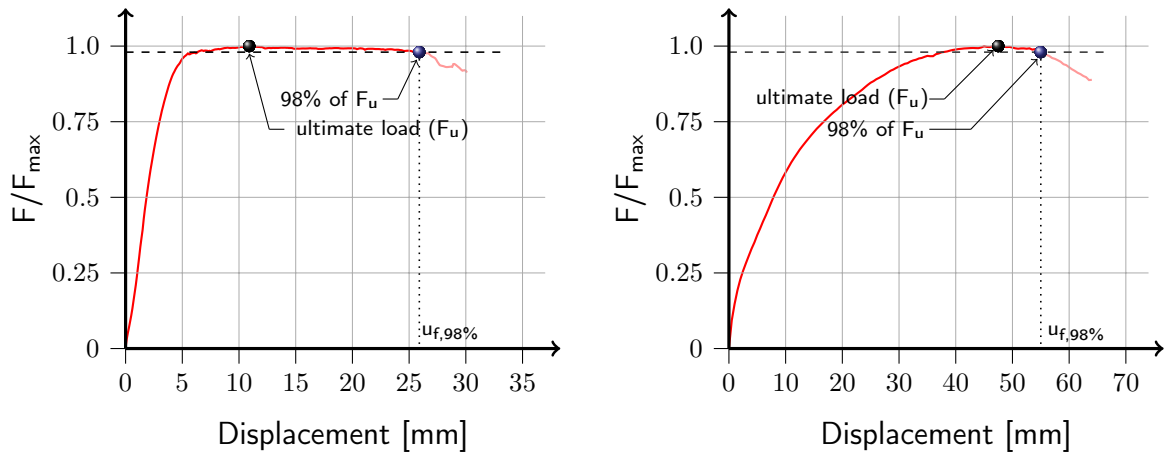
Type of connection	Ductility ratio according to Eq. (4.1)
Joints acting in contact, Shear connections with dowels or bolts with a smaller timber thickness compared to t_{req} , Connections with nails or screws with a length or a fastener length smaller than $9d$, Connections accomplished with nails, screws or bonded-in rods acting in tension, Split ring connections, Nail plates, Glued connections,	$1 < D < 2$
Shear connections with dowels or bolts if t_{req} is abided, Connections with nails or screws with a length or a fastener length greater than $9d$,	$D > 3$

tility ratio of the inserted fasteners is greater than three. Thereby, the higher redundancy of ductile fasteners compared to brittle fasteners is taken into account.

Discussion of the different appraisals

A fundamental question is given by the reference point. EN 12512 [102] & SIA 265:2012 [114] set the reference to the displacement at failure, whereas Smith et al. [69] consider the displacement at ultimate load to evaluate the ductility ratio. Nevertheless, Smith et al. [69] also mention, that the displacement at failure may be used to evaluate the ductility.

This results from the fact that a negative stiffness occurs if the ultimate load is reached before the termination of failure. This means that the connection is in an undefined condition if this behavior is pronounced. On the other hand, a large number of fasteners in timber structures show a distinctive plastic behavior of zero stiffness. A slight increase of the load carrying capacity, due to material inhomogeneities, lead to the declaration as ultimate load per definition. However, to avoid a neglect of the ductile behavior although the load is slightly increased the conditions of failure according to EN 12512 [102] & SIA 265:2012 [114] are tightened for the classification. The failure, and thus the reference displacement ($u_{f,98\%}$), is set to the point, when the load decreases to 98 % of the ultimate load (see Fig. 4.8). Therefore, an acceptable momentary load increase is possible without excluding ductile potential of the fastener. On the other hand, if a connection is losing stiffness the failure is



(a) Pronounced ductile behavior with a small single peak load

(b) Considerable load decrease after reaching ultimate load

Figure 4.8: Representation of the defined failure at 98% of the ultimate load

defined without a considerable gain of plastic deformation.

No attention is given to the shape of the graph when considering the energy based appraisal of the ductility ratio (comp. Eq. (4.11) & Eq. (4.12)). Therefore both, a rather brittle and a ductile behavior, gain the same assessment (see Fig. 4.9).

Jorissen and Fragiacomio [42] suggested a possibility to base the evaluation on the energy by the following equation:

This method divides the total energy (E_d) by the energy up to the point of yielding (E_{py}), which can be found by the methods described in Section 4.2. This method is therefore also placed into the group of relative values.

Another method is based on the initial stiffness of the connection (comp Eq. (4.6) & Eq. (4.7)). Within the consideration of the initial stiffness the ductility factor $D_{s/u}$ or $D_{s/f}$ describe

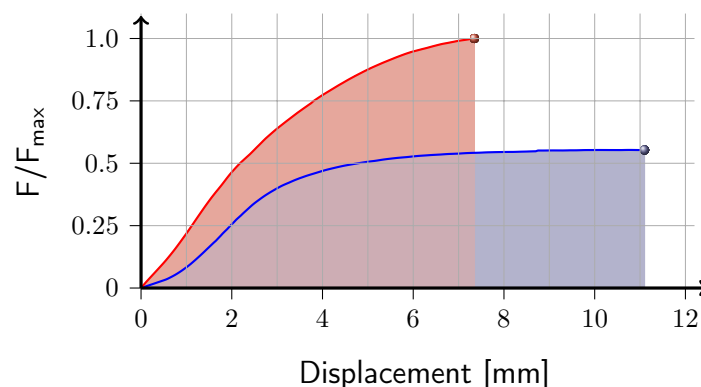


Figure 4.9: Different load-displacement behaviors with almost identical areas

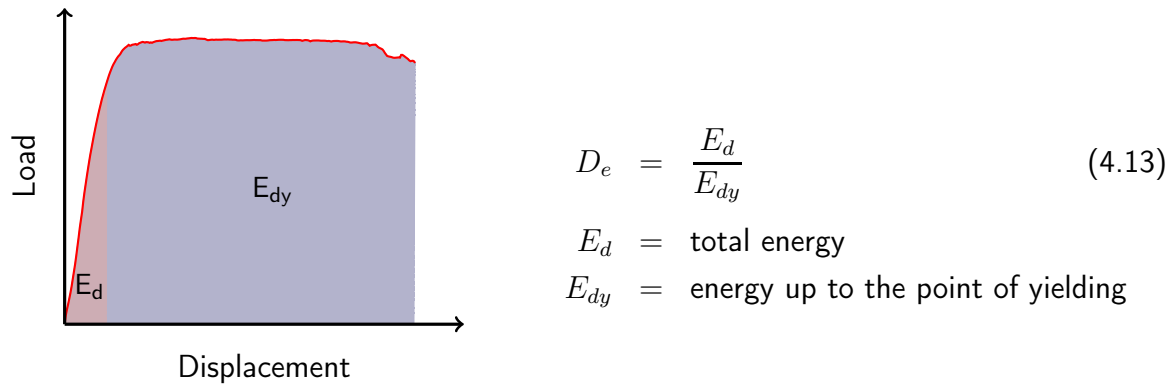


Figure 4.10: Possible approach to define ductility based on the energy by Jorissen and Fragiaco [42]

the ductility ratio as the ratio of the elastic stiffness to an artificial stiffness depending on the displacement at failure and the maximum load till a displacement at 5 mm (see Fig. 4.11). The elastic stiffness is determined from the point of zero to the point of yielding.

If a connection is still in the elastic stage after reaching a displacement of 5 mm, the method inevitably overestimates the ductility ratio due to the chosen force F_1 at a displacement at 5 mm (see Fig. 4.11). The chosen force F_1 gives a low artificial stiffness and therefore a rather high ductility ratio. A modified method could refer to the stiffness at failure (K_f) or with respect to the ultimate stiffness to K_u .

$$D_{u,f} = \frac{K_0}{F_{u,f}} \cdot u_f = \frac{K_0}{K_{u,f}} \quad (4.14)$$

Hence, the real behavior of the connection would be considered instead of an arbitrary based value.

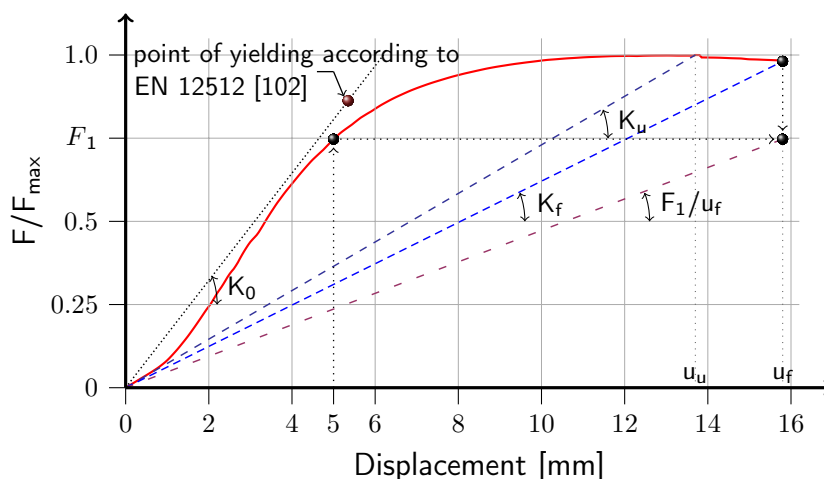


Figure 4.11: Representation of the stiffness based appraisal of the ductility

4.3 Evaluation of different types of fasteners

4.3.1 General

The load-displacement behavior of connections in timber structures differs significantly from each other (see Fig. 4.12). The various behaviors are based on the different load-carrying mechanism of fasteners. Nailed connections behave due to the large slenderness in general ductile, whereas glued connections due to the adhesive bond behave rather brittle (boundary graphs (g) and (a) in Figure 4.12). Connection accomplished with bolts are characterized

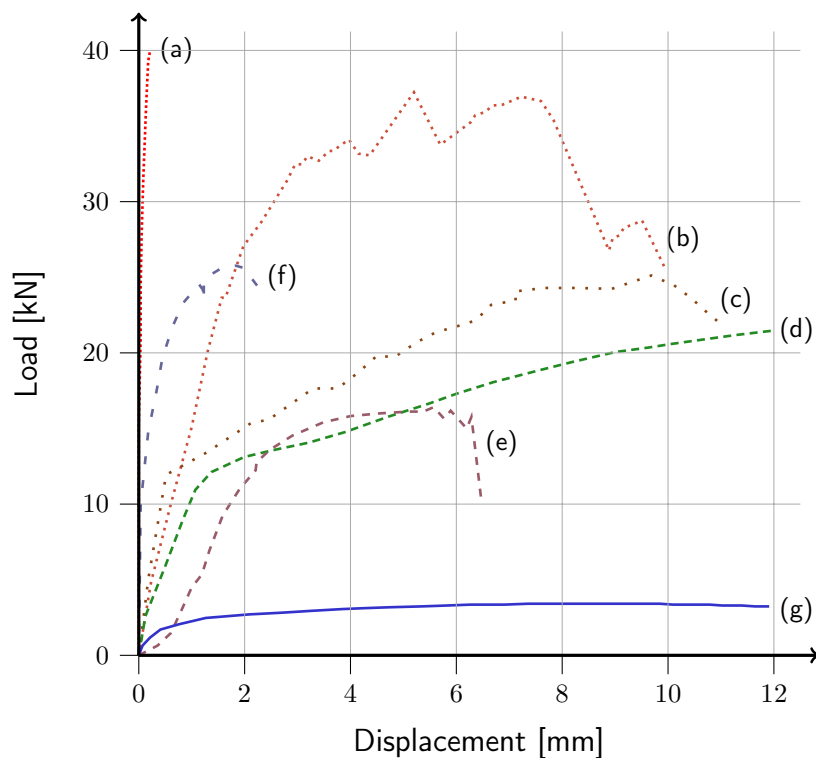


Figure 4.12: Experimental load-displacement studies parallel to the grain in tension: (a) bonded-in rods ($12,5 \cdot 10^3 \text{ mm}^2$), (b) single-sided tapered collar shear plate (100 mm), (c) double-sided teathed shear plate (62 mm), (d) dowel (\varnothing 14 mm), (e) bolt (\varnothing 14 mm), (f) nail plate (10^4 mm^2), (g) nails (\varnothing 4,4 mm) [62]

with a larger initial slip compared to dowels due to the larger tolerances (graph (e) compared to graph (d) in Figure 4.12).

This section analyzes various types of fasteners based on the indicated methods described in the previous section. Within the discussion it has been shown, that some methods are rather unsuitable in the application to classify the ductility of fasteners in timber structures. Therefore the focus to determine the point of yielding is set to the methods of:

(b) EN 12512 [102] (see Fig. 4.3(b))

(b_{mod}) Modified method of [102] as described in Section 4.2.1.2 (see Fig. 4.6)

(e) 5% diameter offset [1] (see Fig. 4.3(e))

(f) EEEP (Equivalent energy elastic-plastic curve) [14] (see Fig. 4.3(f))

Based on the discussion of the ductility ratio the investigations are set to the relative value D_f (comp. Eq. (4.1)), the absolute value D_{fy} (comp. Eq. (4.9)) and the energy based method D_e proposed by Jorissen and Fragiacomio [42] (comp. Eq. (4.13)).

All of the examined load-displacement graphs are shown in Appendix B.

4.3.2 Investigations on dowel typ connections

4.3.2.1 Nailed connections

Section 3.2.5 describes investigations on nailed connections in view of the variation to grain direction; in direction to the grain or perpendicular to the grain conducted by Blaß [6]. The examined nails consisted of a diameter of 3.66 mm with a timber thickness of the side members of 19 mm and 38 mm for the middle member respectively.

Table 4.2: Determination of the point of yielding (u_y) of nailed connections, according to different methods (see Fig. 4.3 & Fig. 4.6)

Test	u_y (b) [mm]	u_y (b _{mod}) [mm]	u_y (e) [mm]	u_y (f) [mm]	u_f [mm]
1A19A	0.31	0.38	0.51	0.60	18.7
23C3A	0.47	0.66	0.64	0.85	17.7
30A-30D	0.60	0.88	0.71	0.98	18.7
40-44	0.56	0.81	0.70	0.91	18.0

The investigations in grain direction were conducted with ten nails per specimen (see Fig. 3.5). The experiments with specimen 1A19A and specimen 23C3A were chosen to determine the specified values to classify the fastener. Hence, the mean value of the 10 single experiments were determined to conduct the investigations on the ductility (see Tab. 4.3). Two series of experiments in view of the influence of the direction perpendicular to grain were also examined (specimens 30A-30D and specimen 40-44). The mean value for experiments were obtained to evaluate the mechanical behavior. Since no information was given if a failure at a certain displacement occurred, the lowest value of the displacements was taken as the displacement at failure for the mean value.

Despite a premature ending of the experiments of about 20 mm [6], all of the experiments

Table 4.3: Determination of the ductility ratio of nailed connections based on Eq. 4.1 & Eq. 4.9

Test	D_f (b)	D_f (b_{mod})	D_f (e)	D_f (f)	D_{fy} (b)	D_{fy} (b_{mod})	D_{fy} (e)	D_{fy} (f)
1A19A	60.92	49.27	36.96	30.95	18.39	18.32	18.19	18.10
23C3A	33.91	23.57	25.65	18.93	17.18	16.95	17.01	16.77
30A-30D	31.14	21.37	26.52	19.11	18.10	17.82	18.00	17.72
40-44	32.19	22.10	25.86	19.74	17.44	17.19	17.30	17.09

show as expected a significant ductile behavior. With a ductility ratio D_f of about 17 to 60, this type of connection is clearly classified as highly ductile based on [69] (see Fig. 4.7). The experiments on specimen 23C3A show a higher ultimate load compared to the the experiments on specimen 1A19A. This is due to notches in the area of the specimen, and therefore to a higher load in view of experiments with an increase of the mean value (see Fig. B.2 & Fig. B.1) [6]. This leads to a shift of the displacement at yielding and a decrease of the ductility ratio (see Tab. 4.3 & Tab. 4.4).

Table 4.4: Determination of the ductility ratio of nailed connections based on Eq. 4.13

Test	D_e (b)	D_e (b_{mod})	D_e (e)	D_e (f)
1A19A	191.62	127.25	93.52	73.32
23C3A	101.13	52.40	62.81	44.11
30A-30D	90.73	49.81	72.24	42.67
40-44	80.72	53.06	64.26	44.75

4.3.2.2 Timber-steel-timber connections

BSB-connections

Investigations on the ductility were carried out on rather slender doweled connections. Information is gathered from the studies of Mischler [89] on BSB-connections with a diameter of 6.3 mm (comp. Sec. 3.2.6). The focus was set on the influence of the timber thickness of the middle member (see t_2 in Fig. 3.10(a)) and the number of fasteners in grain direction. The mean values of the single experiments were taken from [89]. All of the considered experiments consist of a more or less distinctive decrease of the load-displacement. The displacement at failure is set to a decrease of the load until 98% of the maximum load was

Table 4.5: Determination of the point of yielding (u_y) of BSB-connections, according to different methods (see Fig. 4.3 & Fig. 4.6)

Test	u_y (b) [mm]	u_y (b_{mod}) [mm]	u_y (e) [mm]	u_y (f) [mm]	$u_{F_{98\%}}$ [mm]
$t_2=67$ mm	1.64	1.94	2.03	1.82	3.80
$t_2=50$ mm	-	-	-	-	1.41
1 row of bolts in grain direction	0,98	1,26	1,25	1,17	8.81
3 rows of bolts in grain direction	1.52	1.70	1.86	1.53	3.12

reached (comp. $u_{F_{98\%}}$, see Fig. 4.8). The experiments in view of the thickness of the middle timber member were performed with the regular BSB-connection (see Fig. 3.10(a)). The basic geometrical setup was also chosen to perform the experiments in view of the influence of the number of bolts in grain direction. The number of rows varied within the consideration.

It is shown, that no displacement at yielding could be found with the suggested methods for the experiments for a mid-section width of 50 mm (see Tab. 4.5). This means that the connection is generally brittle (see Appendix Fig. B.6). It shows that a minimum timber thickness is required in order to prevent a failure due to splitting. An increase of the mid-section thickness up to 67 mm allows a classification of the connection with a low ductile behavior (see Fig. 4.7).

The danger of a failure due to splitting increases as well with the number of fasteners in grain direction. This is expressed by the ductility ratio (see Tab. 4.6 & Tab. 4.7).

Table 4.6: Determination of the ductility ratio of BSB-connections based on Eq. (4.1) & Eq. (4.9)

Test	D_f (b)	D_f (b_{mod})	D_f (e)	D_f (f)	D_{fy} (b)	D_{fy} (b_{mod})	D_{fy} (e)	D_{fy} (f)
$t_2=67$ mm	2.32	1.96	1.88	2.09	2.16	1.86	1.77	1.98
$t_2=50$ mm	-	-	-	-	-	-	-	-
1 bolt	8.97	7.01	7.03	7.52	7.83	7.55	7.56	7.64
3 bolts	2.06	1.83	1.68	2.03	1.60	1.42	1.26	1.59

Connections with one bolt in grain direction are classified with a ductility ratio between seven and nine as highly ductile. This is underlined by a plastic displacement of about 7.5 mm. Whereas the ductility ratio of unreinforced connections with three dowels in a row significantly decreases. A ductility ratio of smaller than two classifies this kind of connection

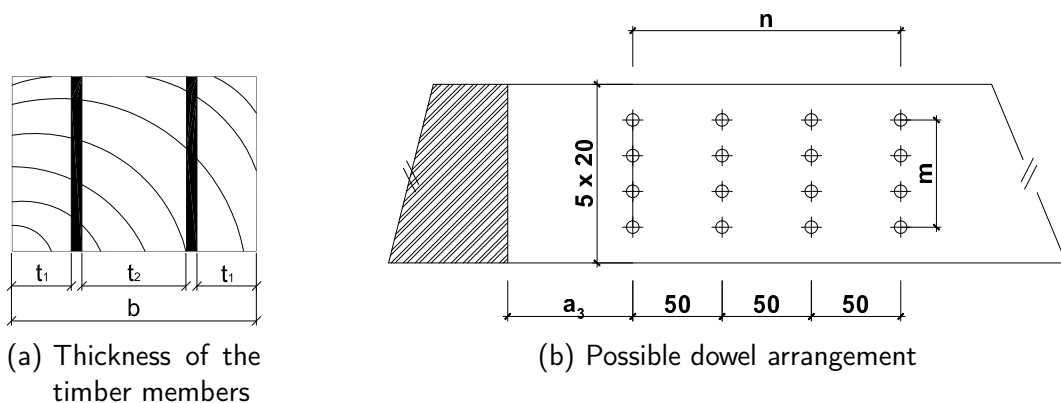
Table 4.7: Determination of the ductility ratio of BSB-connections based on Eq. (4.13)

Test	D_e (b)	D_e (b_{mod})	D_e (e)	D_e (f)
$t_2=67$ mm	4.03	2.94	2.69	3.24
$t_2=50$ mm	-	-	-	-
1 bolt in grain direction	20.41	12.98	12.98	14.86
3 bolts in grain direction	3.25	2.88	2.11	3.25

as a brittle type. The absolute value of the plastic displacement of about 2 mm underpins the classification.

Self-drilling dowels

Further studies on the ductile behavior on multiple slotted connections were performed on self-drilling dowels developed by SFS intec AG (see Fig. 4.13). The idea of self-drilling

**Figure 4.13:** Self drilling dowel developed by SFS intec AG**Figure 4.14:** Geometrical properties of the connections with self-drilling screws

dowels is based on the frequently appearing accuracy problem of the hole in the flitch plate and the hole in the timber member. This type of connector is able to drill the timber elements and up to three slotted steel plates (S 235 JR) with a thickness of 5 mm. Hence a

Table 4.8: Properties of the investigated connections with a diameter of 7mm [56]

Test	Number of slotted plates [-]	Steel grade [$\frac{N}{mm^2}$]	End-distance, a_3 [mm]	Timber dimensions			Arrangement	
				b_1 [mm]	t_1 [mm]	t_2 [mm]	m [-]	n [-]
3E	2	450	50	160	44	60	4	3
3F	2	600	50	160	44	60	4	3
3G	2	450	70	160	44	60	4	3
3H	2	600	70	160	44	60	4	3
4F	3	600 +/- 50	70	180	35	46	4	3
4G	2	600 +/- 50	70	180	45	78	4	3

high accuracy is achieved.

Mischler [56] conducted experiments on self-drilling dowels with a diameter of 5 mm and 7 mm. The focus in the test series 3 was set to the influence of the steel grade and the end distance a_3 (see Fig. 4.14). Test series 4 investigates the influence of the timber thickness. Thus the number of slotted plates was increased with a constant timber thickness. Furthermore, experiments were performed with a dowel diameter of 5 mm.

Table 4.8 shows the properties and the arrangement of the studied connections. The arrangement is described with the character m, which represents the number of dowels

perpendicular to the grain, and the character n, the number of dowels parallel to the grain (see Fig. 4.14(b)). The test setup was performed with one connection on the bottom and one on top of the specimen, which were clamped into the testing machine. Hence the weaker connection of both governed the failure of the test setup (see Fig. 4.15).

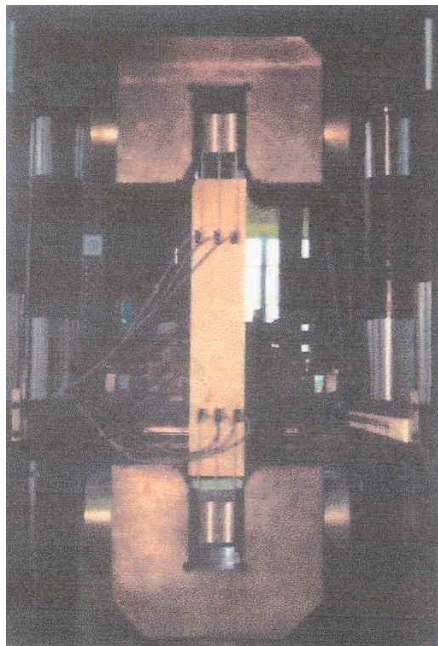


Figure 4.15: Test setup of self-drilling dowels [56]

The decisive displacement was for all tests found as the displacement at 98% of the ultimate load (see Appendix Fig. B.9 up to Fig. B.14).

The investigations on self-drilling dowels show different load slip behaviors depending on the timber thickness and the distance to the loaded end (a_3). The point of yielding shows only a small deviation within the experiments of a diameter of 7mm (see Tab. 4.9). The little variation is assigned to the different steel grades of the

Again, the influence of the timber thickness and the

end distance (a_3) is obvious within the experiments. An increase of the end distance of 50 mm to 70 mm (3E \rightarrow 3G and 3F \rightarrow 3H) decreases the risk of splitting, therefore the ductility ratio increases as well. Due to the application of three slotted plates in the test

Table 4.9: Determination of the point of yielding (u_y) of self-drilling dowels with a diameter of 7mm, according to different methods (see Fig. 4.3 & Fig. 4.6)

Test	u_y (b) [mm]	u_y (b_{mod}) [mm]	u_y (e) [mm]	u_y (f) [mm]	$u_{F_{98\%}}$ [mm]
3E	1.16	1.47	1.62	1.39	3.24
3F	1.17	1.48	1.60	1.38	4.97
3G	1.07	1.38	1.54	1.38	6.63
3H	1.22	1.53	1.62	1.46	7.04
4F	1.11	1.29	1.56	1.17	1.84
4G	1.19	1.47	1.61	1.40	5.55

Table 4.10: Determination of the ductility ratio of self-drilling dowels based on Eq. (4.1) & Eq. (4.9)

Test	D_f (b)	D_f (b_{mod})	D_f (e)	D_f (f)	D_{fy} (b)	D_{fy} (b_{mod})	D_{fy} (e)	D_{fy} (f)
3E	2,80	2,21	2,01	2,33	2,08	1,78	1,63	1,85
3F	4,25	3,35	3,12	3,61	3,80	3,49	3,37	3,59
3G	6,19	4,82	4,32	4,79	5,56	5,26	5,10	5,25
3H	5,75	4,61	4,36	4,83	5,82	5,52	5,42	5,58
4F	1,65	1,42	1,18	1,56	0,72	0,54	0,28	0,66
4G	4,66	3,77	3,45	3,95	4,36	4,07	3,94	4,14

Table 4.11: Determination of the ductility ratio of self-drilling dowels based on Eq. (4.13)

Test	D_e (b)	D_e (b_{mod})	D_e (e)	D_e (f)
3E	5,47	3,57	3,01	3,81
3F	9,20	5,66	5,06	6,39
3G	15,42	9,08	7,62	9,08
3H	13,01	8,23	7,79	9,24
4F	2,48	1,81	1,33	2,27
4G	9,60	6,83	5,76	7,26

setup 4F instead of two slotted plates in the test setup 4G the ultimate load increases. On the other hand, the ductility ratio drops down with a decrease of the timber thickness (see Tab. 4.10 & Tab. 4.11).

Common dowels

Experiments [91] have been conducted to develop a 3D numerical model in order to predict the load-displacement behavior of timber joints. The focus was set to double shear connections with slotted steel plates. The investigations were performed on different timber species (spruce, azobe and beech) with a variation of the number of fasteners in grain direction. The dowels varied in the diameter (12 mm and 24 mm) and in the steel grade. A steel grade of S235 and a high strength steel grade 12.9 was chosen. The tension test on the

Table 4.12: Properties of the considered experiments on common dowels [91]

Experiment	Dowels in grain direction [n]	steel grade [-]	Distance a_1 [mm]	Distance a_3 [mm]	timber properties t [mm]	b [mm]
S12C_1	1	S235	-	84	91	72
S12C_5	5	S235	60	84	91	72
S24C_1	1	S235	-	168	166	144
S24C_5	5	S235	120	168	166	144

dowels showed a higher tension strength as anticipated for the dowels of mild steel S235. The dowels with a diameter of 12 mm showed a tensile strength of 609 N/mm² and the dowels with a diameter of 24 mm a tensile strength of 517 N/mm². With regard to the ductile behavior attention is given to the experiments conducted on regular spruce with a dowel steel grade of S235.

Table 4.13: Determination of the point of yielding (u_y) of common dowels, according to different methods (see Fig. 4.3 & Fig. 4.6)

Test	u_y (b) [mm]	u_y (b_{mod}) [mm]	u_y (e) [mm]	u_y (f) [mm]	u_F [mm]
S12C_1	1.38	2.01	2.01	1.82	9
S12C_5	2.27	2.49	-	-	2.8
S24C_1	0.95	1.17	2.45	1.26	4.65
S24C_5	2.79	3.06	-	-	3.32

Table 4.12 shows the geometrical properties of the considered experiments. The thickness (t) refers to the embedded length of the dowel in the timber section per shear plane, the width (b) of the section is chosen in dependence on the edge distance (a_4) as three times the diameter. Five single experiments were available to determine the mean value of every test setup. Except the mean value of the experiments on connections with a diameter of 12 mm with single fasteners. The fourth experiments on single fasteners with a diameter of 12 mm reached an exceptional ultimate load, followed by a sudden failure. This is assigned to a knot in the dowel region. Hence the embedded strength is of a high value, but also afflicted with a high risk of splitting. Therefore, only four experiments were available to determine the mean value.

Following the previous investigations it is shown, that the ductile behavior of unreinforced connections significantly depends on the number of dowels in a row (see Tab. 4.12). The risk of splitting is the driving parameter in this case. Hence the application of the different methods to determine the displacement at yielding was not in all cases successful. However, the method based on EN 12512 [102] results in a displacement at yielding (see Fig. 4.3(b)). The connections with a single fastener can be classified for both diameters to a moderate to high ductility, whereas the connections with 5 dowels in a row behave rather brittle (see Tab. 4.14 & Tab. 4.15).

Table 4.14: Determination of the ductility ratio of common dowels based on Eq. (4.1) & Eq. (4.9)

Test	D_f (b)	D_f (b_{mod})	D_f (e)	D_f (f)	D_{fy} (b)	D_{fy} (b_{mod})	D_{fy} (e)	D_{fy} (f)
S12C_1	6.52	4.48	4.49	4.94	7.62	6.99	7.00	7.18
S12C_5	1.23	1.12	-	-	0.53	0.31	-	-
S24C_1	4.89	3.96	1.90	3.71	3.70	3.48	2.20	3.39
S24C_5	1.19	1.08	-	-	0.53	0.26	-	-

Table 4.15: Determination of the ductility ratio of common dowels based on Eq. (4.13)

Test	D_e (b)	D_e (b_{mod})	D_e (e)	D_e (f)
S12C_1	16.34	8.76	8.76	10.48
S12C_5	1.48	1.25	-	-
S24C_1	11.60	7.42	2.35	6.89
S24C_5	1.42	1.18	-	-

4.3.2.3 Timber-timber connections

Jorissen [84] carried out various experiments focusing on the load-carrying capacity of multiple timber to timber connections (comp. Sec. 3.2.7). Instead of installing common steel dowels, bolts of grade 4.6 were used without a washer and nut.

Table 4.16: Properties of the considered experiments of timber to timber connections [84]

Experiment	Dowels in	steel	Distance	Distance	timber properties	
	grain direction [n]	grade [-]	a_1 [mm]	a_3 [mm]	t_s [mm]	b_m [mm]
31107	1	4.6	-	84	24	48
39127	9	4.6	60	84	24	48
39157	9	4.6	132	84	24	48
81107	1	4.6	-	84	59	72
89127	9	4.6	60	84	59	72
89157	9	4.6	132	84	59	72

All of the conducted experiments by Jorissen [84] were re-evaluated regarding the ductility during a *COST E55 Short-Therm Scientific Mission (STSM)* [16]. The previous investigations considering the ductility showed, that the timber thickness is one of the driving parameters in achieving a ductile behavior. The study confirms that no ductility could be activated for timber members with a rather low timber thickness of $t_s=12$ mm and $t_m=24$ mm (see also Fig. 3.13(a)). However, within these investigations the focus is set to the influence of the in-between distance a_1 and the number of fasteners in a row. Table 4.16 shows the properties of the examined experiments.

Table 4.17: Determination of the point of yielding (u_y) of timber to timber connections, according to different methods (see Fig. 4.3 & Fig. 4.6)

Test	u_y (b) [mm]	u_y (b_{mod}) [mm]	u_y (e) [mm]	u_y (f) [mm]	u_F [mm]
31107	0.37	0.44	0.99	0.67	8.8
39127	2.17	2.70	2.84	2.38	5
39157	2.06	2.40	2.93	2.42	5.5
81107	0.61	0.73	1.28	1.07	15.2
89127	-	-	4.03	3.49	5.3
89157	3.19	3.86	4.10	4.03	10.75

The investigations showed, that connections with one single bolt behave in a considerably ductile manner. On the reason given for this behavior is set in the point of yielding. The point of yielding develops earlier at experiments conducted with one fastener compared to a number of fasteners in grain direction Table 4.17. In addition to that, the displacement at failure occurs at a later stage with a single fastener. Hence the number of fasteners parallel to grain and the in-between distance have a significant influence on the ductility ratio (see Tab. 4.18 & Tab. 4.19). Therefore no point of yielding could be found for the experiment 89127 with nine dowels in grain direction and an in-between distance of five times the diameter. By increasing the in-between distance to eleven times the diameter, the behavior can be classified to a low ductility (see experiment 89157).

Hence, the ductile behavior is depending on the in-between distance and the number of fasteners in a row in unreinforced connections.

Table 4.18: Determination of the ductility ratio of timber to timber connections based on Eq. (4.1) & Eq. (4.9)

Test	D_f (b)	D_f (b_{mod})	D_f (e)	D_f (f)	D_{fy} (b)	D_{fy} (b_{mod})	D_{fy} (e)	D_{fy} (f)
31107	23.96	19.96	8.93	13.05	8.43	8.36	7.82	8.13
39127	2.31	1.85	1.76	2.10	2.83	2.30	2.17	2.62
39157	2.67	2.29	1.88	2.28	3.44	3.10	2.58	3.08
81107	24.79	20.78	11.86	14.17	14.59	14.47	13.92	14.13
89127	-	-	1.32	1.52	-	-	1.27	1.81
89157	3.37	2.78	2.62	2.67	7.56	6.89	6.65	6.72

Table 4.19: Determination of the ductility ratio of timber to timber connections based on Eq. (4.13)

Test	D_e (b)	D_e (b_{mod})	D_e (e)	D_e (f)
31107	69.02	56.68	17.33	32.00
39127	3.97	2.64	2.41	3.25
39157	4.95	3.66	2.54	3.66
81107	82.95	56.62	24.58	31.25
89127	-	-	1.61	2.11
89157	7.04	4.93	4.40	4.50

Reinforced timber-steel-timber connections

Within the study of Bejtka [82] on optimized connections with fully threaded screws, experiments were performed on reinforced doweled connections with a diameter of 16 mm and 24 mm. One of the main findings was the possibility to neglect the reduction of the number of

Table 4.20: Properties of the considered experiments of reinforced timber-steel-timber connections [82]

	Experiment	Reinforcement per shear plane	steel grade [-]	Distance a_1 [mm]	Distance a_3 [mm]	timber properties t [mm]	b [mm]
Ø 16mm	V30	-	S235	80	170	100	200
	V36 & V37	1	S235	80	170	100	200
	V38 & V39	2	S235	80	170	100	200
Ø 24mm	M1 - M4	-	S235	120	170	100	200
	M5 & M6	1	S235	120	170	100	200
	M7 - M10	2	S235	120	170	100	200

fasteners in grain direction, if the connection is reinforced with fully threaded screws (comp. Sec. 3.2.8).

Table 4.20 shows the properties of the examined experiments. All of the experiments were performed with five dowels parallel to the grain. The reinforcement was placed 10 mm underneath the fasteners within the test setup V and in the middle of two fasteners (60 mm) in the test setup M.

Table 4.21: Determination of the point of yielding (u_y) of reinforced timber-steel-timber connections, according to different methods (see Fig. 4.3 & Fig. 4.6)

Test	u_y (b) [mm]	u_y (b_{mod}) [mm]	u_y (e) [mm]	u_y (f) [mm]	u_F [mm]
V30	0.74	1.06	1.68	0.78	2.0
V36 & V37	1.38	1.76	2.39	2.10	15.3
V38 & V39	1.44	1.88	2.41	2.11	14
M1 - M4	-	-	-	1.70	2.18
M5 & M6	1.84	2.20	3.36	2.19	6.70 *
M7 - M10	2.23	2.85	3.74	2.59	7,79 *

* Displacement at 98% of ultimate load

The reinforcement has a direct influence on the ductile behavior due to the reduction of the risk of splitting. Hence the displacement at failure increase significantly compared to unreinforced connections (see Tab. 4.21). Connections accomplished without any reinforcement (exp. V30 and M1 - M4) are classified as brittle based on Smith et al. [69], whereas reinforced connections increase the ductile behavior significantly to a moderate or high ductile classification.

The increase of the dowel diameter from 16 mm to 24 mm with a constant timber thickness leads to a decrease of the ductility ratio (see Tab. 4.22 & Tab. 4.23). Hence it can be seen, that the slenderness (λ) (comp. Eq. (3.12) & (3.13)) of the connection is also of importance for reinforced connections.

Table 4.22: Determination of the ductility ratio of reinforced timber-steel-timber connections based on Eq. (4.1) & Eq. (4.9)

Test	D_f (b)	D_f (b_{mod})	D_f (e)	D_f (f)	D_{fy} (b)	D_{fy} (b_{mod})	D_{fy} (e)	D_{fy} (f)
V30	2.71	1.89	1.19	2.56	1.26	0.94	0.33	1.22
V36 & V37	11.07	8.69	6.40	7.30	13.92	13.54	12.91	13.20
V38 & V39	9.74	7.46	5.80	6.63	12.56	12.12	11.59	11.89
M1 - M4	-	-	-	1.28	-	-	-	0.48
M5 & M6	3.64	3.05	2.00	3.06	4.87	4.51	3.35	4.51
M7 - M10	3.49	2.74	2.08	3.00	5.56	4.95	4.06	5.19

Table 4.23: Determination of the ductility ratio of reinforced timber-steel-timber connections based on Eq. (4.13)

Test	D_e (b)	D_e (b_{mod})	D_e (e)	D_e (f)
V30	5.38	2.93	1.27	4.27
V36 & V37	31.92	20.22	12.49	15.55
V38 & V39	29.06	18.48	11.43	14.22
M1 - M4	-	-	-	1.58
M5 & M6	7.43	5.32	2.63	5.32
M7 - M10	6.94	4.48	2.86	5.29

4.3.3 Miscellaneous connections

Tube connections

A new and innovative type of connection, the tube connection, was examined by Leijten [88] (comp. Sec. 3.3.2). The load-displacement behavior may be described by a non-linear

Table 4.24: Determination of the point of yielding (u_y) of tube connections, according to different methods (see Fig. 4.3 & Fig. 4.6)

Test	u_y (b) [mm]	u_y (b_{mod}) [mm]	u_y (e) [mm]	u_y (f) [mm]	u_F [mm]
18 mm tube	1.45	1.83	2.51	1.98	15*
35 mm tube	0.61	0.80	2.55	0.92	15*

* The experiments were terminated at a displacement of 15 mm according to EN 26891 [110]

regression model. The model is based on Jaspart and Maquoi [35] which was originally developed in steel engineering.

The regression model for tube connections loaded parallel to the grain form the basis of the investigations with regard to ductility. Two different diameters were examined, tubes with a diameter of 18 mm and with a diameter of 35 mm. Both models meet the minimum requirements developed by Leijten [88] (see Tab. 3.3).

The evaluation of the tube connections shows that this type of connection represents a remarkable ductile fastener. It is clearly classified as high-ductile based on the classification of Smith et al. [69]. The ductile behavior tends to a higher value as evaluated since the experiments were terminated at a displacement of 15 mm according to EN 26891 [110].

Connections accomplished with a tube diameter of 35 mm show a higher initial stiffness compared to the stiffness of a tube with a diameter of 18 mm. Hence, the point of yielding

Table 4.25: Determination of the ductility ratio of tube connections based on Eq. (4.1) & Eq. (4.9)

Test	D_f (b)	D_f (b_{mod})	D_f (e)	D_f (f)	D_{fy} (b)	D_{fy} (b_{mod})	D_{fy} (e)	D_{fy} (f)
18 mm tube	10.35	8.18	5.98	7.59	13.55	13.17	12.49	13.02
35 mm tube	24.45	18.66	5.88	16.34	14.39	14.20	12.45	14.08

Table 4.26: Determination of the ductility ratio of tube connections based on Eq. (4.13)

Test	D_e (b)	D_e (b_{mod})	D_e (e)	D_e (f)
18 mm tube	26.89	17.57	10.77	15.41
35 mm tube	72.57	44.96	8.47	37.24

is initiated at an earlier state (see Tab. 4.24), and the ductility ratio of a tube fastener with a diameter of 35 mm increases compared to a tube fastener with a diameter of 18 mm (see Tab. 4.25 & Tab. 4.26).

Split rings

Investigations on double tapered collar shear plate connectors (type A1, see Fig. 3.20(b)), and double spike shear plate connectors (type C10, see Fig. 3.20(a)) were performed at the Universität Karlsruhe [11] (comp. Sec. 3.4.2). Further investigations were performed

Table 4.27: Properties of the considered experiments of split ring connections [11]

Experiments	Dowel \varnothing [mm]	Number of test	Bolt \varnothing [mm]	Timber dimensions $t_1/t_2/b/l$ [mm]
<i>Double tapered collar shear plate connectors, type A1</i>				
A65N	65	65	M12	45/75/80/160
A128N	128	65	M12	70/115/160/310
<i>Double spike shear plate connectors, type C10</i>				
D50N	50	45	M12	40/70/60/120
D115N	115	45	M24	40/70/140/280

at the Ruhr-Universität Bochum on timber-to-timber connections and on steel-to-timber connections [64]. Shear plate connectors with teeth (Typ C2, see Figure 3.20(f)) and with spikes (Typ C11, vgl. Figure 3.20(d)) were investigated (comp. Sec. 3.4.2 & Sec. 3.4.3), the properties of the examined experiments are given in Table 4.27 and Table 4.28.

Table 4.27 and Table 4.28 show the different tested types of split rings and the associated timber properties. The thickness t_2 indicates the thickness of the steel plate within the test setup C117SH and D115SH.

Another issue of the experiments conducted at the Universität Karlsruhe was the identification of manufacturing inaccuracies. Hence, thin plywood elements have been glued on the

Table 4.28: Properties of the considered experiments of split ring connections [64]

Experiments	Dowel \varnothing [mm]	Number of test	Bolt \varnothing [mm]	Timber dimensions $t_1/t_2/b/l$ [mm]
<i>Shear plate connectors with teeth, type C2</i>				
C117HH	117	5	M20	80/80/150/400
C117SH	117	5	M20	80/8/150/400
<i>Shear plate connectors with spikes, type C11</i>				
D115HH	115	5	M24	60/60/140/400
D115SH	115	5	M24	60/10/140/400

specimens, to prevent any movement of the two shear planes. Just before the beginning of the test, the plywood was partially or fully cut, so no information of the inaccuracies has been lost. This procedure results in a higher stiffness at the beginning of the experiment, followed by a lesser joint stiffness due to the inaccuracies (see Fig. 4.16). The initial stiffness is a decisive parameter in determining the point of yielding by the method of EN 12512 [102]. In order to achieve reliable results, the determination of the initial stiffness was changed since the stiffness at the beginning is affected by the partially cut ply wood. Instead of using the difference between 10 % and 40 % of the maximum load, the stiffness was determined between 30 % and 60 % of the ultimate load (see Fig. 4.16). Hence, the determined stiffness

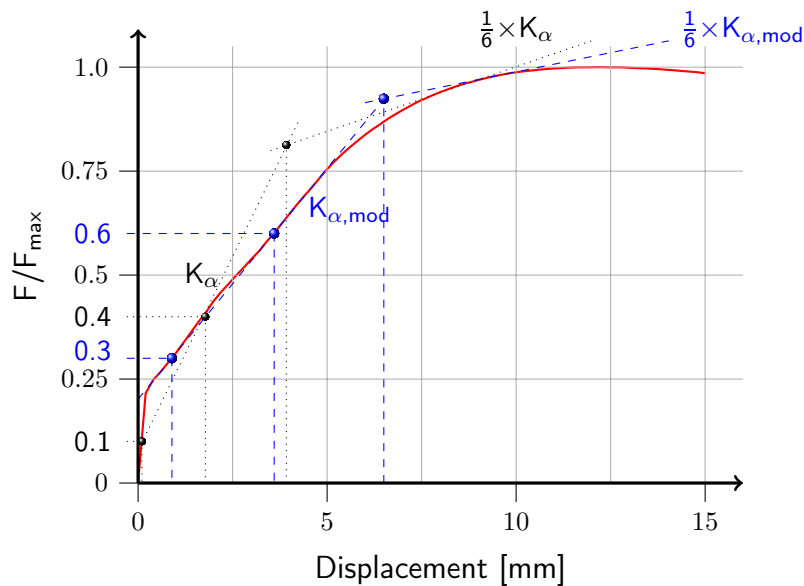
**Figure 4.16:** Modified method to determine the initial stiffness of the series D

Table 4.29: Determination of the point of yielding (u_y) of split rings, according to different methods (see Fig. 4.3 & Fig. 4.6)

Test	u_y (b) [mm]	u_y (b_{mod}) [mm]	u_y (e) [mm]	u_y (f) [mm]	u_F [mm]
A65N	4.58	5.69	7.76	4.39	12
A128N	5.26	7.12	11.98	5.02	13.4
D50N	6.47	7.89	8.71	6.01	15**
D115N	4.24	5.44	9.91	2.90	15***
C117HH	4.21	5.49	10.55	4.40	14.4
C117SH	2.76	3.54	8.90	2.96	12.62*
D115HH	3.12	3.90	9.55	3.64	11.4*
D115SH	2.19	2.85	8.24	2.36	9.88*

* Displacement at 98% of ultimate load

** The experiments were terminated at a displacement of 15 mm according to EN 26891 [110]

*** Displacement of 15 mm is similar to the displacement at 98% of ultimate load

matches well with the experimental results.

Obliviously, the manufacturing accuracy has a large influence on the behavior of split rings. The different experiments show a large variability of results (see Appendix Fig. B.33 to Fig. B.36). Shear plate connectors with teeth and spikes are less susceptible in the manufacturing process than shear plate connectors. Hence, this type of connectors show a pronounced stiffness after overcoming the friction due to tightening of the bolt.

The method based on a 5% diameter offset [1] to determine the point of yielding is most likely not applicable. The inapplicability is caused by the large diameter of those types of fastener. Therefore, the point of yielding is shifted towards the displacement at failure (see Tab. 4.29 and Appendix Fig. B.33 to Fig. B.40).

The investigations on split rings revealed a low to medium ductile behavior (see Tab. 4.30 & Tab. 4.31). Double spike shear plate connectors showed no tendency to fail until a displacement of 15 mm. Since the experiments were performed with the focus on the load-bearing capacity, the experiments were terminated at a slip of 15 mm due to the test procedure according to EN 12512 [102]. It is assumed, that a displacement of 15 mm is the lower limit of the displacement and therefore a higher ductility may be achieved in reality.

The point of yielding occurs at an earlier stage for steel to timber connections with split rings than timber to timber connections with split rings. This is due to the higher deformability of timber. Hence, the ductile behavior increases with steel to timber connections.

Table 4.30: Determination of the ductility ratio of of split rings based on Eq. (4.1) & Eq. (4.9)

Test	D_f (b)	D_f (b_{mod})	D_f (e)	D_f (f)	D_{fy} (b)	D_{fy} (b_{mod})	D_{fy} (e)	D_{fy} (f)
A65N	2.62	2.11	1.55	2.73	7.42	6.31	4.24	7.61
A128N	2.55	1.88	1.12	2.67	8.14	6.28	1.42	8.38
D50N	2.32	1.90	1.72	2.49	8.53	7.11	6.29	8.99
D115N	3.54	2.76	1.51	5.17	10.76	9.56	5.09	12.10
C117HH	3.42	2.62	1.36	3.27	10.19	8.91	3.85	10.00
C117SH	4.57	3.56	1.42	4.27	9.86	9.08	3.72	9.66
D115HH	3.65	2.92	1.19	3.14	8.28	7.50	1.85	7.76
D115SH	4.51	3.47	1.20	4.19	7.69	7.03	1.64	7.52

Table 4.31: Determination of the ductility ratio of split rings based on Eq. (4.13)

Test	D_e (b)	D_e (b_{mod})	D_e (e)	D_e (f)
A65N	4.26	3.08	1.91	4.59
A128N	4.34	72.55	71.17	74.63
D50N	3.58	2.61	2.16	3.98
D115N	5.74	3.94	1.66	9.59
C117HH	6.46	4.12	1.54	5.97
C117SH	9.48	6.11	1.54	7.91
D115HH	7.55	4.96	1.24	5.72
D115SH	8.94	5.58	1.24	7.69

Nail plates

Investigations on nail plate connections were performed by Kevarinmaki [85] on different types of plate connectors (comp. Sec. 3.5). Table 4.32 shows the displacement at yielding for the different types of fasteners. Within the method of a 5% diameter offset based on AF & PA [1], the thickness w_t (see Fig. 3.25) is chosen as the associated diameter.

It is obvious, that the point of yielding occurred at a rather slight shift among the other previously examined connections. Hence, the relative ductility ratio (D_f) classifies nail plate connectors with a high ductility, although the deformation at 98 % of the ultimate force has only a magnitude of 2.5 mm. On the other hand, the absolute plastic deformation (D_{fy}) shows a low plastic deformability of only 2 mm to 2.5 mm (see Tab. 4.33). Therefore, nail plate connections are classified with a low ductile behavior [62]. The minimum required

Table 4.32: Determination of the point of yielding (u_y) of nail plate connections, according to different methods (see Fig. 4.3 & Fig. 4.6)

Test	u_y (b) [mm]	u_y (b_{mod}) [mm]	u_y (e) [mm]	u_y (f) [mm]	u_F [mm]
Fix	0.14	0.21	0.31	0.22	2.56*
TOP 91	0.33	0.47	0.46	0.42	2.29*
W	0.21	0.32	0.41	0.33	2.84*

* Displacement at 98% of ultimate load

displacement ($\delta_{u,k}$) is set to 6 mm. The displacement $\delta_{u,k}$ is defined as a reduction of the smallest displacement within a test series of 10 %.

This follows the rules of EN 1994-1-1 [108, 6.6.1.1] which demands a minimum displacement of a fastener in steel-concrete composite structures (for instance headed studs) in order to classify them as ductile.

Table 4.33: Determination of the ductility ratio of nail plates based on Eq. (4.1) & Eq. (4.9)

Test	D_f (b)	D_f (b_{mod})	D_f (e)	D_f (f)	D_{fy} (b)	D_{fy} (b_{mod})	D_{fy} (e)	D_{fy} (f)
Fix	17.67	11.90	8.19	11.78	2.41	2.34	2.24	2.34
TOP 91	6.86	4.92	4.9	5.47	1.96	1.83	1.83	1.87
W	13.61	8.99	6.92	8.58	2.63	2.52	2.43	2.51

Table 4.34: Determination of the ductility ratio of nail plates based on Eq. (4.13)

Test	D_e (b)	D_e (b_{mod})	D_e (e)	D_e (f)
Fix	47.39	30.02	16.29	30.02
TOP 91	15.11	8.39	9.95	12.08
W	39.78	21.78	14.37	17.41

4.4 Discussion and conclusion

In general, fasteners in timber structures show a low to high ductile behavior. However, the real ductility could not be ascertained for some of the experiments, since the tests were terminated at a displacement of 15 mm. The different carefully chosen methods to determine the point of yielding show a good applicability.

The method based on a 5% diameter offset by AF & PA [1] indicated contradictions. The application on spilt rings is most doubtful, since the rather large diameter shifts the point of yielding far towards the point of failure (see Tab. 4.29). Hence the point of yielding might be within the horizontal plastic plateau (see for instance Fig. B.38). Since punched-out nails have no defined diameter per definition, it is important to define either the nail width, the plate thickness or a combination of both as the diameter. Within the previous investigations the nail width (w_t) was chosen as the corresponding diameter. The determined values of the point of yielding show a good match with the results gained with the modified method based on EN 12512 [102] (see Appendix Fig. B.41 to Fig. B.43).

Within the investigations on nail plate connections it can be seen that it is necessary to pay attention not only to the relative value D_f , but also to the absolute value D_{fy} in order to evaluate the ductility of fasteners (see Fig. 4.17). Therefore, the appraisal given by Smith et al. [69] (see Fig. 4.7) is extended by the absolute plastic deformation D_{fy} (see Tab. 4.35). For the classification of a type of fastener both, the absolute and the relative consideration, should comply with the classification limits. The limiting values are chosen according to the requirements given in EN 1994-1-1 [108]. The initial background of a minimum yield displacement of a headed stud of six millimeters, given in [108], cannot be transferred directly.

Table 4.35: Extension of the ductility classification based on Smith et al. [69]

Classification	Relative consideration	Absolute consideration
Brittle	$D_f \leq 2$	$D_{fy} \leq 1 \text{ mm}$
Low ductility	$2 < D_f \leq 4$	$1 \text{ mm} < D_{fy} \leq 3 \text{ mm}$
Moderate ductility	$4 < D_f \leq 6$	$3 \text{ mm} < D_{fy} \leq 6 \text{ mm}$
High ductility	$D_f > 6$	$D_{fy} > 6 \text{ mm}$

Figure 4.17 shows the necessity of the consideration of both values. Corresponding values of D_f and D_{fy} are illustrated in Figure 4.17 for certain types of fasteners. The chosen values are based on the modified method of EN 12512 [102] (see Fig. 4.6). The method was chosen since it gives more reliable values of the point of yielding compared to the initial method [102].

Only experiments with a group of fasteners are considered. The risk of splitting is smaller in

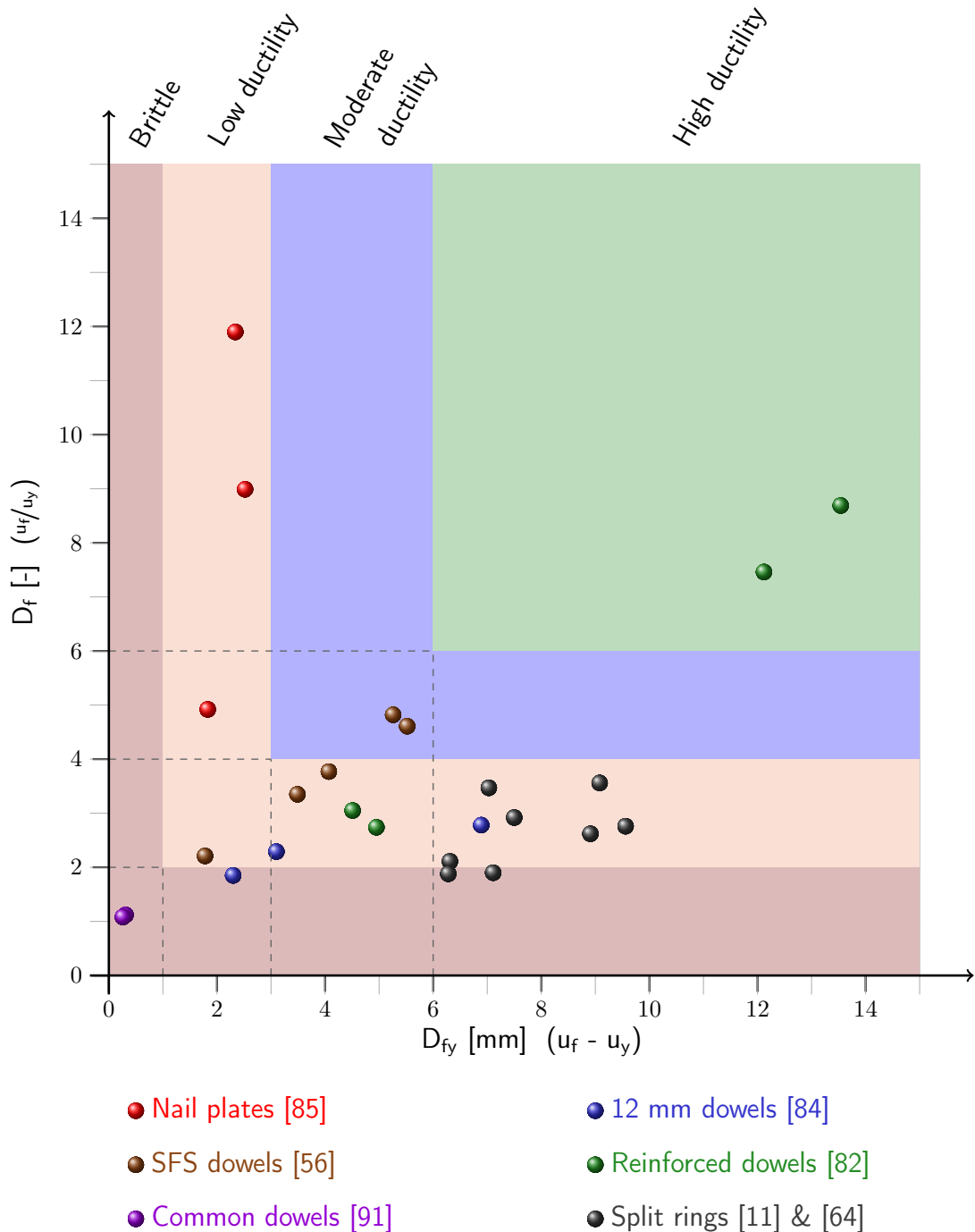


Figure 4.17: Interaction of the relative ($D_f (b_{mod})$) and absolute ($D_{fy} (b_{mod})$) consideration of the ductility ratio

the view of a single fastener compared to a group of fasteners which leads to an increase of the ductile behavior. Tube connections and nailed connections behave in both assessments very well, therefore, those types of connections are not included. On the other hand, non-reinforced doweled steel to timber connections are classified in both assessments as brittle.

The investigations on reinforced dowels show a large variance in-between the two test series. The series V shows a high ductility, whereas the series M a low ductility presented (see Tab. 4.22 and Tab. 4.23).

However, a convincing method is significant to determine the point of yielding. Within these investigations it has been shown, that the method based on EN 12512 [102] and SIA 265:2012 [114] gives reasonable results to determine the point of yielding. The modified method is a bit more conservative but gives a direct point on the graph.

The point of yielding is an artificial point which is not directly located to the actual graph [102, 114]. With regard to the the ductility classification of a fastener, it is not decisive to gain a point of yielding on the actual graph since it is only a reference point.

5 Experimental research

5.1 Introduction

The previous chapter has pointed out that fasteners in timber structures generally exhibit a ductile behavior. Within the investigations reinforced doweled connections showed both, a good relative ductility ratio D_f and a convincing absolute ductile displacement D_{fy} . In order to gain more knowledge, with the view on the ductile behavior, experiments were conducted at the University of Stuttgart. Since doweled connections are a commonly used type of fastening system combined with excellent ductile qualities, reinforced flitch plate connections were chosen to perform the experiments.

Most of the earlier performed experiments were performed based on the rules of EN 26891 [110]. Hence the experiments were in most cases terminated at a displacement of 15 mm. Within this study a possible termination at 15 mm was neglected to achieve the maximum displacement at failure.

The first part of this chapter will discuss the material properties of the experiments. Special attention is given to the steel grade of the dowels and to the timber density. Both parameters are driving parameters in the determination of the load carrying capacity and the deformability of a connection. It is necessary that all of the used dowels within a test setup belong



(a) Pure tension test



(b) Four-point bending moment test

Figure 5.1: Experiments conducted at the University of Stuttgart [46] [47]

to the same material lot.

The second part of this chapter describes the experimental investigations [46] [47]. The performed experiments were in general divided into two parts. Firstly, pure tension tests (see Fig. 5.1(a)) to obtain experiences about the general ductile behavior of connections and secondly four point bending tests (see Fig. 5.1(b)) to achieve the moment-rotation capacity of the previous tested connections, introduced to a joint.

Further investigations are described in the third part of the chapter. Tentative experiments were conducted on reinforced connections loaded perpendicular to the grain to prove the ductile behavior. A further point of view was set to an important application of ductility in the seismic design. Therefore, investigations on a cyclic loading were performed to gain knowledge of the behavior under a changing loading.

The experimental results are evaluated based on the methods discussed and applied in Chapter 4.

The experiments were carried out at the Materials Testing Institute, University of Stuttgart (MPA Stuttgart, Otto-Graf-Institut (FMPE)).

5.2 Description of the specimens

5.2.1 Overview

Table 5.1 shows the matrix of the performed main experiments within [47]. All of the conducted experiments were reinforced with fully threaded screws according to the findings of Bejtka [82] (see Fig. 5.2).

Besides the pure investigations on the ductility performance, attention was also given to the dowel arrangement, the diameter and to the number of slotted plates. The aim of the variation of the dowel arrangement was to examine the influence of the alignment on the moment-rotation capacity within the bending tests. Since all of the timber specimens had a constant width of 180 mm, the influence on the slenderness was examined with the variation of the dowel diameter. Based on the studies of Mischler [89] experiments were also

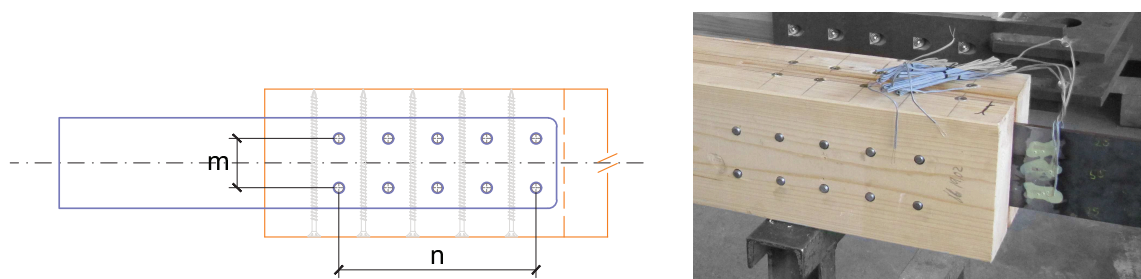


Figure 5.2: Dowel arrangement within the tension experiments

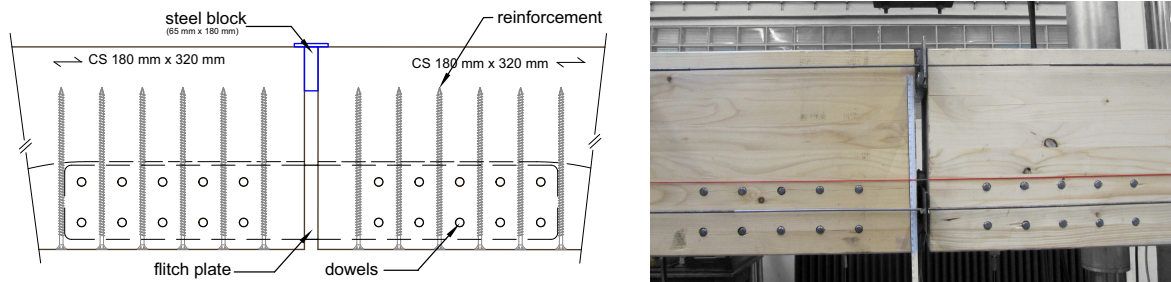


Figure 5.3: Dowel arrangement within the bending experiments

planned on double flitch plate connections. The timber thickness was chosen according to the optimal slenderness ratio given in Equation (3.13).

Table 5.1: Overview of the performed experiments

Test	$f_{u,k}$ [$\frac{N}{mm^2}$]	Number of slotted plates	Number of tests	Geometry			Arrangement	
				b [mm]	t_1 [mm]	t_2 [mm]	n [-]	m [-]
Experiments in tension								
<i>Self-drilling dowels (SFS):</i>								
ZV_7_2×3	579 (550)	2	3 (4)	180	55	58	2 (3)	3
ZV_7_4×2	579 (550)	2	4	180	55	58	4	2
<i>Ordinary dowels Ø 12mm:</i>								
ZV_12_5×2	581 (360)	1	4	180	85	-	5	2
ZV_12_2×4	581 (360)	1	3 (4)	180	85	-	2 (3)	4
ZV_12_3×3	581 (360)	1	4	180	85	-	3	3 (4)
<i>Ordinary dowels Ø 16mm:</i>								
ZV_16_3×2	488 (360)	1	4	180	85	-	3	2
Experiments in bending								
<i>Self-drilling dowels (SFS):</i>								
BV_7_2×3	579 (550)	2	3	180	55	58	2 (3)	3
BV_7_4×2	579 (550)	2	3	180	55	58	4	2
<i>Ordinary dowels Ø 12mm:</i>								
BV_12_5×2	581 (360)	1	3	180	85	-	5	2
BV_12_2×4	581 (360)	1	3	180	85	-	2 (3)	4
BV_12_3×3	581 (360)	1	3	180	85	-	3	3 (4)
<i>Ordinary dowels Ø 16mm:</i>								
BV_16_3×2	488 (360)	1	3	180	85	-	3	2

To achieve a reasonable reliable mean value of the different test setups, four experiments were performed of each configuration within the tension tests, and three experiments within the bending tests (see Fig. 5.3). Two experiments have not been performed due to problems in manufacturing and in the performance of the experiment itself. Therefore 22 experiments in tension and 18 experiments in bending were conducted.

Table 5.1 shows the designation of the single experiments and the corresponding parameters of the specimens. The geometry of the timber fingers is named according to the declaration given in Figure 3.10(a). Figure 5.2 shows the designation of the dowel arrangement. The character *n* indicates the number of fasteners in grain direction. The character *m* describes the number of columns perpendicular to the grain.

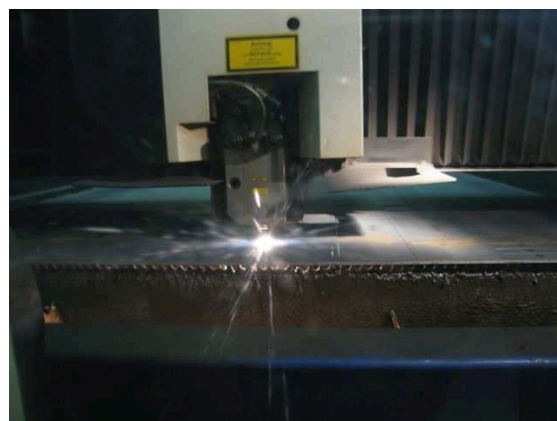
Some of the dowel arrangements needed to be revised due to the high measured tensile strength of the dowels (comp. Sec. 5.2.3.2). Hence, connections were reduced by a column or a row of dowels (see Tab. 5.1). The numbers in brackets within the shown arrangement in Table 5.1 shows the originally planned alignment based on [109]. The necessity is substantiated in order to ensure a ductile behavior of the joint before a possible brittle failure of the timber member next to the joint occur.

5.2.2 Fabrication

Major problems in steel to timber connections are usually resulting from the accuracy of the drilling pattern of the flitch plate to the drills in the timber element. Therefore both, the steel parts and the timber parts were manufactured CNC controlled to minimize the risk of disagreements. Figure 5.4(a) shows the manufacturing process of the timber elements; Figure 5.4(b) the manufacturing process of the steel parts. Within the CNC factoring process in timber structures, the boreholes are drilled from both sides of the specimen. Thereby, a



(a) Timber elements



(b) Steel parts

Figure 5.4: CNC controlled manufactured process

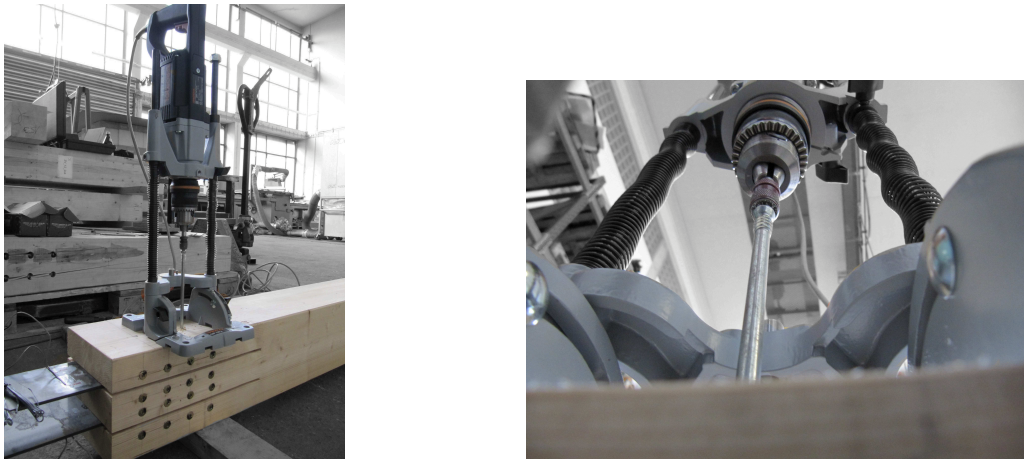


Figure 5.5: Placing of self-drilling dowels

higher degree of accuracy is achieved. The drills have an overlap in the middle of the drilling due to that manufacturing process. In some cases it might happen, that the drills are not in the same position due to a running off the line. This may lead to an elongated hole in the mid-section.

All of the screws and self-drilling dowels were placed by hand. No pre-drilled hole was made, neither by the timber elements, nor by the flitch plates. The assembling was carried out in self-service to avoid hidden defects and to gain knowledge of every specimen (see Fig. 5.5).

5.2.3 Material properties

5.2.3.1 Timber

Timber as a natural growing material is subjected to a large scattering of the material properties. The density, the modulus of elasticity and the moisture content are important parameters in view of the fasteners behavior and of the beam timber element itself.

Therefore, it was of crucial importance to record the material properties at the earliest possible opportunity. The company *MiCROTEC® GmbH, Brixen, Italy*, has agreed to grade 160 lamellae needed to manufacture the timber beams and make them available for further use. The grading was accomplished with the quality scanner 706. Therefore, it was possible to determine the statistical distribution of the density, the modulus of elasticity and of the moisture content during the manufacturing process (see Appendix Fig. C.1 to Fig. C.3).

All of the timber elements were fabricated by *WiEHAG GmbH, Altheim, Austria*. Although in practical use a combined timber grade (e.g. GL24c, GL28c) is appropriate for members stressed in bending, a homogeneous setup was chosen to ensure that all connectors are

with a dynamic procedure in the grading process. The dynamic measurement technology results in a higher modulus of elasticity compared to the statically measured modulus of elasticity given in the code.

There are mainly two different methods to determine the statical modulus of elasticity. On one hand the locally measured modulus of elasticity (MoE_{loc}), which is determined with a four point bending test setup in the area of no shear. On the other hand the globally measured modulus of elasticity (MoE_{glob}) which considers the complete length of a bending test setup. Ravenhorst and van de Kuilen [63] give a relation to determine the local modulus of elasticity by means of the dynamic modulus of elasticity (comp. Eq. (5.1)).

$$MoE_{loc} = 0.92 \cdot MoE_{dyn} \quad (5.1)$$

Based on the findings of [63] the dynamically measured modulus of elasticity turns to a locally measured modulus of elasticity of 11260 N/mm² for the specimens of the tension test setup, and 11930 N/mm² for the specimens used in the bending test setup. The measured mean value corresponds well with a deviation of less than ± 4 % compared to the mean value given in [103]. The standard coefficient of 16 % of the timber members acting in bending is slightly higher as the corresponding coefficient of 13 % given in the Probabilistic Model Code by the Joint Committee on Structural Safety (JCSS) [41].

The ascertained mean value of the density of approximated 444 kg/m³ shows a good accordance with the incorporated value given in EN 14080 [103] of 420 kg/m³. The coefficient of variation is in both cases, tension and bending, almost in accordance with the value given in the Probabilistic Model Code by Joint Committee on Structural Safety (JCSS) [41].

A moisture content of 13.6 % respectively 12.9 % is in the range of 6 % to 15 % to achieve a well acting glueing [103]. Furthermore the density of no lamellae differs more than 5 % from each other EN 14080 [103]

5.2.3.2 Dowels

The choice of the dowels for the experiments were set to a self-drilling system from **SFS intec, Heerbrugg, Switzerland** on one hand and to ordinary dowels ordered with a steel garde of S235 JR on the other hand. The ordinary dowels were manufactured by **HMR Jacob GmbH, Osterhofen**.

Properties

The dowels were ordered directly from the manufacturer to minimize the risk to obtain dowels with different mechanical properties. This is of utmost importance to achieve a comparability of the experiments within a test setup and additionally of the interaction between the tension experiments and the bending experiments. Figure 5.7 shows exemplarily the segmentation



Figure 5.7: Segmentation of a semi-finished product

of a semi-finished product during the order process. A six meter long round profile bar forms the basis in the production of dowels. In the stage of planning attention was given that all dowels of a connection belong to one semi-finished product. Furthermore samples were ordered of every semi-finished product to gain knowledge of the differences between the various semi-finished products. The single dowels were delivered for a set of corresponding experiments belong to the same semi-finished product. Therefore 16 tensile experiments with a diameter of 12 mm and three experiments with a diameter of 16 mm have been conducted to prove the accordance. Measurements on arbitrary chosen dowels were performed to prove the dimensional accuracy. Neither the ordinary dowels nor the SFS dowels showed significant deviations of the dowels. No statistical determination could be performed since the deviations were too small.

Tensile tests were conducted at the beginning of the experiments to prove possible differences in the various dowel parts (see Fig. 5.8). Table 5.3 shows the the material properties of the performed tensile experiments. Since the self-drilling dowels are an industrially produced product with a large quantity, only three dowels were tested. The biggest contribution was given by the ordinary dowels with a diameter of 12 mm; 16 semi-finished products were needed to manufacture the required dowels for the experiments. The coefficient of variation shows



Figure 5.8: Tensile test on an ordinary dowel

Table 5.3: Statistical properties of the tensile tests of the installed dowels

	Mean value $\left[\frac{N}{mm^2}\right]$	Number of samples	Standard deviation $\left[\frac{N}{mm^2}\right]$	Coefficient of variation [%]
self-drilling dowels \varnothing 7mm	579	3	5,97	1,0
dowels \varnothing 12mm	581	16	3,46	0,6
dowels \varnothing 16mm	488	3	9,84	2,0

that the different semi-finished products belong to the same batch. Hence a homogenous dowel connection was installed in every experiment, in every test setup and in the complete experiment setup. The gained knowledge in the tension tests can therefore be transferred to experiments acting in bending.

The mean tensile strength of 579 N/mm² of the self-drilling dowels is within the range of 550 N/mm² -0 / +100 N/mm² given in [56]. Table 5.4 shows the rules of hot rolled steel products of steel grade S235 JR. Steel dowels with a diameter of 16 mm show an enhanced tensile strength compared to the values given in [95]. However, the measured tensile strength is still in the range given in EN 10025-2 [100]. The tensile strength of ordinary dowels with a diameter of 12 mm show a strongly enhanced tensile strength, which is higher than the

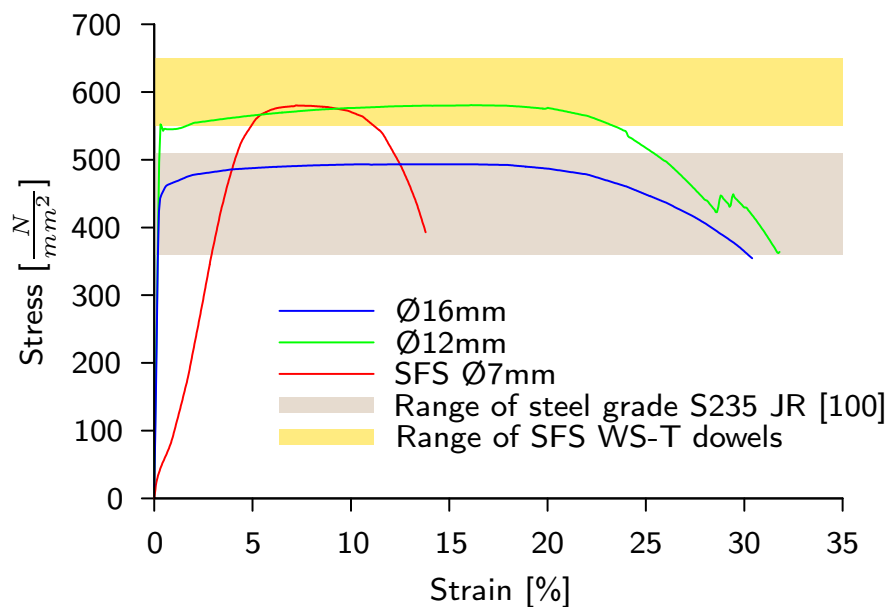
**Figure 5.9:** Stress-strain relationship of the different dowels

Table 5.4: Classification of the ordinary dowels based on the rules of EN 10025-2 [100]

	Ordered steel grade	measured tensile strength	Tensile strength according to EN 10025-2 [100]
dowels Ø 12mm	S235 JR	581 $\frac{N}{mm^2}$	360 to 510 $\frac{N}{mm^2}$
dowels Ø 16mm	S235 JR	488 $\frac{N}{mm^2}$	360 to 510 $\frac{N}{mm^2}$

upper bound given in EN 10025-2 [100] (see Fig. 5.9).

An enhanced tensile strength was also examined by Werner [93] and in further consequence by Schickhofer et al. [68]. Tensile strength values over 600 N/mm² were examined on S235 JR dowels in the study of [68]. Sandhaas [91] reports also on an enhanced tensile strength of ordinary dowels of a steel grade S235 JR. The tensile tests showed a strength of 638 N/mm² for a diameter of 12 mm, and 541 N/mm² for dowels with a diameter of 24 mm.

Figure 5.9 shows the general stress-strain relationship of the mean values of the tensile tests. The clamping of the self-drilling dowel specimens were difficult to carry out, since self-drilling dowels consist of a small diameter combined with a rather small length. Hence a slip occurred in the clamping device. Thus the displayed strain ratio does not match with the actual modulus of elasticity. Within this consideration, the absolute tensile strength is of interest, thus the slip does not influence the actual tensile strength.

Yield moment of fasteners

The formation of plastic hinges within dowel type fasteners forms the basis of a ductile behavior of connections in timber structures. For a circled cross-section the yield moment is found as:

$$M_{y,k} = f_{y,k} \cdot \frac{d^3}{6} \quad (5.2)$$

based on the general mechanics of the full plastic capacity.

Investigations on screws of grade 4.6 and 5.6 in steel structures loaded systematically in bending, showed that the 5 %-quantile value of the yield stress is less than 67 % of the tensile stress [67] (comp. Eq. (5.3)). Therefore the first estimation is given to:

$$M_{y,k} = 0,67 \cdot f_{u,k} \cdot \frac{d^3}{6} \quad (5.3)$$

The previous investigations are based on a bending angle of 10°, which is not compatible with the rules given in EN 409 [111]. A bending angle of 45° is required on dowel type fasteners according to [111]. The maximum yield moment is not achieved at an angle of

10°, since the plastic hinge is not fully developed. Investigations of Blaß et al. [10] showed that the yield moment has to be increased by 19 % for a bending angle of 45°. Equation (5.3) turns to:

$$M_{y,k} = 1,19 \cdot 0,67 \cdot f_{u,k} \cdot \frac{d^3}{6} = 0,8 \cdot f_{u,k} \cdot \frac{d^3}{6} \quad (5.4)$$

Equation (5.4) formed the calculation basis of the yield moment of the pre-standard ENV 1995-1-1 [112, Eq. (6.5.1.2e)].

Further investigations were conducted to gain knowledge on the dependency of the yield moment on the bending angle [10]. Since the maximum load-carrying capacity is found as the maximum value until a displacement of 15 mm occurs, the density of the timber and the tensile strength of the dowels are chosen in such a way, that a preferably smaller bending angle develops. Based on the investigations, Blaß et al. [10] proposed an equation to determine the yield moment of fasteners in timber structures as follows:

$$M_{y,k} = 0,3 \cdot f_{u,k} \cdot d^{2,6} \quad (5.5)$$

The proposal is nowadays applied in the standards and gives the principle to determine the yield moment depending on the tensile strength of the fastener.

Figure 5.10 shows the dependency of the different approaches to determine the yield moment. It can be seen, that the yield moment is less for the derived Equation (5.5) compared

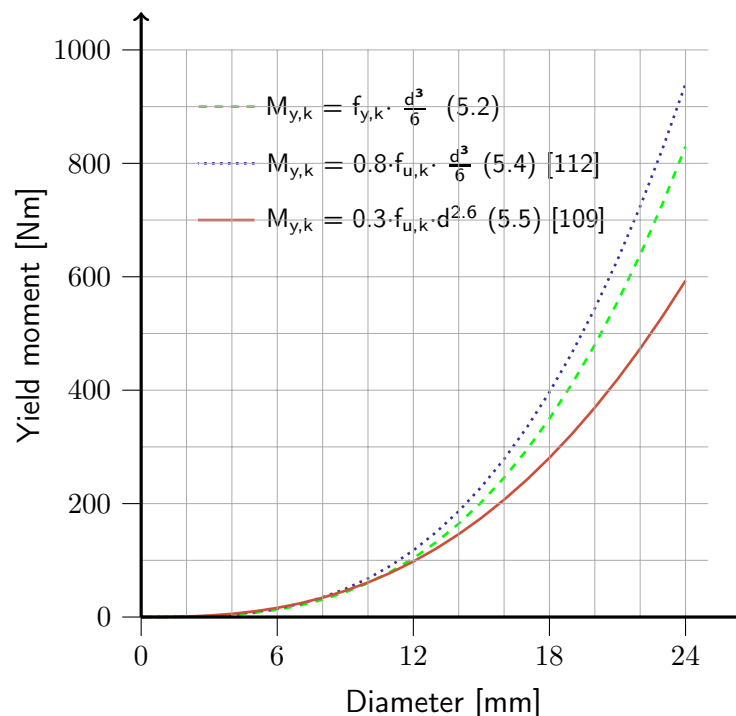


Figure 5.10: Comparison of the different methods to determine the yield moment

to Equation (5.4). Since rather thick dowels have not fully formed a plastic hinge, within a displacement of 15 mm, it was considered that Equation (5.4) determines a yield moment which is too high.

Besides the pure tensile tests, experiments on the yield moment of the used dowels were performed at the Karlsruhe Institute of Technologie. Hence, four dowel samples were examined with a dowel diameter of 7 mm and 12 mm, respectively three samples with a diameter of 16 mm. Table 5.5 gives the statistical parameters of the conducted experiments on the yield moment. The yield moment was determined based on a bending angle of $110^\circ/d$ [111]

Table 5.5: Statistical parameters of the determination of the yield moment

	110°/d [111]						45°				
	n	MV	max	min	St. dev.	COV	MV	max	min	St. dev.	COV
		[Nm]	[Nm]	[Nm]	[Nm]	[%]	[Nm]	[Nm]	[Nm]	[Nm]	[%]
Ø 7mm	4	28.45	29.29	27.47	0.82	3	33.13	33.78	32.14	0.72	2.2
Ø 12mm	4	147.7	158.8	139.3	8.1	5.5	177.7	189.6	188.2	8.1	4.5
Ø 16mm	3	324.9	342.0	306.7	17.7	5.5	399.8	419.2	377.2	21.2	5.3

and on the other hand at an angle of 45° . In order to compare the different steel dowels, the results of the yield moments (M_α) were standardised to a bending angle of 45° (\bar{M}_α). Blaß et al. [10] developed an approximation to determine the standardised yield moment of dowels and bolts depending on the bending angle (comp. Eq. (5.6)).

$$\bar{M}_{(\alpha)} = \frac{\bar{M}_{(\alpha,d)}}{\bar{M}_{(\alpha=45^\circ,d)}} = (0.866 + 0.00295 \cdot \alpha) \cdot \left(1 - e^{\left(\frac{-0.249 \cdot \alpha}{0.866}\right)}\right) \quad (5.6)$$

Figure 5.11 shows the comparison of derived yield moments to Equation (5.6). It can be seen that the approximation of [10] matches well with the results of the ordinary dowels (see Fig. 5.10). It is not possible to compare the different initial stiffness of the SFS dowels with a diameter of 7 mm due to the standardization to an angle of 45° . The point of yielding of high strength steel dowels occur at a later point, therefore the SFS dowels appear to behave with a lesser stiffness compared to ordinary dowels. All of the conducted experiments show a good accordance within the steadily increasing plastic area.

The comparison of the different equations to determine the yield moment shows that the currently valid method determines the yield moment conservatively (see Tab. 5.6). On the other hand the previous equation contained in ENV 1995-1-1 [112] corresponds to the yield moment with a higher accuracy compared to the examined test results.

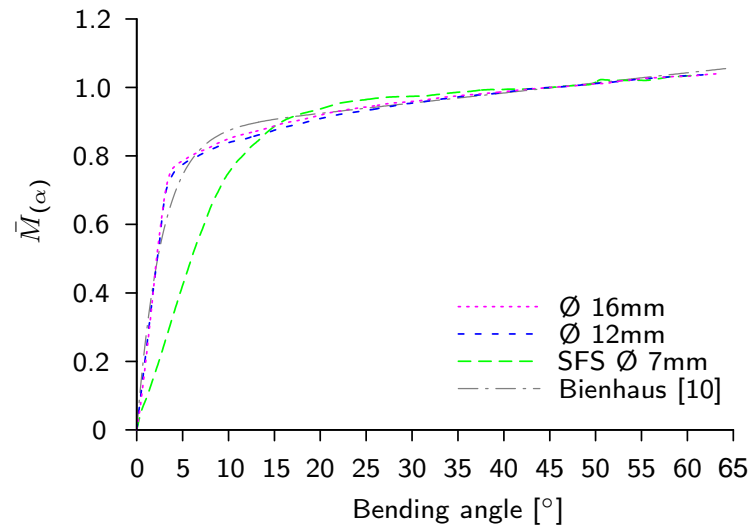


Figure 5.11: Mean value of the derived yield moments compared to Equation (5.6)

Table 5.6: Comparison of the examined yield moments with Equation (5.5) & Equation (5.4)

	MV	$M_{y,k}$ [109]	$M_{y,k}$ [112]	Deviation to [109]	Deviation to [112]
	[Nm]	[Nm]	[Nm]	[%]	[%]
Dowels \varnothing 7mm	28.45	27.35	26.58	-3.8	-6.9
Dowels \varnothing 12mm	147.7	111.5	133.86	-24.5	-9.4
Dowels \varnothing 16mm	324.9	235.5	266.51	-39.1	-18

5.2.3.3 Steel elements

In addition to the investigations on the material properties of the timber lamellae and the dowels, experiments were conducted on steel sheets used to cut out the different flitch plates (see Fig. 5.12(b)). Three dumbbell specimens were cut out of each plate in the direction of rolling and perpendicular to the rolling direction (see Fig. 5.12(a)). Table 5.7 shows the properties of the different plates. The five millimeter thick flitch plates were ordered with a steel grade of S235 JR and the eight millimeter thick flitch plates of a grade S355 JR. The tensile strength is within the limits of EN 10025-2 [100] for both steel grades.

It becomes obvious that the elastic limit ($R_{p0.2}$) and the tensile strength is slightly higher in the direction of rolling compared to the direction perpendicular to rolling.

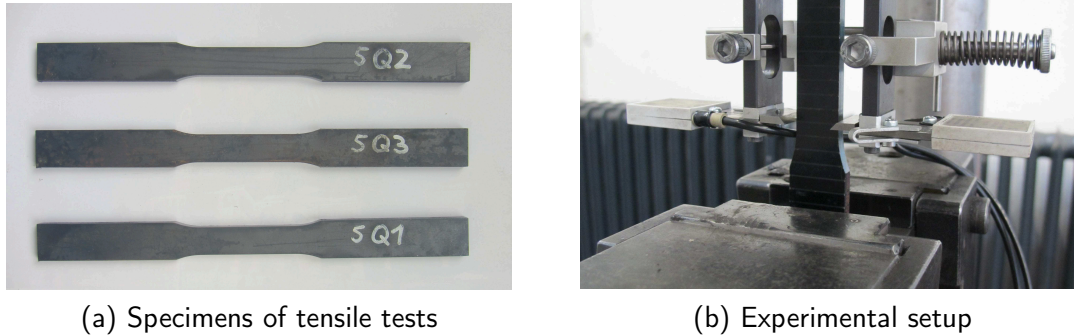


Figure 5.12: Tensile experiments on the steel sheets of the flitch plates

Table 5.7: Statistical properties of the tensile tests of the steel plates

		Mean value	Number of samples	Standard deviation	Coefficient of variation
		$\left[\frac{N}{\text{mm}^2}\right]$		$\left[\frac{N}{\text{mm}^2}\right]$	[%]
t=5mm, para	$R_{p0.2}$	315.3	3	10.96	3.5
	R_m	414.4	3	7.46	1.8
t=5mm, perp	$R_{p0.2}$	303.2	3	4.27	1.4
	R_m	394.3	3	1.66	0.4
$t_1=8\text{mm}$, para	$R_{p0.2}$	466.6	3	2.20	0.5
	R_m	537.0	3	1.10	0.2
$t_1=8\text{mm}$, perp	$R_{p0.2}$	459.4	3	7.12	1.6
	R_m	524.8	3	0.50	0.1
$t_2=8\text{mm}$, para	$R_{p0.2}$	465.2	3	4.06	0.9
	R_m	530.6	3	1.75	0.3
$t_2=8\text{mm}$, perp	$R_{p0.2}$	448.8	3	8.71	1.9
	R_m	522.0	3	2.71	0.5

5.3 Experiments on connections in tension

5.3.1 Test setup

All of the experiments in tension were performed on a servo-hydraulic 1000 kN testing machine. The testings were carried out displacement controlled with a speed of 0.4 mm per minute. The tension specimens had a cross-section of 180 mm times 180 mm. The slots were executed 2 mm wider compared to the width of the flitch plates.

All the experiments in tension, which had taken place in other experiments were planned with a connection on the top and bottom of the specimen. In some cases both of the connections were similar. However, in such a testing method always the weaker connection tends to fail and provides only information about the weaker load-carrying behavior. In some other cases the connection on top of the specimen was designed with a higher load carrying capacity. Hence only the bottom connection was likely to fail, independent of the top connection. To

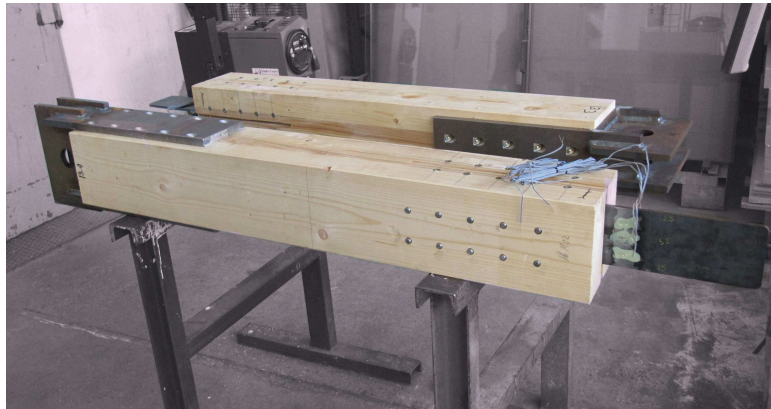


Figure 5.13: Specimens prepared before testing

gain knowledge about the ductile behavior of weak and strong connections a test setup was chosen which examines only one connection. Since fully threaded screws become more and more important, a cover was designed on top of the specimens which was adjusted with fully threaded screws on top (see Fig. 5.13). Such connections have a high load carrying capacity combined with a high stiffness. However, fully threaded screws behave contrary to the research approach since the connection acts in general in a brittle way [49]. The cover was fixed with a bolt at the top of the testing machine. The flitch plate was fixed with clamping jaws at the bottom of the testing machine. Hence an uncomplicated installation of the specimen was reached.

The tension tests were carried out in accordance with EN 26891 [110], as already stated. To gain the important knowledge about the ultimate plastic behavior, it was necessary to revise the rules. Figure 5.14 shows the modified test procedure. The modification does not claim on a termination at a displacement of 15 mm, it continues the testing process until

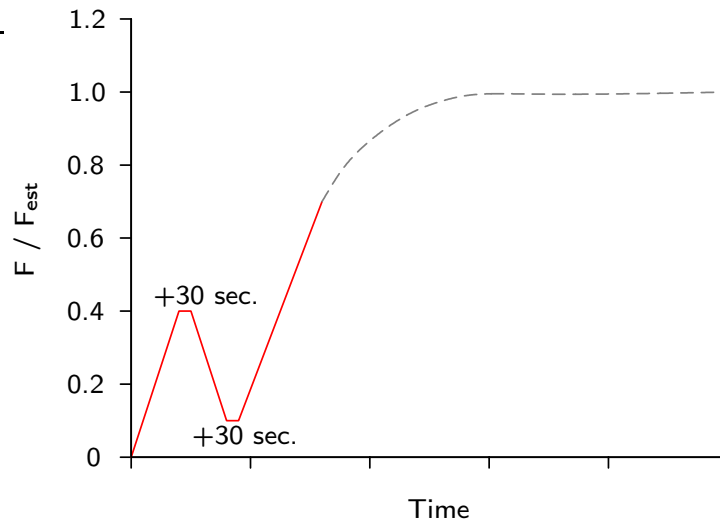


Figure 5.14: Modified test procedure in accordance with EN 26891 [110]

a defined failure occurs. The general procedure is a loading up to 40 % of the estimated maximum load, with a breakpoint of 30 seconds. Afterwards the sample is unloaded until a load level of 10 % is reached. Again, a breakpoint is given for 30 seconds. The specimen is loaded with a continuing displacement in the last loading process till a failure is reached. The failure is either defined as rupture, or as a load decrease to 80 % of the maximum load.

Measuring equipment

The general measuring equipment is displayed in Figure 5.15. Two inductive displacement transducers were placed on either side of the specimen, in the center line of the dowel arrangement, which also form the central axis of the experiment.

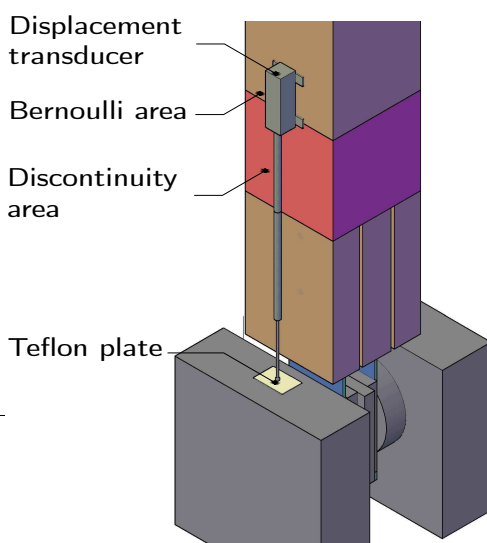


Figure 5.15: Measuring equipment

The fixing of the transducers on the specimens, was shifted out of the discontinuity-area to a undisturbed area of the connection. This area is know as the Bernoulli area (see Fig. 5.15). Locally occurred stress concentrations are in general retrenched in this area. Therefore, the fixing points of the transducers were shifted 180 mm upwards, which coincides with the width of the timber element. The tip of the measuring element was placed on a teflon plate which was placed on the base element of the clamping jaw.

Although the top of the specimen was fixed with a hinge to the testing machine, it could not guarantee that no clamping effect occurs on the bottom fixing due to imperfections. Hence, uniaxial strain gauges were placed on the flitch plates. Therefore, stresses due to bending could be detected.

5.3.2 Results of the experiments on connections in tension

The experimental program implied two different types of dowels with three different diameters. On one hand SFS-WS self-drilling dowels with a diameter of 7 mm, and on the other ordinary dowels with a diameter of 12 mm and 16 mm. The joints with self-drilling dowels were accomplished as double flitch plate connections. Attention was given to the slenderness in the design of the connection. According to Equation (3.13) the optimal slenderness for the mid-section is found as 6.1 (comp. Eq. (5.7)). The embedded strength is calculated according to Equation (3.9) with a density based on Table 5.2. The yield moment is found based on Equation (5.5) with an actual tensile strength given in Table 5.3.

$$\lambda_{exist} = \frac{t_2}{d} = \frac{58}{7} = 8.3 \geq = 1.4 \cdot \sqrt{\frac{8 \cdot M_{u,95}}{f_{h,05} \cdot d^3}} = 1.4 \cdot \sqrt{\frac{8 \cdot 27356}{33,82 \cdot 7^3}} = 6.1 \quad (5.7)$$

The timber thickness t_1 should range between 0.5 to 0.67 of t_2 according to [89] to achieve a ductile behavior (comp. Sec. 3.2.6). Considering a drillbit with a length of 11.8 mm, the actual governed embedded length of the dowel in the side member is 36.2 mm and therefore in the demanded range. Hence the requirements to form a ductile connection are abided.

The slenderness ($\lambda=t/d$) for connections accomplished with a single flitch plate was found as 7.1 for dowels with a diameter of 12 mm, and 5.3 for dowels with a diameter of 16 mm respectively. The rather low slenderness of the 16 mm diameter was chosen as an lower boundary in view of ductility.

The dowel arrangement varied within the different diameters to discuss the influence of the alignment on the ductility and on the load-carrying capacity.

Experiments with a dowel diameter of 7 mm

Figure 5.16 shows the load-deflection behavior of self-drilling dowels with a diameter of 7 mm. The different experiments are standardized to the characteristic load-carrying capacity ($F_{V,Rk}$) based on the actual material properties according to EN 1995-1-1 [109] and DIN EN 1995-1-1/NA [99]. Hence it is possible to compare the different experiments.

Two different load-displacement behaviors could be observed within the test series of 7 mm dowels. The initial stiffness fits well in both cases. The first behavior is characterized by a decrease of the initial stiffness with a constant load increase till rupture. This behavior could be examined on the first and fourth experiment of a dowel arrangement with four dowels

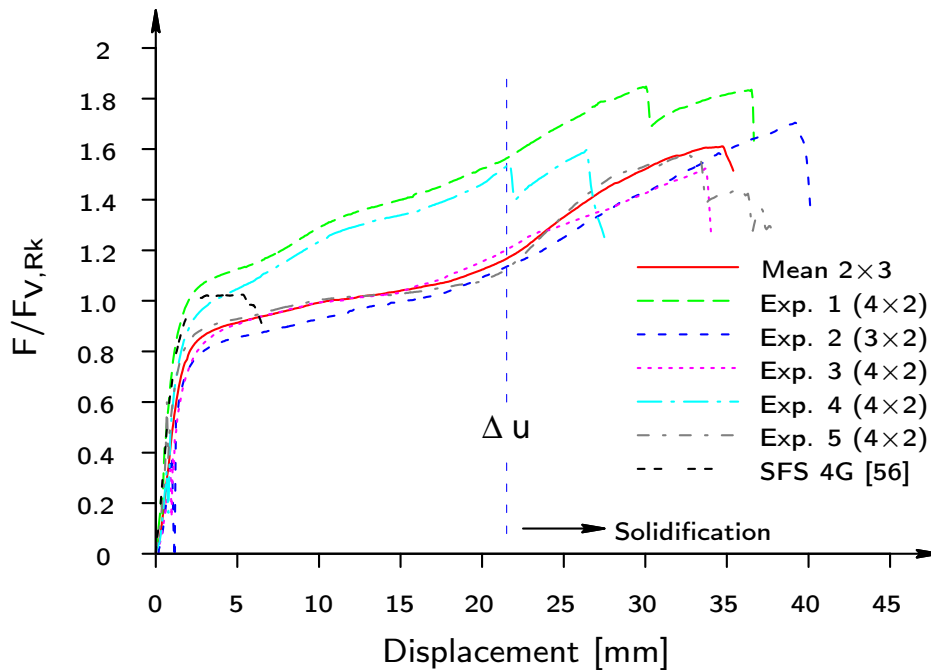


Figure 5.16: Load-deflection behavior of self-drilling dowels with a diameter of 7 mm

in grain direction and two dowel columns. Due to the sharp increase of the ultimate load compared to the calculated ultimate load, one row of dowels was removed in the second experiment. However, the load-displacement behavior turned to the second different modulus in the second experiment. The second modulus was characterized by a pronounced plastic plateau following the initial stiffness. After a displacement of about 20 mm to 22 mm a desired solidification occurred (see Fig. 5.16).

Since this modulus showed a different behavior compared to the first experiment, the dowel arrangement was changed to the originally planned alignment of 4×2. Each load-displacement modulus occurred twice in the test series with 4×2 dowels.

The behavior can be justified as follows. The connection is in both cases in the elastic stage at the beginning. A plastic hinge is formed based on the mechanical model of Johansen [37], thus a plastic plateau occurs in the load-displacement behavior. After reaching a displacement of approximately 50 % of the distance of the reinforcement (Δu), which is the distance of the dowel to the reinforcement, a steady load increase was observed (see Fig. 5.17(a)). In the stage of solidification, the dowel got cramped between the reinforcement, therefore the mechanical model changed and it was possible to increase the load (see Fig. 5.17(b)). On the other hand, the steady load increase in the load-slip behavior of the first modulus is justified with an instantaneous activation of the reinforcement. A locally higher timber strength within the connection may lead to an immediate activation of the fully threaded screws. Since the stiffness is approximately the same for the steady load increase and of the solidification, this is a possible explanation of this phenomena.

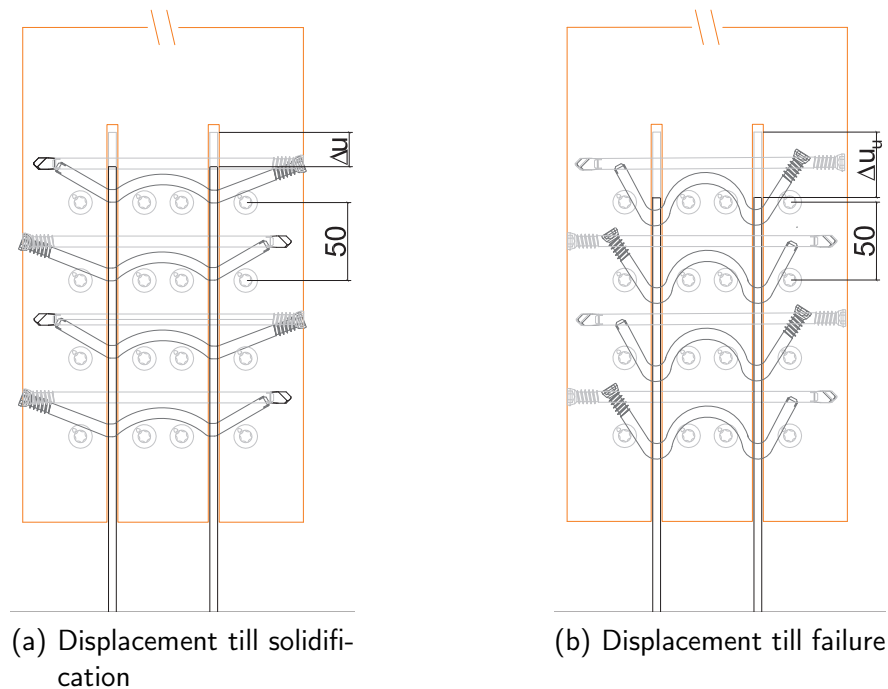


Figure 5.17: Different mechanical properties to declare the solidification on self-drilling dowels

The original connection with 3×3 dowels was revised due to the experience of the previous tests series. One row of dowels was withdrawn to a new arrangement of 2×3 dowels. Only three experiments were performed with the arrangement of 2×3 dowels, since one experiment with 3×2 dowels was conducted additionally in the test series of 4×2 dowels. The displayed mean value in Figure 5.16 consists therefore only of three tests. All experiments of the dowel arrangement with 2×3 dowels showed a solidification

The load-displacement behavior of an unreinforced connection (SFS 4G) [56] is incorporated to Figure 5.16. A clear increase of the ductile behavior due to the reinforcement could be achieved. The dimensions of the specimens and the end and in-between distances of the dowels were almost identical.

The general failure mode was a local block shear failure in the mid-section (t_2) of the connection. However, the failure load was approximately 1.6 times higher than the calculated load according to EN 1995-1-1 [109], with a displacement of 30 mm to 35 mm.

Experiments with a dowel diameter of 12 mm

Experiments on three different dowel arrangements were performed with a diameter of 12 mm. Figure 5.18 shows the mean values of the different experiments. Again, to compare the different experiments the load-displacement behaviors are standardized to the ultimate load

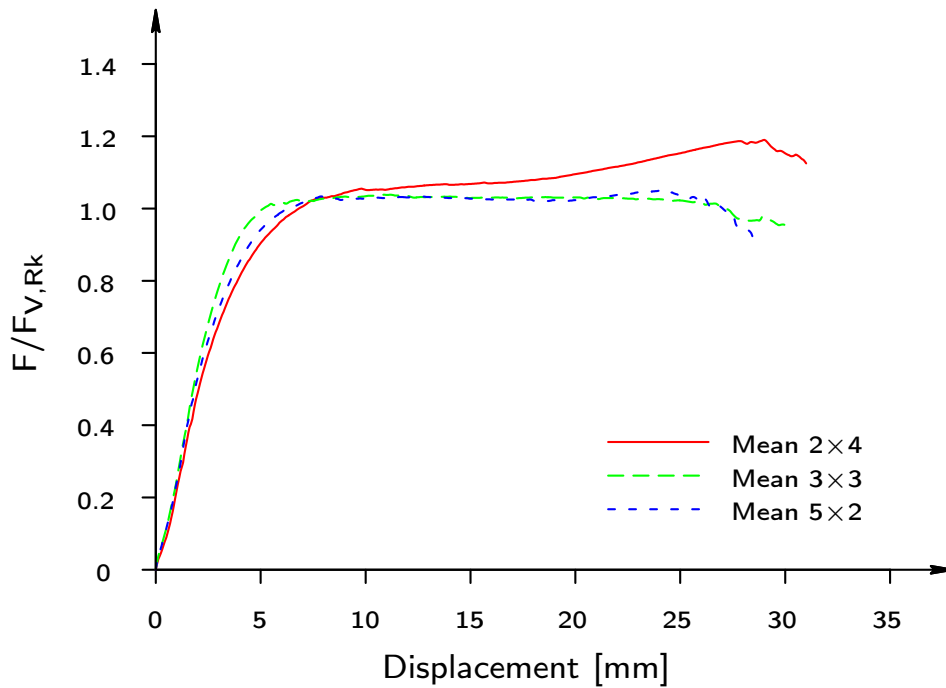


Figure 5.18: Load-deflection behavior of ordinary dowels with a diameter of 12 mm

($F_{V,Rk}$) based on the actual material properties according to EN 1995-1-1 [109] and DIN EN 1995-1-1/NA [99]. The mean values are based on four experiments per dowel arrangement, except the test series of 2×4 dowels where the mean value is based on three experiments. Although all of the specimens were manufactured CNC controlled (comp. Sec. 5.2.2), it was not possible to assemble one connection due to the large differences in the hole pattern.

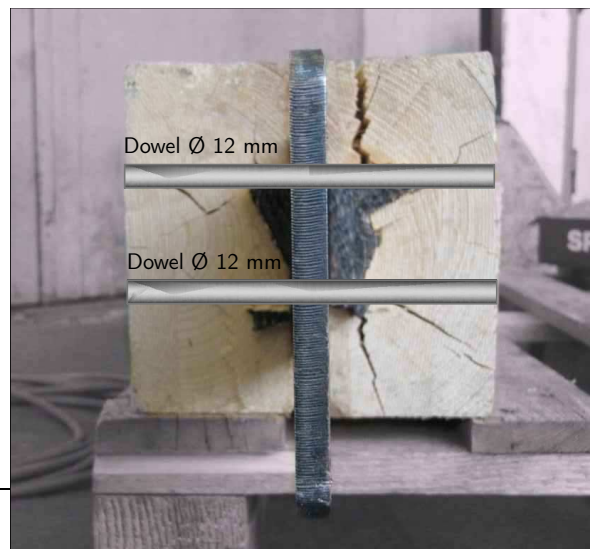


Figure 5.19: Local block shear failure after reaching a large displacement

All the different experiments show a good accordance of the initial stiffness and of the ultimate load-carrying capacity. The ultimate displacement of 25 mm to 30 mm shows a considerable ductile behavior. Hence it can be confirmed, that the effective number of fasteners (n_{ef}) according to EN 1995-1-1 [109] can be neglected if the connection is reinforced with fully threaded screws [82].

The typical failure of the experiments was a local block shear failure (see Fig. 5.19)

Experiments with a dowel diameter of 16 mm

The experiments with a diameter of 16 mm were performed in order to gain knowledge of a reinforced connection with a marginal embedded length of the dowel to gain a ductile behavior.

The first conducted experiment showed an unexpectedly significant ductile behavior (see Fig. 5.20). The failure occurred at a displacement of 32 mm as a result of a local timber failure. The second experiment failed due to a bending-tension failure at the bottom of the slot (see Fig. 5.21(a)) at a displacement of about 7 mm. The bending stresses at the slot were caused by the tilting of the dowel. The third experiment was conducted without any strengthening to gain knowledge of the different failure modes. The experiment failed after 10 mm again caused by a combination of bending and tension. The fourth experiment was strengthened by fully threaded screws to prevent a loading due to bending and tension at the bottom of the slotting. The screws were attached on each side of the flitch plate (see Fig. 5.21(b)).

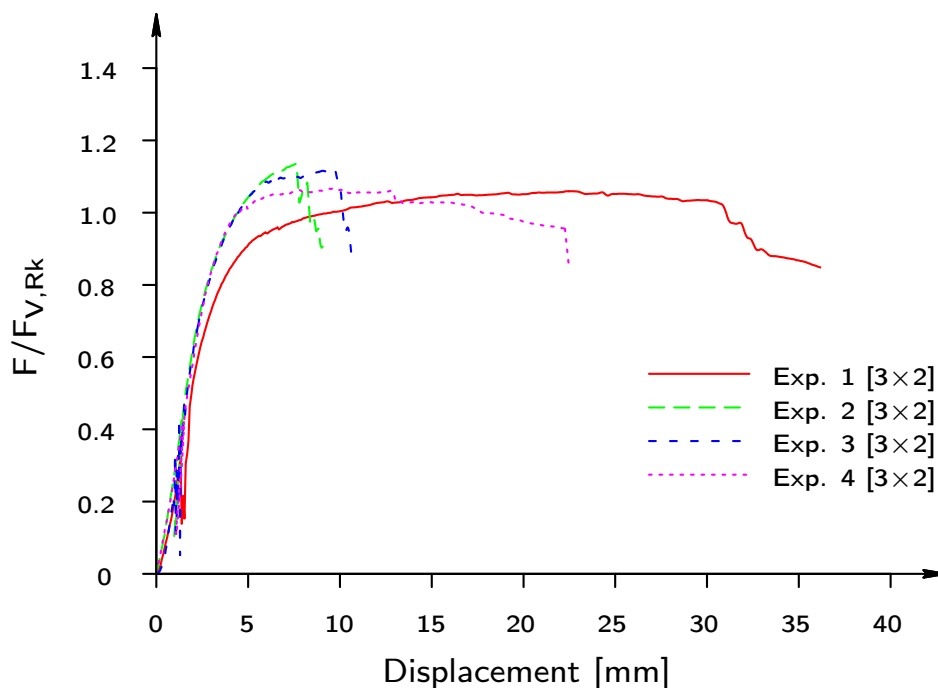


Figure 5.20: Load-deflection behavior of ordinary dowels with a diameter of 16 mm

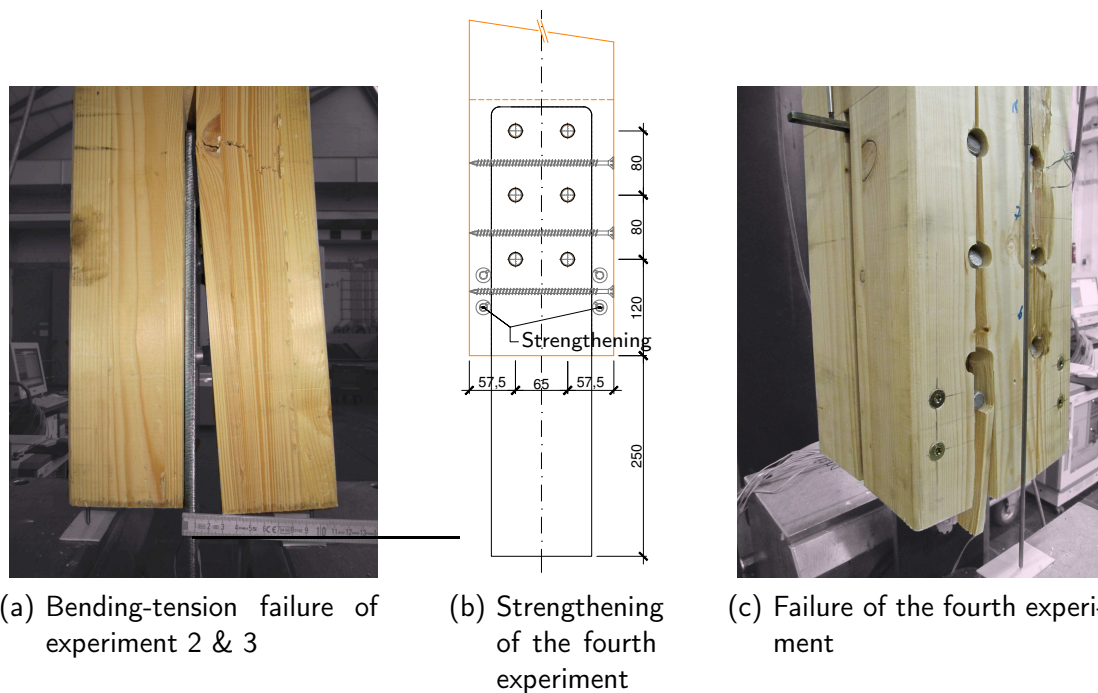


Figure 5.21: Experiments with a dowel diameter of 16 mm

The preventive measure led to an increase of the displacement to approximately 20 mm. A local block shear failure occurred along the dowels columns (see Fig. 5.21(c)). However, the test series with a diameter of 16 mm showed that the behavior is rather brittle compared to the previous experiments.

5.3.3 Ductility evaluation

The methods to evaluate the ductility are explained and discussed in Chapter 4 (see page 47). The investigations on the conducted experiments are based on the selected and explained methods.

The mean value was determined within a test setup to evaluate the ductile behavior. The failure of the mean value was set to the earliest failure within a group.

Table 5.8 shows the determined point of yielding and the displacement at failure. The displacement at failure was set to the displacement at 98 % of the ultimate load (see Fig. 4.8), which was in all cases governed.

The point of yielding increases slightly for reinforced connections with self drilling dowels, whereas the displacement at failure increases significantly (comp. Tab. 5.8 & Tab. 4.9). This supports the claim that it is indispensable to reinforce dowel type connections in view of ductility.

Two investigations with a dowel arrangement of 4×2 on self-drilling dowels were carried out

Table 5.8: Determination of the point of yielding (u_y) of the performed experiments in tension, according to different methods (see Fig. 4.3 & Fig. 4.6)

Test	u_y (b) [mm]	u_y (b_{mod}) [mm]	u_y (e) [mm]	u_y (f) [mm]	u_F [mm]
7_2×3	1.60	1.90	2.05	2.51	34.97*
7_4×2 (a)	1.32	1.58	1.78	2.08	26.56*
7_4×2 (b)	1.57	1.77	1.99	2.43	33.49*
12_2×4	3.27	4.27	3.85	4.36	29.45*
12_3×3	3.23	3.89	3.98	3.74	25.60*
12_5×2	3.15	4.09	3.64	3.81	25.47*
16_3×2	2.72	3.32	3.94	3.26	7.55*

* Displacement at 98% of ultimate load

since two different failure modes occurred. The failure mode (a) represents the characteristic line with a slightly increasing load within the plastic area. Failure mode (b) is described by a horizontal plateau followed by a solidification. The analysis of the two different modi showed that the point of yielding of modus (a) is in general slightly earlier compared to modus (b). The failure occurred at a lower displacement as well. This is caused by the steady load increase. The experiments on self-drilling dowels with an arrangement of 2×3 dowels show the same load-displacement behavior. This is reflected in the ductility parameters. Both test setups obtained most similar data.

Table 5.9: Determination of the ductility ratio on the performed experiments in tension based on Eq. (4.1) & Eq. (4.9)

Test	D_f (b)	D_f (b_{mod})	D_f (e)	D_f (f)	D_{fy} (b)	D_{fy} (b_{mod})	D_{fy} (e)	D_{fy} (f)
7_2×3	21.83	18.40	17.06	13.91	33.37	33.07	32.92	32.46
7_4×2 (a)	20.07	16.76	14.92	12.78	25.23	24.97	24.78	24.48
7_4×2 (b)	21.31	18.90	16.83	13.78	31.92	31.72	31.50	31.06
12_2×4	9.00	6.89	7.65	6.75	26.18	25.18	25.60	25.09
12_3×3	7.93	6.58	6.43	6.85	22.37	21.71	21.62	21.87
12_5×2	8.10	6.23	7.00	6.69	22.33	21.38	21.83	21.67
16_3×2	2.78	2.28	1.92	1.69	4.83	4.23	3.61	3.08

Table 5.10: Determination of the ductility ratio on the performed experiments in tension based on Eq. (4.13)

Test	D_e (b)	D_e (b_{mod})	D_e (e)	D_e (f)
7_2×3	69.55	50.03	41.78	31.07
7_4×2 (a)	66.23	44.57	36.11	27.82
7_4×2 (b)	64.35	51.35	42.36	30.97
12_2×4	23.17	14.25	16.99	13.69
12_3×3	17.69	12.25	11.71	13.48
12_5×2	18.48	11.81	14.88	13.50
16_3×2	4.53	3.09	3.36	2.64

The parameters determined on experiments with a dowel diameter of 12 mm are closely related regardless of the arrangement. The experiments on reinforced self-drilling dowels and on reinforced ordinary dowels are classified as highly ductile based on the extended ductility classification (comp. Tab. 5.9 & Tab. 5.10). The classification of the experiments on dowels with a diameter of 16 mm confirms the brittle behavior (see Tab. 4.9).

5.3.4 Summary and conclusions

Summary

Table 5.12 to Table 5.14 show a summary of the main findings in the experiments. X-ray scans were performed to gain knowledge about the bending angles of the dowels (see App. E). The displayed bending angles α_1 to α_4 on double flitch plate connections are determined as a mean value of all measured angles along one shear plane (see Fig. 5.22(a)). On the other hand, the bending angle α_1 on single flitch plate connections is the bending angle of the dowel itself (see Fig. 5.22(b)). The coefficient of variation of the bending angle is higher on connections accomplished with a dowel diameter of 7 mm. The higher variation could be related with the greater influence of the fully threaded screws and their position.

The ultimate load has a rather low variation per dowel for a diameter of 16 mm. In this case a COV of 3.5 % was determined, The COV for self-drilling dowels with a diameter of 7 mm and the COV for dowels with a diameter of 12 mm is with 6.1 % and 7.6 % respectively still low. All of the experiments except the tests on 16 mm showed a large displacement at ultimate load. This is followed in most cases by a nearby displacement at 98 % of the ultimate load compared to the ultimate displacement. This indicates that the failure occurred often just after reaching ultimate load.

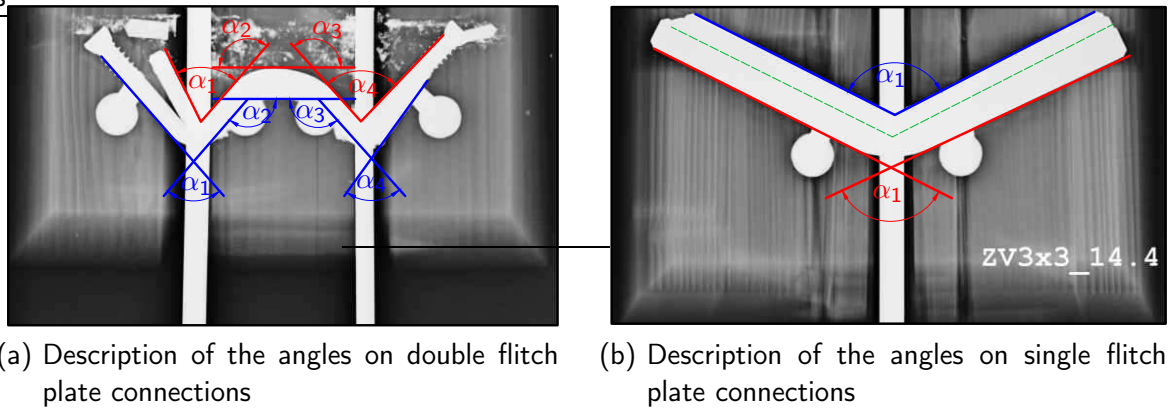


Figure 5.22: Determination of the bending angle at failure

The design of the connections predicted the formation of all plastic hinges within the fasteners. However, only the mid-section of the connections with a dowel diameter of 7 mm met the provision. A still ductile behavior with one plastic hinge per shear plane was found for all other cases. A larger embedded length is required for the examined bigger yield moment of the fasteners (see Tab. 5.5). Therefore, the system between fastener and timber was only able to form one plastic hinge per shear plane. The failure modes (FM) are displayed following the rules of EN 1995-1-1 [109].

The slip modulus (K_{ser}) was determined based on the rules of EN 26891 [110] (comp. Eq. (5.8)). The slip modulus of one dowel was calculated to determine the variation with a type of fastener.

$$K_{ser} = \frac{0.4 \cdot F_{max}}{v_{i,mod}} \quad (5.8)$$

$$v_{i,mod} = \frac{4}{3} \cdot (v_{04} - v_{01}) \quad (5.9)$$

with : v_{01} : Displacement at 10 % of ultimate load
 v_{04} : Displacement at 40 % of ultimate load

The lowest variation in the slip modulus, with a COV of 12,4 %, was determined on ordinary dowels with a diameter of 16 mm, followed by the dowels with a diameter of 12 mm with a COV of 13,7 %.

Table 5.11: Mean densities of the specimen with $4 \times 2 \text{ } \varnothing 7 \text{ mm}$ dowels

	7_4x2_1	7_3x2_2	7_4x2_3	7_4x2_4	7_4x2_5
Mean density	450.8 kg/m ³	415.2 kg/m ³	410.2 kg/m ³	463.2 kg/m ³	437.8 kg/m ³

Table 5.12: Connection test results of tension experiments on self drilling dowels with a diameter of 7 mm

Exp.	No. of dowels	F_{max} [kN]	u_u [mm]	u_f (98% F_{max}) [mm]	FM			K _{ser}				Bending angle [°]				COV [%]			
					t_1	t_2	t_i	t_i	t_i	K_{ser} [kNmm]	α_1	α_2	α_3	α_4	α_1	α_2	α_3	α_4	
E	4×2_1	293.1	29.9	30.1	(d)	(m)	(d)	(d)	119.9	79.0	130.0	142.5	94.4	12.4	2.5	2	12.4		
	4×2_3	241.3	33.7	33.8	(d)	(m)	(d)	(d)	75.1	89.9	137.4	151.9	82.5	12.6	4.4	21.8	7.8		
	4×2_4	252.9	26.4	26.5	(d)	(m)	(d)	(d)	110.5	86.8	137.3	137.8	93	11.6	2.0	2.8	6		
	4×2_5	251.1	32.7	33.4	(d)	(m)	(d)	(d)	96.5	83.1	141.5	145.8	88.4	11.3	5.8	5.6	12.5		
	2×3_1	197.9	38.4	39.1	(d)	(m)	(d)	(d)	65.9	84.8	138.5	136.8	77.8	6.2	6.3	4.4	15.6		
E	2×3_2	191.3	40.8	41.3	(d)	(m)	(d)	(d)	58.7	69.2	128.7	127.5	74.8	5.7	0.6	2.8	7.5		
	2×3_3	202.5	33.6	34.8	(d)	(m)	(d)	(d)	75.1	86.8	139.2	139.3	81.7	8.0	1.2	1.4	9.3		
Ø	3×2_1	202.8	39.2	39.4	(d)	(m)	(d)	(d)	54.1	82.0	135	130.7	76.5	6.3	4.2	3.5	11.7		

Table 5.13: Connection test results of tension experiments on ordinary dowels with a diameter of 16 mm

Exp.	No. of dowels	F_{max} [kN]	u_u [mm]	u_f (98% F_{max}) [mm]	FM		K _{ser} [kNmm]	Bending angle [°]		COV [%]
					t_1	t_i		α_1	α_1	
E	3×2_1	246.9	22.3	27.8	(d)	(d)	79.2	124.7	0.8	
	3×2_2	264.5	7.3	7.4	(d)	(d)	84.9	148.3	2.1	
E	3×2_3	261.2	9.3	9.5	(d)	(d)	96.0	156.5	0.5	
	3×2_4	248.6	9.3	12.7	(d)	(d)	71.6	156.5	0.5	

Table 5.14: Connection test results of tension experiments on ordinary dowels with a diameter of 12 mm

Exp.	No. of dowels	F_{\max} [kN]	u_u [mm]	u_f (98% F_{\max}) [mm]	FM		K_{ser} [kNmm]	Bending angle [°]		COV [%]
					t_1	$t_{\bar{1}}$		α_1	α_1	
2×4_1	8	266.3	29.0	29.2	(d)	(d)	54.2	117.9	1.7	
2×4_2	8	258.2	30.7	31.1	(d)	(d)	63.9	108.8	1.0	
2×4_4	8	231.8	32.6	32.8	(d)	(d)	58.9	119.8	1.3	
3×3_1	9	242.4	29.8	30.0	(d)	(d)	64.6	127.3	1.0	
3×3_2	9	248.0	18.6	21.0	(d)	(d)	70.3	133.3	1.1	
3×3_3	9	251.9	7	23.3	(d)	(d)	78.4	129.3	0.7	
3×3_4	9	257.5	9.4	12.1	(d)	(d)	66.8	127.7	1.2	
5×2_1	10	259.5	7.8	8.0	(d)	(d)	87.2	134.2	1.0	
5×2_2	10	291.0	23.1	24.3	(d)	(d)	68.9	127.3	1.6	
5×2_3	10	275.9	8.0	16.6	(d)	(d)	77.5	131.4	0.9	
5×2_4	10	297.1	25.2	25.4	(d)	(d)	64.5	132.9	1.0	

The experiments on self-drilling dowels showed the highest variation with a COV of 18,7 %. It is noticeable that the connections on self-drilling dowels with a steady slight load increase in the plastic area (modulus 1, see Fig. 5.16) have the highest slip modulus. This is a further indication of a higher density of timber of those connections.

The analysis of the grading data shows, that the mean density of the specimens of the experiment one and four is indeed higher compared to the other specimens (see Tab. 5.11).

Conclusions

To draw a conclusion, it has been shown, that it is possible to achieve connections with a ductile behavior under tension. The driving parameter is the prevention of a possible splitting of the timber which was achieved by self drilling screws. The evaluation based on the selected

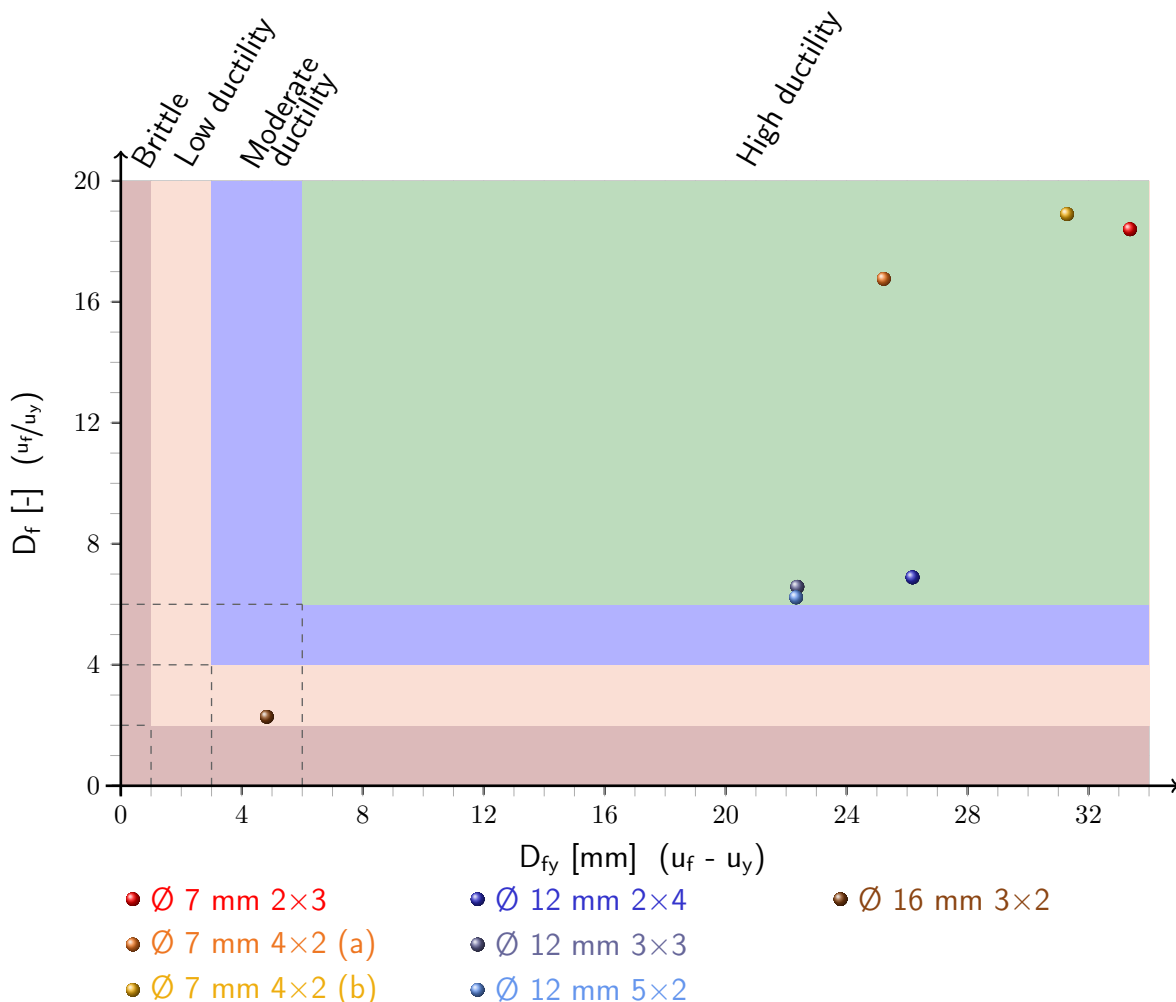


Figure 5.23: Illustration of the determined absolute (D_{fy} (b_{mod})) and relative (D_f (b_{mod})) ductility ratios

classification methods shows that the experiments can be rated as highly ductile (see Fig. 5.23). The experiments with a dowel diameter of 16 mm failed prematurely, due to a tension - bending failure of the timber fingers. Since a doweled connection provides bolts within a group of fasteners, that failure is normally not governed.

The investigation also established that it is possible to achieve a limit deformation of 20 mm - 30 mm. In order to gain benefits of the plastic deformation, investigations need to be conducted to assess the formation of a plastic hinge.

5.4 Experiments on joints in bending

5.4.1 Test setup

A possible formation of plastic hinges is based on moment resisting joints. To gain knowledge of feasibility of such joints it is indispensable to perform experiments. Hence four-point bending tests were conducted to prove the rotational capacity of moment resisting joints. The bending moment was transferred by a defined compression zone (steel block 65 mm × 180 mm) on the top and the previous tested dowel arrangements in the tension zone (see Fig. 5.24). The cross-section of the timber beams was 180 mm × 320 mm. The beams

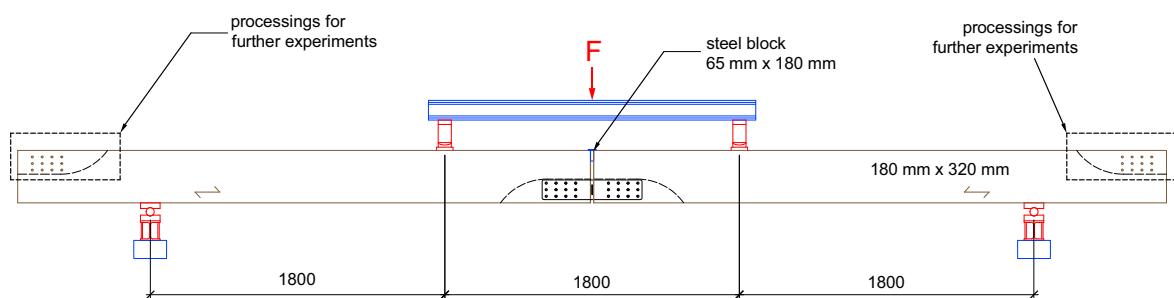


Figure 5.24: Test setup of the four-point bending test

were designed in such a way, that a yielding of the connection takes place before the net cross-section fails in a brittle manner. To gain the greatest benefit of the timber beams, it was tried to use each beam twice. Therefore the beam was slightly elongated with a second connection prefabrication at the end (see Fig. 5.24). The specimens were removed and the proved joint was sawn out. The beams were rotated by 180 degrees and the second connection was installed.

A 400 kN hydraulic jack was installed in the middle of the test setup which transferred the load via a crossbar to the third points of the specimen. To prove the splitting of the initiated force, a load cell was installed between the traverse and the calotte on the beam. Hence the



Figure 5.25: Failure at preliminary experiments due to tension perpendicular to the grain

actual acting moment could be recalculated.

The configuration of the group of dowels was reinforced with self-drilling fully threaded screws (\varnothing 8 mm) as well (see Fig. 5.26(a)). Preliminary experiments had pointed out that a bending moment emerged due to the rotation on either side of the joint. Hence stresses perpendicular to the grain direction occurred besides shear stresses on the timber side members (see Fig. 5.25). As a result of the observation, fully threaded screws were extended above the upper row of the dowels to absorb the stresses perpendicular to the grain, additionally to the prevention of a possible timber splitting at the dowel arrangement (see Fig. 5.26(b)).

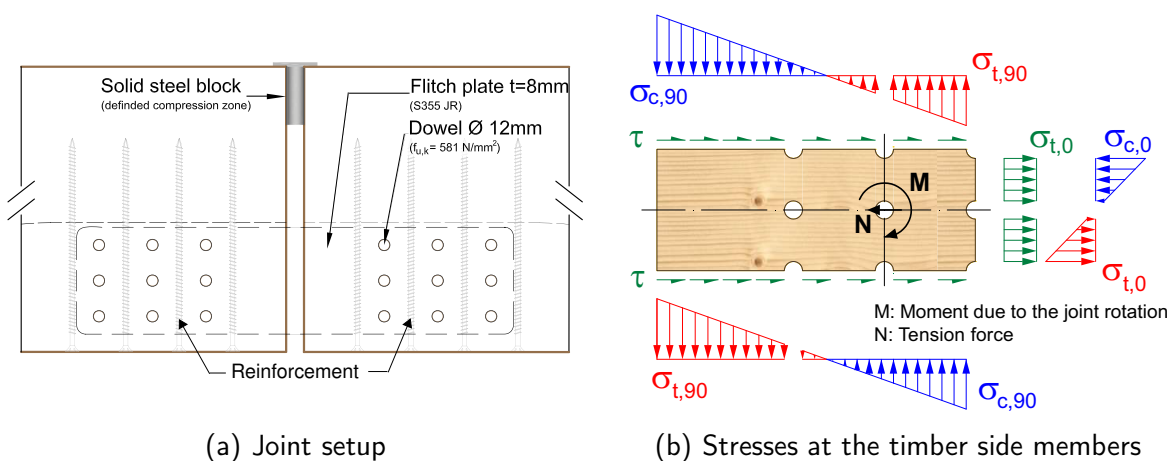


Figure 5.26: Reinforcement and additional stresses on joints loaded in bending

Measuring equipment

The measurement devices were attached in accordance with the previously described load distribution. Two inductive displacement transducers were placed in the compression and tension zone on each side of the joint (see Fig. 5.27). The displacement transducers were placed at the undisturbed area therefore the attachment was shifted 180 mm towards the supports.

The transducers were placed in the middle of either the compression zone or of the center line of the dowel group. Hence the displacement was clearly measured. To attach the tips of the measuring devices, small steel plates were welded on the compression block and to the flitch plates as supports for the tips.

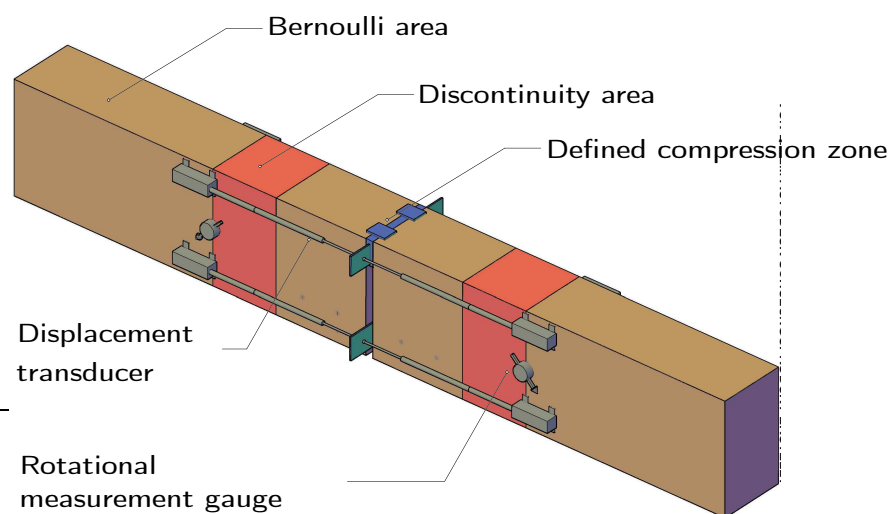


Figure 5.27: Measuring equipment on the experiments in bending

In addition to the displacement transducers, rotational measurement gauges were installed in the middle of the beam height. The distance from the connection to the fixing was also chosen to 180 mm. Therefore the rotation was recorded on every side of the joint. Furthermore, strain gauges were installed to gain knowledge about the stresses in the flitch plates.

5.4.2 Results of the experiments on joints in bending

Four point bending tests were performed in order to examine the behavior of moment resisting joints. The aim of the experiments was to gain knowledge of the rotational capacity of such joints. The geometrical properties of the single components were equal to the tension experiments, in order to compare the different results and to check the subsequent developed component model (comp. Sec. 6).

The mean value of the rotation on the left and right hand side was determined as a first

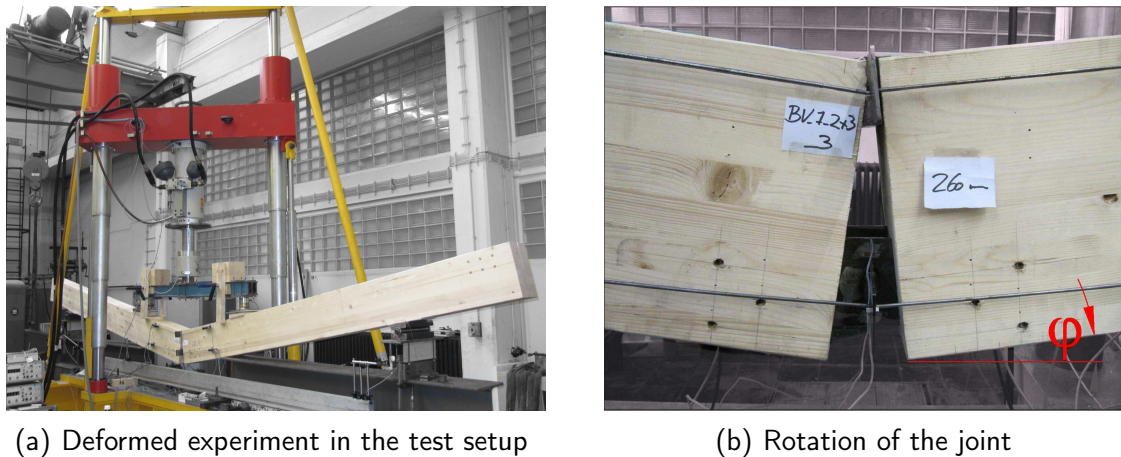


Figure 5.28: Four-point bending experiment

step. Furthermore, the mean value of the rotation on the left and right hand side was ascertained for the evaluation and the comparability of the single experiments. Hence the displayed mean value consists of four different measuring points. The rotations refer to the original neutral position of either side of the joint (see Fig. 5.28(b)). The test procedure was stopped on defined points to gain knowledge on the relaxing behavior of the joint. This lead to discontinuities within the graphical representation of the

moment-rotation behavior. Furthermore, the experiments were completely driven back at a rotation φ of about 80 mrad. This became necessary because the hydraulic jack was completely extended at this point. A wedge was placed within the readjustment between the timber beam and the calotte, since the adjusted rotation acquires high values (see Fig. 5.29).

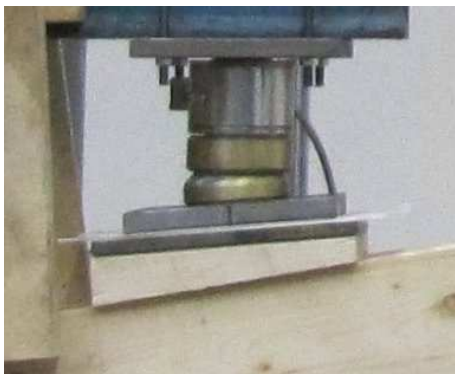


Figure 5.29: Required wedge

The position of the flitch plate was measured in all experiments. It was stated that the flitch plates hardly moved from the horizontal position. Therefore, it was ensured that the right and left side of the joint acted in the same way.

Experiments with a dowel diameter of 7 mm

Figure 5.30 shows the mean values of the moment-rotation behavior on double flitch plate connections with self-drilling dowels. The different test results are normalized to the maximum achieved bending moment of 51.7 kNm of the second experiment with an arrangement of 4×2 dowels.

The general behavior followed the behavior achieved in the tension tests. A linear-elastic

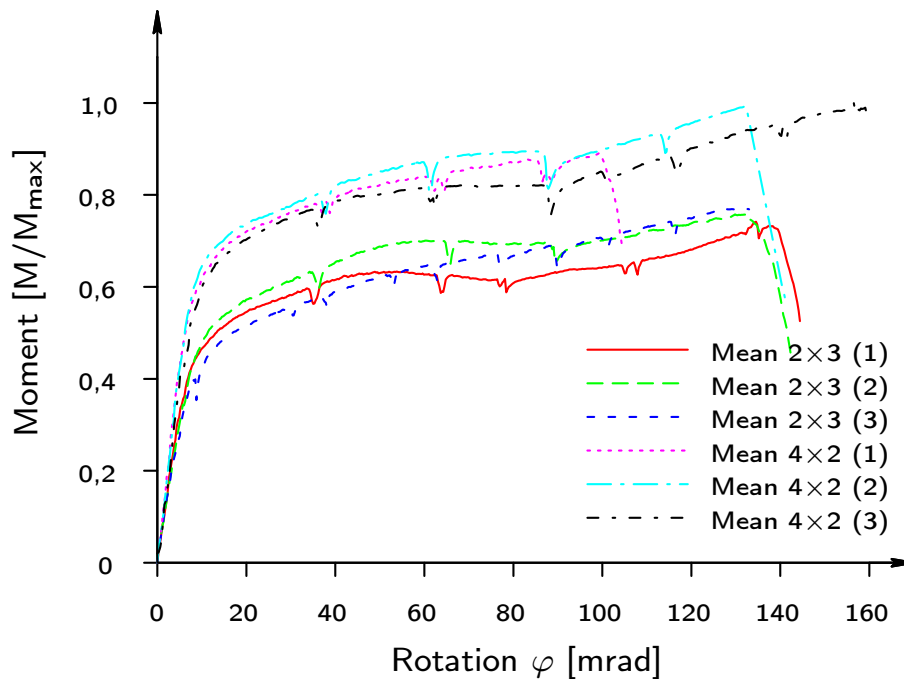


Figure 5.30: Moment-rotation behavior with a dowel diameter of 7 mm

behavior was observed at the beginning of the experiments. The stiffness decreased followed by a plastic deformation. All experiments with a dowel arrangement of 4×2 dowels showed a solidification at about $80 - 90$ mrad (modus b). The test setup with an alignment of 2×3 dowels showed the same behavior as the first and second experiment. The third experiment differed, a slightly steady increasing of the moment occurred without a pronounced solidification (modus a).

The first experiment of the dowel alignment of 4×2 dowels failed at a rotation of about 100 mrad. This was caused by a rather poor timber quality due to a timber failure of the middle member. The second and the third experiment showed a ductile behavior. The experiments showed, that stretched connections in the tension zone (4×2) are more endangered by a failure of the mid-section compared to compact connections of 2×3 dowels. This is caused by the higher stresses perpendicular to the grain in combination with shear along the outside margin on stretched connections (see Fig. 5.26(b)).

Experiments with a dowel diameter of 12 mm

The mean values of the experiments performed with an diameter of 12 mm are displayed in Figure 5.31. The results of the experiments are normalized to the maximum achieved bending moment of 64.1 kNm of the second experiment with a dowel arrangement of 5×2 dowels. All of the conducted experiments showed a pronounced ductile behavior of approximately 140 mrad ($\approx 8^\circ$). One exception is given by the second experiment with a dowel arrangement of 5×2 dowels. The experiment failed at an earlier stage due to the combination of shear and

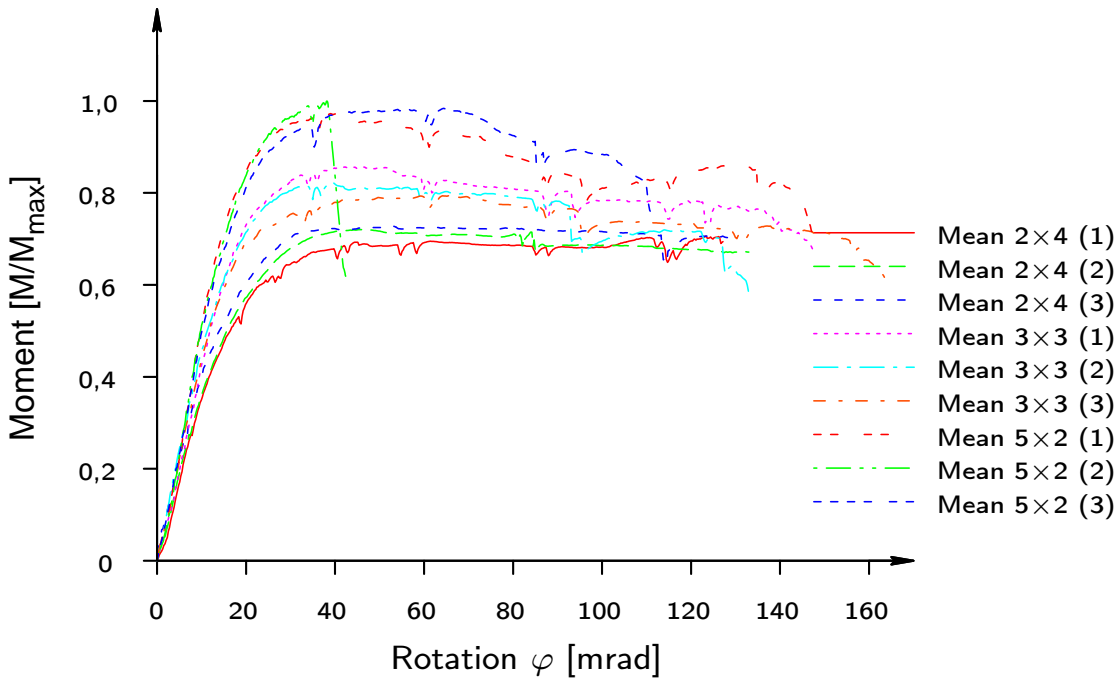


Figure 5.31: Moment-rotation behavior with a dowel diameter of 12 mm

stresses perpendicular to the grain. However, stretched connections tend to fail due to high stresses perpendicular to the grain in combination with shear stresses in the lowest dowel row (see Fig. 5.32). Therefore the first experiment of this test series failed also due to the same failure mode. On the other hand, the third experiment was the only joint which failed due to a bending tensile failure of the flitch plate at a rotation of approximately 110 mrad. The experiments on joints were consciously performed although the experiments in tension exhibited a high load-carrying capacity. Hence, the pre-design load of the joint was exceeded. However, the experiments with 5×2 dowels were performed despite the knowledge of a higher load carrying capacity to gain information of the influence of stretched arrangements on the

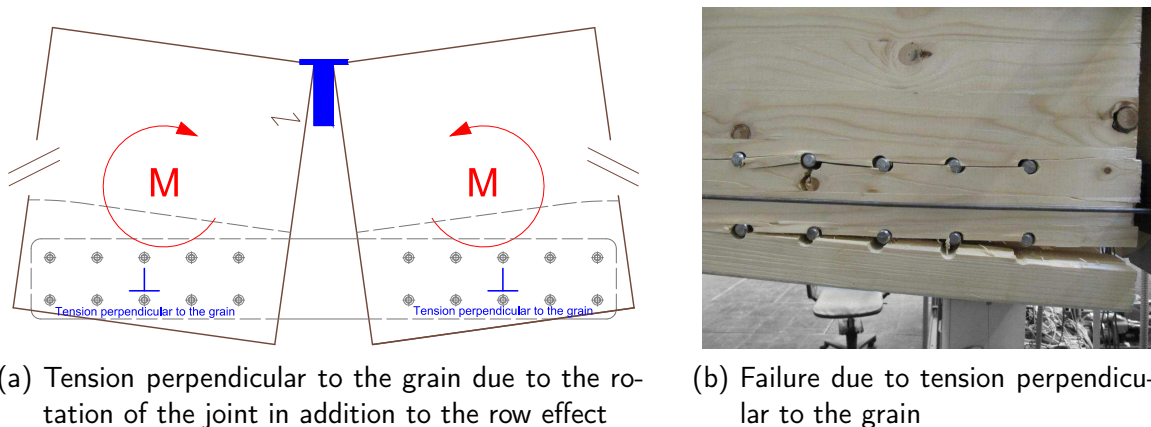


Figure 5.32: Typical failure on stretched arrangements

rotational capacity of joints.

It is apparent that the influence of a decreasing plastic plateau is more pronounced in stretched dowel arrangements 5×2 compared to wider alignments 2×4 (see Fig. 5.31). This is caused due to a geometrical influence, which is explained in Section 6. Furthermore it is evident that the moment load carrying capacity is not only dependent on the number of dowels but also on the arrangement. Ten dowels in two columns (5×2) achieve the highest moment load carrying capacity. On the other hand, the load carrying capacity of eight dowels in 4 columns (2×4) achieved a moment load carrying capacity of about 70 % of the joint with ten dowels. This gives first information of a possible influence of an inner lever arm.

Experiments with a dowel diameter of 16 mm

The experiments with a dowel diameter of 16 mm were conducted although the experiments in tension showed a rather brittle failure.

The tests showed a significant rotational capacity, contrary to the findings of the tension testing. The testing had to be terminated at a rotation of 160 mrad. The timber beams

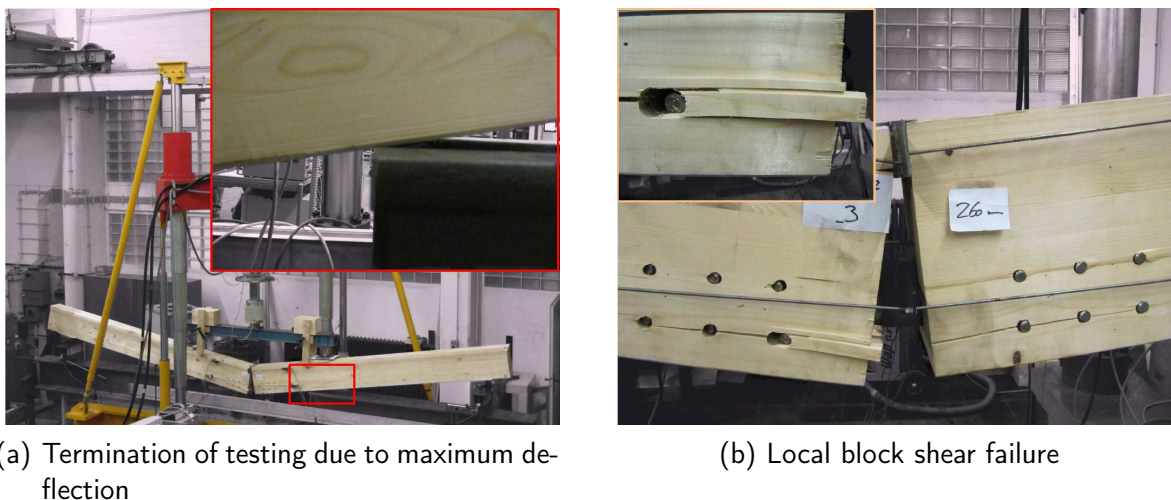


Figure 5.33: Observations within the test setup with 16 mm dowels

touched the supporting beam of the experiment setup at this stage (see Fig. 5.33(a)). The typical failure was a local block shear failure along the dowels (see Fig. 5.33(b)), which occurred at a large rotation.

Figure 5.34 shows the results of the three experiments with a dowel diameter of 16 mm. The experiments were normalized to the maximum bending moment of 55.3 kNm, achieved at the first experiment. The initial stiffness and the moment carrying capacity fits well within the test-setup. The slot pattern of the beams was only partially at the bottom of the specimens in contrast to the tension experiments with a slot from one side of the element to the other. The timber side members were linked to the beam on the top by fully threaded screws.

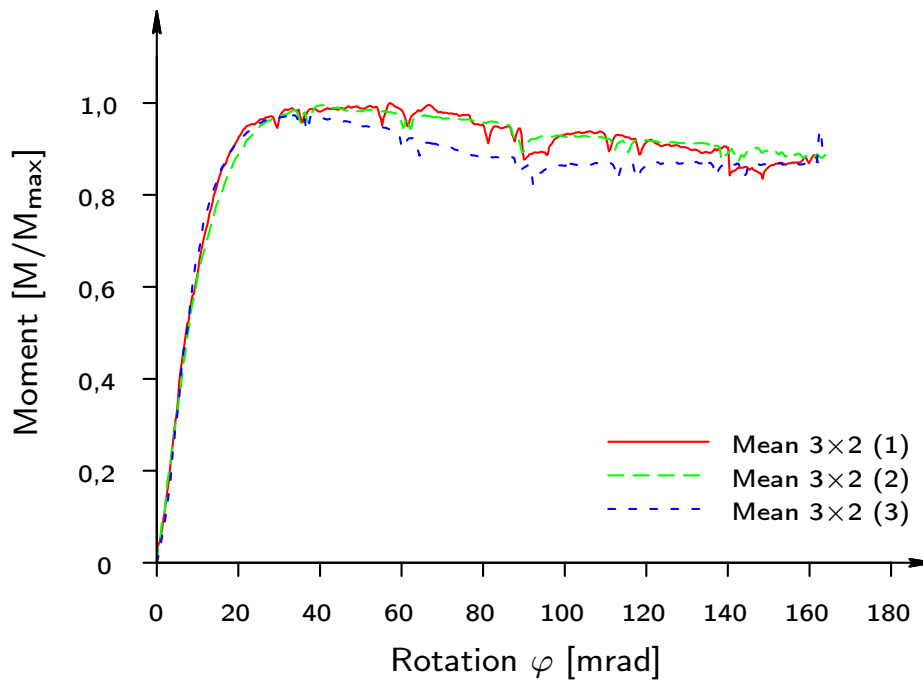


Figure 5.34: Moment-rotation behavior with a dowel diameter of 16 mm

The danger of a bending tension failure was therefore reduced. A slight decreasing of the moment load carrying capacity was observed as well, which agrees well with the findings of the experiments with a diameter of 12 mm.

5.4.3 Ductility evaluation

Table 5.15 shows the rotation at yielding of the different experiments conducted in bending. The evaluation is based on the methods explained in Section 4.2.

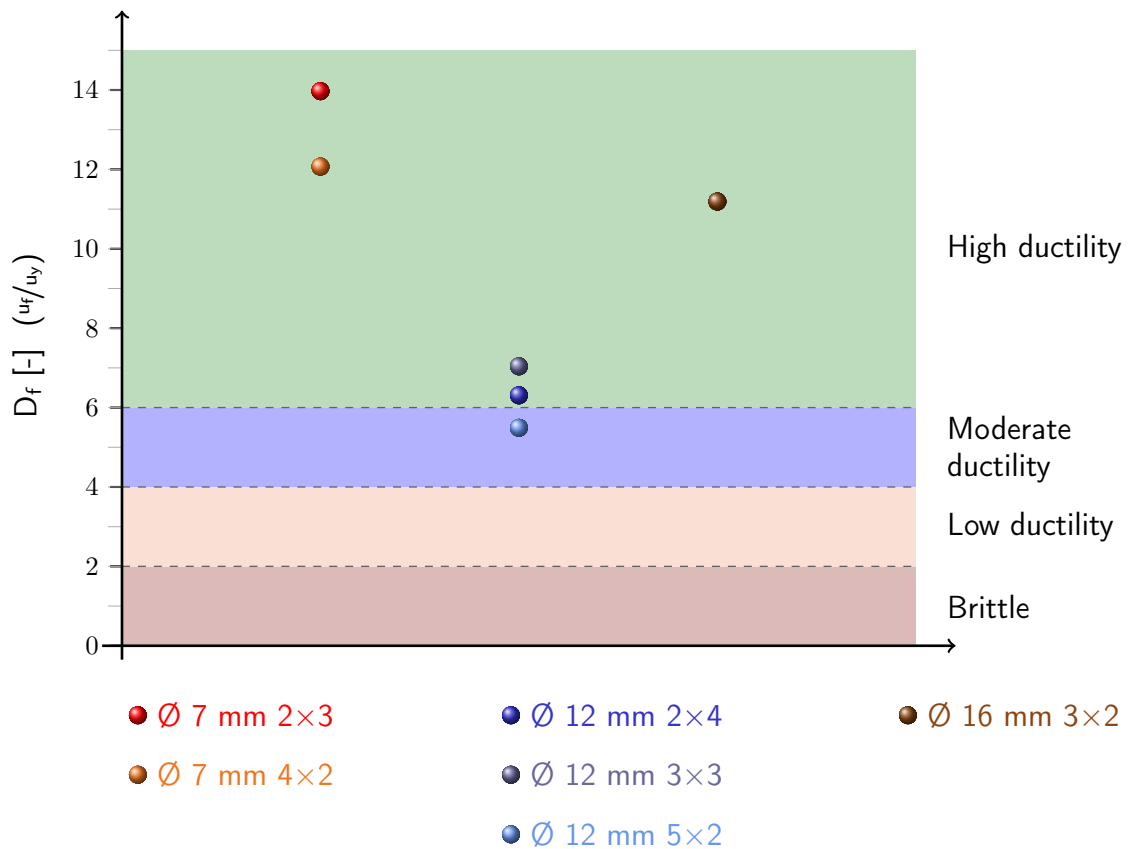
Table 5.15: Determination of the point of yielding (φ_y) of the performed experiments in bending (comp. Sec. 4.2.1.2)

Test	φ_y (b) [mrad]	φ_y (b _{mod}) [mrad]	φ_y (f) [mrad]	φ_F [mrad]
7_2×3	7.44	9.51	10.67	132.8
7_4×2	6.73	8.38	9.58	101.1
12_2×4	15.02	20.14	18.33	127.2
12_3×3	15.62	18.92	17.60	133.2
12_5×2	16.78	20.33	18.57	111.6
16_3×2	11.20	14.50	13.34	162.6

Table 5.16: Determination of the ductility ratio on the performed experiments in bending based on Eq. 4.1 & Eq. 4.13

Test	D_f (b)	D_f (b_{mod})	D_f (f)	D_e (b)	D_e (b_{mod})	D_e (f)
7_2×3	17.85	13.97	12.45	49.65	32.87	26.98
7_4×2	15.02	12.07	10.55	42.10	28.53	22.61
12_2×4	8.47	6.31	6.94	20.07	11.86	14.20
12_3×3	8.53	7.04	7.57	18.47	12.89	14.80
12_5×2	6.65	5.49	6.01	13.76	9.65	11.39
16_3×2	14.48	11.19	12.16	34.92	21.44	25.01

It is not possible to apply the method of a 5% diameter offset by AF & PA [1] on experiments in bending, since a contradiction occurs within the definition. The abscissa shows the rotation φ which does not conform with the definition of the point of yielding. The point of yielding is defined as a certain percentage of the dowel diameter (see Fig. 4.3(e)). Therefore, no

**Figure 5.35:** Illustration of the determined relative ductility ratio (D_f (b_{mod}))

conclusion could be drawn for the definition given by AF & PA [1].

The ductile behavior and therefore the classification of the joint strictly depends on the chosen fasteners. Attention has to be given, to the issue if the joint is able to activate the ductility of the fasteners itself to form a plastic hinge. Therefore, the classification of the joints is based on the relative ratio (D_f). The appraisal given by Smith et al. [69] classifies all experiments as highly ductile (see Table 5.16 & Figure 5.35). The experiment with a dowel diameter of 12 mm and an arrangement of 5×2 forms an exception. The classification as moderate ductile is based on the elongated alignment of the dowels, which causes an earlier failure (see Fig. 5.35). However, a rotational capacity of over 100 mrad underlines the significant ductile behavior of the conducted experiments (see Tab. 5.15).

5.5 Miscellaneous experimental research

5.5.1 Introduction

The previous experiments pointed out, that stresses perpendicular to the grain have a large influence on the ability to form a plastic hinge. Therefore the testing matrix was extended to gain knowledge of reinforced doweled connection loaded perpendicular to the grain [51]. Furthermore, the ductile behavior is currently embedded within the seismic design. Hence experiments were conducted under a cyclic loading to gain knowledge of the ductile behavior under a changing load [73].

5.5.2 Experiments in tension perpendicular to the grain

Figure 5.36 shows the general test setup of the conducted experiments perpendicular to the grain. This type of connection can be for instance installed at overlapped purlins and contributes to a possible load redistribution of the system [51].

The general idea was a test setup with a testing of two specimens next to each other. Each specimen consisted of four dowels with one shear plane (see Fig. 5.36(a)). The dowels of the different specimens met each other at the center line of the test setup. The load was introduced via a halved HEB 220 profile and fully threaded screws to both mid-section timber members. The two side members were tied back with two U-profile members at the edges of the specimens (see Fig. 5.36(b)). Each side of the connection was reinforced with two fully threaded screws to prevent a splitting of the timber.

The chosen dowels had a diameter of 12 mm and were ordered with a steel grade of S235 JR. Tensile experiments were also carried out to prove the actual tensile strength. The examination showed a steel strength of 573 N/mm^2 . The mean density of the experiments was determined to 456.5 kg/m^3 [51]. The experiments were performed in accordance with the rules of EN 26891 [110] as well.

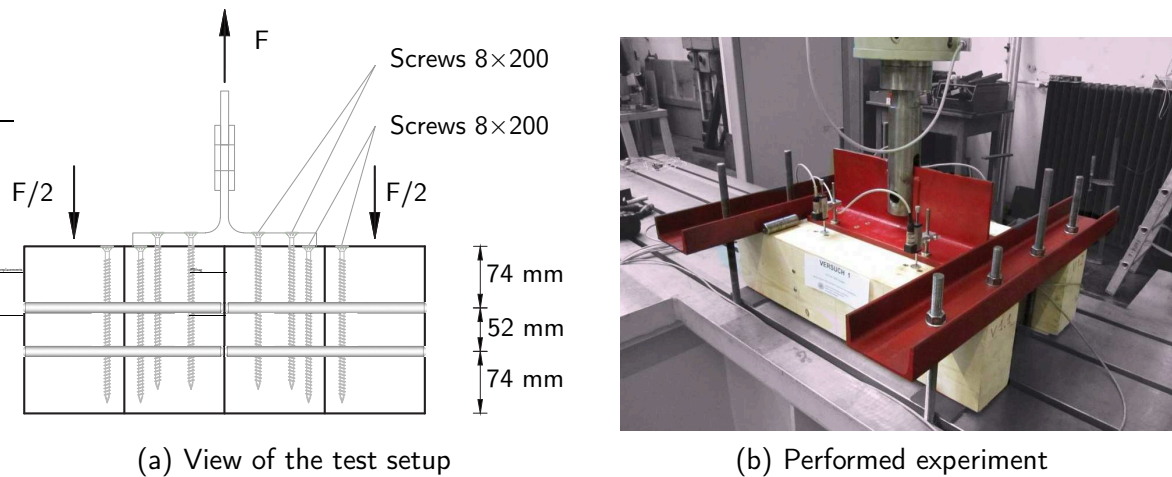


Figure 5.36: Experiments perpendicular to the grain [51]

Measuring equipment

The displacement transducer were placed at mid-section to record the relative displacement between the two timber members at the position of the dowels (see Fig. 5.36(b)). The absolute displacement was measured between the middle timber members and the testing apparatus. Hence the position of the middle members was recorded and possible load inequalities could be detected.

It was ensured that locally non-uniform displacements as well as inequalities within the single connections could be recognized with the chosen measuring equipment.

Results of the experiments

Four experiments on connections perpendicular to the grain were performed to prove a possible ductile behavior. Figure 5.37 shows the mean value of four connections within one experiment. The evaluation of the different load-deflection behaviors within one experiment showed, that all dowels participated in almost equal parts on the load transfer. Only marginal differences could be measured within the different connections.

The fourth experiment was conducted with only four dowels instead of eight dowels to gain more knowledge of the interaction between the single connections. The general load-displacement behavior remained the same compared to the experiments with eight dowels (see Fig. 5.37; Exp. 4 (doubled)). Hence it can be expected that all dowels are acting in the same way.

The general load-displacement differs greatly from the behavior parallel to the grain direction. The experiments perpendicular to the grain exhibit no pronounced plastic plateau. A steady load increase with a slight decreasing of the stiffness was detected. This phenomenon is caused by a rupture of single wood fibers and an activation of the nearby fibers (see Fig.

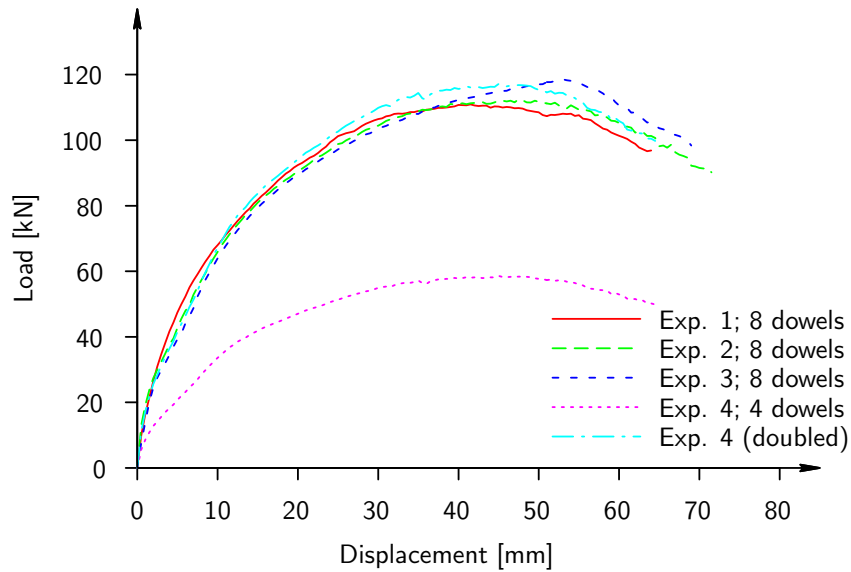


Figure 5.37: Load-displacement behavior of connections perpendicular to grain [51]

5.38). The single fibers are acting as a rope effect supported by the reinforcement screws. The load carrying capacity based on the ascertained material properties is calculated to 7.56 kN according to DIN EN 1995-1-1/NA [99]. However, the experiments showed an ultimate load of almost 15 kN per shear plane at a displacement of approximately 43 mm, which is almost twice as much. Considering the rules of EN 26891 [110], which describe the ultimate load within a displacement of 15 mm, gives an ultimate load of 10.2 kN.



(a) View on the shear plane



(b) Timber member with rope effect

Figure 5.38: Timber failure on experiments perpendicular to the grain [51]

5.5.3 Cyclic testing

The behavior under a cyclic loading is a further important parameter in view of the ductile behavior of fasteners. This is especially of interest in case of a dynamic load for instance in case of an earthquake.

Experiments under a cyclic loading were performed in order to evaluate the ductile behavior under a changing load [73]. The experiments were conducted based on the rules of EN 12512 [102].

The dowel arrangement was chosen following the connection accomplished with 3×3 dowels with a diameter of 12 mm (see Fig. 5.39(a)). Therefore it was possible to compare the experiments with each other. The connection was modified in such a way, that the slotting within the timber member was set with a larger distance to the flitch plate. Hence the flitch plate could move without triggering the timber member. A further modification was carried out at the top of the specimen. The connection at the top of the specimen was changed in such a way, that it was possible to transfer also compression forces without a considerable clearance.

The timber embedding of the dowel was deformed in both load directions due to the cyclic loading (see Fig. 5.39(b)). Therefore, the gap at zero-crossing became wider within the hysteresis diagram due to a local plasticization of the timber member.

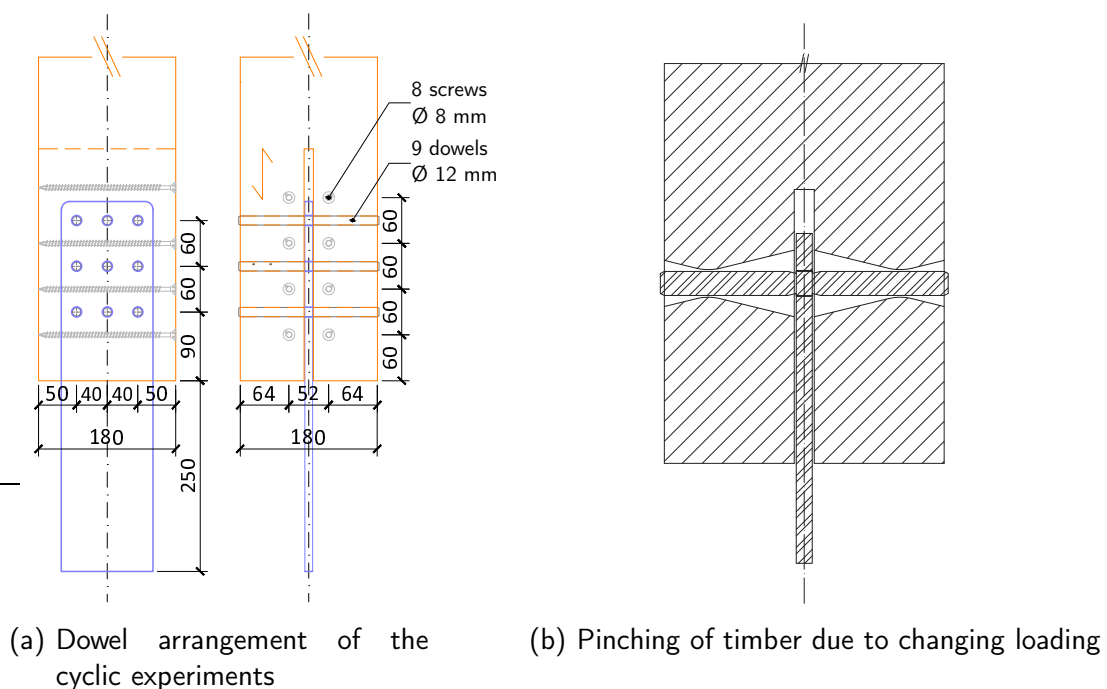


Figure 5.39: Cyclic testing

Test procedure

The test procedure of a cycling testing is based on the displacement of yielding of the static experiments according to EN 12512 [102]. The ascertained displacement at yielding was found to 3.2 mm based on [102] (see Table 5.17 on page 125). A displacement of 3 mm was set to the determination of the testing procedure. The loading speed has to be between 0.02 mm/s and 0.2 mm/s [102].

The first experiment out of four was set as a pre-testing to gain knowledge of the general behavior. The following experiments were performed with a loading speed of 0.067 mm/s (4 mm/min).

The loading process was set as follows (see Fig. 5.40):

1. Cycle

- Compression loading until 25 % of $u_y = -0,75 \text{ mm}$ is reached
- Relief till zero-crossing
- tension loading until 25 % of $u_y = 0,75 \text{ mm}$ is reached
- Relief till zero-crossing

2. Cycle

- Compression loading until 50 % von $u_y = -1,5 \text{ mm}$ is reached
- Relief till zero-crossing
- tension loading until 50 % von $u_y = 1,5 \text{ mm}$ is reached
- Relief till zero-crossing

3. to 5. Cycles (series of three cycles)

- Cycles following the benchmarks of the 2. cycle until 75 % of the displacement at yielding
 $\pm 0,75 \cdot 3,0 \text{ mm} = \pm 2,25 \text{ mm}$

6. to 8. Cycles (series of three cycles)

- Cycles following the benchmarks of the 2. cycle until 100 % of the displacement at yielding
 $\pm 1,0 \cdot 3,0 \text{ mm} = \pm 3,0 \text{ mm}$

In the following a series of 3 cycles

- Cycles following the benchmarks of the 2. cycle until 200 % of the displacement at yielding
 $\pm 2,0 \cdot 3,0 \text{ mm} = \pm 6,0 \text{ mm}$
- Cycles following the benchmarks of the 2. cycle until 300 % of the displacement at yielding

$$\pm 3,0 \cdot 3,0 \text{ mm} = \pm 9,0 \text{ mm}$$

- Cycles following the benchmarks of the 2. cycle until 400 % of the displacement at yielding
 $\pm 4,0 \cdot 3,0 \text{ mm} = \pm 12,0 \text{ mm}$
- Cycles following the benchmarks of the 2. cycle until 500 % of the displacement at yielding
 $\pm 5,0 \cdot 3,0 \text{ mm} = \pm 15,0 \text{ mm}$
- Cycles following the benchmarks of the 2. cycle until 600 % of the displacement at yielding
 $\pm 6,0 \cdot 3,0 \text{ mm} = \pm 18,0 \text{ mm}$
- The displacement is increased till a failure or a displacement of 30 mm occurs.

The cycles at 300 % and 500 % of the displacement at yielding is not implemented in EN 12512 [102]. However, the additional steps were introduced to reach a higher number of cycles.

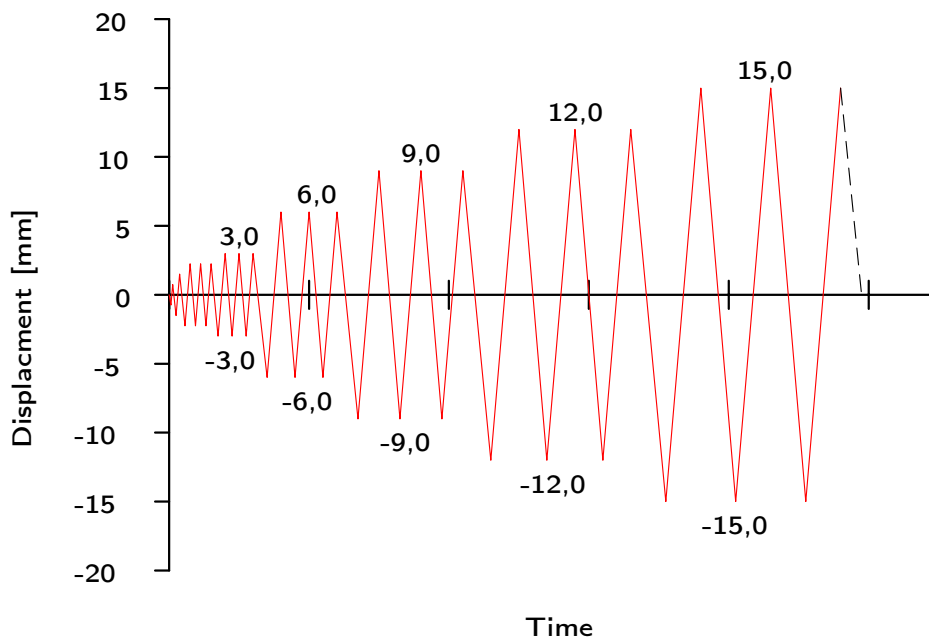


Figure 5.40: Load procedure of the cycle testings

Results of the experiments

The pre-testing was performed with the load procedure according to EN 12512 [102]. The cycles at 300 % and 500 % were not implemented at the first testing. The loading in com-

pression could be performed in the step of the displacement increase from 9 mm to 12 mm. The reloading in tension lead to a decrease of the load. This was caused by a splitting at the slotting. The load decreases under 80 % of the maximum load which resulted in the termination of the experiment.

The specimen of the second experiment was modified in such a way that two fully threaded screws were placed 40 mm above the top edge of the flitch plate to prevent a splitting of the timber at the slotting (see Fig. 5.41(a)). The experiment failed after the 12th cycle due to a tension-bending failure at the slotting (see Fig. 5.41(b)). The tension-bending failure is caused by an inclination of the dowel as a result of the formation of a plastic hinge. The inclination lead to a pushing together of the two timber side members within the compression loading. On the other hand, the timber members splayed apart under a tension loading which leads to bending stresses at the edge of the slotting followed by a failure (see Fig. 5.42(a) & Fig. 5.44(a)).

This shows that it is important to protect connections against such a failure with bolts in a connection instead of dowels. The use of bolts instead of dowels was no alternative, since bolts have a different load-carrying capacity. This is caused by a different steel grade and the rope effect due to the washer and the nut. The spreading of the two timber members was prevented by two fully threaded screws next to the flitch plate (see Fig. 5.42(b)). The connection was not influenced by the screws, but the danger of a possible splitting was re-

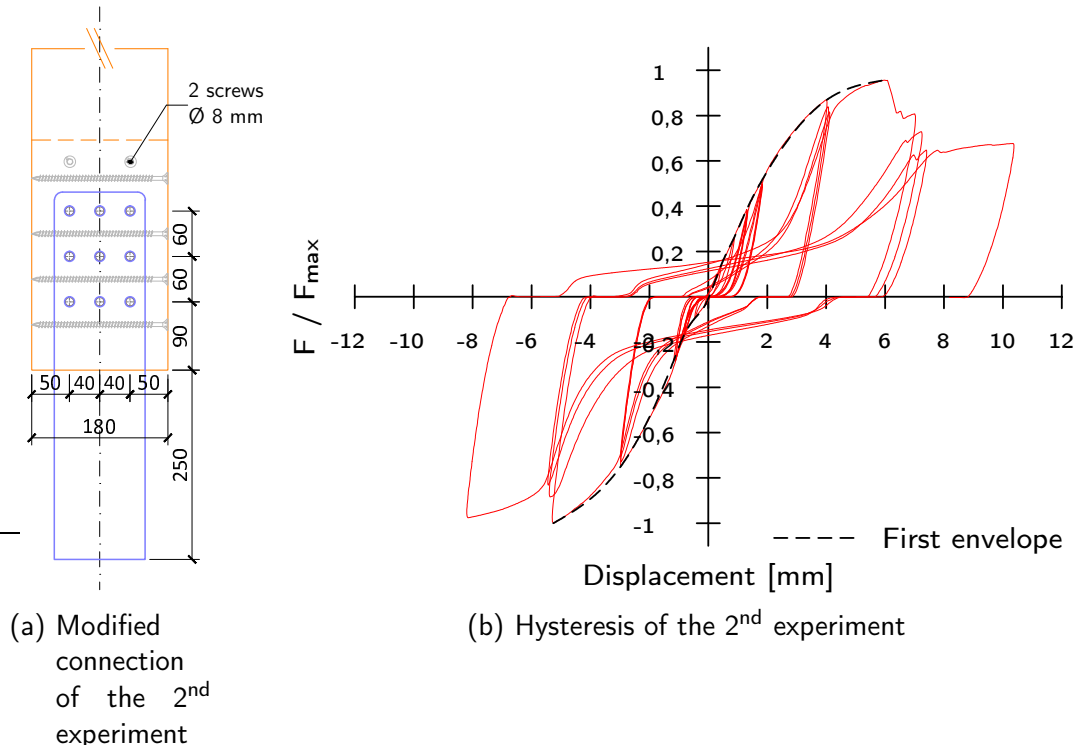


Figure 5.41: Modification and result of the 2nd cyclic experiment

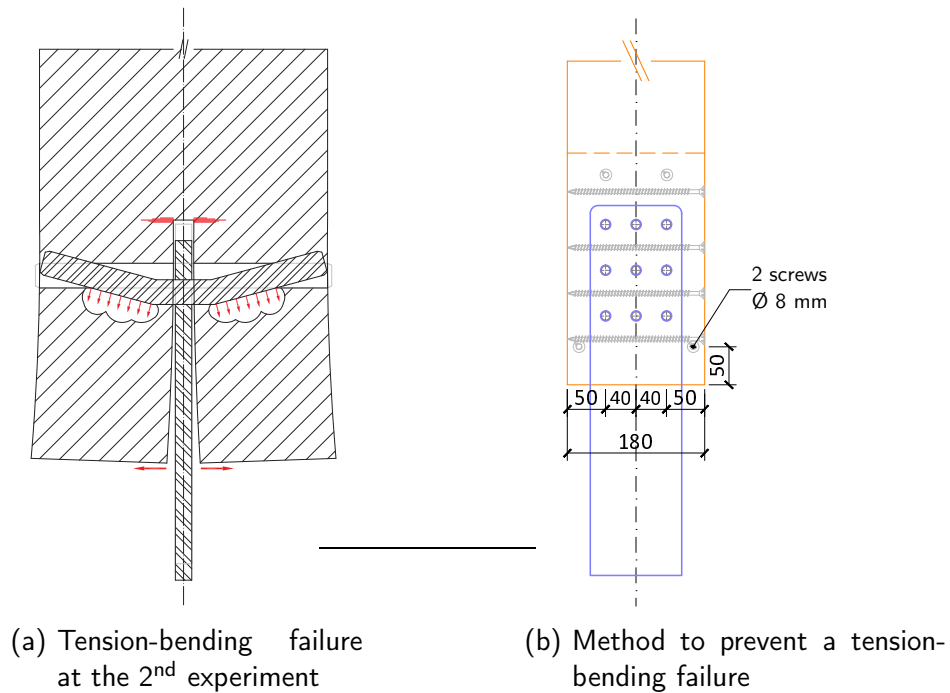


Figure 5.42: Modifications of the 3rd and 4th experiments

duced. A decrease of the load was noticed after the 12th cycle at the third and fourth cyclic experiment (see Figure 5.43 & Figure 5.45). The reason for a load decrease was a local block shear failure in the third testing. Hence a significant load decrease occurred between the 12th and 15th cycle in tension (see Fig. 5.44(b)). A local splitting of the timber combined

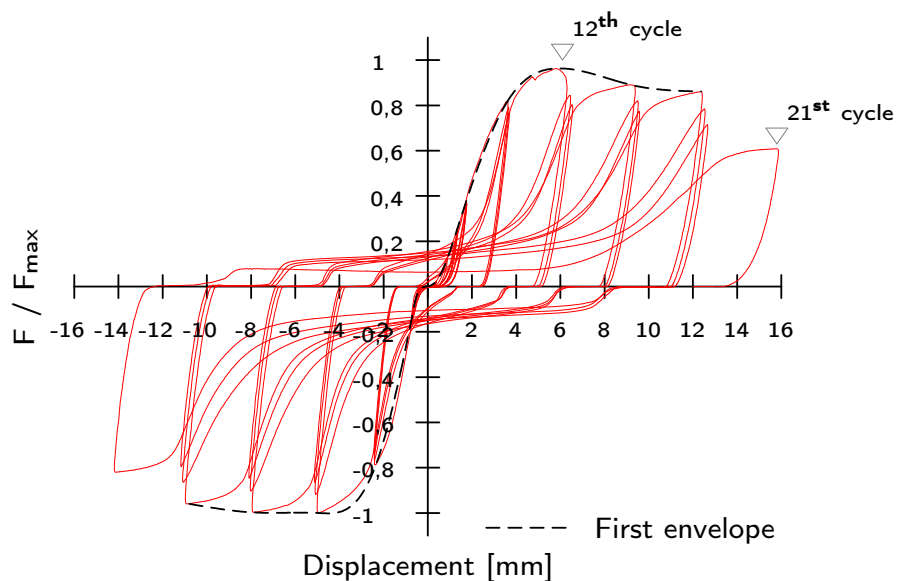


Figure 5.43: Hysteresis in the 3rd experiment

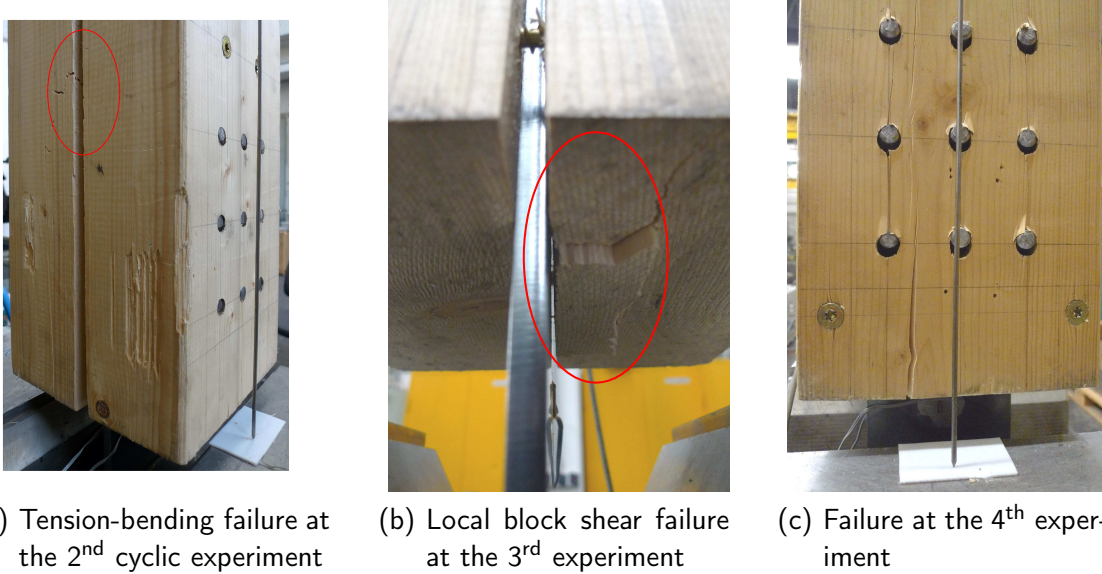


Figure 5.44: Failure modes of the different specimens [73]

with high embedding stresses caused the failure in the fourth experiment (see Fig. 5.44(c)). A load decrease of 80 % of the ultimate load was detected at the 21st cycle (~ 15 mm displacement) at both experiments.

Figure 5.46 shows the comparison of the mean value of the static experiments with an arrangement of 3×3 dowel with the first envelope of the different experiments. The first envelope encloses the first cycles of the test series (see Fig. 5.43 & Fig. 5.45). The different

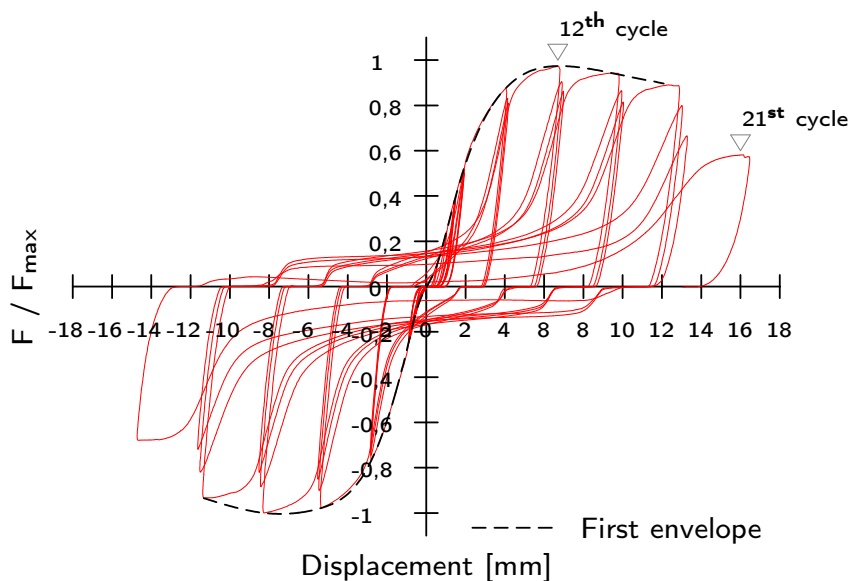


Figure 5.45: Hysteresis in the 4th experiment

behaviors are divided by the maximum load, which was achieved in the second experiment. It is recognized that the ultimate load is higher within the cyclic testings compared to the static loading. This is caused due to the short but rather fast loading in the cyclic experiments. This reflects the Madison curve, which describes the behavior of timber depending on the load duration and the moisture content. Investigations of [33] confirm this phenomenon. The ultimate displacement within the cyclic loading achieved approximately 40 % of the displacement at ultimate load compared to the static testings (see Fig. 5.46).

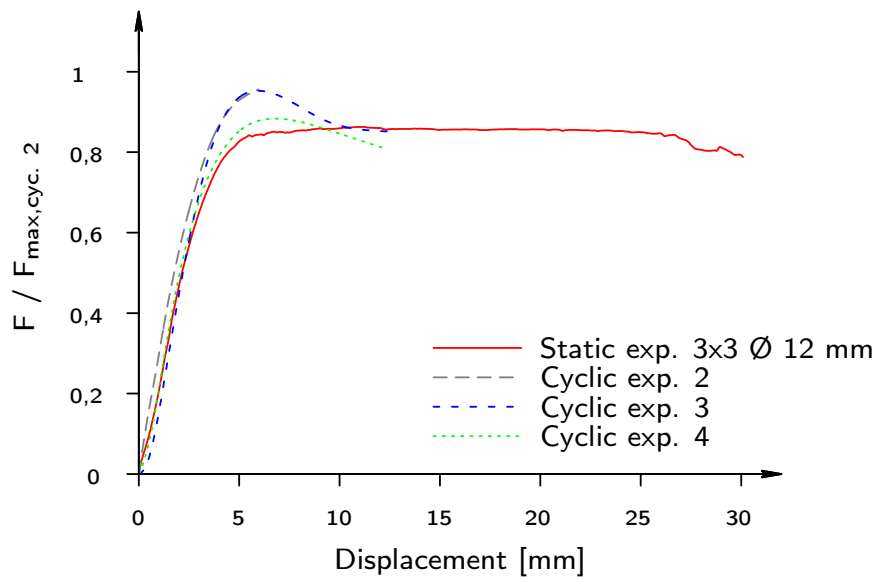


Figure 5.46: Comparison of the first envelope with the static testing

Ductility evaluation

The point of yielding changed significantly with a variation of the load direction. It is shifted towards ultimate load due to the lower embedment strength (see Tab. 5.17). A local splitting along the grain direction could be prevented by the application of fully threaded screws.

Table 5.17: Determination of the point of yielding (u_y) on miscellaneous experiments (comp. Sec. 4.2.1.2)

	u_y (b) [mm]	u_y (b_{mod}) [mm]	u_y (e) [mm]	u_y (f) [mm]	u_F [mm]
Ø 12 perp. to grain	11.33	16.42	7.53	12.54	55.15*
Ø 12 cyclic loading	3.20	3.80	4.34	3.85	12.34
Ø 12_1×1	1.78	2.41	2.28	2.65	41.34

* Displacement at 98% of ultimate load

Table 5.18: Determination of the ductility ratio on miscellaneous experiments based on Eq. (4.1) & Eq. (4.9)

	D_f (b)	D_f (b_{mod})	D_f (e)	D_f (f)	D_{fy} (b)	D_{fy} (b_{mod})	D_{fy} (e)	D_{fy} (f)
Ø 12 perp. to grain	4.87	3.36	7.32	4.40	43.82	38.73	47.62	42.61
Ø 12 cyclic loading	3.86	3.25	2.84	3.20	9.14	8.54	8.00	8.49
Ø 12_1×1	23.18	17.13	18.11	15.61	39.52	38.89	39.02	38.65

This leads to a displacement at maximum load of 47.5 mm. Based on the absolute ductility ratio D_{fy} (comp. Sec. 4.2.2), this type of connection is classified as high ductile. However, the point of yielding is shifted towards ultimate load, therefore the connection is classified as low to moderate ductile based on the relative ductility ratio D_f (see Table 5.18 & Figure 5.47). Hence this type of connection is classified as low ductile behavior.

The cyclic experiments suffered a decrease of the displacement at failure. Within the cyclic experiments the ultimate load was not taken as the displacement at 98 % of the ultimate load. A decrease of the load at a certain stage is a typical behavior within cyclic experiments. Therefore the rules given in EN 12512 [102] have been used. The ductility ratio is determined as the quotient of the displacement at failure (u_f) and the displacement at yielding (u_y) (comp. Eq. (4.1)).

The ascertained displacement at yielding decreases slightly at the cyclic experiments compared to the static experiments (see Tab. 5.17). This is caused by a higher stiffness in the area of the transition of the elastic behavior to the plastic behavior. Therefore, the displacement is dropping down. The cyclic testing is classified as low to moderate ductile see Table 5.18 & Figure 5.47).

Additional experiments were conducted with a diameter of 12 mm, with only one dowel.

Table 5.19: Determination of the ductility ratio on miscellaneous experiments based on Eq. 4.13

	D_e (b)	D_e (b_{mod})	D_e (e)	D_e (f)
Ø 12 perp. to grain	9.75	5.52	19.44	8.53
Ø 12 cyclic loading	8.19	5.82	4.53	5.67
Ø 12_1×1	64.69	40.36	43.22	33.48

These experiments have been conducted to gain knowledge about the initial stiffness in regard to the influence of the number of fasteners (comp. Sec. 6.4.2). The experiments are evaluated within this context with view on the ductility. It is clearly shown that the point of yielding occurs at a much lower displacement compared to the experiments conducted with a certain amount of dowels (see Table 5.8 & Table 5.17). This behavior provides an initial orientation of the stiffness. It can be noted that the stiffness of a connection with a single fastener changes compared to a group of fasteners. The displacement at yielding is approximately twice as high compared to a group of fasteners. More detailed investigations are given within the discussion of the initial stiffness (comp. Sec. 6.4.2).

The danger of splitting is dropping down for connections with only one fastener [84]. Hence, the ultimate deflection and therefore, the ductility ratio is increasing significantly (see Tab. 5.19).

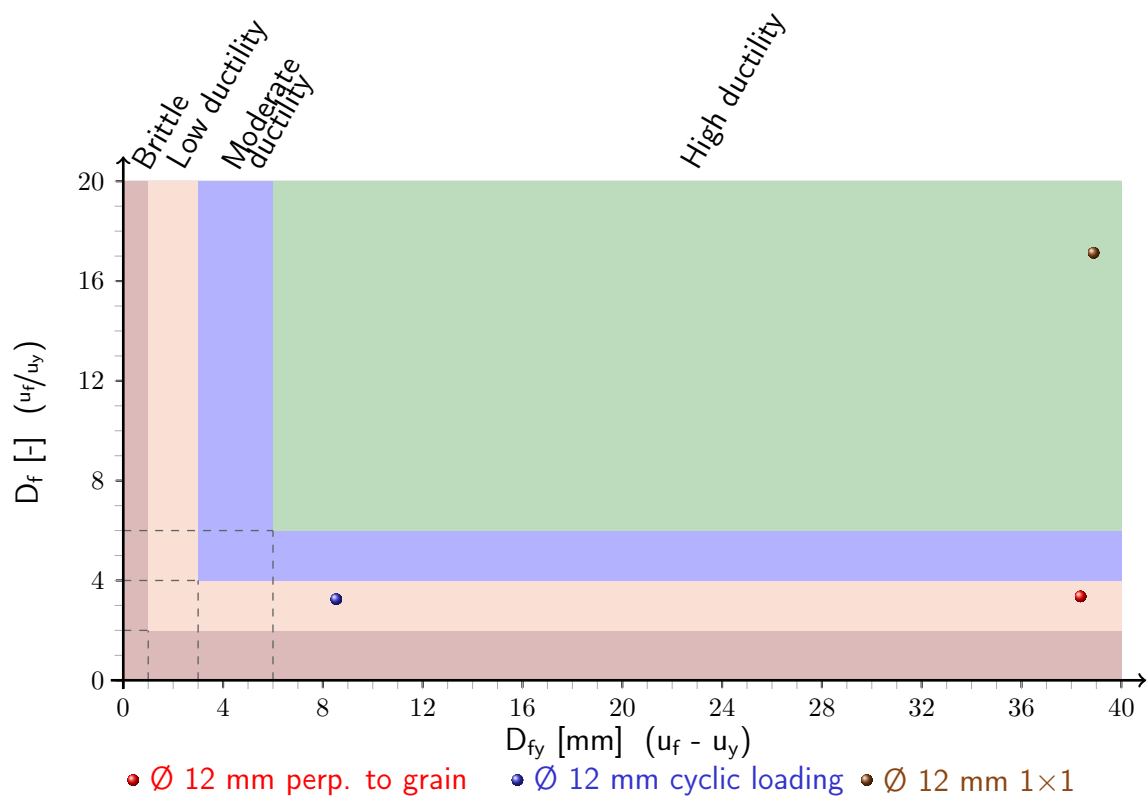


Figure 5.47: Illustration of the determined absolute ($D_{fy} (b_{mod})$) and relative ($D_f (b_{mod})$) ductility ratios

5.6 Summary

The experiments on dowel type connections showed a significant ductile behavior if the dowel arrangement is not endangered by a failure due to splitting. The prevention of such a failure was achieved with fully threaded screws [82], which is a common method nowadays. A desired load increase after a level of ductility was observed at the experiments on double flitch plate connection with self-drilling screws. This is a further important advantage of the reinforcement within a dowel type connection. An increase of the stiffness and therefore an increase of the load occurred approximately at the distance of reinforcement to the fastener. It is not possible to generalize this behavior, since it was only observed on dowels with a diameter of 7 mm. It is supposed that the ratio of the dowel diameter to the stiffness of the reinforcing element is the driving parameter for this desired behavior.

Neither the ultimate load nor the load-displacement behavior of the conducted experiments in tension with a certain diameter are influenced by the dowel arrangement. The results of Bejtka [82] could be confirmed that no reduction of the load-carrying capacity is necessary on connection arrangements reinforced with fully threaded screws.

The designed system of a 16 mm diameter combined with an embedding of 85 mm gives a rather low slenderness of the connection system. This type of connection failed due to a tension-bending failure of the timber fingers at the slotting in a brittle manner. However, this type of failure is prevented in the practical application due to the use of some bolts instead of dowels.

Four-point bending experiments were conducted besides the pure experiments in tension. All of the performed testings showed a considerable rotational capacity under a bending loading. The dowel arrangement is influencing the moment-rotation capacity. Stretched arrangements (5×2 dowels) showed an increase of the moment resistance with a decrease of the rotation, whereas for a wide arrangement (2×4 dowels) a rather constant moment-rotation exhibited. High stresses occurred at the undermost dowel row, which leads to a timber splitting along the row. Therefore it is suggested to use a rather compact alignment instead of a stretched arrangement.

In addition to the experiments loaded parallel to the grain, experiments perpendicular to the grain were conducted. A brittle splitting of the connection was prevented due to the reinforcement of the connection. Hence the ultimate load and the displacement were increased. This type of connection showed a high deformability. However, since the point of yielding increased significantly compared to connections loaded parallel to the grain, the relative ductility ratio drops significantly. Hence this type of connection is classified as low ductile.

Within the view of ductility the behavior under a changing load is also of importance. Therefore, experiments under a cyclic loading were performed to prove the behavior under such a loading. The first experiments failed due to high bending-tension stresses at the slotting as

a consequence of a spreading of the two timber side elements. The connection was modified with fully threaded screws to prevent the spreading without influencing the general connection. Although the ductile behavior was reduced due to the changing load, the modified connection could be classified with a low to moderate ductile behavior. The experiments showed, that it is important to prove a connection not only under a monotonic loading, but also under a cyclic loading.

The additional experiment with only one 12 mm dowel showed that the displacement at yielding decreased for all chosen definitions. Further investigations on the different behavior are given within the next chapter.

All of the conducted experiments showed a ductile behavior of reinforced connections. In order to bridge the gap to introduce the non-linear behavior to the standards, it is indispensable to develop a design procedure with a reliable model. Reliable not only in the view of the ultimate load, but also in the view in depicting the non-linear behavior.

6 Analytical determination of the rotation capacity

6.1 General

In order to implement the elastic-plastic design method to timber engineering, it is important to develop a model which describes the behavior of connections and joints in a reliable manner. Reliable not only within the view of the moment-carrying capacity, but also on the prediction of the rotational capacity. A mechanical model has been developed, based on the conducted experiments, to describe the rotational capacity of plastic hinges in a reasonable way. Therefore, the model has to describe the available rotational capacity and the plastic moment load capacity.

Intensive investigations on semi-rigid joints in steel structures were conducted in the eighties at the Institute of Timber- and Steel Structures in Innsbruck under the leadership of Professor F. Tschammernegg [5, 78, 79]. The developed design philosophy, the so called component model, divides the overall joint into single load carrying components. The single components are characterized as a spring with their specific load carrying behavior (see Fig. 6.1). This model is also well known as the *Innsbruck component model*. This type of mod-

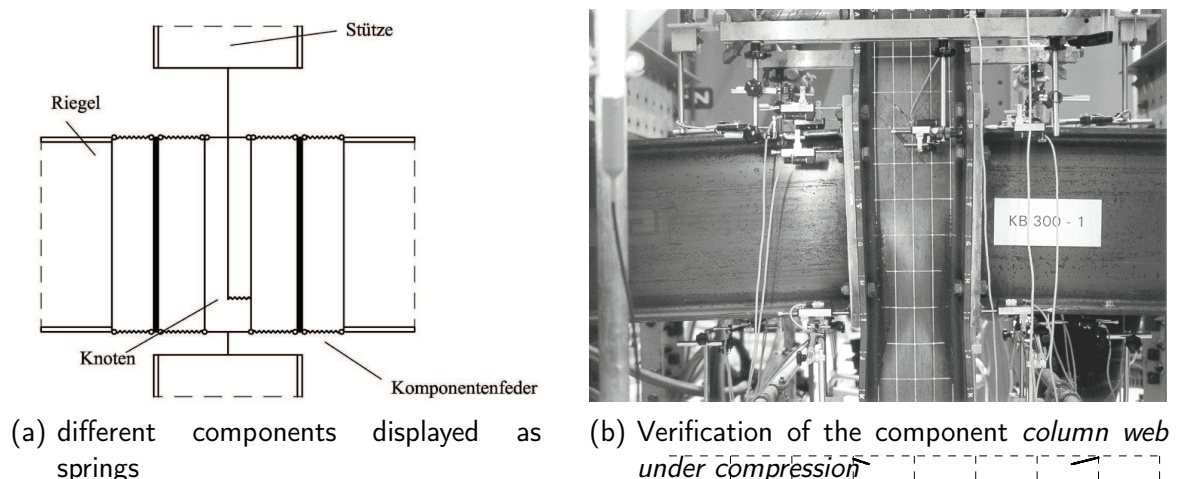


Figure 6.1: Modeling of a semi-rigid joint [87]

eling is currently implemented in the standardization of steel structures [107] and composite structures [108].

Further investigations were carried out at the Institute of Structural Design at the Universität Stuttgart under the supervision of Professor U. Kuhlmann. Kühnemund [87] dealt with the available rotational capacity of semi-rigid joints in steel structures. The focus was set to the component *column web under compression*. Another study was performed on the verification of the rotation on partial strength joints in composite structures. The main focus was set on the verification of the rotational capacity [92].

Jaspart et al. [36] gives an extensive overview of the available regulated single components and their application.

The following components are currently known among others:

- Bolts under a tension loading
- Bolts under a shear loading
- End plate joints
- Column web under tension loading
- Column web under compression loading
- Concrete under a compression loading

The moment-rotation capacity is gained by assembling the different single components (see Fig. 6.1(a)). Figure 6.2 shows the moment-rotation behavior of a semi-rigid joint exemplarily with the appropriated parameters based on [107]. The stiffness $S_{j,ini}$ describes the initial stiffness of the joint. If the moment at the joint is smaller than the elastic moment ($M_{j,sd} \leq 2/3 \cdot M_{j,pl,Rd}$) the stiffness $S_{j,ini}$ has to be taken into account. The reduced stiffness ($S_{j,ini}/\eta$) may be used as a simplification until the plastic moment load carrying capacity is reached ($2/3 \cdot M_{j,pl,Rd} \leq M_{j,sd} \leq M_{j,pl,Rd}$) (see Fig. 6.2). A bilinear assumption can be used if the elastic-plastic design method is used [48], [107]. The rotational capacity ϕ_{Cd} describes

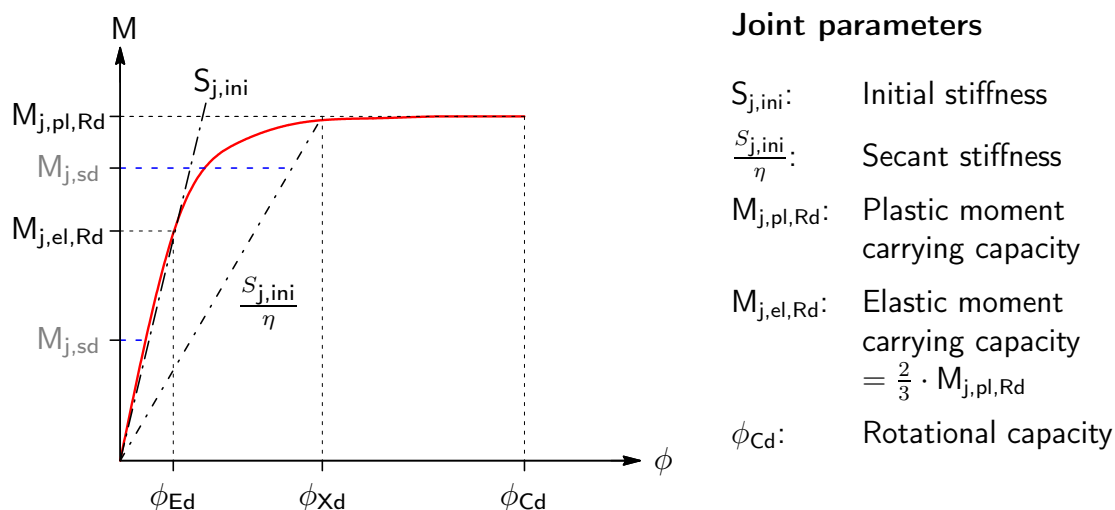


Figure 6.2: Parameters of the moment-rotation of a joint behavior based on EN 1993-1-8 [107]

the rotation at rupture or the rotation if the actual moment $M_{j,SD}$ drops below the plastic moment capacity $M_{j,pl,Rd}$.

A simplified method is presented in the following to predict the rotational capacity of joints in timber structures. The method follows the principle of the previously described method to retain known systems. Therefore, the lack of knowledge regarding EN 1995-1-1 [109] is closed to implement the elastic-plastic design method in timber structures.

6.2 Identification of the different components

6.2.1 Introduction of the single components

The different detected components of the examined joint are described and discussed in the following. Figure 6.4 shows exemplarily an examined joint with the different components. Hence the flitch plate connection in the tension zone forms a main component. The transfer of the compression force is ensured via a defined steel block and forms a further main component. Fully threaded screws ($\varnothing 8 \text{ mm} \times 200 \text{ mm}$) were placed on the top of the joint to avoid a laterally tension failure perpendicular to the grain at the bottom of the steel block (see Fig. 6.3). The load-displacement behavior was not influenced by the reinforcing application.

The development of the component model was mainly conducted on the experiments with a dowel diameter of 12 mm. A dowel diameter of 12 mm was chosen since it implies three different test setups. The stretched arrangement with 5×2 dowels, a rather compact alignment of 3×3 dowels and a wide arrangement with 2×4 dowels. Therefore a sufficient cover of different arrangements was ensured and the influence of dowel arrangement can be discussed.



Figure 6.3: Reinforcement at the compression zone

The validation of the developed component model was performed on all conducted experiments.

Pre-testings had been conducted to investigate the development of tension perpendicular to the grain with an increasing of the rotation. It has been shown that the experiments suffered stresses perpendicular to grain which lead to a brittle rupture in the area of transition from the elastic to the plastic behavior. The fully threaded screws were elongated to absorb in addition stresses perpendicular to the grain (see Fig. 6.4).

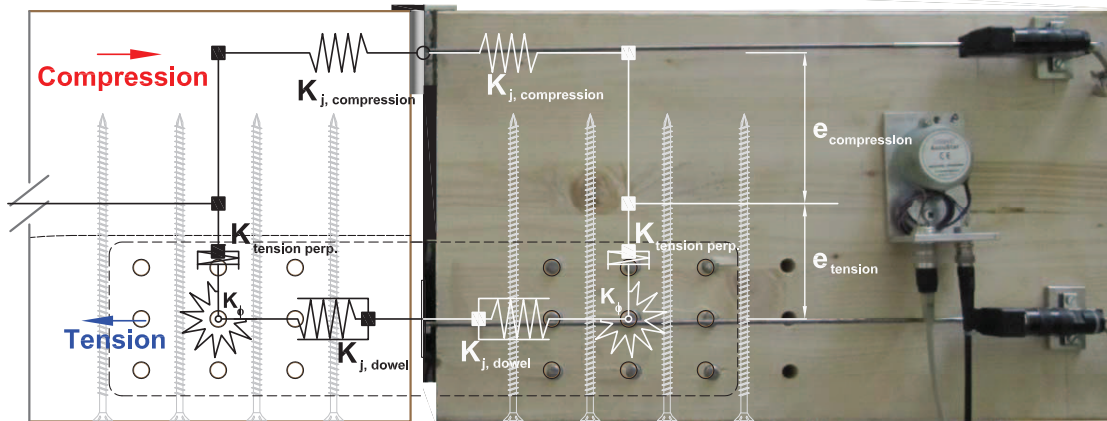


Figure 6.4: Single components of the examined joint

6.2.2 Components acting in compression

Displacement transducers were placed on the joint in the middle of the steel block to gain knowledge of the mechanical behavior of the component $K_{compression}$. A measuring device was placed on either side of the connection in the front and in the back to locate possible differences in the performance under a loading (see Fig. 6.4). Figure 6.5 shows the typical deformation of the tested joints. The steel block was always flush with the interface of the timber beam at one side, whereas large deformations occurred at the other side suffered by large rotations.

The load-displacement behavior within the compression zone is displayed in Figure 6.6. The different behaviors of either side of the joint is clearly shown. It is obvious that the left side of the joint was acting only in the elastic range. On the other hand, the right side of the connection was initially also acting in an elastic way. The elastic deformation was followed

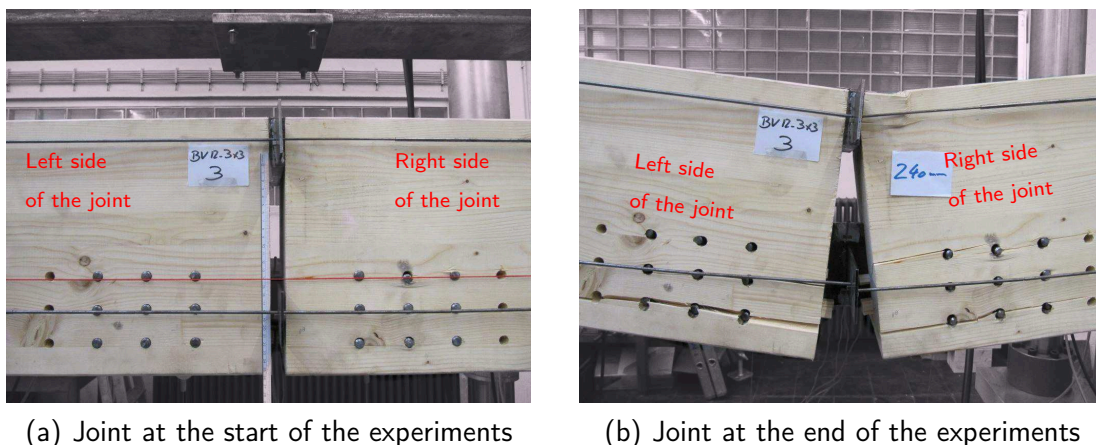


Figure 6.5: Deformations within the compression zone

by large plastic deformations and a partial buckling of the timber fibers.

The steel block within the compression zone remained constant in all experiments. Therefore it was possible to determine the behavior for the chosen geometrical parameters.

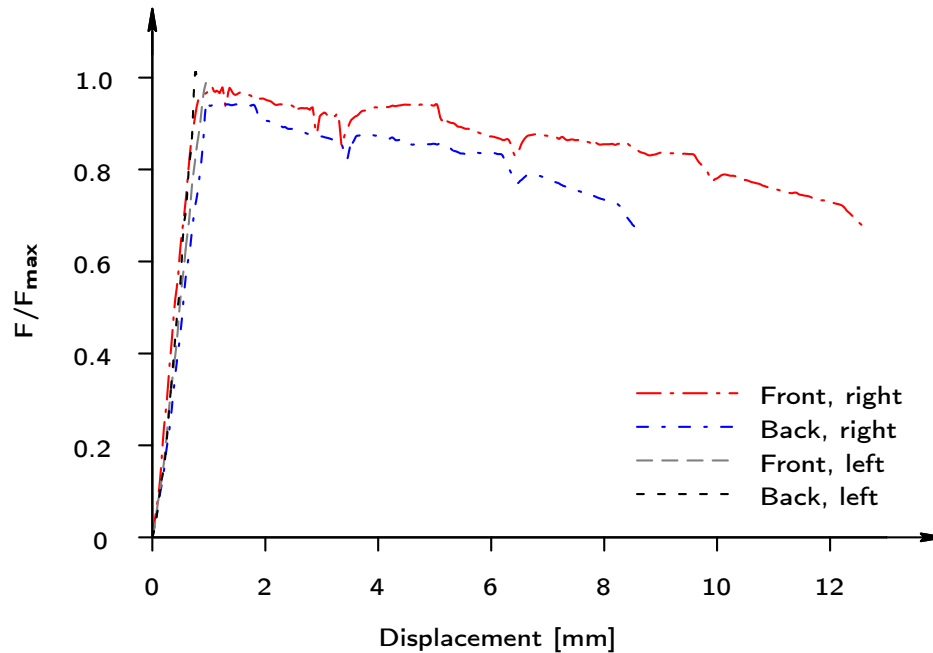


Figure 6.6: Behavior of the component acting in compression, displayed on a dowel arrangement of $3 \times 3 \text{ } \varnothing 12 \text{ mm}$

Determination of the component acting in compression $K_{\text{Compression}}$

The tracked load-deflection behavior of the experiments formed the base to determine the stiffness of the compression zone. Hence the mean values of the front- and backside of each beam was determined. The stiffness of the compression zone was determined according to the rules of EN 26891 [110]. The compression zone had a dimension of $65 \text{ mm} \times 180 \text{ mm}$, which was the corresponding width of the actual beam (see Fig. 6.4). The following equations were applied:

$$K_{\text{Compression}} = \frac{0.4 \cdot F}{v_{i,\text{mod}}} \quad (6.1)$$

$$v_{i,\text{mod}} = \frac{4}{3} \cdot (v_{04} - v_{01}) \quad (6.2)$$

with :

v_{01} : Displacement at 10% of the ultimate load

v_{04} : Displacement at 40% of the ultimate load

Table 6.1: Determined values of $K_{\text{compression}}$ based on the experiments [kN/mm]

Experiment	\varnothing 7 mm						\varnothing 16 mm		
	2×3			4×2			3×2		
	1	2	3	1	2	3	1	2	3
Right	317.1	335.5	244.0	307.0	386.9	377.1	355.4	355.4	329.9
Left	295.1	239.6	207.6	262.2	253.9	270.1	299.2	287.4	271.76

Experiment	\varnothing 12 mm								
	2×4			3×3			5×2		
	1	2	3	1	2	3	1	2	3
Right	341.2	374.8	363.6	231.8	333.3	290.7	355.7	253.9	305.6
Left	323.1	337.0	357.1	289.6	267.3	280.8	270.1	266.8	212.2

Number of samples : 36 pieces
 Mean : **300 kN/mm**
 COV : 15.8 %

The ascertained stiffness values of the component acting in compression are displayed in Table 6.1. A mean value of 300 kN/mm was determined as a mean value of the stiffness. The coefficient of variation is slightly higher compared to the value of 13 % given in [41] for the modulus of elasticity.

To classify the results of the evaluation, the value is compared with the stiffness of a notch within TCC structures since this is a similar loading. Experiments on notched connections with a timber grade of GL32h and a depth of 40 mm showed a stiffness of 387 kN/mm [2]. The experiments had a width of 220 mm, and the modulus of elasticity (E_{dyn}) was examined to 14759.9 kN/mm. Therefore, the determined stiffness of 300 kN/mm on a 180 mm wide beam is within the range of the identified value in TCC structures.

6.2.3 Components acting in tension

The experiments performed on flitch plate connections in tension form the basis of the component acting in tension. The load-slip behavior has been specified in the first test series (comp. Sec. 5.3). The general behavior was measured on both sides of the joint in the front and in the back to have a closer look at the general behavior of the joint. The load-deflection behavior of the connection on either side of the joint matches well, except for the initial stiffness. Due to a higher density of the beam on the left hand side the stiffness

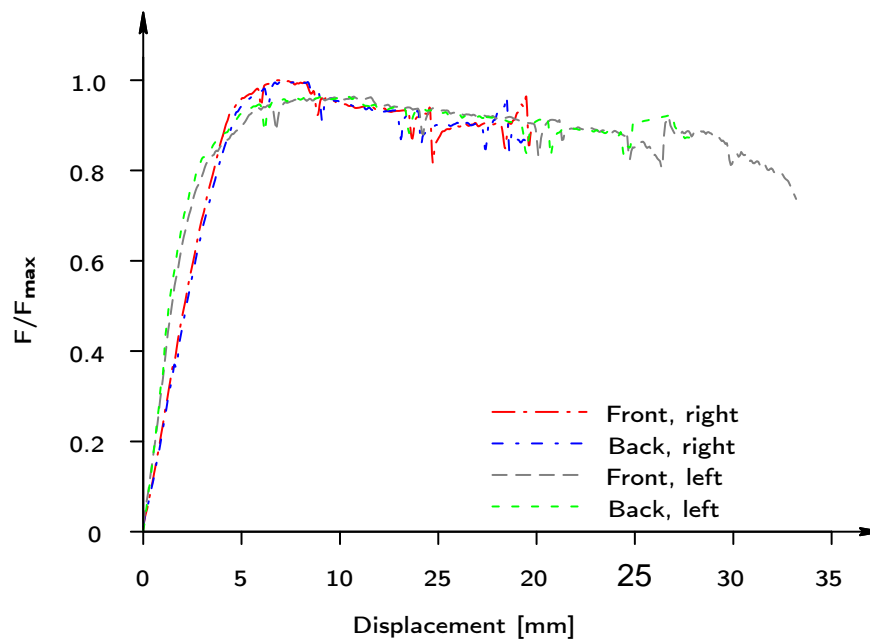


Figure 6.7: Comparison of the load-displacement behavior of the left and right side of the joint (Exp. 12_3x3_1)

on the left side was higher compared to the right side (see Fig. 6.7). In addition, the left side of the joint achieved a slightly larger displacement compared to the right side. Both sides of the joint act nearly in the same way, therefore the rotation of the joint was nearly similar on both sides. Since the contribution of the displacement in compression was higher on the right hand side, the deformation in tension decreased.

The initiated bending moment was divided by the inner lever arm to determine the actual force within the dowel type connection. The inner lever arm was defined as the length from the center of the dowel connection to the center of the compression zone, which was assumed to be rectangular distributed at this investigation (see Fig. 6.8(a)). The studies showed that the inner lever arm has a large contribution on the component model. Thus the inner lever arm is more closely examined.

Influence of the inner lever arm

The detected moment-rotation behavior was divided by the inner lever arm to recalculate the load-displacement behavior of the connection with dowel-type fasteners. Two different stress distributions in the compression zone were assumed. A rectangular distribution as a lower bound (see Fig. 6.8(a)) and a triangular distribution as an upper bound (see Fig. 6.8(b)). Figure 6.9 shows the comparison of the mean value determined within the pure tension experiments with a dowel diameter of 12 mm and an arrangement of 3×3 and the ascertained load-displacement behavior in the tension zone of the bending experiments. The investigation

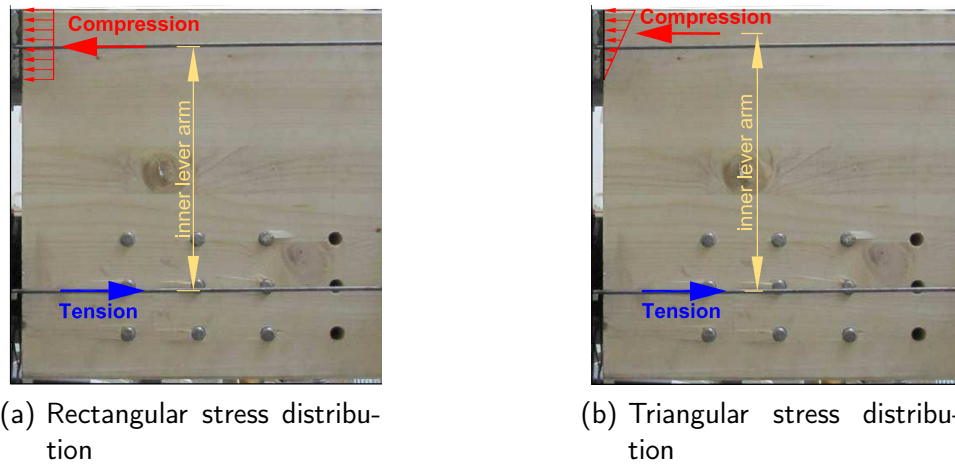


Figure 6.8: Assumption of the inner lever arm

was performed with the first and the third experiment in bending. The displayed mean value of the bending experiments implied the behavior of the right and left hand side of the joint. The comparison of the different assumptions within a dowel arrangement of 3×3 does not allow a reliable prediction. Both the assumption of a rectangular stress distribution and the triangular stress distribution show in one case a reliable solution (see Fig. 6.9).

It can be seen, that the assumption of the inner lever arm is a driving parameter in the design of the component model. Hence, further investigations were performed on the stress distribution at the compression zone to gain knowledge of the approach of the inner lever arm. The steel plates within the tension zone formed a further part of the component in tension. However, the deformations are rather small compared to the deformations of the dowels. Therefore, no closer focus was set on this component.

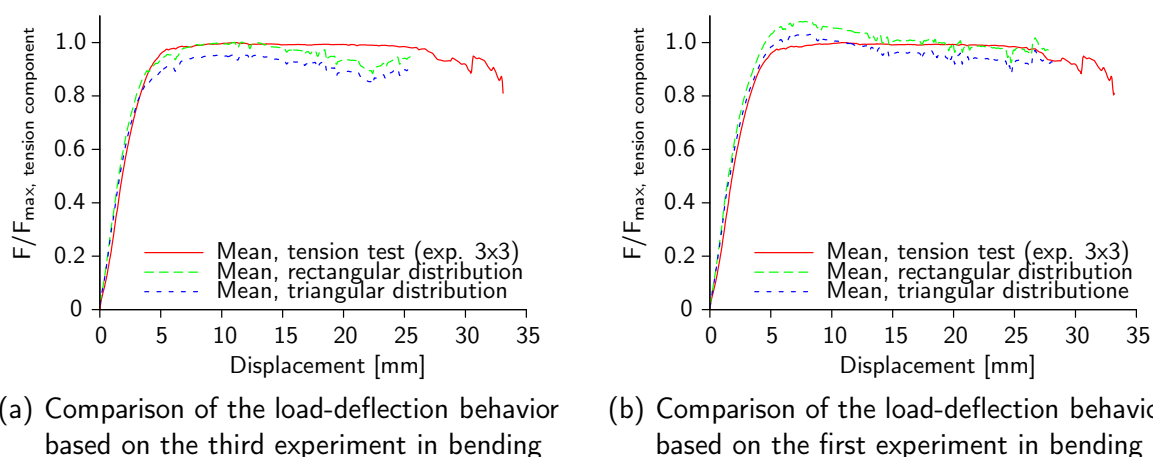


Figure 6.9: Accordance of the determined load-displacement behavior within the tension zone compared with the pure tension testings (\varnothing 12mm 3×3)

Stress distribution at the compression zone

Strain gauges were placed on the edge of the compression zone, to gain knowledge of the strain distribution within the compression zone. The gauges had a length of 60 mm. The

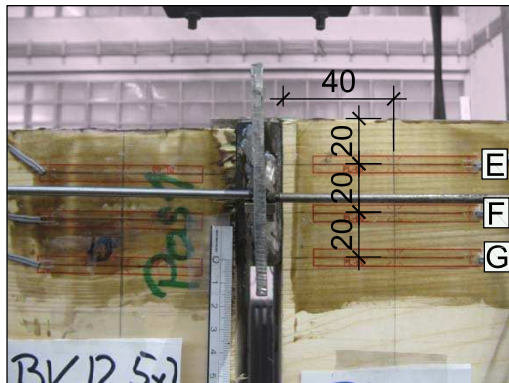


Figure 6.10: Arrangement of the strain gauges

first gauge (E) was placed with a distance of 20 mm from the top of the beam, the following gauges (F & G) had an in between distance of 20 mm as well (see Fig. 6.10). The gauges were placed on certain beams on the front and back on both sides of the joint. It is in general well known, that gauges are highly sensitive. Therefore, only one set of gauges could be evaluated on the experiment with an arrangement of 5×2 dowels (\varnothing 12 mm) to gain knowledge of the compression stresses. Since the left side achieved large deformations, only the right side could be evaluated. The middle gauge ($F_{(b)}$) at the back side got damaged before or during the loading process. Therefore, it was not possible to display the behavior. Figure 6.11 shows the strain distribution at certain stages within the compression zone. The moment rotation behavior of the joint is also displayed to gain insight into the joint

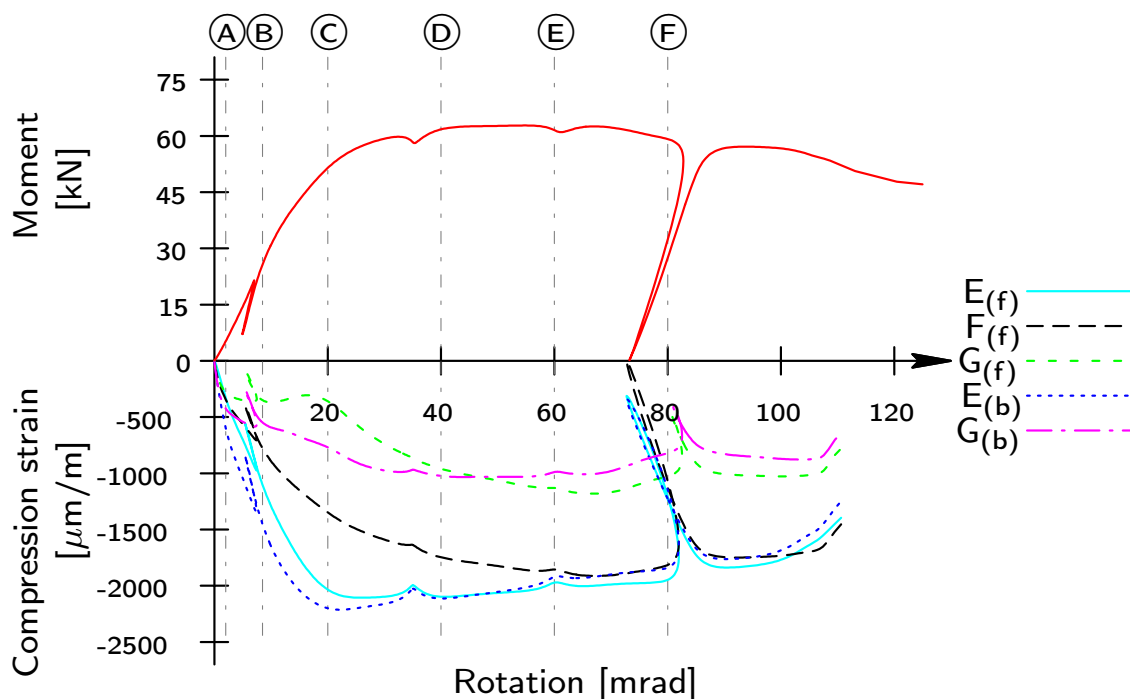
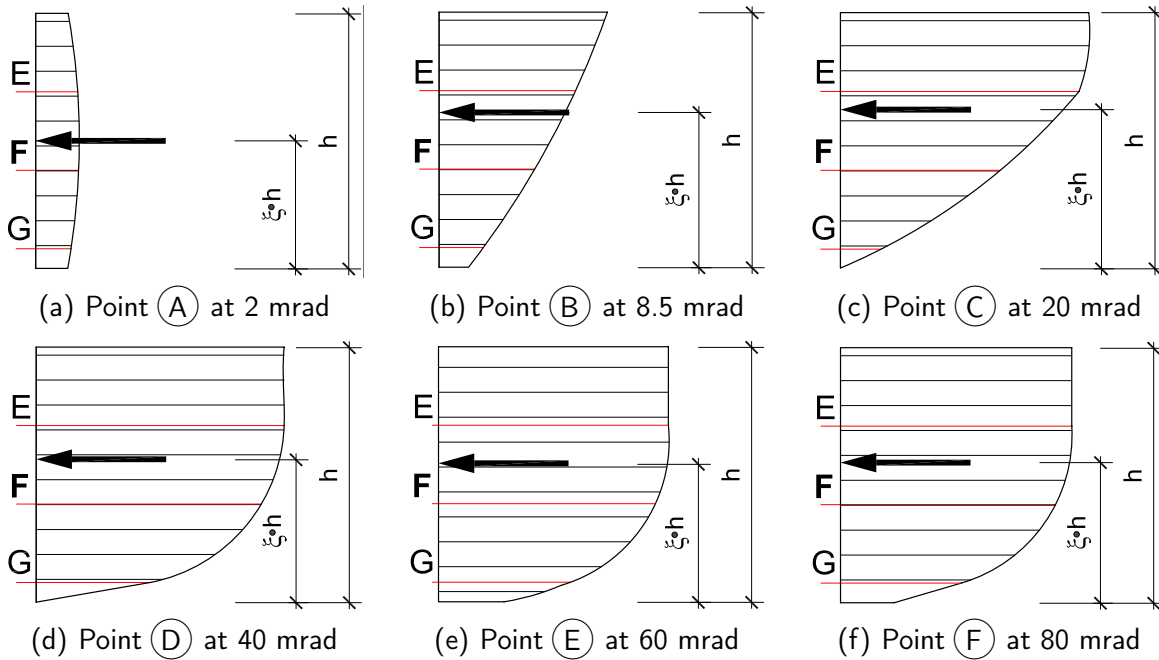


Figure 6.11: Strain development within the compression zone in accordance with a proceeding of the rotation (f=front, b=back)



h = height of the steel block (65 mm (see Fig. 5.26(a)))

Figure 6.12: Compression strain distribution at certain rotation steps

behavior. It is obvious that the strain at the top fibers of the compression zone were following the moment-rotation behavior. Figure 6.12 shows the ascertained strain distribution at the compression zone for different steps of the rotation ((A) \mapsto (F)). The yielding of the joint occurred approximately at a strain of 2.1 ‰ at the measuring point (C). This reflects to stresses of approximately 27.2 N/mm² with a mean value of the modulus of elasticity of 12967 N/mm² (see Tab. 5.2). A stress value of 27.2 N/mm² does not reflect the absolute possible compression stresses in grain direction [83]. However, the left side already reached the ultimate strain. Hence the asymptotically compression strength raised and stresses were redistributed within the system. The asymptotically final compression strength can reasonably be assumed as 80 % to 90 % of the ultimate compression strength [32].

Further investigations were conducted to gain information about the compression zone. Therefore, the strains were integrated for every rotational step on the corresponding compression block using Equation (6.3).

$$R_{\varepsilon} = \int_A \varepsilon_x dA \quad (6.3)$$

The center of gravity was subsequently determined based on Equation (6.4) to find the acting point of the resultant.

$$x_{R_{\varepsilon}} = \frac{1}{R_{\varepsilon}} \int \varepsilon_x \cdot Z dA \quad (6.4)$$

Based on the geometrical properties it was possible to prove the strain distribution within the compression zone. Hence the resultant compression force is calculated for every rotation step according to the law of Hooke. The determined force in the compression zone is compared with the tension force acting in the dowel arrangement, which should show an equilibrium. The tension force acting in the dowels is calculated as the quotient of the actual bending moment to the actual lever arm. Table 6.2 shows the previously described parameters. It

Table 6.2: Determined parameters based on the compression zone

	(A) 2 mrad	(B) 8.5 mrad	(C) 20 mrad	(D) 40 mrad	(E) 60 mrad	(F) 80 mrad
x_{R_ε} [mm]	32.50	39.40	40.20	36.40	35.30	35.70
$F_{\text{compression}}$ [kN]	51.34	138.90	220.41	273.26	265.22	262.22
F_{tension} [kN]	30.39	119.47	233.04	281.57	269.86	267.06
$F_{\text{comp.}} / F_{\text{tens.}}$	41 %	14 %	-6 %	-3 %	-2 %	-2 %
ξ	0.50	0.61	0.62	0.56	0.54	0.55

is obvious that the measured strain distribution for low values of the rotation do not match with the recalculated values. One possible explanation of the differences between both values may possibly be situated in the three dimensional strain situation. The fibers at the edges could be stressed before the fibers in the mid section are stressed at the beginning of loading. The stresses are balanced with a further loading, which leads to a homogenous distribution within the plastic plateau.

The factor ξ describes the ratio of the distance from the bottom edge of the compression

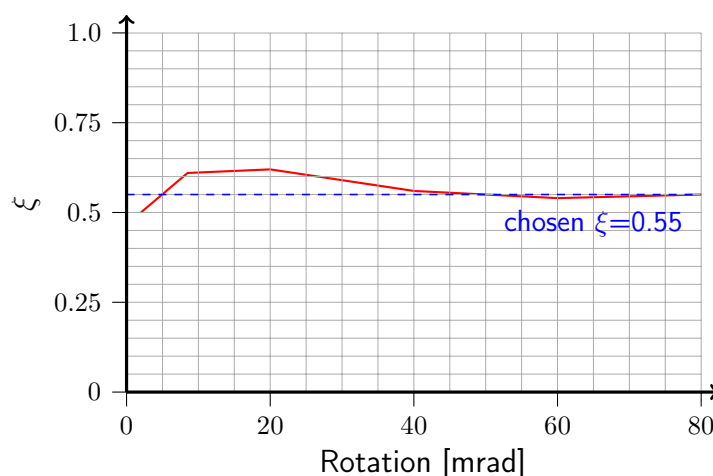


Figure 6.13: Illustration of the determined factor ξ depending on the rotation

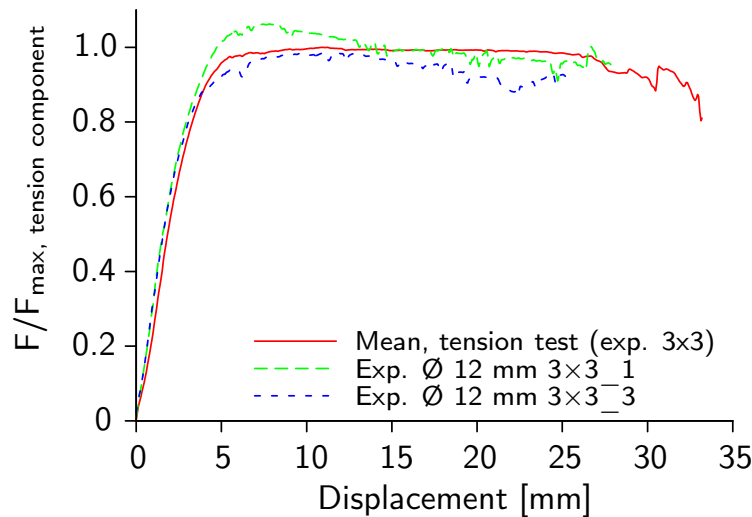


Figure 6.14: Results of the application with $\xi = 0.55$

block to the resultant force of the compression block (see Fig. 6.12). It can be seen, that a rather rectangular stress distribution is formed at the beginning of the loading. This changes rapidly to a triangular stress distribution at the intersection point between an elastic behavior to a plastic behavior. A parabola shaped distribution occurs within the plastic zone. An average ξ - factor for the determination of the lever arm within the compression zone is delineated to 0.55 (see Fig. 6.13).

Figure 6.14 shows the application of the proposed factor ξ . Both recalculated load-displacement behaviors of the dowels within the tension zone achieved from the bending experiment $\text{Ø } 12 \text{ mm } 3 \times 3_1$ and $\text{Ø } 12 \text{ mm } 3 \times 3_3$, show a good accordance with the pure load-displacement behavior evaluated within the tension experiments, except the ultimate load within the calculation of the first experiment, which is slightly higher.

6.2.4 Rotation of a group of dowels

The dowel arrangement induced a bending moment at the connections due to the rotation of the joint. The magnitude of the bending moment is determined by:

$$M_\phi = K_\phi \cdot \phi \quad (6.5)$$

with

$$K_\phi = K_{dowel} \cdot I_P$$

The moment-rotation behavior follows thereby the general load-deflection behavior of the dowel (K_{dowel}). The acting force at the compression zone respectively the normal force in the flitch plate is reduced due to the adjusting moment in the connection. The overall moment

of the joint is calculated by the following equation:

$$\begin{aligned} M_{joint} &= M_{\phi} + F_t \cdot e_t + F_c \cdot e_c \\ &= M_{\phi} + F_{t/c} \cdot e \end{aligned} \quad (6.6)$$

with

M_{ϕ} :	Moment at the dowel arrangement (comp. Eq. (6.5))	e_t :	Lever arm from the center line to the center of the dowel arrangement (see Fig. 6.4)
$F_{t/c}$:	Force acting in tension and/or compression	e_c :	Lever arm from the center line to the center of compression zone (see Fig. 6.4)
e :	Inner lever arm, depending on the assumed stress distribution within the compression zone (see Fig. 6.8)		

Strain gauges were placed on the flitch plate to gain information of the stresses in the flitch plate. The gauges were placed 20 mm from the top and bottom edge of the flitch plate on the front and on the back of the plate. Figure 6.15 shows the strain of the certain gauges in accordance with the rotation. It is obvious that the strain increases on the bottom of the flitch plate and decreases on the top due to the moment released by the rotation. This shows that a bending moment is acting at the connections. The bending moment increases with a growing rotation until a yielding of the dowels takes place.

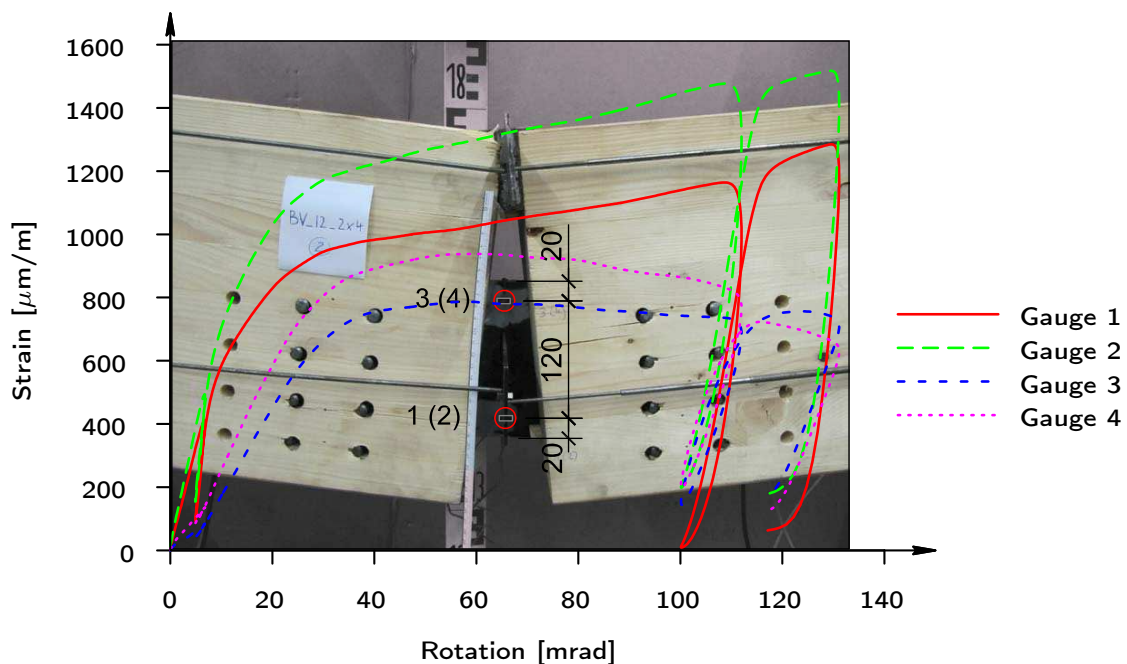


Figure 6.15: Strain distribution at the flitch plate

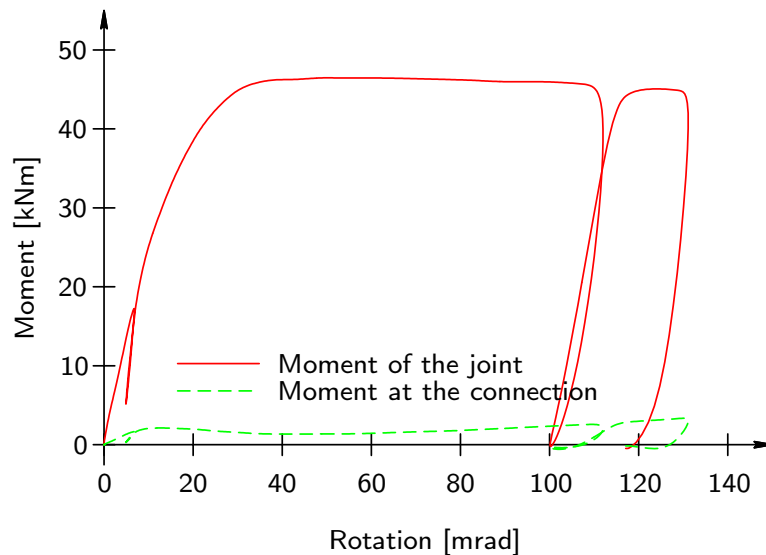


Figure 6.16: Moment share of the dowel arrangement on the overall bending moment of the joint (Exp. 2 with 2×4 dowels $\varnothing 12$ mm)

An unusual behavior was observed. The strain gauges placed at position 2, 3 and 4 did not place back to zero strain at the complete unloading at approximately 100 mrad. Although the investigations on the material properties showed that the steel section is in the elastic range at a strain of $1500 \mu\text{m}/\text{m}$ (comp. gauge 1). Furthermore, the strains on either side of the plate showed a pronounced difference. This could be due to a not centered flitch plate since a gap of 1 mm of each side to the timber was considered.

The bending moment within the flitch plate was calculated based on the strain measurements of the plate (see Fig. 6.15 & Fig. 6.16). A linear elastic stress distribution was assumed in the calculation. It can be seen that the proportion of the moment induced by the dowel arrangement is approximately 7 % for an arrangement with 2×4 dowels ($\varnothing 12$ mm).

Numerical determination

The dowels are stressed with an additional force perpendicular to the lever arm from each fastener to the center of the dowel arrangement (see Fig. 6.17). The additional component is considered within the numerical determination of the moment introduced by the rotation of the dowel alignment. The additional forces are divided into a horizontal component and a vertical component. In sum, these components are in equilibrium and do not form a resultant effect. Due to the equilibrium of the inner forces and the bending moment the various components depend on each other. The bearing resistance is found for every rotation step by using an iteration process. Therefore, the load deflection behavior of the pure tension experiment is divided into certain steps. The stiffness of the dowel arrangement is determined for every

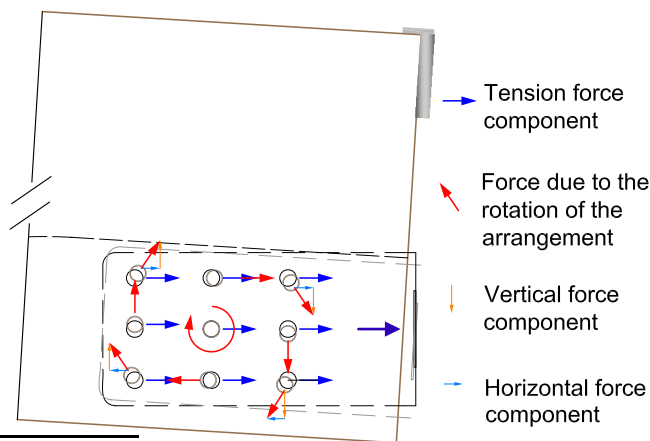


Figure 6.17: Components within the dowel arrangement

single step. If other hand, if the compression stiffness is considered, it is necessary to apply the iteration process to determine the actual rotation and thereby the distribution of the moment. Five iteration steps were conducted within every step. However, a good convergence was found in general after two iteration steps.

Considering a center of the stresses within the compression zone at $0.55 \times h$ from the bottom of the steel

block, it can be seen that the achieved moment-rotation behavior matches well with the mean value of the corresponding bending experiments (see Fig. 6.18). The stiffness and the ultimate load of the determined behavior are slightly higher within the transition of the elastic to the plastic area. The determined behavior matches in general well with the mean of the experiments on a arrangement of 3×3 dowels. The slight decrease of the moment capacity has not received any consideration since it is caused by a geometrical effect which is described at a later stage.

The moment of the dowel arrangement hold approximately 7 % to 8 % of the overall bending moment of the joint.

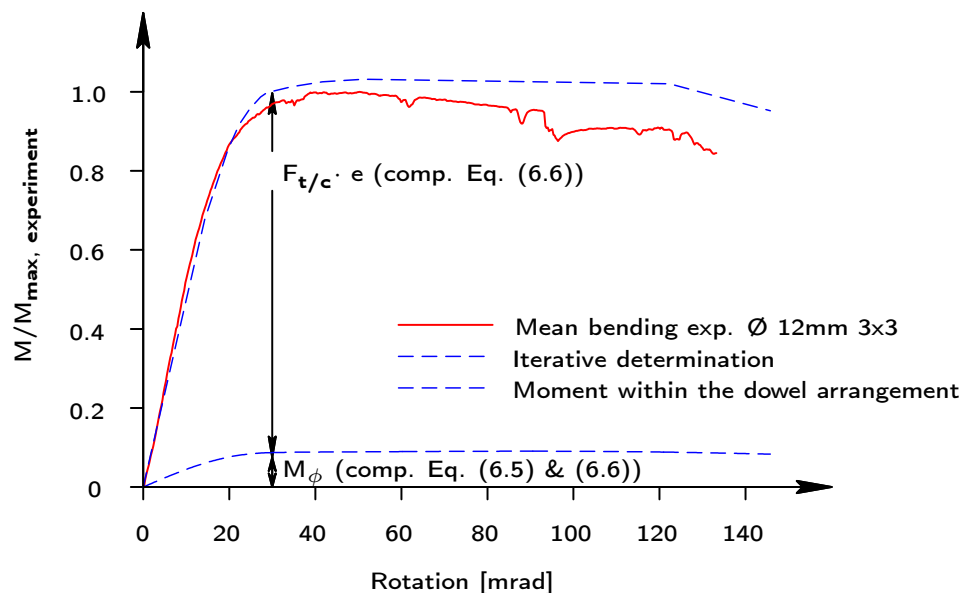


Figure 6.18: Distribution of the determined moment of the joint and the ratio of the moment at the dowel arrangement in comparison with the experimental result

6.3 Verification of the model

6.3.1 Comparison of the measurement results of the experiments on joints in bending

Inclinometers were provided within the design of the experiments besides the pure displacement transducers in the tension and compression zone (comp. Sec. 5.4). Therefore, it was possible to prove the results of the moment-rotation behavior based on the transducers with the tension- and compression zone with the results of the inclinometer. The distance between the transducer placed at the compression zone and the transducer in the tension zone forms the inner lever arm in the determination of the moment-rotation behavior (see Fig. 6.4).

The results based on the transducers show a well match with the inclinometer measurements (see Fig. 6.19). The left side of the joint shows a good accordance with initial stiffness whereas the right side underestimates the initial stiffness. This is associated with the stiffness of the dowel arrangement in the tension zone. The initial stiffness of the dowel group on the right hand side shows a smaller stiffness compared to the left side.

Having a look at the plastic area, the right side of the joint has a smaller rotation compared to the inclinometer measurement (see Fig. 6.19(b)). On the other hand, the left side of the joint indicated a larger rotation compared to the inclinometer measurement (see Fig. 6.19(a)). The differences of the magnitude of the rotation is substantiated by the larger deformations in the tension zone. The deformation in the tension zone is larger at the left side of the joint after a displacement of approximately seven millimeters compared to the right side (see Fig. 6.20). The overall rotation was compensated by the larger deformations

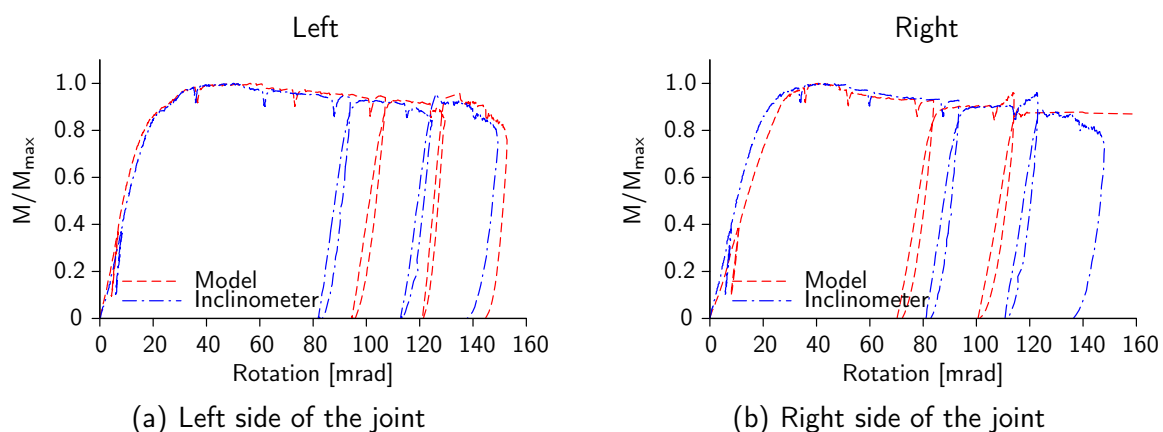


Figure 6.19: Comparison of the moment-rotation behavior based on the component model with the measurements of the inclinometers of the first experiment with 3×3 dowels (\varnothing 12 mm)

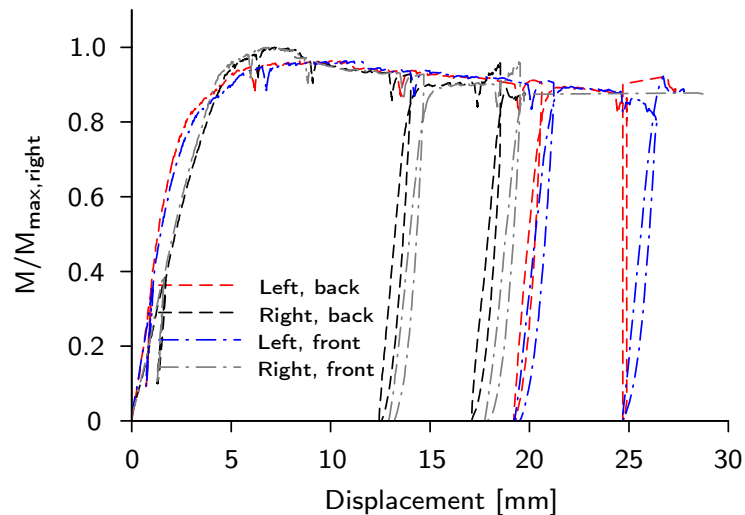


Figure 6.20: Load-deflection behavior of the left and right side of the dowel arrangement (Exp. 12_3x3_1)

in the compression zone at the right side of the joint.

Both sides of the joint show a significant ductile behavior despite the discussed differences.

6.3.2 Validation based on individual components

6.3.3 General

The previous investigations have shown, that it is in general possible to describe the moment-rotation behavior of a joint with the component model. The single explained components are assembled within these investigations. The study refers to the experiments conducted with a dowel arrangement of 3×3 dowels (\varnothing 12 mm). The ascertained moment-rotation behavior determined with the component model are compared with the mean of the inclinometer measurements of the left and right side of the corresponding performed bending experiments.

6.3.4 Discussion of the parameters

Different moment-rotation behaviors were performed in order to discuss the influence of the various components.

Modeling without considering the rotational stiffness

The component model was applied as a first step without the consideration of the rotational stiffness (comp. Sec. 6.2.4). The resultant within the compression zone is acting at a

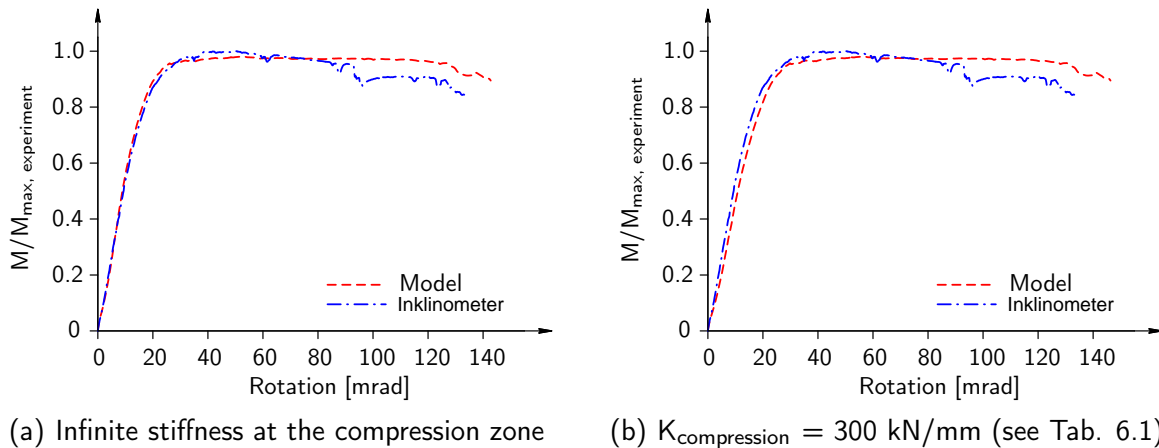


Figure 6.21: Comparison of the component model considering the stiffness at the compression zone ($\text{Ø}12 \text{ } 3 \times 3$)

distance of $0.55 \times h_{\text{compression-zone}}$ from the bottom of the steel block (see Fig. 6.12) within this study. Both approaches, with an infinite stiffness and a stiffness of 300 kN/mm , correspond well with the findings based on the inclinometer measurements (see Fig. 6.21). Figure 6.21(a) shows the determined moment-rotation behavior without considering the stiffness at the compression zone. The initial stiffness and the ultimate load matches well with the moment-rotation behavior conducted in the experiments. If attention is given to the stiffness of the compression zone, the initial stiffness is slightly underestimated compared to the experiments in bending (see Fig. 6.21(b)).

Modeling considering the rotational stiffness

The component model has been extended by considering the rotational stiffness. Again, the resultant at the compression zone is set to 55 % of the height of the steel block within this study.

The bending moment increases in both cases due to the additional bending moment at the connections at either side of the joint (see Fig. 6.18). The acting tension force has been calculated based on an iteration process. This was necessary since the magnitude of the forces depend on the actual rotation of the joint. Hence the corresponding bending moment is calculated based on Equation (6.6).

Figure 6.22 shows the results considering the rotational stiffness. As already stated, the results of the component model are compared with the mean of the experiments in bending with a dowel arrangement of 3×3 . The determined moment-rotation behavior conducted with the component model shows in both cases a very good match with the initial stiffness. The approximation without considering the stiffness at the compression zone, generates a higher stiffness at the transfer from the elastic to the plastic behavior (see Fig. 6.22(a)).

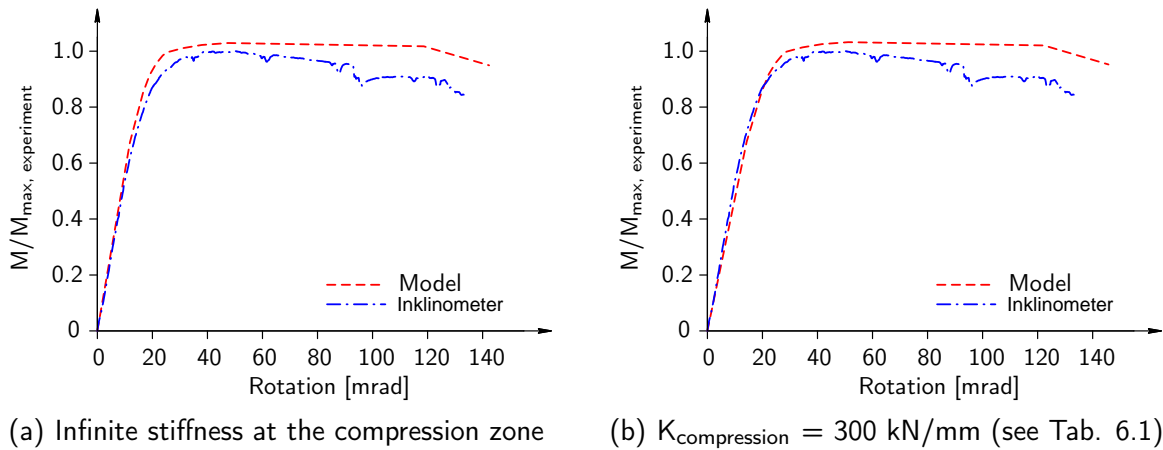


Figure 6.22: Comparison of the component model considering the rotational stiffness and the stiffness at the compression zone ($\varnothing 12 \text{ 3x3}$)

However, this transitional zone is better identified considering the compression stiffness (see Fig. 6.22(b)).

Both approximations obtain a higher ultimate load compared with the experimental studies. Furthermore the decrease of the moment carrying capacity is not represented with the model. Therefore, further investigations are required to calibrate the component model.

6.3.5 Geometrical conditions

The present state of the component model shows a very good match of the ultimate stiffness and a slightly higher ultimate load compared with the experimental results. However, the ultimate moment capacity and the decrease of the moment capacity is not represented.

The decrease of the ultimate moment capacity within the plastic level is caused by a geometrical effect. The inner lever arm is shortened due to the rotation of the joint which leads to a decrease of the inner lever arm by the distance $\Delta_{\text{lever arm}}$ (see Fig. 6.23). The center of the fastener arrangement is turning around the pivot point with a certain distance r . The pivot point of the joint is set to the corner of the top edge of the beam.

The shortening of the beam is calculated using the following correlations:

$$\Delta_{\text{lever arm}} = \sqrt{b^2 - u_i^2} \quad (6.7)$$

$$b = 2 \cdot r \cdot \sin\left(\frac{\phi}{2}\right) \quad (6.8)$$

with

$$r = \sqrt{a_{\text{End}}^2 + a_{\text{Top}}^2} \quad (6.9)$$

(see Fig. 6.23)

ϕ = Rotation of either side of the joint

u_i : Displacement

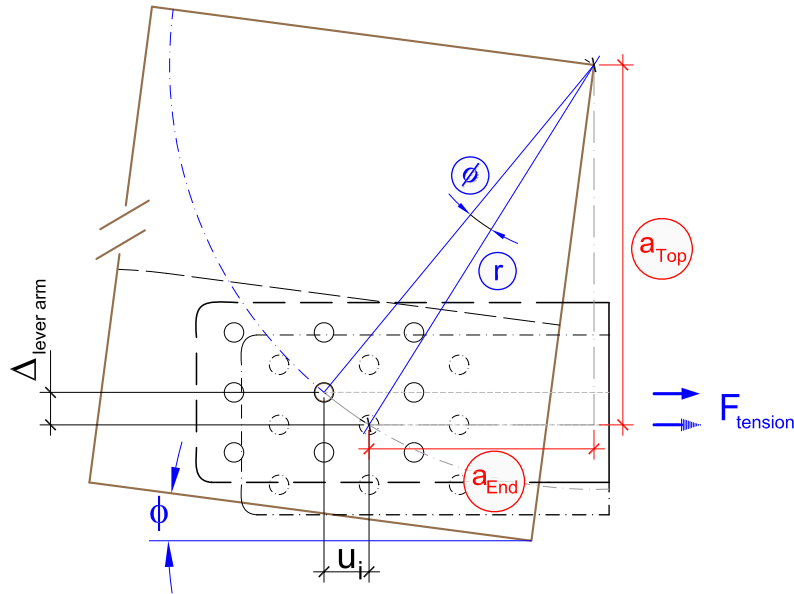


Figure 6.23: Shortening of the inner lever arm due to joint rotation

Figure 6.24 shows the determined results of the component considering the geometrical conditions. Both approaches match the experimental result very well. The approximation with an infinitive stiffness at the compression zone shows a very good correlation within the initial stiffness and the ultimate load (see Fig. 6.24(a)). On the other hand, considering the stiffness at the compression zone, the initial stiffness is slightly underestimated (see Fig. 6.24(b)). However, the transfer from the elastic to the plastic area is well displayed.

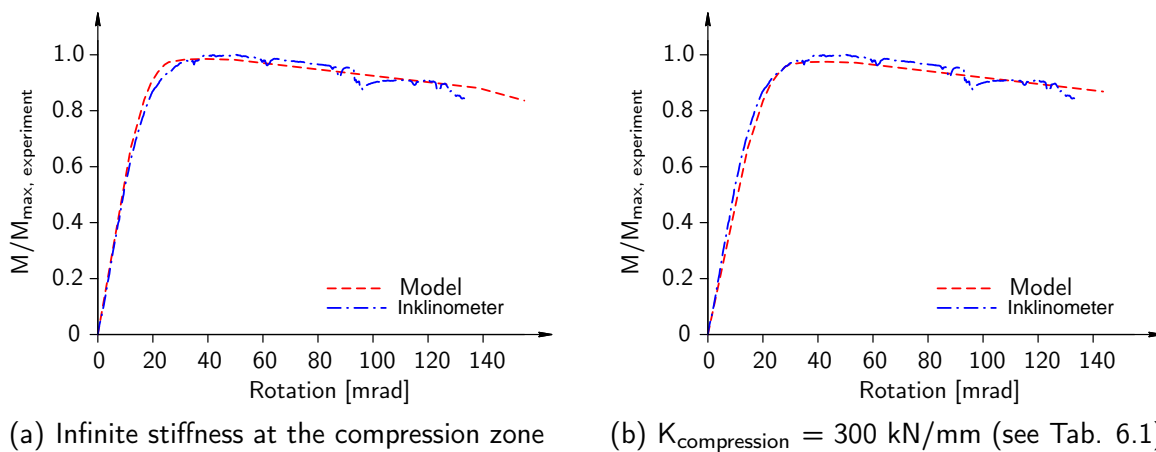


Figure 6.24: Comparison of the component model considering the rotational stiffness and the geometrical influence ($\text{Ø}12 \text{ 3x3}$)

6.3.6 Summary

The single components were added stepwise to discuss the influence of the single elements. After discussing the stress distribution at the compression zone, and therefore the dimension of the inner lever arm, the focus was set on the influence of the stiffness of the compression zone and the rotational stiffness. Furthermore a geometrical discontinuity was identified, explained and discussed. The introduced mechanical model, based on the component model, shows a good match with the experimental results in bending.

Since the determination of the nonlinear behavior is not applicable in practical use, a practical approach is formulated based on a multi-linear graph.

6.4 Simplification - proposal of a practical application

6.4.1 Introduction

To implement the component model, and therefore the nonlinear behavior of joints, it is necessary to develop a simplified procedure which describes the behavior in a reliable manner. Reliable not only in view of the load bearing resistance, but also concerning deformability. A known and regulated method is chosen to introduce the nonlinear method. The load-deflection behavior of the connection is shown as a trilinear graph (see Fig. 6.25). The various sections differ in the magnitude of the stiffness (K_i).

The simplification is performed based on the mean of the conducted experiments in tension with a diameter of 12 mm.

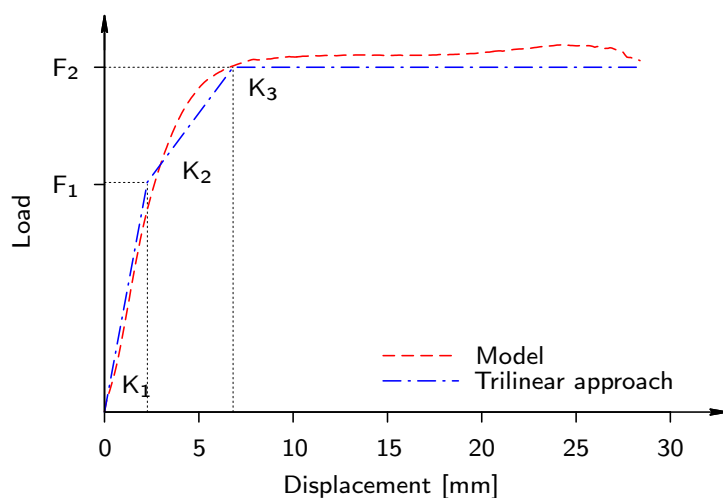


Figure 6.25: Simplification of the load-deflection behavior as a trilinear approach

6.4.2 Discussion of the initial stiffness

The initial stiffness (K_1) forms one of the most important input parameters to describe the load-deflection behavior as a trilinear approach. The initial stiffness of the experiments was calculated based on the rules of EN 26891 [110] (comp. Eq. (6.1)) on the mean of the conducted experiments with a dowel diameter of 12 mm. The experimentally derived value of the stiffness was found as 3747,8 N/mm.

Table 6.3: Determined stiffness K_{ser} [N/mm] based on various standards and densities

		ρ_{mean}	ρ_k	$\rho_{experiment}$
DIN 1052 [95]	(comp. Eq. (6.9))	5164.46	4444.54	5603.92
EN 1995-1-1 [109]	(comp. Eq. (6.10))	$2 \cdot 4490.84$	$2 \cdot 3864.82$	$2 \cdot 4872.97$
SIA 265:2012 [114]	(comp. Eq. (6.11))	$2 \cdot 4201.01$	$2 \cdot 3995.96$	$2 \cdot 4316.94$

The following densities have been applied:

$$\rho_{mean} = 420 \text{ kg/m}^3 [103] \quad \rho_k = 380 \text{ kg/m}^3 [103] \quad \rho_{experiment} = 443,5 \text{ kg/m}^3 \text{ (see Tab. 5.2)}$$

$$K_{ser} = \frac{\rho_k^{1.5} \cdot d}{20} \quad (6.9) \quad K_{ser} = \frac{\rho_m^{1.5} \cdot d}{23} \quad (6.10) \quad K_{ser} = 3 \cdot \rho^k \cdot d^{1.7} \quad (6.11)$$

Certain stiffness values based on various standards were determined to evaluate the magnitude achieved by the experiments (see Tab. 6.3). All of the standard related stiffness values overrate the ascertained stiffness value.

The embedded determination of the stiffness value based on EN 1995-1-1 [109] & SIA 265:2012 [114] allows a doubling of the stiffness value. This is related to the fact, that the conducted experiments to define the stiffness value were performed on timber to timber connections. Deformations are gained on either side of the connections per shear plane on timber to timber connections. The stiffness is therefore only half of the steel to timber stiffness whereas only one timber member is stressed and deformed. A doubling of the stiffness is certainly not confirmed.

As a point of fact it is necessary to discuss the stiffness value. Jorissen [84] also stated that the observed stiffness values of the conducted experiments considerably differ from the equation suggested in ENV 1995-1-1 [112], which is equal to the equation of DIN 1052 [95] (comp. Eq. (6.9)). Jorissen [84] introduced a factor k_{bolt} for multiple bolted connections. Equation 6.9 becomes:

$$K_{ser} = k_{bolt} \cdot \frac{\rho_k^{1.5} \cdot d}{20} = 0.3 \cdot \frac{\rho_k^{1.5} \cdot d}{20} \quad (6.12)$$

per shear plane.

Having a closer look at the performed experiments conducted by Jorissen [84] and described

in Section 3.2.7, Figure 6.26(a) shows the different load-displacement behavior with various numbers of fasteners in grain direction on timber connections with two shear planes. It can be seen, that the initial stiffness, determined per bolt, of a connection with a single fastener is by far higher compared to the connections with a certain number of fasteners. On the other hand, the initial stiffness on connections with a certain number of fasteners differ only slightly from each other. Sandhaas [91] conducted experiments on steel-to-timber connections as described in Section 4.3.2.2. The experiments with a diameter of 24 mm show the same findings (see Fig. 6.26(b)). A connection with a single dowel shows a higher stiffness compared to a multiple bolted connection.

The findings are verified with further experiments on a flitch plate connection with one single fastener. The test setup was similar to the conducted experiments on multiple bolted connections performed at the University of Stuttgart (comp. Chap. 5) [47]. Four tests were performed to gain knowledge of the load-displacement behavior. The used dowels belonged to the same lot as the main experiments. A slightly lower density of 438 kg/m^3 was measured.

Figure 6.27 shows the load-slip behavior of the conducted experiments with a dowel diameter of 12 mm. In order to ensure comparability, the certain load-slip behaviors are standardized to a single fastener with two shear planes. The conducted experiments present a higher stiffness of a single fastener as well. The doubling of the stiffness of a single fastener cannot be confirmed either. A stiffness of approximately 6500 N/mm per shear plane differs considerably from the values based on the codes [95, 109, 114].

The difference of the stiffness between a single fastener and a group of fasteners can be explained on the initial slip of each fastener within the connection. Unlike a single fastener, the initial slip of a group of fasteners does not act at the same stage. This means that a various displacement is required for each fastener till a force is transmitted. Hence the initial

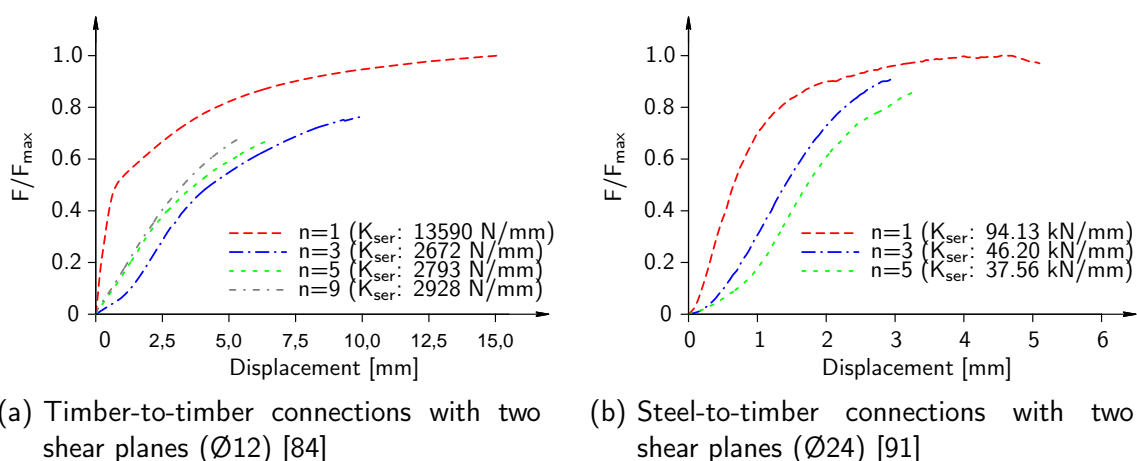


Figure 6.26: Comparison of the initial stiffness of various numbers of fasteners in grain direction (K_{ser} is determined per bolt)

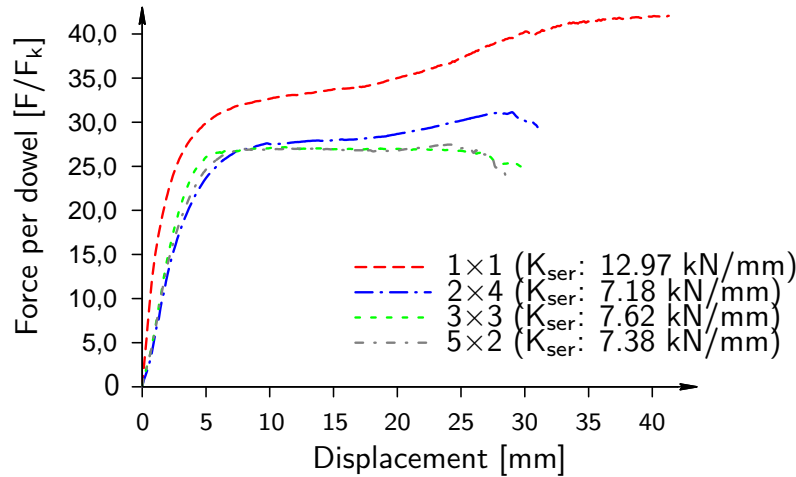


Figure 6.27: Comparison of the initial stiffness with a various number of fasteners on a flitch plate connection ($\text{Ø}12$; K_{ser} is determined per bolt)

slip is shifted along the elastic stage and leads to a decrease of the initial stiffness.

The initial stiffness matches well with the conducted experiments, if the doubling of the stiffness is not considered. The initial stiffness K_1 is therefore in the further consequence determined based on the equation formulated in EN 1995-1-1 [109] (comp. Eq. (6.10)) with the mean value instead of the characteristic value for the density.

6.4.3 Simplification of the load-deflection behavior

A simplified model has been developed to give a first approach for the practical application. The approach is consistent with known methods which are implemented in EN 1993-1-8 [107], which is a known and already applied method. Figure 6.28 shows the parameters to describe the behavior as a trilinear graph.

The characteristic load-bearing capacity ($F_{v,Rk}$) is a further important parameter to develop the approach. The ultimate characteristic load for flitch plate connections is given by [99, 109]:

$$F_{v,Rk} = \min \begin{cases} f_{h,1,k} \cdot t_1 \cdot d & (f) \\ f_{h,1,k} \cdot t_1 \cdot d \left(\sqrt{2 + \frac{4 \cdot M_{y,Rk}}{f_{h,1,k} \cdot d \cdot t_1^2}} - 1 \right) & (g) \\ \sqrt{2} \cdot \sqrt{M_{y,Rk} \cdot f_{h,1,k} \cdot d} & (h) \end{cases} \quad (6.13)$$

It is important, that the governing equation is either case **g** or **h**. Both cases consider a yielding of the fasteners which is of high importance if ductile behavior is applied.

The first part of the triangular graph is characterized by the initial stiffness and two thirds of the load-bearing capacity. Hence the first describing point is found by:

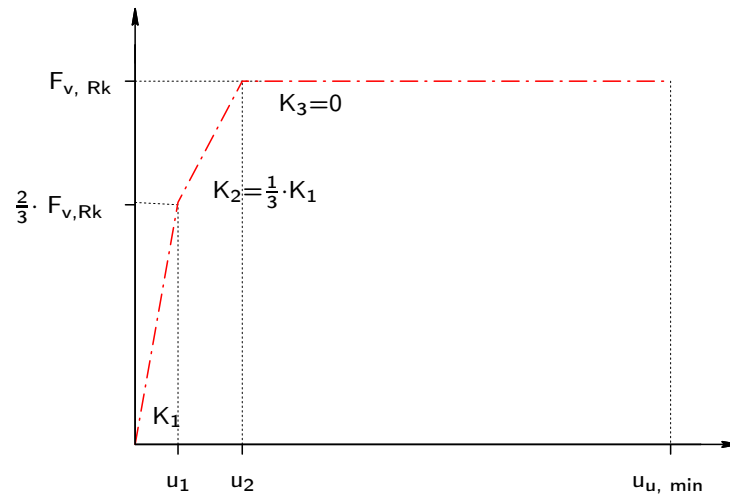


Figure 6.28: Possible description of the load-deflection behavior of a dowel connection under tension, following the regulations of [107]

$$F_1 = \frac{2}{3} \cdot F_{v,Rk} \quad (6.14) \quad u_1 = \frac{F_1}{K_1} = \frac{\frac{2}{3} \cdot F_{v,Rk}}{\frac{\rho_k^{1,5}}{23} \cdot d} \quad (6.15)$$

The stiffness of the second part is given by a stiffness of one third of the initial stiffness. Hence the second point is achieved by:

$$F_2 = F_{v,Rk} \quad (6.16) \quad u_2 = u_1 + \frac{\Delta F}{\frac{1}{3} \cdot K_1} = u_1 + \frac{F_{v,Rk}}{K_1} = \frac{\frac{2}{3} \cdot F_{v,Rk}}{K_1} + \frac{F_{v,Rk}}{K_1} = \frac{5}{3} \cdot \frac{F_{v,Rk}}{K_1} \quad (6.17)$$

The third part is characterized by an infinitesimal stiffness.

To describe the load-displacement behavior it is necessary to consider the ultimate displacement (u_u). A statistical study has been performed based on the experiments with a dowel diameter of 12 mm and 7 mm to gain knowledge of the plastic level. The explained 98 % percentile value is chosen for the statistical determination (see Tab. 5.14). Table 6.4 shows the main parameters gained from the study. The statistical distribution was chosen as log-normal distributed. The coefficient of variation shows a higher value for a diameter of 12 mm compared to a diameter of 7 mm. This results primarily from the fact that a plastic plateau is formed with a rather low stiffness, whereas a diameter of 7 mm shows an assigned stiffness. Hence the displacement of 98 % of the ultimate load is in the range of the displacement of failure and hardly varies. On the other hand, the displacement of 98 % of the ultimate load has a higher scattering due to high influence of an uncertain ultimate load within the plastic plateau (see Fig. 4.8).

To describe the ultimate displacement the 2 % percentile and the mean is applied and given

Table 6.4: Statistical parameters of the ultimate displacement (u_u)

	Ø 12 mm	Ø 7 mm
Mean	24.8 mm	34.9 mm
COV	32.0 %	15.0 %
2% percentile	12.4 mm	25.4 mm

within the further investigations.

6.5 Application and justification of the simplified model

6.5.1 General

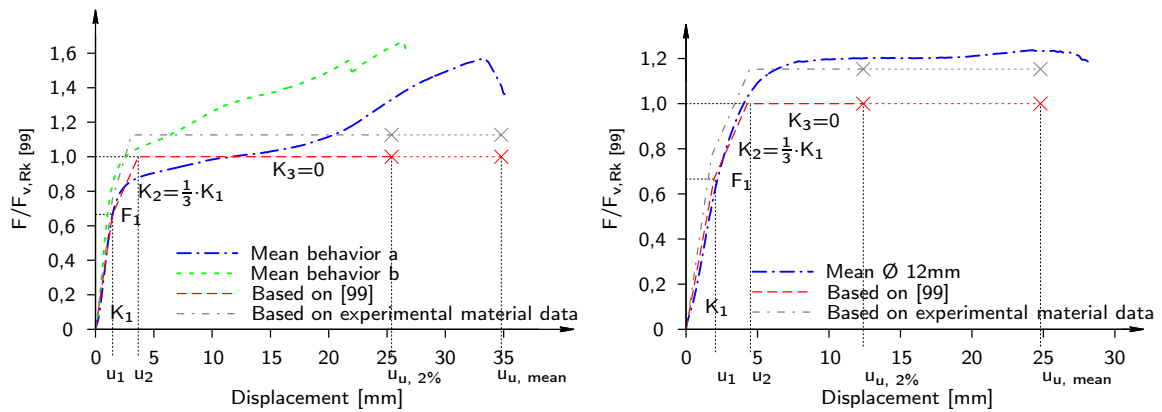
The previous introduced methods are applied to compare the trilinear approach with the actual load-displacement behavior gained from the performed experiments. Again, the justification is based on the mean of the experiments with a dowel diameter of 12 mm.

In a first step the component acting in tension is discussed, which is in a further step implemented to the developed component model to describe the moment-rotation behavior of a joint.

6.5.2 Load-displacement behavior

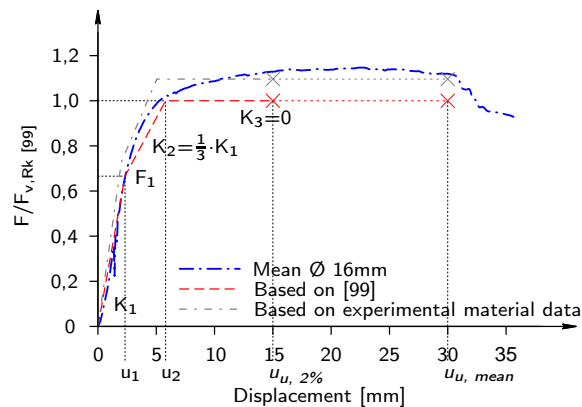
Figure 6.29 shows the comparison of the gained load-displacement behavior based on the simplified model and the mean value obtained with all experiments in a test setup. Two different proposals are shown. On the one hand the initial material properties (comp. Sec. 5.2.3), and on the other the material properties according to the standards. Within the standardized determination a characteristic timber density (ρ_k) of 380 kg/m³ [103] was chosen. Due to the increased tensile strength of the dowels, a steel grade of S355 ($f_{u,k}=510$ N/mm²) was chosen for the study on a diameter of 12 mm and 16 mm, and a tensile strength of 550 N/mm² for the dowels with a diameter of 7 mm.

The load bearing resistance of the conducted experiments show a good conformity with the trilinear approaches based on the initial properties. Since the input values of the standardized determination are lower than the actual properties, the load bearing resistance underestimates the experimental value with a diameter of 12 mm (see Fig. 6.29(b)) and 16 mm (see Fig. 6.29(c)). Investigations on a dowel diameter with 16 mm has also been conducted although the connections failed rather brittle (comp. Sec. 5.4). The displacement at failure was



(a) Results of the investigations with a diameter of 7 mm

(b) Results of the investigations with a diameter of 12 mm



(c) Results of the investigations with a diameter of 16 mm

Figure 6.29: Comparison of the load-displacement curve as a trilinear approach with the mean value of the experiments of the tension component

supposed as 30 mm, and the displacement at 98 % of the ultimate load is estimated to 15 mm.

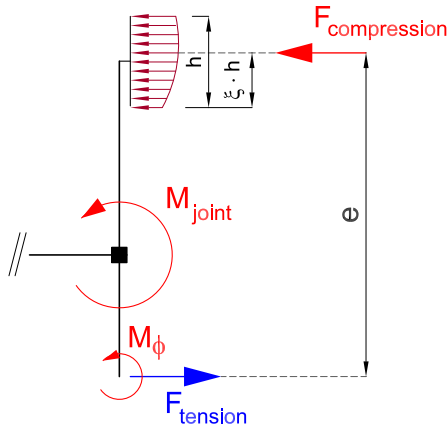
The initial stiffness of the experiments with a dowel diameter of 7 mm matches well with the conducted experiments. Considering EN 26891 [110], the maximum load within a displacement of 15 mm confirms the ultimate calculated load and the experimental results. All of the experiments show a pronounced ductile behavior. However, a direct comparison of the model with the results is hardly possible, since the experiments behave either with a constantly increasing load or a solidification.

6.5.3 Moment-rotation behavior

The previous section has shown a good accordance of the simplified trilinear approach, considering the experimental material properties. Since the trilinear approach with a diameter

of 7 mm was hardly possible, the experiments with this type of dowel is not closer exemplified in this section (see Fig. 6.29(a)).

Figure 6.30 shows the general approach to determine the load-displacement behavior as described in the previous sections.



with:

- M_{joint} : Moment at the joint
- M_{ϕ} : Moment triggered by the rotation of the connection (comp. Sec. 6.2.4)
- e : Inner lever arm (comp. Sec. 6.3.5)
- h : Height of the compression block

Figure 6.30: Depiction of the general model to describe the moment-rotation behavior

In order to simplify the determination of the moment-rotation behavior, factors are introduced to describe the behavior (see Tab. 6.5). Each of the represented data values is calculated based on the following equations:

$$M_{joint} = F_{v,Rk} \cdot e \cdot k_{\phi,e} \cdot k_{\phi,M} \tag{6.18}$$

$$\phi_{con} = \frac{u_{con}}{e \cdot k_{\phi,e}} \tag{6.19}$$

The different values of the load-displacement behavior are given as described in the previous section. The center of the compression zone was set to $0.55 \times h$ (see Tab. 6.2) from the bottom of the compression zone to determine the inner lever arm.

Both, the approach based on the material data given by DIN EN 1995-1-1/NA [99] and

Table 6.5: Introduced factors to determine the moment-rotation behavior

Factor	Description	Value
$k_{\phi,M}$:	This factor accounts for the moment within the dowel arrangement due to the rotation of the connection	1.08
$k_{\phi,e}$:	This factor accounts for the change of length of the inner lever arm due to the rotation of the connection	$\frac{e - \Delta_{lever\ arm}}{e}$
u_{con} :	Displacement of the connection	

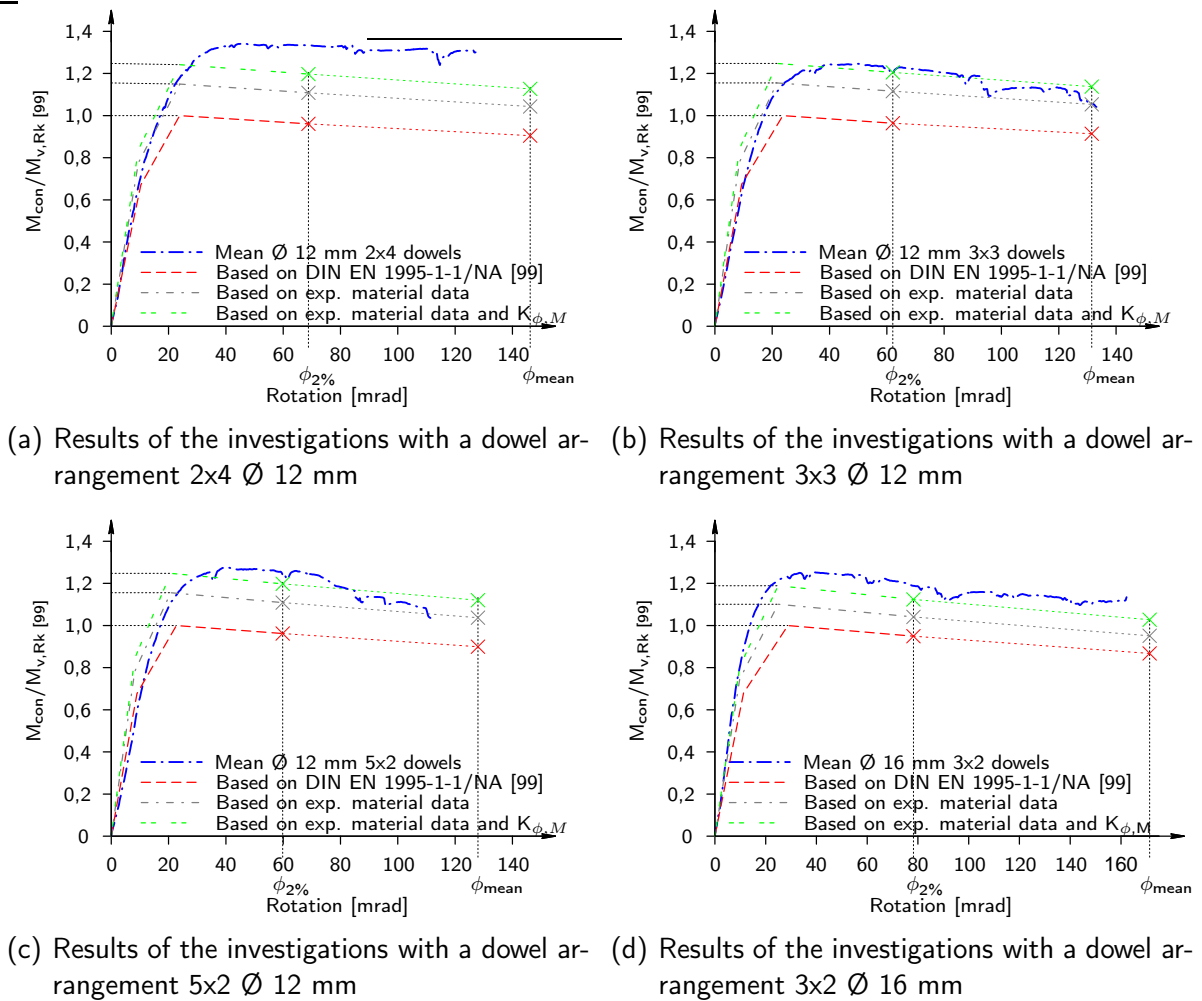


Figure 6.31: Comparison of the moment-rotation approach and the mean behavior of the corresponding experiment

investigated in the experiments underestimate the moment capacity of the connection (see Fig. 6.31). This characteristic is owed to the rotational stiffness. The given fact is represented by introducing the factor $k_{\phi,M}$. Considering the rotational stiffness, the ultimate moment capacity matches well with the results given by the experiments (see Fig. 6.31). An underestimation of the ultimate moment is only given within the experiments with a dowel diameter of 12 mm and a dowel configuration of 2x4 dowels (see Fig. 6.31(a)). This could be related with a generally higher load bearing capacity of the connection. The general load increase is between 22 % and 27 % percent compared to the bearing resistance calculated based on the material data given by the code (see. Fig. 6.31(b) to Fig. 6.31(d)). However, the increase of the ultimate load within the experiment with a dowel arrangement of 2x4 dowels is 34 % higher (see Fig. 6.31(a)).

The second important parameter is the rotational capacity of the connection. The ultimate rotation given by the experiments is for all experiments overestimated based on the mean

value of the ultimate displacement. On the other hand, the rotation capacity based on the 2 % percentile of the conducted experiments (see Tab. 6.4) gives a reliable rotation capacity of the joint.

The initial stiffness is slightly overestimated for dowels with a diameter of 12 mm. This is connected with the fact that the simplified model does not take the stiffness of the compression zone into account.

6.6 Summary

The analytical determination of the rotation capacity shows that it is in general possible to define the single components to describe the behavior of a connection with dowel type fasteners based on the component method. The single component of the dowels acting in tension was pointed out and discussed. It was possible to represent the behavior of connections with dowel-type fasteners as a trilinear approach based on known methods. Therefore, it is possible to describe the ductile behavior of such connections and bridge the gap to implement it in the standard for the application in elastic-plastic design methods [109, 5.1(3)].

For structures able to redistribute the internal forces via connections of adequate ductility, elastic-plastic methods may be used for the calculation of the internal forces in the members.

Since a hardening takes place on reinforced connections with self-drilling dowels, it was hardly possible to describe the load-deflection behavior and therefore a moment-rotation behavior. However, this is a desired behavior and needs more attention in further investigations.

The discussion on various connections showed that uncertainties take place due to the fluctuation of the material properties. Not only concerning the timber members, but also concerning the properties of the steel dowels.

The impact of the material scattering, first and foremost of the timber elements, is examined in more detail within the next chapter.

7 Effects of the material scattering

7.1 General

The inherent material properties of timber are characterized by the natural growth and the constantly exposed weather conditions in the lifetime of trees. Hence the properties are subjected to a highly distinctive material scattering. Particularly, the scattering of the density, the modulus of elasticity or similar properties have a great influence on the behavior, not only within a certain section (e.g. joints, supports, etc.) but also within a complete structural system. For instance Werner [93] and Jorissen [84] report on the bearing capacity of connections with dowel-type fasteners with the main focus on the

- embedment strength of the timber,
- splitting sensitivity,
- geometrical properties of the connection and
- mechanical fixing of the fastener within the timber

in dependence on the dispersive material properties.

The material varieties are not only locally placed, but also of global extent. The research work in grading in fact could prove that the material properties (e.g. density, bearing resistances, etc.) depend on the location of growth. First investigations showed that sawn timber from the south-eastern parts of Europe have a lower bending resistance than sawn timber from middle and northern European areas [71].

In the description of the experiments (comp. Sec. 5.2.3) it has been shown that the material properties and the coefficient of variation of the manufactured boards are subjected to a large variance. This confirms that it is significant to consider the material scattering, not only in view of the bearing capacity in bending ($f_{t,0} \Rightarrow f_m$), the load carrying capacity of fasteners (ρ_{den}) but also with attention to the deformation behavior (E_0).

In order to introduce plastic hinges into timber structures it is inevitable to consider these natural conditions.

7.2 Introduction of an over-strength factor

7.2.1 General

Within steel structures it is under certain requirements possible to form plastic hinges either in the structural element or in the joint. Conversely, in timber structures it is only possible to develop plastic hinges in the joint.

Regardless of the subsequent application of the ductility it is of the utmost importance to guarantee a plastification of the ductile element within timber structures before a brittle element fails. Paulay and Priestley [59] developed the capacity design method with view on the earthquake safety of reinforced concrete and masonry structures. The capacity design method considers over-strength values within a structural system and introduces a factor, which ensures that no brittle element fails with a certain probability. As an example of a

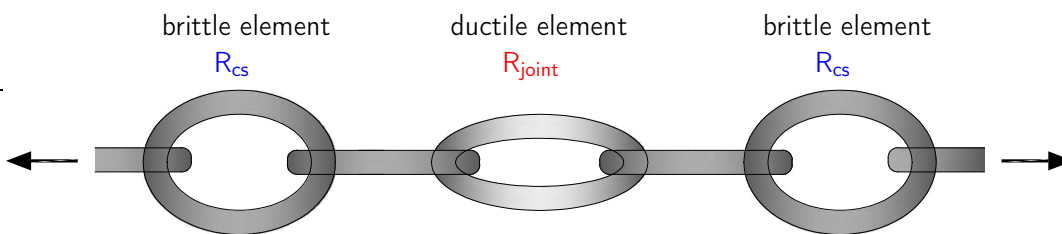


Figure 7.1: Series of different structural elements [59]

series of different structural elements, represented as chain links, Figure 7.1 shows that the bearing resistance of the brittle elements have to be higher than the bearing resistance of the ductile element. If both bearing members consist of the same bearing resistance, the likelihood of a brittle failure is considerable.

In order to avoid a brittle failure, the factor k_{cs} is introduced. The factor is defined as the quotient of the bearing resistance of the joint (R_{joint}), the ductile element, to the bearing resistance of the timber member (R_{cs}), the brittle element, next to the joint. The factor ensures with a certain probability that the ductile element yields before a brittle failure occurs.

$$\frac{M_{joint}}{M_{cs}} \leq k_{cs} \quad (7.1)$$

$$k_{cs} < 1.0$$

The current version of the Swiss timber code already implements an over-strength factor if ductility is required [114, 4.6.3.1]. The introduced factor is indicated by 1.2. It has to be stated, that the given over-strength factor in SIA 265:2012 [114] is a multiplier for the brittle element to gain a certain strength in order to have a ductile failure. Within this work the over-strength factor is the reciprocal showing a certain reduced strength of the ductile element. Hence, the over-strength factor (k_{cs}) is between zero and one (comp. Eq. (7.1)).

Figure 7.2 describes the general influence of the introduced over-strength factor on the load bearing situation at a joint in timber structures. Within the system analysis the factor k_{cs}

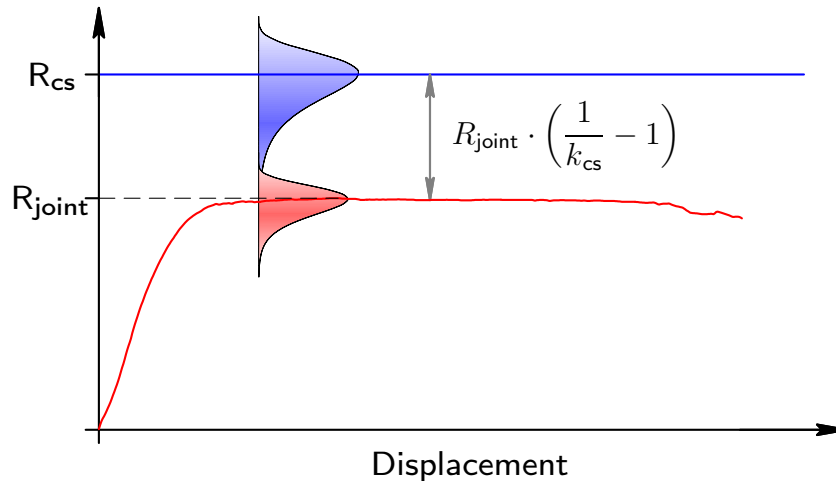


Figure 7.2: Representation of the over-strength factor k_{cs}

has to consider the material scattering not only in view of the bearing resistance of the cross-section, but also with respect to the load capacity of the joint. Furthermore, attention has to be given to possible interactions of material properties which are driving parameters on both, the bearing resistance of the cross-section and the load capacity of the joint.

7.2.2 Representation of the failure probability

7.2.2.1 Basic rules

Figure 7.3(a) shows a possible density distribution of two variables x_1 and x_2 . The peak of the density distribution characterizes the highest probability of occurrence and is defined by the mean values of both variables.

The limit state function is given by the zero points of:

$$g(x_1, x_2) = x_2 - x_1 \quad (7.2)$$

The results of Equation (7.2) can be summarized as follows (see Fig. 7.3(b)):

- $g(x_1, x_2) > 0$ The limit state is not reached, thus the variation is on the safe set.
- $g(x_1, x_2) < 0$ The limit state is reached, thus the variation is on the failure set.
- $g(x_1, x_2) = 0$ Meets exactly the limit state and is thus indifferent.

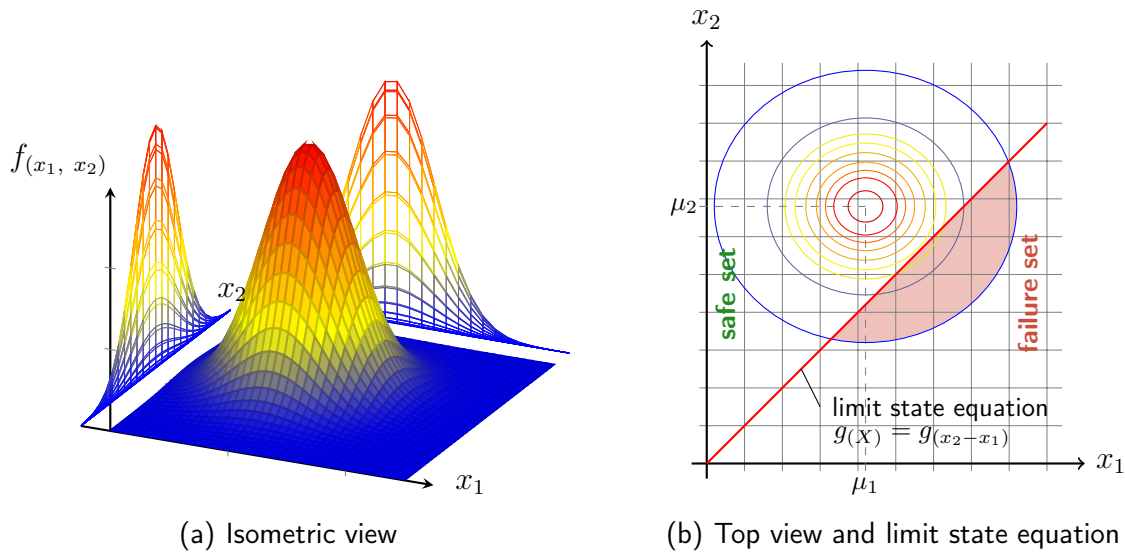


Figure 7.3: Illustration of a possible density distribution [58]

The magnitude of the failure probability (P_f) is defined as [25]:

$$P_f = P(g(x_1, x_2) < 0) = P(g(X) < 0) = \int_{D(g(X) < 0)} f_X(X) dX \quad (7.3)$$

and is represented by the volume of the red shaded area in Figure 7.3(b).

Within Equation (7.3) X represents the vector of the two variables x_1 and x_2 , and D the area where Equation (7.2) reaches a value smaller than zero.

For normal distributions, the probability of failure can be found as:

$$P_f = \Phi(-\beta) \quad (7.4)$$

Whereas the factor β in Equation (7.4) represents the so called reliability index and Φ is the Gaussian distribution. Table 7.1 shows the correlation of the beta-index and the failure probability.

Table 7.1: Correlation of P_f and β

β	0	1	2	3	4	5	6	7	8	9	10
P_f	0.5	1.587 $\cdot 10^{-1}$	2.275 $\cdot 10^{-2}$	1.350 $\cdot 10^{-3}$	3.169 $\cdot 10^{-5}$	2.871 $\cdot 10^{-7}$	9.901 $\cdot 10^{-10}$	1.288 $\cdot 10^{-12}$	6.285 $\cdot 10^{-16}$	1.145 $\cdot 10^{-19}$	7.770 $\cdot 10^{-24}$

7.2.2.2 Demands on the failure probability

The principle of the failure probability was introduced the first time in the late sixties in North America [4]. In the early eighties it was introduced in Germany by DIN Deutsches Institut für Normung e.V. [21]. The approach differs significantly from the previous considerations, since it was accepted, that not all hazards can be excluded. In fact the point of view was set to the handling and estimation of possible structural failures [21].

The consequences of a possible failure specify the target value of the reliability. Therefore the required reliability is mainly based on the limit state (ULS or SLS) and the consequences respectively the economic damage. DIN Deutsches Institut für Normung e.V. [21] classifies buildings in three different safety categories (see Tab. 7.2). The required reliability is then

Table 7.2: Safety categories of buildings [21]

Possible consequences		Class
Mainly concerning the ultimate limit state	Mainly concerning the serviceability	
No serious danger to safety of life, relatively small economical effects	Limited limitation in use, relatively small economical effects	1
Serious danger to safety of life and/or serious economical effects	Significant limitation in use, serious economical effects	2
Major importance of the building to the public	Major limitation in use, major economical effects	3

assigned to the different safety classes (see Tab. 7.3).

The currently valid EN 1990 [104] adopted the approach and introduced consequence classes as well. The consequence classes (CC) are directly associated with the introduced reliability classes (RC) (see Tab. 7.4). Table 7.5 shows the minimum required reliability index depending on the reliability class. Within the reliability class 2, Table 7.5 is extended by the consideration of fatigue and the serviceability limit state (see Tab. 7.6).

Table 7.3: Required reliability index β in a one year period [21]

	Safety class		
	1	2	3
Ultimate limit state (ULS)	4.2	4.7	5.2
Serviceability limit state (SLS)	2.5	3.0	3.5

Table 7.4: Definition of consequence classes EN 1990 [104]

Consequence Class	Description	Examples of buildings and civil engineering works
CC3	High consequence for loss of human life, or economic, social or environmental consequences very great	Grandstands, public buildings where consequences of failure are high (e.g. a concert hall)
CC2	Medium consequence for loss of human life, economic, social or environmental consequences considerable	Residential and office buildings, public buildings where consequences of failure are medium (e.g. an office building)
CC1	Low consequence for loss of human life, and economic, social or environmental consequences small or negligible	Agricultural buildings where people do not normally enter (e.g. storage buildings), greenhouses

Table 7.5: Recommended minimum values for the reliability index β (ULS) EN 1990 [104]

Reliability class	Minimum values for β	
	1 year reverence period	50 year reverence period
RC3	5.2	4.3
RC2	4.7	3.8
RC1	4.2	3.3

Table 7.6: Target reliability index β for class RC2 structural members EN 1990 [104]

Limited state	Target reliability index	
	1 year	50 year
Ultimate	4.7	3.8
Fatigue		1.5 to 3.8
Serviceability (irreversible)	2.9	1.5

The Joint Committee on Structural Safety (JCSS) [38] gives another extension by the relative costs of the safety measure for the reliability index (see Tab. 7.7). The shaded value

Table 7.7: Tentative target reliability indices β (and associated target failure rates) [38]

Relative costs of safety measure	Minor consequence failure	Moderate consequence failure	Large consequence failure
Low	$\beta=3.1$ ($P_f \approx 10^{-3}$)	$\beta=3.3$ ($P_f \approx 5 \cdot 10^{-4}$)	$\beta=3.7$ ($P_f \approx 10^{-4}$)
Normal	$\beta=3.7$ ($P_f \approx 10^{-4}$)	$\beta=4.2$ ($P_f \approx 10^{-5}$)	$\beta=4.4$ ($P_f \approx 5 \cdot 10^{-5}$)
High	$\beta=4.2$ ($P_f \approx 10^{-5}$)	$\beta=4.4$ ($P_f \approx 5 \cdot 10^{-5}$)	$\beta=4.7$ ($P_f \approx 10^{-6}$)

in Table 7.7 is recommended by [38] for most of the common design situations. The recommendation refers to the ultimate limit state and to a one year reference period [86]. Another aspect is the type of failure and the resulting consequences. The type of failure are classified according to [38] as:

- a) ductile failure with reserves in the strength (e.g. resulting from strain hardening)
- b) ductile failure with no reserves in the strength
- c) brittle failure

A ductile failure has an inherent warning system, whereas a brittle element fails without warning. Hence brittle structural elements should be designed for a higher reliability level [38].

It has been shown, that reinforced dowel type connections have a significant ductile behavior, which in some cases even behave with reserves in the strength. Therefore, the importance of ductile connections is also emphasized in view of the reliability.

7.2.3 Determination of the structural reliability

7.2.3.1 General

The reliability index β is given as the smallest distance of the limit state equation to the peak of the density distribution. The resultant point on a linear limit state function is represented as the design point (see Fig. 7.4). In order to determine the reliability index β the independent normal distributed variables x_1 and x_2 are normalized into standardized normal distributed random variables u_1 and u_2 with Equation (7.5) and Equation (7.6). Therefore, the random variables u_1 and u_2 have zero means and uniform standard deviation [86].

$$u_1 = \frac{x_1 - \mu_1}{\sigma_1} \quad (7.5)$$

$$u_2 = \frac{x_2 - \mu_2}{\sigma_2} \quad (7.6)$$

The inclination of the limit state function (g_U) is changing and depends on the ratio of the

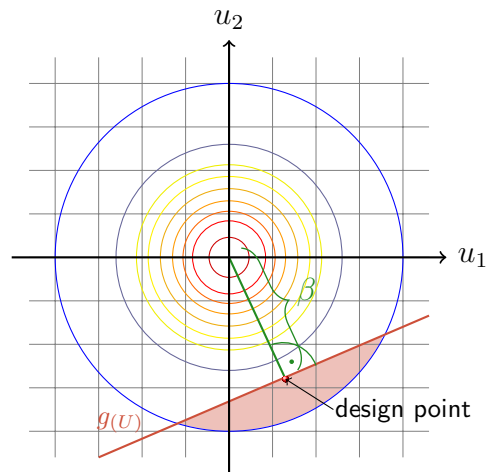


Figure 7.4: Standardized normal distributed variables [58]

standard deviation of σ_1 to σ_2 [58]. The limit state function turns into:

$$\begin{aligned} u_2 \cdot \sigma_2 + \mu_2 - u_1 \cdot \sigma_1 - \mu_1 &= 0 \\ u_2 \cdot \sigma_2 - u_1 \cdot \sigma_1 + \mu_2 - \mu_1 &= 0 \end{aligned} \quad (7.7)$$

By standardizing Equation 7.7 the general *Hessian normal form* is obtained.

$$u_2 \cdot \frac{\sigma_2}{\sqrt{\sigma_1^2 + \sigma_2^2}} - u_1 \cdot \frac{\sigma_1}{\sqrt{\sigma_1^2 + \sigma_2^2}} + \frac{\mu_2 - \mu_1}{\sqrt{\sigma_1^2 + \sigma_2^2}} = 0 \quad (7.8)$$

Therefore, the distance and thus the reliability index β for a linear limit state function is

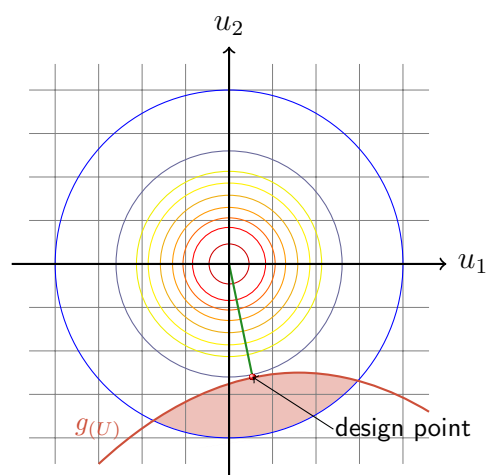


Figure 7.5: Standardized normal distributed variables with a nonlinear limit state function [58]

given by:

$$\frac{\mu_2 - \mu_1}{\sqrt{\sigma_1^2 + \sigma_2^2}} = \beta \quad (7.9)$$

The previous described method is only suitable for linear state functions and normal distributed variables. Only a limited number of limit state functions fulfill these conditions. Figure 7.5 shows the geometrical situation with a nonlinear limit state function and two standardized normal distributed random variables u_1 and u_2 . It becomes obvious that the minimum distance cannot be found by applying the *Hessian normal form*.

7.2.3.2 First order reliability method

There are different approaches to determine the structural reliability for non-linear limit state functions with various distributed variables [22].

Well known are the First Order Reliability Method (FORM) and Second Order Reliability Method (SORM) to determine the failure probability with a n-dimensional density. Both methods form an iterative approach to find the design point. The following optimization problem has to be solved [86]:

$$\beta = \min_{u \in \{g(u)=0\}} \sqrt{\sum_{i=1}^n u_i^2} \quad (7.10)$$

One possible iterative approach (FORM) is described hereafter according to Spaethe [70]. The iteration process starts with an arbitrary chosen vector x^k , $k=0$. The start vector can be estimated based on the expected value. All of the non-normal distributed variables are approximated to normal distributed variables. A good approach is found if both the density and the distribution function are equal in x^k [70]. The standard deviation of the approximated normal distribution is found by:

$$\sigma_{\tilde{X}_i}^{(k)} = \frac{1}{f_{X_i}(x_i^{(k)})} \varphi \left(\Phi^{-1} \left(F_{X_i}(x_i^{(k)}) \right) \right) \quad (7.11)$$

The mean value is given as:

$$\mu_{\tilde{X}_i}^{(k)} = x_i^{(k)} - \sigma_{\tilde{X}_i}^{(k)} \Phi^{-1} \left(F_{X_i}(x_i^{(k)}) \right) \quad (i = 1, 2, \dots, n) \quad (7.12)$$

The density and the distribution function are exemplary shown for a log-normal distribution

$$\begin{aligned} f_{X_i}(\tilde{x}_i^{(k)}) &= \frac{1}{\sigma_{\tilde{X}_i} \cdot \tilde{x}_i^{(k)} \cdot \sqrt{2 \cdot \pi}} \exp \left(-\frac{(\ln \tilde{x}_i^{(k)} - \mu_{\tilde{X}_i})^2}{2 \cdot \sigma_{\tilde{X}_i}^2} \right) \\ &= \frac{1}{\sigma_{\tilde{X}_i} \cdot \tilde{x}_i^{(k)}} \varphi \left(\frac{\ln \tilde{x}_i^{(k)} - \mu_{\tilde{X}_i}}{\sigma_{\tilde{X}_i}} \right) \end{aligned} \quad (7.13)$$

$$\begin{aligned}
 F_{X_i}(\tilde{x}_i^{(k)}) &= \frac{1}{\sigma_{\tilde{X}_i} \cdot \sqrt{2 \cdot \pi}} \int_0^{\tilde{x}_i^{(k)}} \frac{1}{u} \exp\left(-\frac{(\ln u - \mu_u)^2}{2 \cdot \sigma_u}\right) du \\
 &= \Phi\left(\frac{\ln \tilde{x}_i^{(k)} - \mu_{\tilde{X}_i}}{\sigma_{\tilde{X}_i}}\right)
 \end{aligned}
 \tag{7.14}$$

Figure 7.6 shows the approximation of a log-normal distributed density to a normal distributed density using Equation (7.11) & Equation (7.12). If all of the variables are approximated

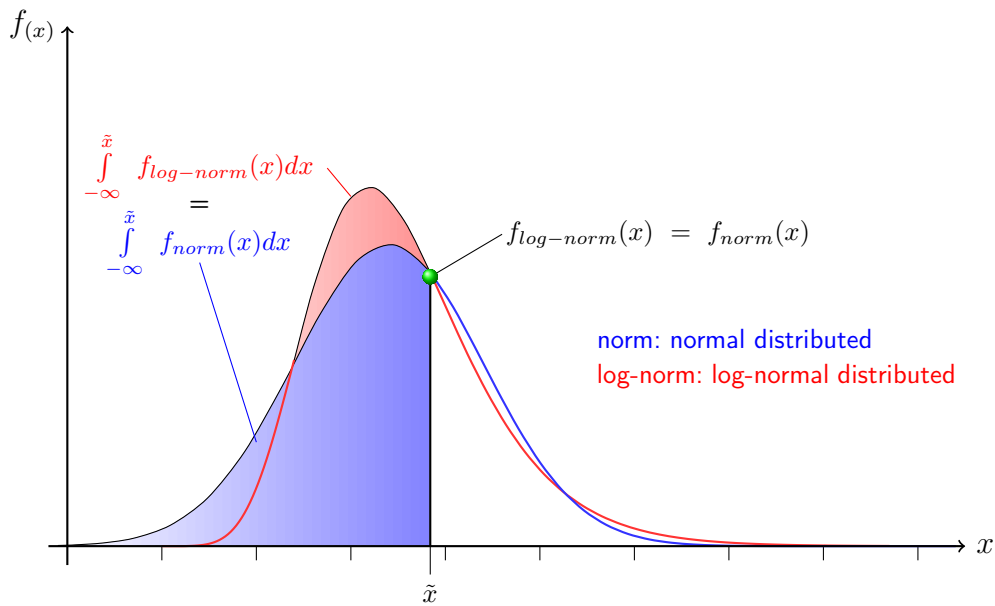


Figure 7.6: Representation of the approximation of a log-normal distributed density to a normal distributed density

to the normal distributed density, the variables are normalized into standardized normal distributed random variables. According to Equation (7.5) and Equation (7.6) the following equation is given:

$$u_i^{(k)} = \frac{x_i^{(k)} - \mu_{\tilde{x}_i}^{(k)}}{\sigma_{\tilde{x}_i}^{(k)}} \quad (i = 1, 2, \dots, n)
 \tag{7.15}$$

The limit state function and the partial derivations are determined in a further step.

$$\left. \frac{\partial g}{\partial u_i} \right|_{u=u^{(k)}}
 \tag{7.16}$$

To ascertain the $\beta^{(k)}$ value within the iteration step, it is important to calculate the coefficients $\alpha_i^{(k)}$ of the tangential hyperplane to $g(u) = 0$ in the point U^k .

$$\alpha_i^{(k)} = \frac{-\left. \frac{\partial g}{\partial u_i} \right|_{u=u^{(k)}}}{\sqrt{\sum_{j=1}^n \left(\left. \frac{\partial g}{\partial u_j} \right|_{u=u^{(k)}} \right)^2}} \quad (i = 1, 2, \dots, n) \quad (7.17)$$

If the limit state function ($g_{(U^k)}$) is greater than 0 the reliability index β^k is given by:

$$\beta^{(k)} = \frac{g_{(U^k)} - \sum_{j=1}^n u_j^{(k)} \left. \frac{\partial g}{\partial u_j} \right|_{u=u^{(k)}}}{\sqrt{\sum_{j=1}^n \left(\left. \frac{\partial g}{\partial u_j} \right|_{u=u^{(k)}} \right)^2}} \quad (7.18)$$

An enhanced start vector for the next iteration step can be determined by

$$x_i^{(k+1)} = \mu_{\tilde{X}_i}^{(k)} + \alpha_i^{(k)} \cdot \sigma_{\tilde{X}_i}^{(k)} \cdot \beta^{(k)} \quad (i = 1, 2, \dots, n) \quad (7.19)$$

The reliability index β is found if $x_i^{(k+1)} \approx x_i^{(k)}$.

The relative importance of the random variables may be interpreted by the components of the vector α [86].

7.2.3.3 Monte-Carlo simulation

Another method to determine the reliability index is using the Monte-Carlo simulation. The method is named after the well known casino in Monte-Carlo. The casino posted regularly tables of randomized numbers which are based on the results of their roulette [34]. Metropolis and Ulam [54] picked up the suggestion to simulate the magnitude of parameters based on random numbers. This was the beginning of the Monte-Carlo simulation.

The numerical approach is based on a stochastically formulated model, for instance a limit state function ($g(x)$). Thereby numerous randomized experiments are conducted with a variety of random variables x_i .

To represent the properties of the variables, randomized numbers (p_n) are conducted in the range between 0 and 1. The distribution function of the variable x_i is known, therefore the magnitude associated with the randomized number is found by:

$$X = F^{-1}(P) \quad (7.20)$$

Figure 7.7 shows exemplarily the determination of the variable x_n , in this case the timber density based on the known distribution function and the density. If the randomized num-

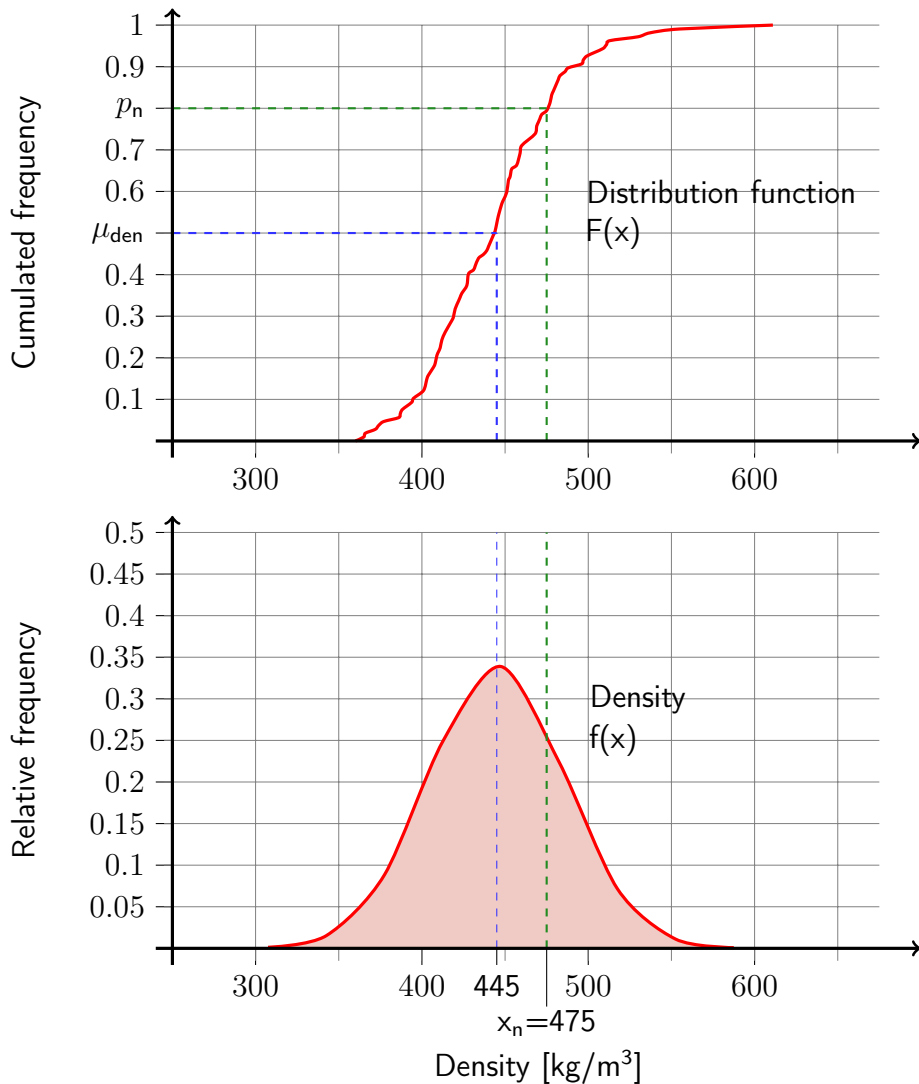


Figure 7.7: Determination of randomized variables based on the distribution function

bers (p_n) are uniformly distributed, which is assumed, the determined variables follow the distribution function F_x . The ascertained variables are implemented into the stochastically formulated model.

The outcome of the randomized experiment is either on the safe set ($g(x) > 0$) or on the failure set ($g(x) \leq 0$). According to Equation (7.3) the failure probability can be found as [86]:

$$P_f = P(g(x) < 0) = \lim_{n \rightarrow \infty} \frac{n_f}{n} \quad (7.21)$$

with:

- n = number of randomized experiments
- n_f = number of experiments on the failure set

EN 1990 [104] refers directly to the artificial experiments. Based on Equation (7.9) the reliability index can be found as:

$$\beta = \frac{\mu_g}{\sigma_g} \quad (7.22)$$

where μ_g represents the mean value of the artificial experiments and σ_g the corresponding standard deviation.

Accuracy of the Monte-Carlo simulation

The Monte-Carlo simulation represents a rather time-consuming method since a considerable computing time is necessary. In order to estimate the number of simulations it is necessary to have a closer look at the accuracy of the method.

The expected value x can be found within a set of n samples (x_1, x_2, \dots, x_n). Hence the function

$$\bar{x} = \frac{1}{n} \sum_{k=1}^n x_k \quad (7.23)$$

gives an unbiased value [34]. Based on the central limit theorem, the sample variance is found by

$$\sigma^2 = \frac{1}{n-1} \sum_{i=1}^n (x_k - \bar{x})^2 \quad (7.24)$$

Applying the law of large numbers, the sample variance converges with a probability 1 to $\text{Var}(X)$ [65]. Hence the confidence interval for x is given by:

$$\left(\bar{x} - z_{(1-\alpha/2)} \frac{\sigma}{\sqrt{n}}, \bar{x} + z_{(1-\alpha/2)} \frac{\sigma}{\sqrt{n}} \right) \quad (7.25)$$

The term $z_{(1-\alpha/2)}$ represents the $(1-\alpha/2)$ quantile of the standard deviation [65]. For instance, for $\alpha=0.1$ the term $z_{(1-\alpha/2)}=z_{0.95}$ results to 1.645.

It is shown that the uncertainty depends on the number of samples and is directly proportional to $1/\sqrt{n}$. The failure probability is a rather small number, e.g. in the magnitude of 10^{-6} (see Tab. 7.1). Rubinstein and Kroese [65] give a proposal to determine the relative error κ by:

$$\kappa \approx \sqrt{\frac{1}{n \cdot P_f}} \quad (7.26)$$

Hence 10^8 simulations should be calculated in order to achieve a result with a relative error of $\kappa=0.1$. Assessing the computing time Figure 7.8 shows the relative error depending on the failure probability for 10^8 simulations. It can be shown that the number of simulations is a good balance between computing time and a possible error. A number of simulations of 10^8 is also proposed by Köhler [86].

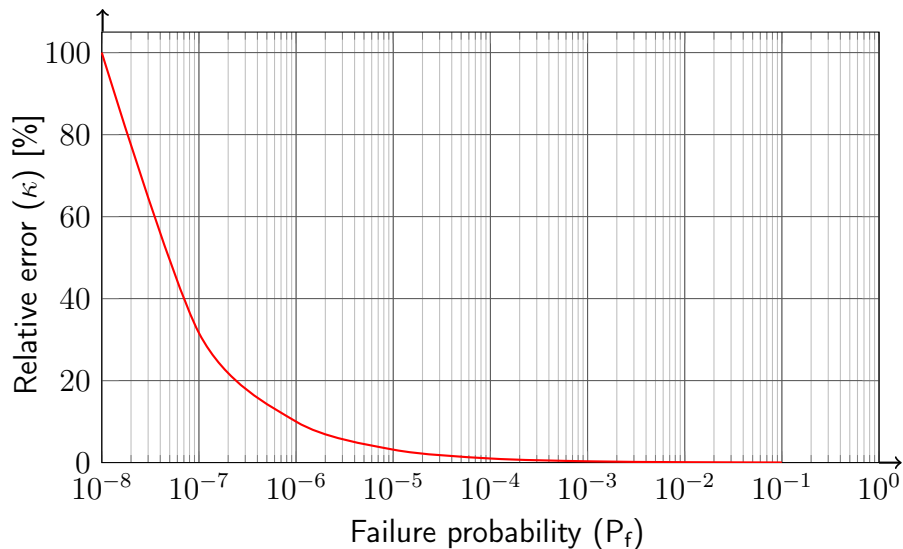


Figure 7.8: Illustration of the relative error κ depending on the failure probability for 10^8 simulations

7.2.4 Reliability based investigations to determine the over-strength factor

Within these investigations the focus is set to the Monte-Carlo simulation to determine the over-strength factor. The first order or second order reliability method does not throw too much light onto the problem, since it is not possible to introduce an if-statement in the limit state function. This is necessary to consider the different failure modes [37] within the calculation of the load bearing resistance of the dowels.

The key element of the reliability based investigations is formed by the limit state function. It is generally formulated as [104]:

$$g = R - E \quad (7.27)$$

with:

$$R = \text{resistance}$$

$$E = \text{effect}$$

Therefore, the limit state function turns into the failure set if the effect (E) is higher than the resistance (R). Within this consideration the over-strength factor ensures, that no brittle failure occurs before the ductile element is activated. Hence the load carrying capacity of the connection is set as an effect (E) and the load bearing resistance of the beam is set to the resistance (R). If the impact, due to the load carrying capacity of the dowel type connection, is greater than the bearing resistance of the beam, an undesirable brittle failure occurs. The Monte-Carlo simulation is based on the conducted experiments. Figure 7.9 gives an overview of the geometrical dimensions and the internal forces acting on the beam. The resistance of

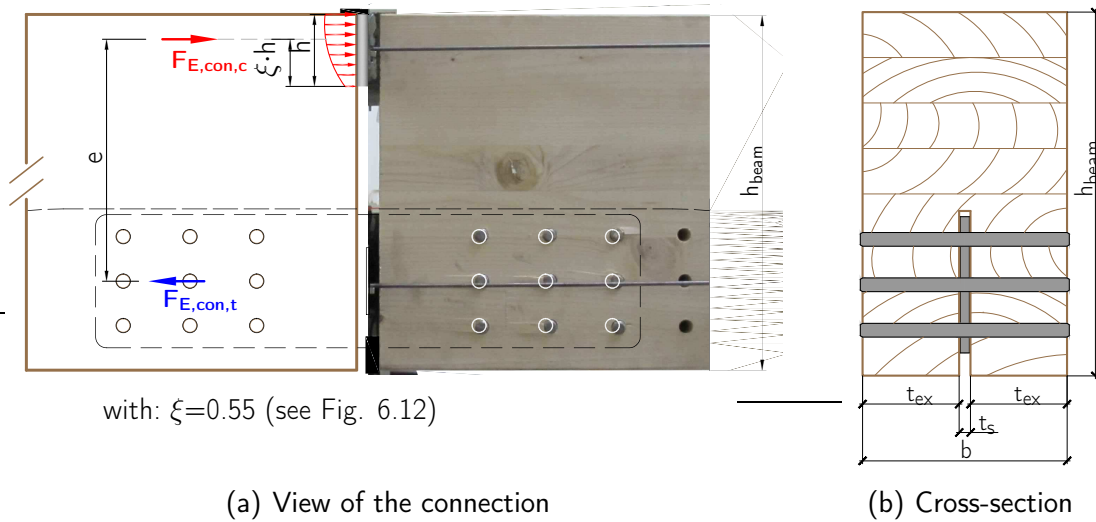


Figure 7.9: Overview of the investigated joint

the beam is found by:

$$R = W_{net} \cdot f_m \quad (7.28)$$

whereas the section modulus is determined with regard to the weakening as a result of the machining of the connection itself (see Fig. 7.9(b)). On the other hand the effect on the beam is given by:

$$E = F_{E,con,t} \cdot e \quad (7.29)$$

with:

$$\begin{aligned} F_{E,con,t} &= \text{tension force in the dowel group (see Fig. 7.9)} \\ e &= \text{inner lever arm (see Fig. 7.9)} \end{aligned}$$

Thus the basic limit state function is defined as:

$$g = W_{net} \cdot f_m - k_{\phi,M} \cdot F_{E,con,t} \cdot e = M_{cs} - k_{\phi,M} \cdot M_{joint} \quad (7.30)$$

In order to cover the over-strength behavior, the factor $\kappa_{cs,i}$ is introduced. The parameter $\kappa_{cs,i}$ was varied to determine the reliability index β . Based on the component model, the factor $k_{\phi,M}$ is implemented, which takes account of the internal bending moment due to the rotation of the joint (see Tab. 6.5). The factor $k_{\phi,e}$ was set to 1.0, since the factor leads to an decrease of the effect to the beam caused by the bending moment.

The failure probability of the limit state function therefore depends on $\kappa_{cs,i}$, which forms in a further step the over-strength factor k_{cs} .

$$g = W_{net} \cdot f_m - X_M \cdot \kappa_{cs} \cdot k_{\phi,M} \cdot n \cdot F_{E,con,t} \cdot e = M_{cs} - X_M \cdot \kappa_{cs} \cdot k_{\phi,M} \cdot M_{joint} \quad (7.31)$$

Depending on the connection, n represents the number of fasteners within the joint. The variable X_M accounts to uncertainties of the model.

Figure 7.10 shows the general calculation process for connections with two shear planes which is implemented in a C++ Programm. Within the calculations a parabolic stress distribution with $\xi=0.55$ was applied in the compression zone (see Fig. 7.9). Therefore, the effect of the flitch plate connection is the most relevant. The number of simulations for every limit state function is 10^8 as described in subchapter 7.2.3.3.

The input variables are the basis of the Monte-Carlo simulation, and described in the following.

Geometrical input variables

The production accuracy of the beam elements showed a very good level of dimensional consistence. Nevertheless, a production tolerance of approximately ± 1 mm has been assumed in the width and height of the cross-section (see Tab. 7.8). The formation of the compression zone is accomplished with a steel plate which is not subjected to a variation.

On the other hand, it has been noticed, that the slot cutter for the flitch plate is afflicted with a marginal inaccuracy. As already stated, the slot of the flitch plate is normally on each side produced one millimeter wider compared to the thickness of the flitch plate. To take into account the inaccuracy of the slot cutter, a coefficient of variation for the width of the slot of 5 % (see Fig. 7.9(b)) is assumed.

The verification of the dowel diameter showed an insignificant deviation of the parameter. This is also confirmed by Joint Committee on Structural Safety (JCSS) [39]. Nevertheless, a coefficient of variation of 0.1 % has been introduced to take account for a possible deviation. Both, the variance in the thickness of the timber side member and the variance of the diameter are considered in the calculation of the section modulus in every calculation step. The stress distribution in the compression zone was chosen in accordance with Chapter 6. Therefore, the determined factor ξ of 0.55 is appropriated within the Monte-Carlo simulation (see Tab. 6.2).

Material input variables

The material properties have been monitored during the grading process (comp. Chap. 5.2.3). Therefore, it was possible to perform a statistical performance of the boards manufactured within the specimens of the test setups. Hence the statistical values of the density have been determined only for the manufactured boards within the connection (see Tab. 7.11). In order to determine the bearing resistance of the beams, the statistical values of the tension strength have been calculated for all boards within the relevant beams.

Table 7.9 shows the statistical values for the manufactured boards within the bending specimens. The required characteristic values were calculated as the 5 % quantile value with a

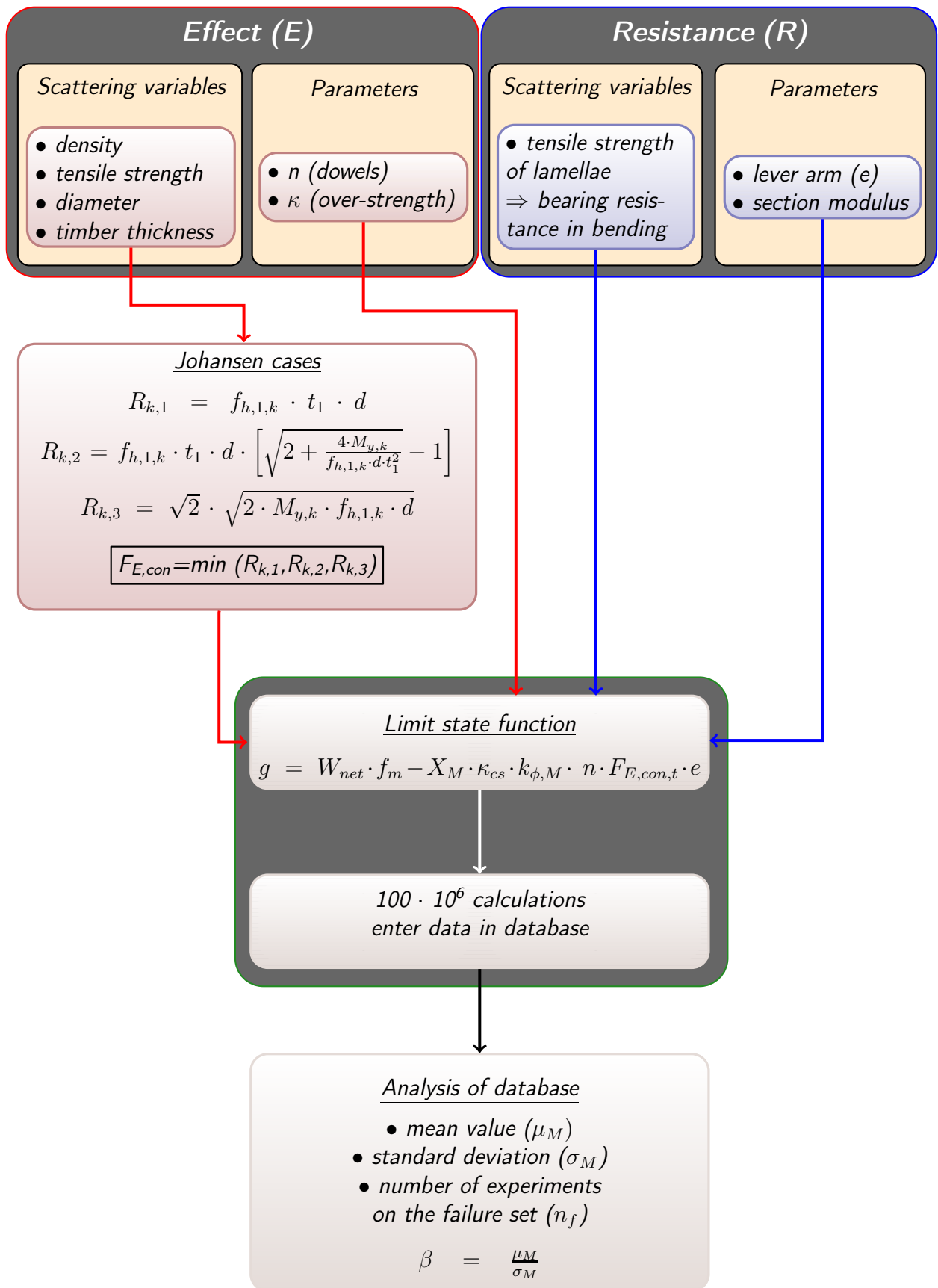


Figure 7.10: Program flow of the Monte-Carlo simulation

Table 7.8: Geometrical input variables for the Monte-Carlo simulation

Experiment	7 mm		12 mm			16 mm
	2x3	4x2	2x4	3x3	5x2	2x3
<u>Cross-sectional dimensions [mm]</u>						
Height (h)	←		320			→
Distribution	←		normal			→
COV	←		0.015 *			→
Width (b)	←		180			→
Distribution	←		normal			→
COV	←		0.025 *			→
Height of compression zone	←		65			→
<u>Timber thickness [mm]</u>						
Distribution	←		normal			→
Member		$t_{s1}-t_m-t_{s2}$		t_m		t_m
Mean value		$t_m=58$		85		85
COV	←		0.05 **			→
<u>Dowel diameter [mm]</u>						
Distribution	←		normal			→
Mean value		7		12		16
COV	←		0.001 ***			→

* DIN 18203-3:2008-08 [97] allows a tolerance of 2 mm at the most for a member length less than 2 m. Based on the knowledge of CNC controlled timber engineering it is known, that the range is about 5-tenth of a millimeter

** The coefficient of variation is assigned to the inaccuracy of the slot cutter, therefore the chosen coefficient gives a reliable number.

*** Based on the receiving inspection, it was noticed that the dimension has hardly any variation.

log-normal distribution [41].

The bending strength (f_m) depends highly on the tension strength of the boards. EN 1194 [101] gives an approach to determine the bending strength based only on the tension strength of the boards.

$$f_{m,k} = 7 + 1.15 \cdot f_{t,l,k} \quad (7.32)$$

Besides the characteristic tension strength of the boards ($f_{t,l,k}$) the tension strength of the finger joint connections ($f_{t,j,k}$) is of significance. Therefore [13] developed formulations to determine the bending strength depending on the tension strength of the boards and the

Table 7.9: Tension strength of the manufactured boards within the bending specimens

Experiment	7 mm		12 mm			16 mm
	2x3	4x2	2x4	3x3	5x2	2x3
Tension strength $f_{t,l}$ [N/mm ²]						
Mean value	27.59	28.46	27.04	29.06	27.41	28.25
St. dev	8.75	9.17	8.58	9.18	9.95	10,17
COV	0.32	0.32	0.32	0.32	0.36	0.36
Characteristic value	15.81	16.15	16.25	16.69	15.37	14.98

finger joints.

$$f_{m,k} = 3,45 + 0,998 \cdot f_{t,j,k} - 0,0211 \cdot f_{t,j,k}^2 - 0,0163 \cdot f_{t,l,k}^2 + 0,0358 \cdot f_{t,j,k} \cdot f_{t,l,k} \quad (7.33)$$

for $13 \text{ N/mm}^2 \leq f_{t,l,k} \leq 21 \text{ N/mm}^2$

$$f_{m,k} = -17,4 + 2,29 \cdot f_{t,l,k} - 0,0322 \cdot f_{t,j,k}^2 + 0,0114 \cdot f_{t,j,k} \cdot f_{t,l,k} \quad (7.34)$$

for $22 \text{ N/mm}^2 \leq f_{t,l,k} \leq 35 \text{ N/mm}^2$

where:

$f_{t,l,k}$: characteristic tension strength of the boards

$f_{t,j,k}$: characteristic tension strength of the finger joint

Equation (7.33) is suitable for lamellae with a tension strength between 13 and 22 N/mm² and Equation (7.34) for lamellae with a tension strength between 22 and 35 N/mm².

EN 14080 [103] refers to the bending strength of the finger connections instead of the tension strength of the finger joints (comp. Eq. (7.35)).

$$f_{m,k} = -2.2 + 2.5 \cdot f_{t,l,k}^{0.75} + 1.5 (f_{m,j,k}/1.4 - f_{t,l,k} + 6)^{0.65} \quad (7.35)$$

with:

$f_{m,j,k}$: characteristic bending strength of the finger joint connection

The determined values according to Equation (7.32), (7.33), (7.34) & (7.35) are valid for a beam height of 600 mm. Therefore the different depth factors need to be applied in order

to achieve the bending strength of a beam height with 320 mm (comp Eq. (7.36 - 7.38)).

$$\text{EN 1194 [101]} : k_{size} = \left(\frac{b}{150}\right)^{0.05} \cdot \left(\frac{h}{600}\right)^{0.1} \quad (7.36)$$

$$\text{Blaß et al. [13]} : k_h = 1.19 - 3.73 \cdot 10^{-4} \cdot h + 1.04 \cdot 10^{-7} \cdot h^2 \quad (7.37)$$

$$\text{EN 1995-1-1 [109]} : k_h = \min\left(1.1, \left(\frac{600}{h}\right)^{0.1}\right) \quad (7.38)$$

Table 7.10 shows the different characteristic values of the bending strength within the different test setups. Since no information of the bending strength of the finger joints ($f_{m,j,k}$) exists, a known value from a glulam producer of 31.85 N/mm² is used, which is slightly higher than the minimum required value based on [103] of 30 N/mm². The tension strength of the finger joints ($f_{t,l,k}$) is given by [103]:

$$f_{f,t,l} = \frac{f_{m,j,k}}{1.4} \quad (7.39)$$

EN 1194 [101] decreases the bending strength for a smaller height than the reference height of 600 mm, both the depth factor based on Blaß et al. [13] and EN 1995-1-1 [109] increases the bending strength due to a smaller beam height, which reflects the state of the art.

The ascertained values based on Blaß et al. [13] show a good accordance with the target value of a GL24h strength class. The model introduced by Blaß et al. [13] reaches a very good accuracy with a slight variation of 6% between the experimental values and the estimated values by Frese et al. [27]. Therefore, the model based on Blaß et al. [13] has been chosen to determine the bending strength of the beam elements.

Within the Monte-Carlo simulation the mean values are of interest. Therefore, the mean

Table 7.10: Characteristic bending strength depending on different approaches

Experiment	7 mm		12 mm			16 mm
	2x3	4x2	2x4	3x3	5x2	2x3
EN 1194 [101]	23.86 (25.18)	24.23 (25.57)	24.34 (25.68)	24.82 (26.19)	23.38 (24.67)	22.95 (24.22)
Blaß et al. [13]	25.99 (24.04)	26.10 (24.14)	26.13 (24.16)	26.26 (24.29)	25.84 (23.90)	25.71 (23.78)
EN 14080 [103]	27.20 (25.54)	27.40 (25.73)	27.45 (25.78)	27.70 (26.01)	26.94 (25.30)	26.71 (25.08)

Note: The values in brackets refer to the bending strength without the consideration of the beam height.

values are determined based on the determined characteristic values (see Tab. 7.10) and a log-normal distribution with a coefficient of variation of 15% [41].

Table 7.11 shows the input variables of the Monte-Carlo simulation with its statistical parameters.

Table 7.11: Material input variables for the Monte-Carlo simulation

Experiment	7 mm		12 mm			16 mm
	2x3	4x2	2x4	3x3	5x2	2x3
<u>model uncertainty X_M [-]</u>						
distribution	←		log-normal [41]			→
mean value	1	1	1	1	1	1
st. dev.	0.1	0.1	0.1	0.1	0.1	0.1
COV	0.1	0.1	0.1	0.1	0.1	0.1
<u>timber density ρ [kg/m³]</u>						
distribution	←		normal [41]			→
mean value	436.4	432.5	441.7	449.6	440.3	460.7
st. dev.	31.5	33.3	48.9	42.1	42.5	43.0
COV (actual)	0.072	0.076	0.111	0.094	0.096	0.093
COV (applied)	←		0.1 [41]			→
<u>bending strength f_m [N/mm²]</u>						
distribution	←		log-normal [41]			→
mean value	33.59	33.73	33.77	33.94	33.40	33.23
COV [41]	←		0.15 [41]			→
<u>tensile strength f_u [N/mm²]</u>						
distribution	←		log-normal [40] & [86]			→
mean value	579		581			488
st. dev.	5.97		3.46			9.84
COV	←		0.04 [40]			→

Consideration of correlated material properties

The introduced limit state function consists of two correlated parameters, the timber density (ρ_{den}) and the bearing resistance in bending (f_m). In order to consider the dependency of both material properties it is necessary to link the characteristics. If the correlation is not considered, a high bearing resistance of the beam (f_m) combined with a rather low density (ρ_{den}) might be generated. In this case a high value of the factor k_{cs} is generated by the Monte-Carlo simulation and may distort the gained results. Figure 7.11 shows the general de-

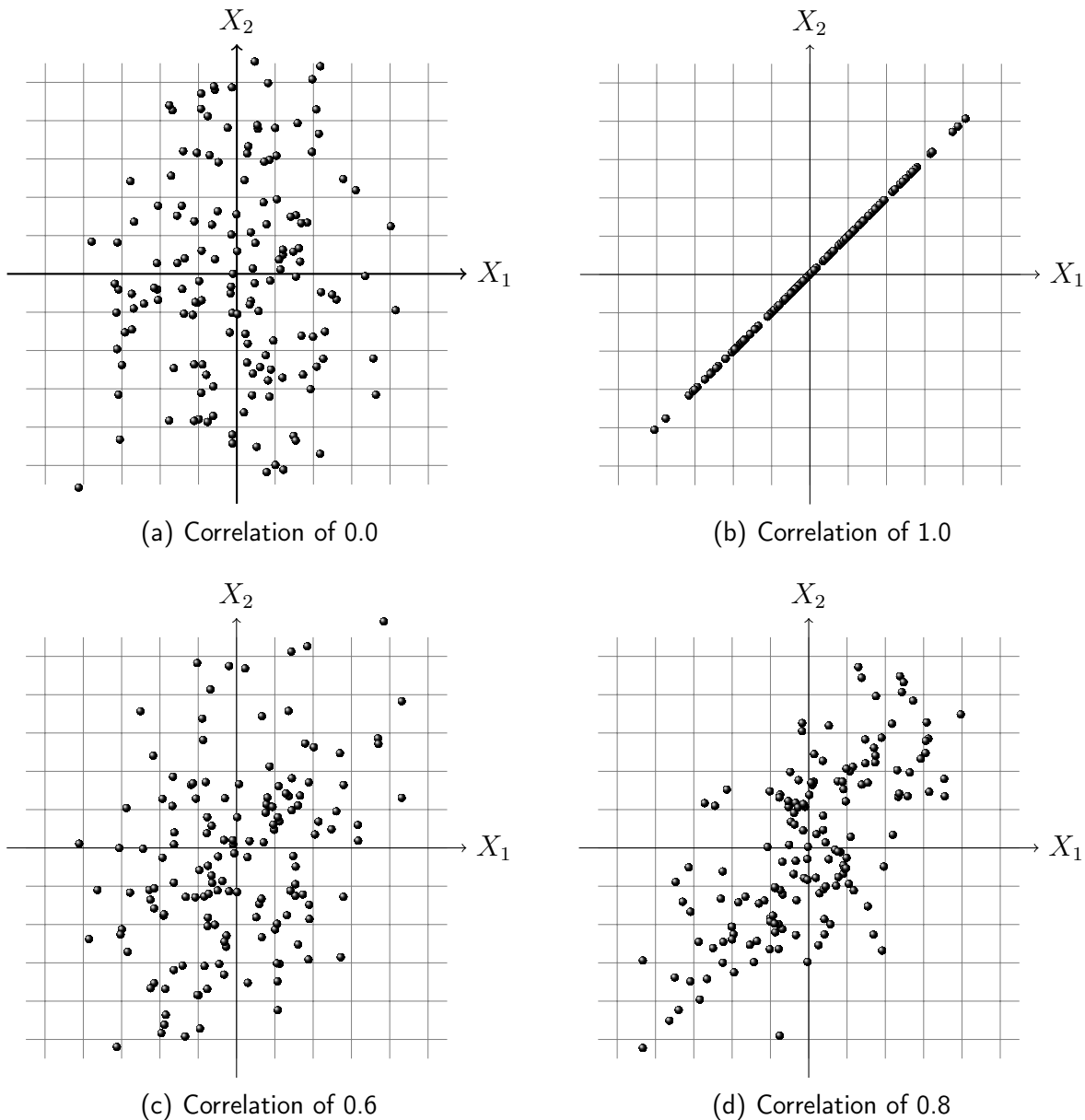


Figure 7.11: Different correlations of two properties

pendency of two correlated properties with different correlation coefficients. If two properties (X_1 & X_2) are almost independent, an arbitrary arrangement of the different characteristics is the consequence (see Fig. 7.11(a)). On the other hand, if two properties are completely dependent on each other the arrangement turns into a straight line. This means for instance, that if the property X_1 attributes the mean value as characteristic, the property X_2 holds also the mean value (see Fig. 7.11(b)). Figure 7.11(c) & 7.11(d) present an intermediate correlation of two properties, which is generally the case. The correlation coefficients of the mechanical properties of timber are displayed in Table 7.12. It has to be mentioned, that these values are quantified by judgment [86] & [41].

Table 7.12: Correlation coefficients of timber [41]

	E_m	ρ_{den}	$R_{t,0}$	$R_{t,90}$	$E_{t,0}$	$E_{t,90}$	$R_{c,0}$	$R_{c,90}$	G_v	R_v
R_m	0.8	0.6	0.8	0.4	0.6	0.6	0.8	0.6	0.4	0.4
E_m		0.6	0.6	0.4	0.8	0.4	0.6	0.4	0.6	0.4
ρ_{den}			0.4	0.4	0.6	0.6	0.8	0.8	0.6	0.6
$R_{t,0}$				0.2	0.8	0.2	0.5	0.4	0.4	0.6
$R_{t,90}$					0.4	0.4	0.2	0.4	0.4	0.6
$E_{t,0}$						0.4	0.4	0.4	0.6	0.4
$E_{t,90}$							0.6	0.2	0.6	0.6
$R_{c,0}$								0.6	0.4	0.4
$R_{c,90}$									0.4	0.4
G_v										0.6

with:

R_m = Bending strength

E_m = Bending MOE

ρ_{den} = Density

$R_{t,0/90}$ = Tension strength

$E_{t,0/90}$ = Tension MOE

$R_{c,0/90}$ = Compression strength

R_v = Shear strength

G_v = Shear modulus

The correlation coefficients can be classified as follows. A factor of 0.8 represents a high correlation, a factor of 0.6 a medium correlation, a low correlation is represented by 0.4 and 0.2 shows a very low correlation [86].

Based on the values of the machine grading process of the processed lamellae, Figure 7.12 shows the correlation of the density and the associated tension strength of the boards ($n=107$). It should be noted that the proposed correlation coefficient of 0.4 (see Tab. 7.12), cannot be confirmed within the experiments. Instead a correlation of approximately 0.8 can be stated.

As previously discussed, the bearing resistance of the beams in bending is based on the resistance in tension ($f_{t,k}$) of the processed lamellae and determined according to Blaß et al. [13]. Since the evaluated data show a high correlation and Joint Committee on Structural Safety (JCSS) [41] proposes a correlation coefficient 0.6 between the density and the bending resistance (see Tab. 7.12), a coefficient of 0.6 is applied within the Monte-Carlo simulation.

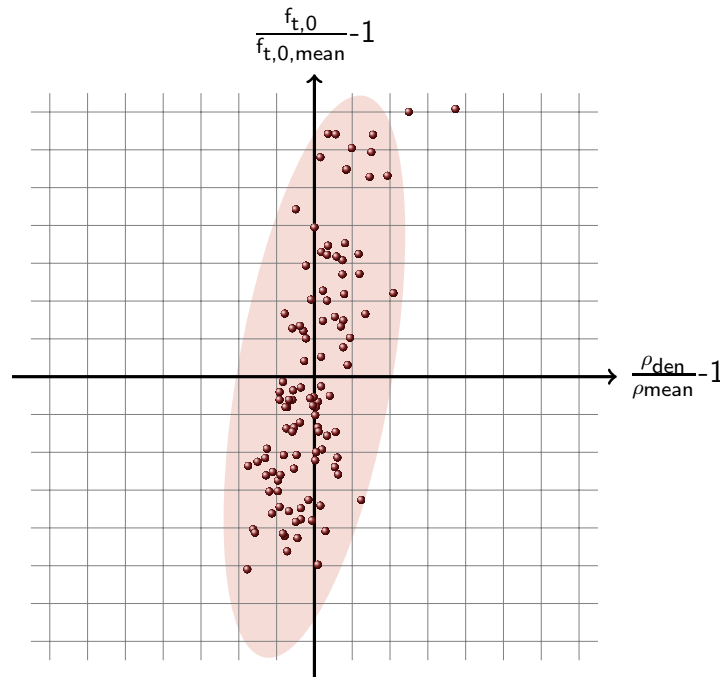


Figure 7.12: Correlation of the density and the tension resistance of the manufactured lamellae within the bending experiments

Application of the correlation coefficient

In order to consider the dependency within the Monte-Carlo simulation of correlated material properties it is necessary to determine the relationship of the liable random numbers. In general there are two possibilities to determine correlated random numbers, either with the Eigenvektor decomposition of the correlation matrix, or with the Cholesky decomposition of the correlation matrix. Within this study only the Cholesky decomposition is applied.

A correlation matrix C is given by the application of the introduced values (see Tab. 7.12), the matrix should be symmetrical and positive definite. The Cholesky decomposition divides a symmetrical, positive definite matrix into its products of an upper triangular matrix and its conjugate transpose (comp. Eq. (7.40)).

$$C = U^T U \quad (7.40)$$

$$\begin{bmatrix} C_{11} & C_{12} & C_{13} \\ C_{21} & C_{22} & C_{23} \\ C_{31} & C_{32} & C_{33} \end{bmatrix} = \begin{bmatrix} U_{11} & 0 & 0 \\ U_{21} & U_{22} & 0 \\ U_{31} & U_{32} & U_{33} \end{bmatrix} \begin{bmatrix} U_{11} & U_{21} & U_{31} \\ 0 & U_{22} & U_{32} \\ 0 & 0 & U_{33} \end{bmatrix}$$

The upper matrix U can be determined with the following equations:

$$U_{i,i} = \sqrt{C_{i,i} - \sum_{k=1}^{i-1} U_{i,k}^2} \quad (7.41)$$

$$U_{j,i} = \frac{1}{U_{i,i}} \left(C_{j,i} - \sum_{k=1}^{i-1} U_{j,k} U_{i,k} \right) \quad (7.42)$$

A vector R consisting of uncorrelated random numbers can be transformed to correlated random numbers by using the matrix U .

$$R_c = RU \quad (7.43)$$

$$\begin{bmatrix} R_{c,11} & R_{c,12} & R_{c,13} \end{bmatrix} = \begin{bmatrix} R_{11} & R_{12} & R_{13} \end{bmatrix} \begin{bmatrix} U_{11} & U_{21} & U_{31} \\ 0 & U_{22} & U_{32} \\ 0 & 0 & U_{33} \end{bmatrix}$$

Therefore different depending properties can be considered within the performance of a Monte-Carlo simulation.

Applying Equation (7.41) and Equation (7.42) to the existing two correlated variables the upper triangular matrix is found by:

$$U = \begin{bmatrix} 1 & C \\ 0 & \sqrt{1-C^2} \end{bmatrix} \quad (7.44)$$

Therefore the two uncorrelated sequences X_1 and X_2 are generated into two correlated sequences $X_{c,1}$ and $X_{c,2}$ by:

$$X_{c,1} = X_1 \quad (7.45)$$

$$X_{c,2} = C \cdot X_1 + \sqrt{1-C^2} \cdot X_2 \quad (7.46)$$

The new sequence $X_{c,2}$ has a correlation of C , with the uncorrelated sequences X_1 and X_2 , to the sequence $X_{c,1}$.

7.2.5 Results of the Monte-Carlo Simulation

The results of the Monte-Carlo simulation were evaluated based on the formulas given in Section 7.2.3.3. The mean is given by Equation (7.23) and the standard deviation as the square root of the variance given by Equation (7.24) (comp. page 173). Figure 7.13 displays the cumulated frequency of the results of the limit state function achieved by the Monte-Carlo simulation with a dowel diameter of 12 mm and an arrangement of 3×3 dowels. The parameter κ_{cs} in Equation (7.31) was set to 1.0 within the determination. It is shown, that

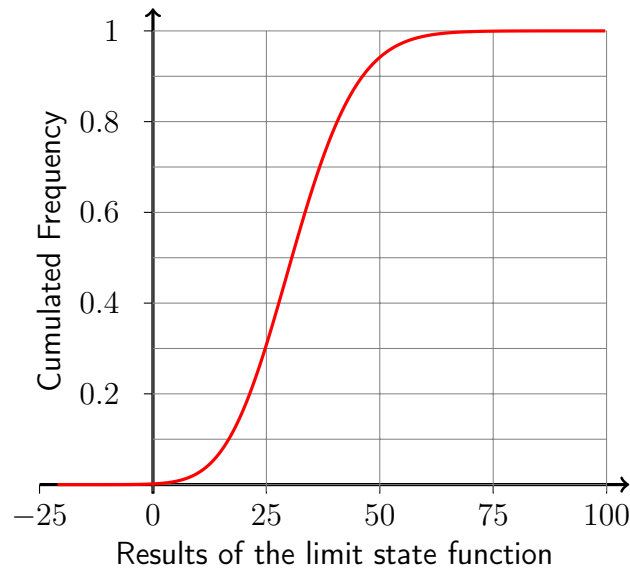
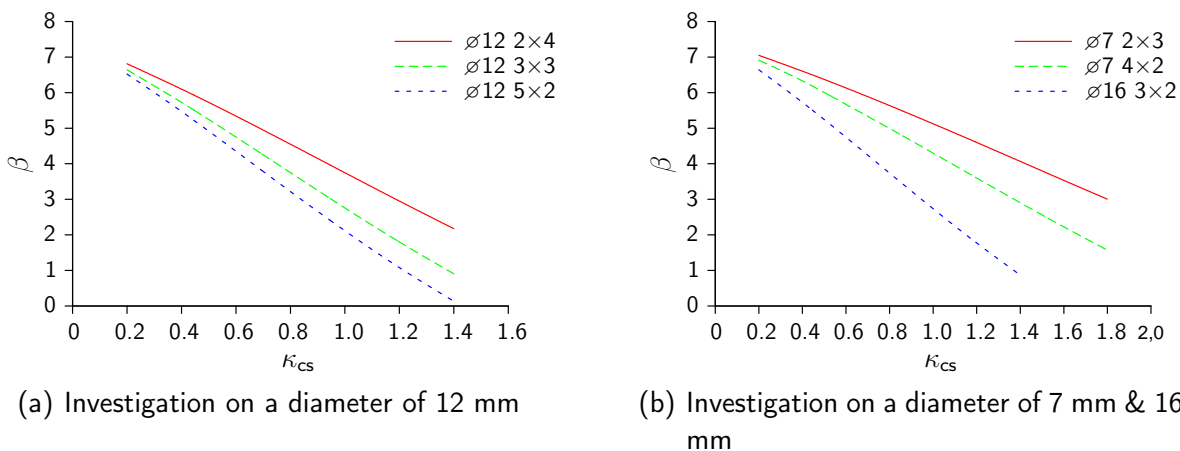


Figure 7.13: Exemplary displayed cumulated frequency of the results of the limit state function

for certain arbitrary chosen values within the Monte-Carlo simulation a failure occurs per se. The Monte-Carlo simulation was conducted with a step of 0.2 for the κ_{cs} value for every test series. The corresponding reliability indexes β , obtained by the Monte-Carlo simulation using Equation (7.22), are given in Figure 7.14 for the examined dowel diameters [17]. It becomes obvious that the load-carrying capacity of the fasteners and the design of the connection have a direct influence on the reliability index β . Hence, the reliability index decreases with a larger extent for a dowel arrangement of 5×2 compared to a dowel arrangement of 2×4 dowels. This is caused by two factors, which are the following: On one hand the number of



(a) Investigation on a diameter of 12 mm

(b) Investigation on a diameter of 7 mm & 16 mm

Figure 7.14: Factor κ_{cs} for different reliability indexes β of various dowel arrangements

fasteners and on the other hand the larger lever arm of the connection designed with 5×2 fasteners. Therefore, the bending moment capacity of the connection increases on a larger scale and the reliability index decreases.

A hidden over-strength factor is inevitably integrated within the design of joints. This is the result of the differences in the design of the bearing resistance of the cross-section ($M_{cs, design}$) and the design of the load-carrying capacity of the joint ($M_{j, design}$).

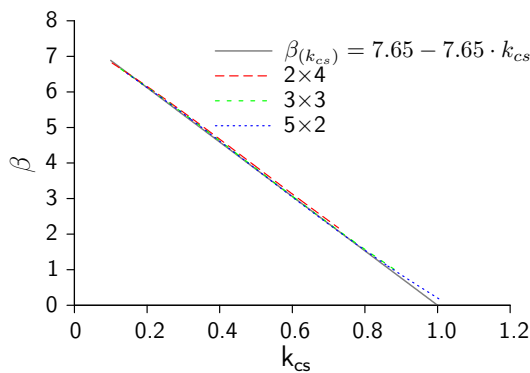
All of the designed connections have an inherent over-strength factor, since it is hardly possible to design the bearing resistance of the connection equal to the bearing resistance of the net cross-section. Within the design of the joints of the experiments a difference of the moment bearing resistance of the joint ($M_{j, performed}$) to the bearing resistance of the cross-section ($M_{cs, performed}$) between 0.32 and 0.72 was considered. Therefore, the normalized over-strength factor k_{cs} can be found by:

$$k_{cs} = \kappa_{cs} \cdot \frac{M_{j,performed}}{M_{cs,performed}} \quad (7.47)$$

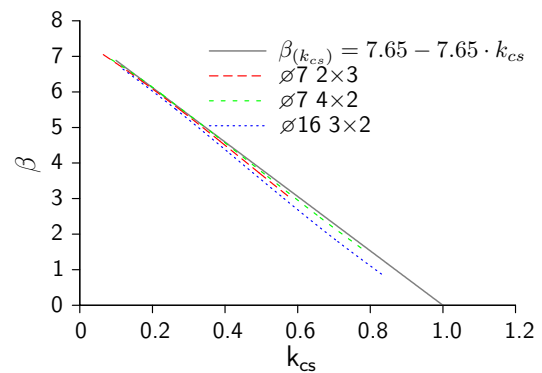
The values $M_{j, performed}$ and $M_{cs, performed}$ are determined based on the mean input values of the Monte-Carlo simulation (comp. Table 7.11). Figure 7.15 shows the normalized over-strength factors k_{cs} of the different reliability indexes β for the considered joints. The obtained reliability line can be expressed by:

$$\begin{aligned} \beta(k_{cs}) &= 7.65 - 7.65 \cdot k_{cs} \\ &= 7.65 \cdot (1 - k_{cs}) \end{aligned} \quad (7.48)$$

$$k_{cs} = 1 - \frac{\beta(k_{cs})}{7.65} \quad (7.49)$$



(a) Investigation on a diameter of 12 mm



(b) Investigation on a diameter of 7 mm & 16 mm

Figure 7.15: Over-strength factor k_{cs} depending on the reliability index β based on properties given in Table 7.11

The reliability line is valid for all analysed connections. Hence the reliability line makes no difference, neither on the dowel diameter nor on the number of shear planes. Therefore, the gradient of the reliability line does not change and can be applied without any correction coefficients for different diameters and (or) number of shear planes.

The verification of the conducted reliability line shows a reliability index β of zero for a k_{cs} value of one. A reliability index of zero gives a failure probability (P_f) of 0.5. This means that the system is in an indifferent condition. This is a reasonable number since both the effect and the resistance are of the same magnitude.

By applying the developed reliability line, it is possible to give an over-strength factor for certain circumstances. Hence an over-strength factor of 0.6 should be applied for an incident with a minor consequence of failure and low costs of safety measures ($\beta = 3.1$ see Tab. 7.7). On the other hand, the over-strength factor increases with the consequence of failure. For large consequences of failure with high costs of safety measures an over-strength factor of 0.38 should be used ($\beta = 4.7$ see Tab. 7.7).

7.3 Influence on the beam end-rotation

7.3.1 General

The variance of the material scattering has not only an influence on the bearing resistance of the structural element or the load carrying capacity of fasteners, but also on the flexibility of structural members. Therefore the influence of the variance of the modulus of elasticity on the beam end-rotation is analyzed.

If a plastic hinge is formed within a statically indeterminate structure, it is possible to redistribute internal actions to lesser utilized structural elements (comp. Fig. 7.16(a) & Chap. 1). A precondition to see the benefits of the plastic hinges is a sufficient rotation capacity (ϕ_{joint}) of the joint. The rotational capacity ensures that the postulated rotation is sufficient to redistribute internal actions.

Besides a targeted redistribution, a structure or structural elements require rotational capacity

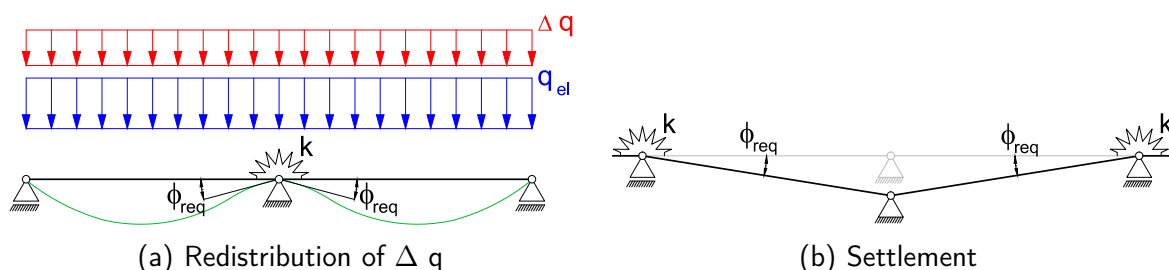


Figure 7.16: Required rotational capacity ϕ_{req}

in case of an overstrain situation. If the joint does not fulfil the required rotational capacity, a failure may occur. Overstrain situations may be caused by:

- exceptional actions (earthquake, etc.)
- settlements (see Fig. 7.16(b))
- failure of structural elements
- long term effects

Figure 7.16 shows the required beam end-rotations in order to compensate overstrains on a structure.

The required rotational capacity of joints is analyzed in this chapter based on the beam-line method (comp. Sec. 7.3.2). Thereby attention is given to the variance of the modulus of elasticity.

7.3.2 Determination of the material impact factor k_{mat}

The beam-line method was developed in the nineteen-thirties by [3]. The aim of the method is to determine the required rotation of semi-rigid joints. Hence the examined structural element is extracted from the main structure see. Fig. 7.17 & Fig. 7.18(b)) to analyze the required rotational capacity of the joints for a certain load (\tilde{q}).

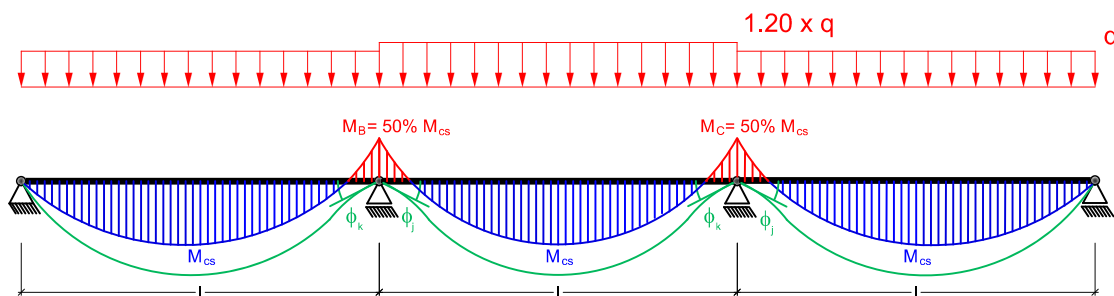


Figure 7.17: Structural system with the maximal loading for a certain bending moment at the support

Depending on the ratio of $M_{joint}/M_{cross-section}$, the line given between (A) and (B) (beam-line) in Figure 7.18(a) shows the required rotational capacity of a joint (ϕ_j respectively ϕ_k) in order to redistribute internal actions. The moment-rotation behavior of the joint is exemplary integrated into Figure 7.18(a) for an arbitrarily chosen ratio of $M_{joint}/M_{cross-section}$ of 0.5, which reflects a reliability index β of 3.8. The chosen factor gives an in between value of the previously defined factor k_{cs} . The red shaded area represents in this case the critical values for $M_{joint}/M_{cross-section}$ with a decrease of the reliability index as discussed. The intersection point of the moment-rotation behavior of the joint with the beam-line indicates a sufficient rotational capacity.

The beam-line of a semi-rigid joint is given by two boundary conditions of the rotation. For a rigid connection the ratio of $M_{\text{joint}}/M_{\text{cross-section}}$ turns to one, with a rotation at the supports of zero (comp. (A) in Fig. 7.18(a)). On the other hand for a hinged connection the rotation is given by $\tilde{q} \cdot l^3 / (24 \cdot EI)$ represented by (B) in Figure 7.18(a). Where \tilde{q} represents the total load applied on the beam element (see Fig. 7.18(b)).

The required rotational capacity for one side of the joint is determined by:

$$\phi_{i,\text{req}} = (1 - k_{cs}) \cdot \frac{\tilde{q} \cdot l^3}{24 \cdot EI} \tag{7.50}$$

The graphical solution given in Figure 7.18 shows the required rotational capacity of either side of the joint (ϕ_j respectively ϕ_k). The total rotational capacity of the joint is found by:

$$\phi_{\text{req}} = \phi_{k,\text{req}} + \phi_{j,\text{req}} \tag{7.51}$$

The rotations $\phi_{k,\text{req}}$ and $\phi_{j,\text{req}}$ describe the required rotation of the connected elements on the right and left hand side of the joint (see Fig. 7.17).

The joint must have at least a rotational capacity which exhibits the required rotation. Considering the material variance of timber the following equation of condition is given.

$$k_{\text{mat}} \cdot \phi_{\text{req}} \leq \phi_{\text{joint}} \tag{7.52}$$

where k_{mat} covers the influence of the material variance of structural elements.

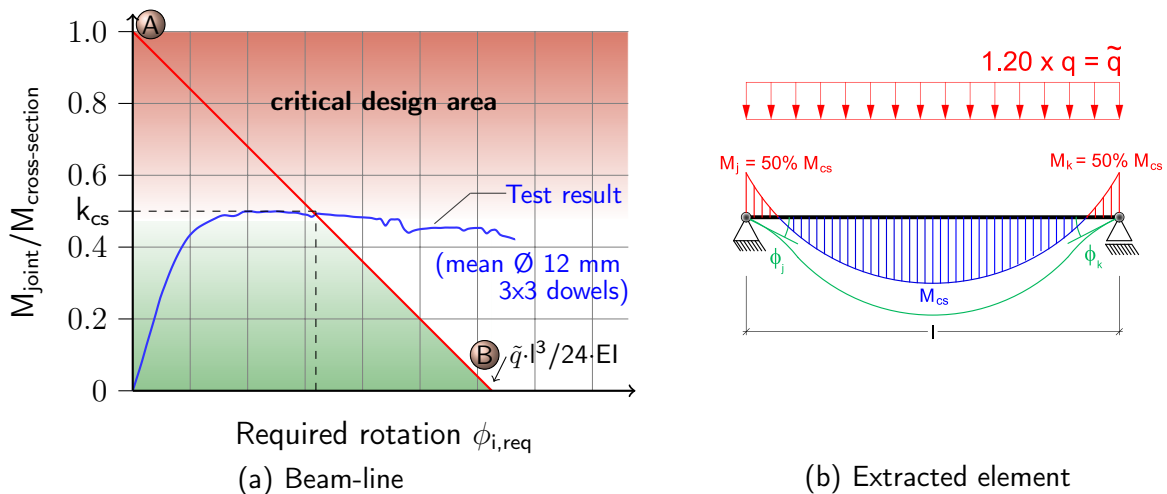


Figure 7.18: Required rotational capacity of a joint with respect to a certain bending moment distribution of a structural element

Deflection curve

The influence of the material variance is found by applying the deflection curve. Based on the beam-line method, a certain bending moment distribution with respect to the ratio of $M_{\text{joint}}/M_{\text{cross-section}}$ is introduced to a beam element (see Fig. 7.18(b)). Solving the differential equation

$$w''_{(x)} = - \frac{M_{(x)}}{(EI_{eff})_{(x)}} \quad (7.53)$$

$$w'_{(x)} = - \phi_{(x)} = - \int \frac{M_{(x)}}{(EI_{eff})_{(x)}} dx + C_1 \quad (7.54)$$

$$w_{(x)} = - \int \int \frac{M_{(x)}}{(EI_{eff})_{(x)}} dx dx + C_1 x + C_2 \quad (7.55)$$

by a numerical integration, the end-rotations $\phi_{k,req}$ and $\phi_{j,req}$ (see Fig. 7.18(b)) are determined for the appropriate bending moment distribution. The modulus of elasticity has a direct influence on the deflection of a beam element and therefore on the rotation as well (comp. Eq. (7.53)). Following the findings of Ehlbeck et al. [23] a computer model has been developed to analyze the influence of the material variance and therefore to quantify the developed factor k_{mat} . The general calculation process is displayed in Figure 7.20. Therefore, the single lamella of each glulam beam has been divided into 150 mm long cells with a reference thickness of 40 mm which represents the general thickness of the lamellae (see Fig. 7.19). A statistically assigned modulus of elasticity is allocated to each cell, where the statistical distribution of each board is log-normal [41], and the distribution within the board is normal [18]. Every step in length was calculated 100000 times with a scattering of



Figure 7.19: Variance of the modulus of elasticity within a beam element

the modulus of elasticity within the cells. The length of the beam was extended by the cell length of 150 mm. The effective bending stiffness for every step in length of the beam is found by:

$$EI_{(eff)} = \sum (E_i \cdot I_i) + \sum (E_i \cdot A_i \cdot a_i^2) \quad (7.56)$$

with

- $E_{i(\text{eff})}$ Effective stiffness of every step in length
- E_i Modulus of elasticity of each cell
- I_i Moment of inertia of each cell
- A_i Area of each cell
- a_i Lever arm of each cell to the centroid

The input data given in Table 7.13 have been used in order to run the program.

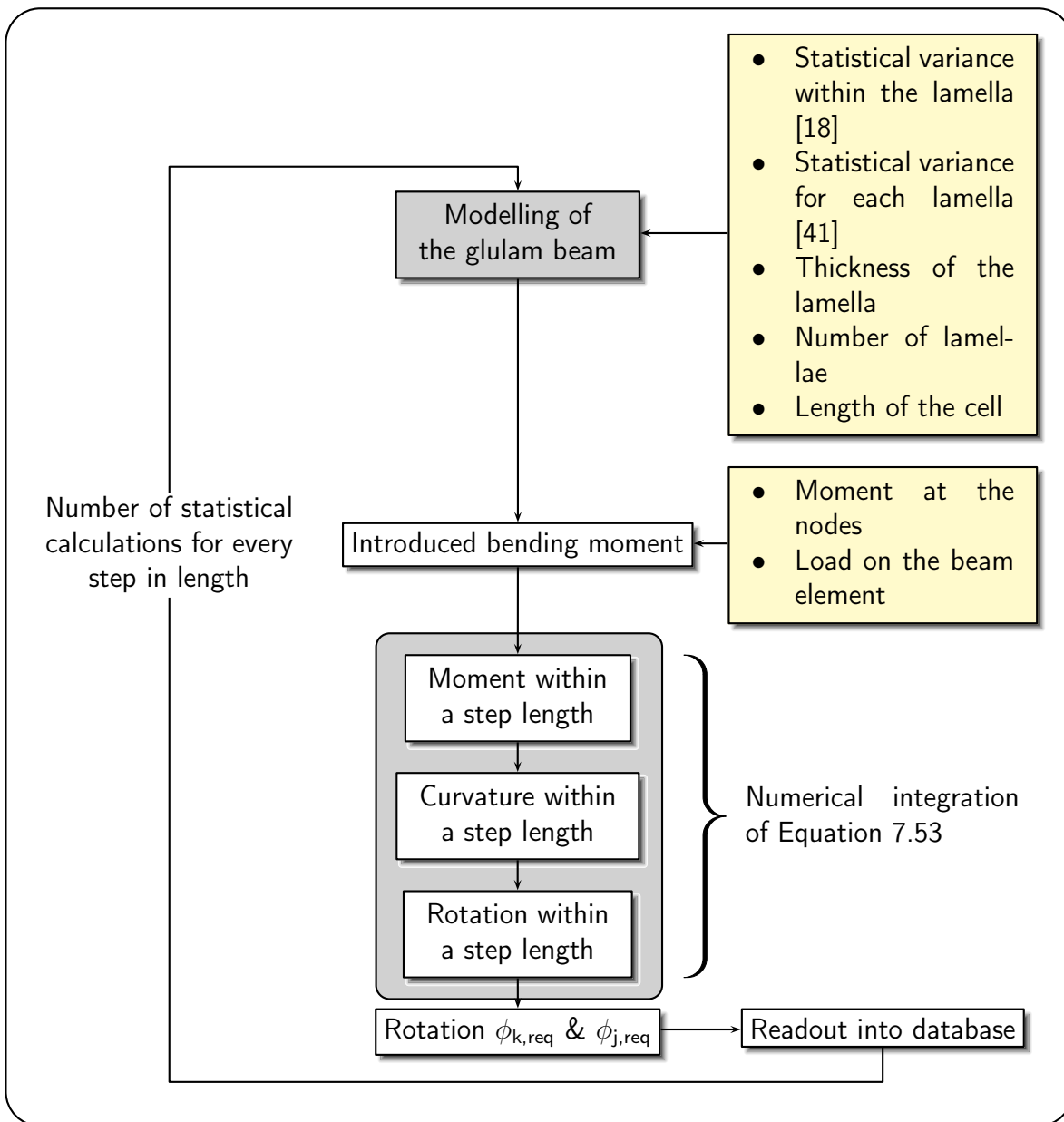


Figure 7.20: Calculation process to determine the factor k_{mat}

Table 7.13: Input data

Value	Magnitude	Source
$E_{0,\text{mean}}$: 11600 $\frac{N}{mm^2}$	DIN 1052 [95]
COV of each board	: 0.13	Joint Committee on Structural Safety (JCSS) [41]
COV within the board	: 0.069	Colling and Scherberger [18]
Number of calculations	: 100000	

7.3.3 Parametrical study and results

A parametrical study was conducted in order to analyze the influence of the variation of the modulus of elasticity.

The following parameters were examined:

- Length of the beam element
- Height of the beam element
- Bending moment distribution
- Height of the lamellae

The influence of the variance of the modulus of elasticity has an effect on the required rotation of the beam. Figure 7.21 shows the required beam end-rotation $\phi_{k,\text{req}}$ and $\phi_{j,\text{req}}$ for the appropriate bending moment distribution. Within this study, the intended bending moment distribution is equal for all beam lengths. Hence the uniformly distributed load was recalculated for every step to achieve the specified bending moment distribution. Therefore, the required rotation has a linear dependency on the beam length (comp. Eq. (7.50)). The

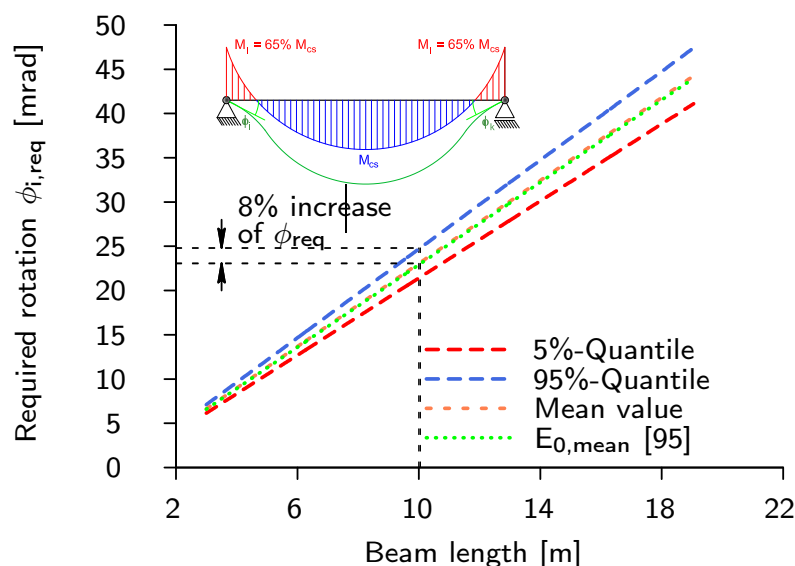


Figure 7.21: Required beam end-rotation of a beam element with a cross-section of 180 mm / 400 mm

mean value of the required rotation based on the computer program follows the calculation without a variance of the modulus of elasticity. This confirms that the modulus of elasticity of each lamella and within each lamella scatters with a variation coefficient with regard to the mean value of the design code.

Assuming a glulam beam with a length of 10 m manufactured in timber grade GL24c, the required rotation increases of approximate 8% compared to a calculation with the same bending moment distribution, but with a constant modulus of elasticity of 11600 N/mm² [95] (see Fig. 7.21).

This has an important influence on the design of the joint. The calculation with respect to the mean value according to DIN 1052 [95] gives a smaller required rotation than the analyzed 5% quantile value with the variance of the modulus of elasticity. If the required rotation is not achieved, the structural element fails due to an insufficient existing rotation capacity of the joint.

A similar but slightly different required rotation arises if the intended bending moment of the beam element is changed. Following the deflection curve, the deflection and therefore the rotation at the supports depend on the internal forces and therefore on the uniformly distributed load which is applied to the structural element (comp. Eq. (7.53) - Eq. (7.55)). Hence, the beam element was loaded with varying types of uniformly distributed loads, in order to analyze the influence of different load configurations on the required rotations. For a uniformly distributed load on a beam with a constant cross-section of 180 mm × 400 mm the required rotation varies from 7.7% to 8% (see Fig. 7.22).

The thickness of the lamellae had a constant value of 40 mm within the investigations on the beam height. A variation of the beam height follows directly Equation (7.53). Hence, an

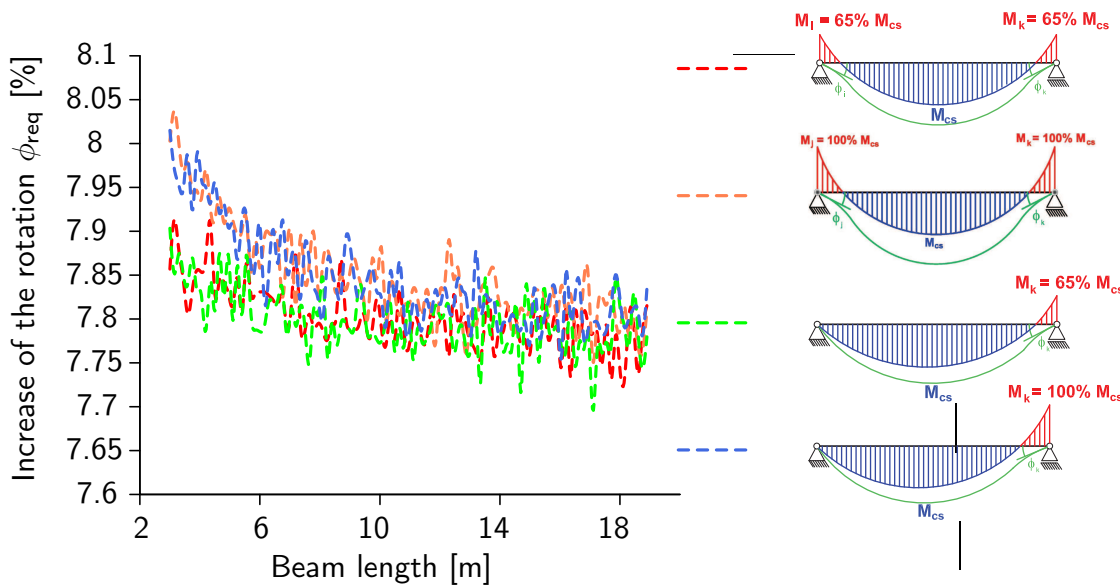


Figure 7.22: Increase of the beam end-rotation depending on the bending moment distribution

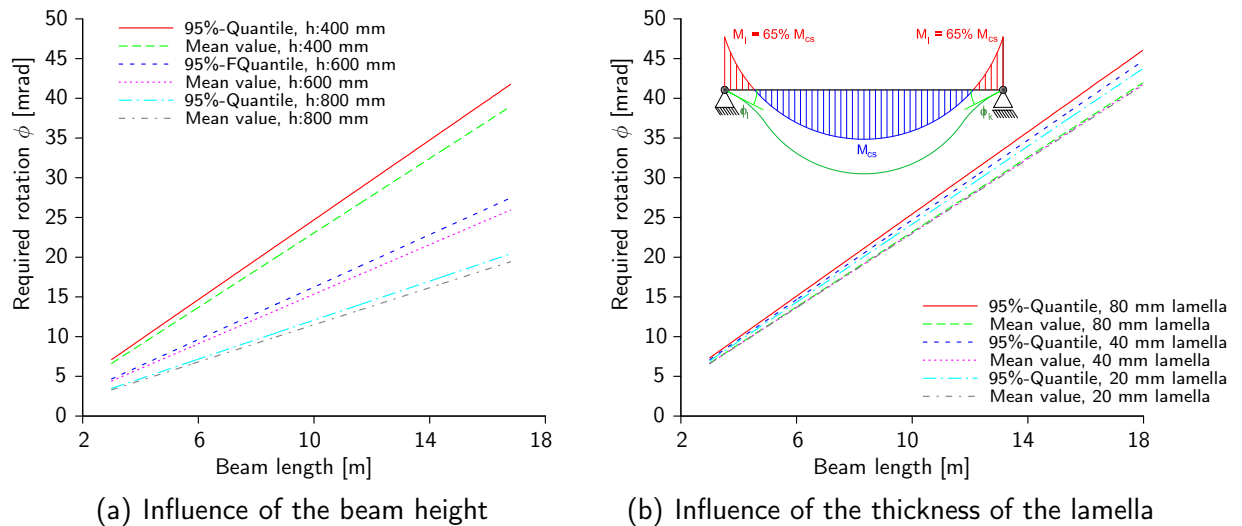


Figure 7.23: Investigations on the influence of the beam end-rotation

increase of the beam height leads to a decrease of the required rotation (see Fig. 7.23(a)). A further aspect could be noticed within the statistical evaluation. The required rotation declines slightly with an increase in the number of lamellae at a constant beam height. Since the height of the lamellae remains constant, the number of lamellae increases as well. Therefore, the coefficient of variation decreases with every step of length decrease and the 95% quantile value approaches to the mean value. Hence, the required rotation decreases.

The same effect can be noticed within the observation of the influence of the height of the lamellae. The required rotation decreases for a constant beam height of 400 mm and a variation of the height of the lamellae (see Fig. 7.23(b)). The statistical distribution for every step in length is reflected. A decrease of the lamella height leads to an increase of the number of lamellae. Therefore, the cross-section becomes more homogeneous, and the 95% quantile value leads to the mean value.

Based on the conducted investigations a factor

$$k_{\text{mat}} = 1.10 \quad (7.57)$$

should be considered (comp. Eq. (7.52)). The usual processed thickness of the lamellae is between 33 mm and 41 mm. Therefore, the developed investigations show an upper bound.

7.4 Summary and conclusion

It has been shown that the material scattering of timber has a large influence on the implementation of the ductility in timber structures.

A reliability line was developed to determine an over-strength factor for certain incidents. Within this study the dependency of certain material properties were considered to avoid unrealistic values within the ultimate limit state function. The material input values are based on the values given by the grading process. On the other hand, the coefficient of variation and the statistical distribution is set to the values given by the Joint Committee on Structural Safety (JCSS) [40, 41].

The consideration of an over-strength factor is already of importance. Within the earthquake design, a certain behavior coefficient is applied depending on the type of used connection. This approach is in general correct, but only little information is given about the required over-strength of the joint to ensure a ductile behavior to justify the applied behavior coefficient. If the ductile behavior is applied within the elastic-plastic design methods, it is indispensable to define an over-strength factor to ensure a ductile behavior of the joint before a brittle timber failure takes place.

A further requirement is the rotation capacity of the joint if forces are specifically redistributed. This study was conducted to ascertain the influence of the material scattering on the end-rotation of the beam. It has been shown that the beam end-rotation has to be increased by 7.8 % compared to the calculation based on a homogenous material assumption. In order to propose a practical application, this phenomenon should be observed by an increase of the required end-rotations of 10 %.

8 Requirements on the joint stiffness

8.1 Introduction

Within statically indeterminate structures the stiffness of the structural members have a significant influence on the load distribution within the considered structure. Joints in timber structures are neither hinged nor fully rigid.

According to [60] and [107], joints in timber structures may generally be classified into three different types.

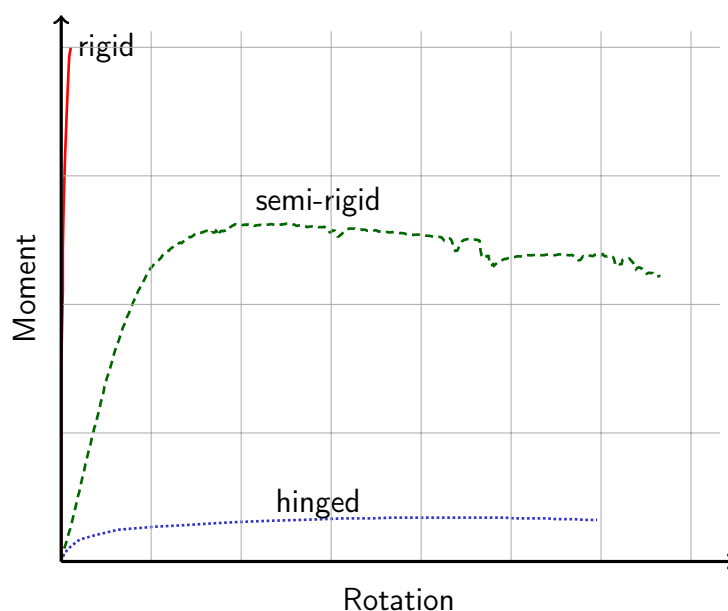


Figure 8.1: Joint classification based on the joint stiffness

If a joint has no rotations, relative to the member rotation, it is classified as rigid. This is ensured with an almost infinitive stiffness.

On the other hand, a hinged or pinned joint is able to transfer normal forces and shear forces without the development of significant moments. A classified pinned or hinged joint should be able to allow rotations at the joint.

A semi-rigid joint neither accomplishes the criteria of a hinged joint nor of a rigid joint. A semi-rigid joint is able to transfer all of the internal actions and provides a previsible degree of interaction between the members (see Fig. 8.1).

Experimental investigations have been conducted on different types of connections [62] (see Fig. 4.12 on page 57). Bonded-in rods show a stiff behavior, but they act rather brittle if the bearing resistance is set to the gluing line instead to a failure of the steel rod itself (see Fig. 4.12 [a]). This type of connection can be classified as rigid according to [60]. On the other hand, nails show a ductile behavior with a rather low stiffness, depending on the number of fasteners (see Fig. 4.12 [g]). This type of connection can either be classified as semi-rigid or as hinged.

All of the other examined connections show a clear semi-rigid behavior.

The influence of the joint stiffness and the resulting consequences on the load distribution are examined on multi-span beams within this section.

8.2 Consideration of the joint stiffness on a two span beam

8.2.1 General

Within this study the joint is located at the center support and behaves with a certain stiffness. The system is carrying a uniformly distributed load. An equal spacing is considered on either side of the mid support (see Fig. 8.2(a)). In order to achieve generally applicable results, the stiffness of the joint is given as a ratio of $3 \cdot \frac{EI}{l}$, which describes the stiffness of a single beam (see Fig. 8.2(b)).

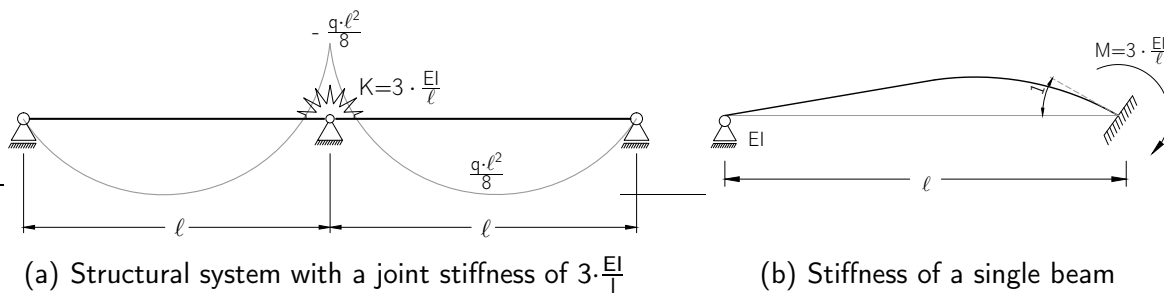


Figure 8.2: Basic principles of the investigations on the joint stiffness [15]

8.2.2 Required joint stiffness

By applying the force method [31] the maximal possible uniformly distributed load for the two span beam is given by:

$$q = M_{joint} \cdot \left(\frac{8}{l^2} + 12 \cdot \frac{EI}{K \cdot l^3} \right) \quad (8.1)$$

where:

- q : uniformly distributed load
- M_j : bearing resistance of the joint
- M_{cs} : bearing resistance of the cross-section
- K : joint stiffness

Assuming the maximum bending moment at mid-span on either side of the center support, the magnitude of the bending moment is found with:

$$M_{cs} = q \cdot \frac{l^2}{8} - \frac{|M_j|}{2} \quad (8.2)$$

Joining Equation (8.1) and Equation (8.2) a minimal required stiffness of the joint is found for certain ratios of M_{joint} and $M_{cross-section}$. The magnitude of the required joint stiffness is given as [15]:

$$K \geq \frac{3 \cdot EI \cdot M_j}{l \cdot (2 \cdot M_{cs} - M_j)} \quad (8.3)$$

Figure 8.3 shows the possibility of a redistribution of internal actions, for certain ratios of M_{joint} to $M_{cross-section}$. The minimum stiffness is represented by the line \overline{ABC} in Figure 8.3.

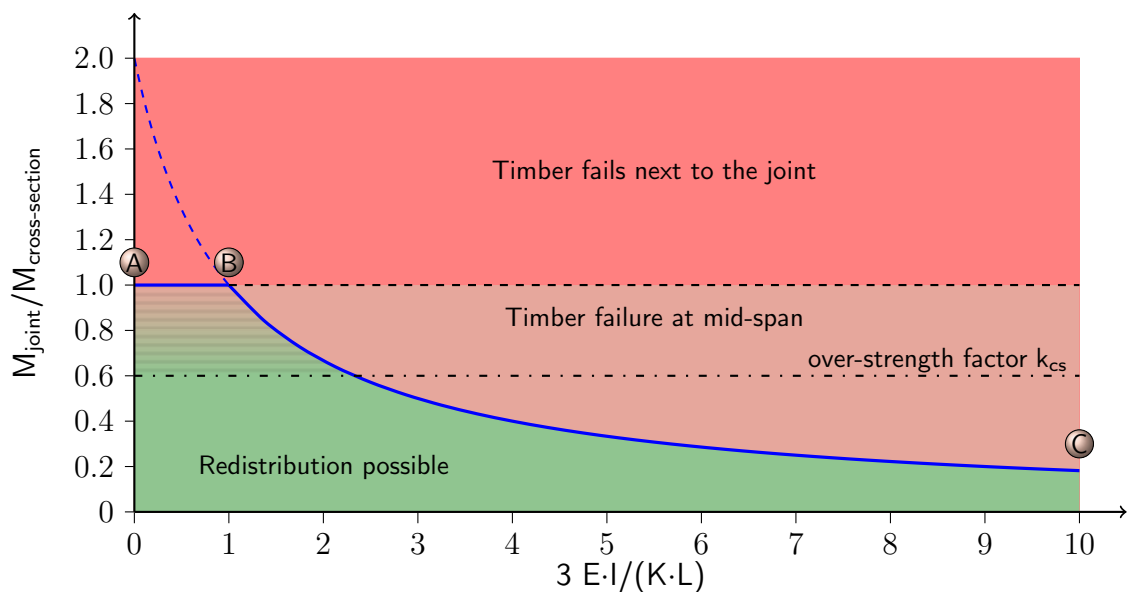


Figure 8.3: Minimal required joint stiffness in order to activate the joint ductility [15]

Consider M_{joint} and $M_{cross-section}$ as equal, for defined levels of the stiffness below $3 \cdot \frac{EI}{l}$, a timber failure at mid-span will occur (line \overline{BC} in Figure 8.3). This is caused by an earlier reaching of the ultimate stresses at mid-span. In this case, the joint is still in the elastic range, while the cross-section fails.

If the stiffness of the joint is $3 \cdot \frac{EI}{l}$ (point B in Figure 8.3) the ultimate bending moment at mid-span and at the joint is reached simultaneously. No plastic rotation of the joint is required. On the other hand, if the stiffness of the joint is higher than $3 \cdot \frac{EI}{l}$, the joint reaches the plastic plateau and redistributes internal actions by a sufficient rotation capacity. A larger bearing resistance of the joint compared to the bearing resistance of the cross-section leads to a timber failure next to the joint (line \overline{BC} in Figure 8.3). Attention has to be given to the joint design in general. As discussed in Section 7.2, the ultimate ratio of M_{joint} to $M_{\text{cross-section}}$ has to be chosen in such a way, that the probability of failure is within the structural requirements (comp. Sec. 7.2.2).

8.3 Further Investigations

8.3.1 General

Further investigations have been conducted by [51] on a multi-span beam. Systems with overlapping purlins are a widespread system, which is generally used in barns and storage halls. The requirements on the joint stiffness of such a system is therefore of further interest. The investigations were focused on a multiple span beam with five sections of equal lengths (see Fig. 8.4). The procedure follows the approach of [15] as described in Section 8.2. For

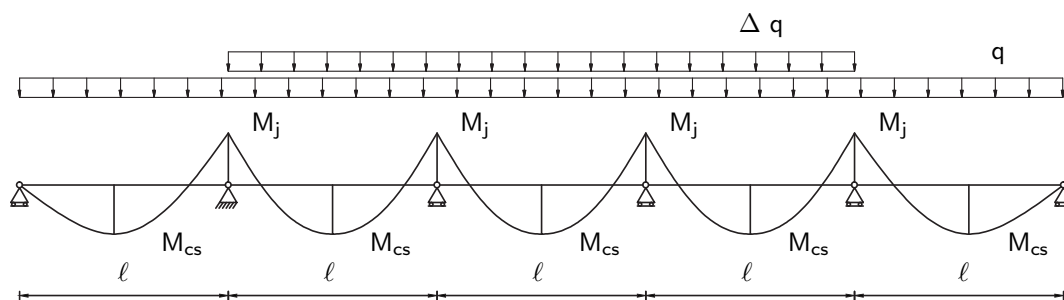


Figure 8.4: Considered structural system [51]

a multiple span beam it is necessary to distinguish between the supports on the side and the middle supports, since the bending moment diagram has a pronounced discontinuity.

8.3.2 Required joint stiffness

Side support: The limit for the required stiffness in order to activate the ductile behavior of the side joint in a multi-span beam, needs to fulfil the following equation [51]:

$$K \geq \frac{-3 \cdot EI \cdot \left(\sqrt{5 \cdot \left(\frac{M_j}{M_{cs}} \right)^2 + 8 \cdot \left(\frac{M_j}{M_{cs}} \right) + 16} + 7 \cdot \left(\frac{M_j}{M_{cs}} \right) - 4 \right)}{l \cdot \left(11 \cdot \left(\frac{M_j}{M_{cs}} \right) - 16 \right)} \quad (8.4)$$

- K : joint stiffness
- M_j : bearing resistance of the joint
- M_{cs} : bearing resistance of the cross-section

If the joint consists at least of a stiffness of:

$$K \geq \frac{3 \cdot EI \cdot (\sqrt{29} + 3)}{5 \cdot l} \quad (8.5)$$

both the moment at the support and the moment at the first beam element are equal. Figure 8.5 illustrates the separation of the different failure modes, which are initiated depending on the stiffness of the joint.

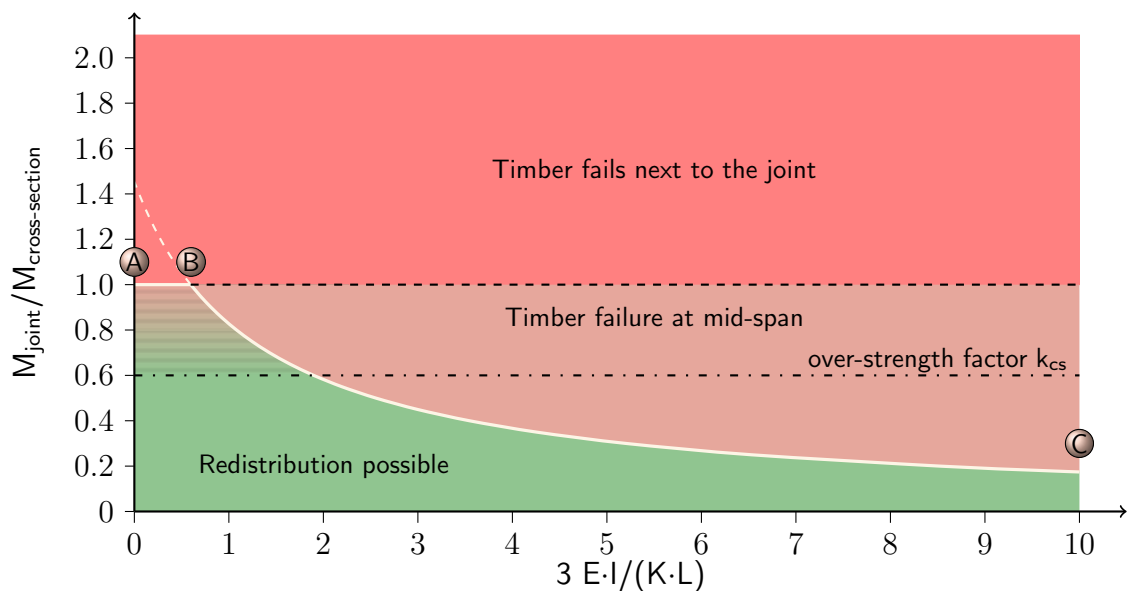


Figure 8.5: Minimum required joint stiffness at the second support of a multi span beam in order to activate the joint ductility [51]

Middle support: At the middle support the following stiffness is required in order to activate the ductile behavior of the joint [51]:

$$K \geq \frac{3 \cdot EI \cdot \left(\sqrt{-3 \cdot \left(\frac{M_j}{M_{cs}}\right)^2 + 8 \cdot \left(\frac{M_j}{M_{cs}}\right) + 16} + 5 \cdot \left(\frac{M_j}{M_{cs}}\right) - 4 \right)}{l \cdot \left(7 \cdot \left(\frac{M_j}{M_{cs}}\right) - 12 \right)} \quad (8.6)$$

In order to achieve an equal magnitude of the bending moment at the support and at the joint, a stiffness of the joint of

$$K = \frac{3 \cdot EI \cdot (\sqrt{21} + 1)}{5 \cdot l} \quad (8.7)$$

is required. In this case, a bending moment of $q \cdot \frac{l^2}{12}$ is obtained.

Figure 8.6 gives the minimum joint stiffness in order to exploit the joint ductility.

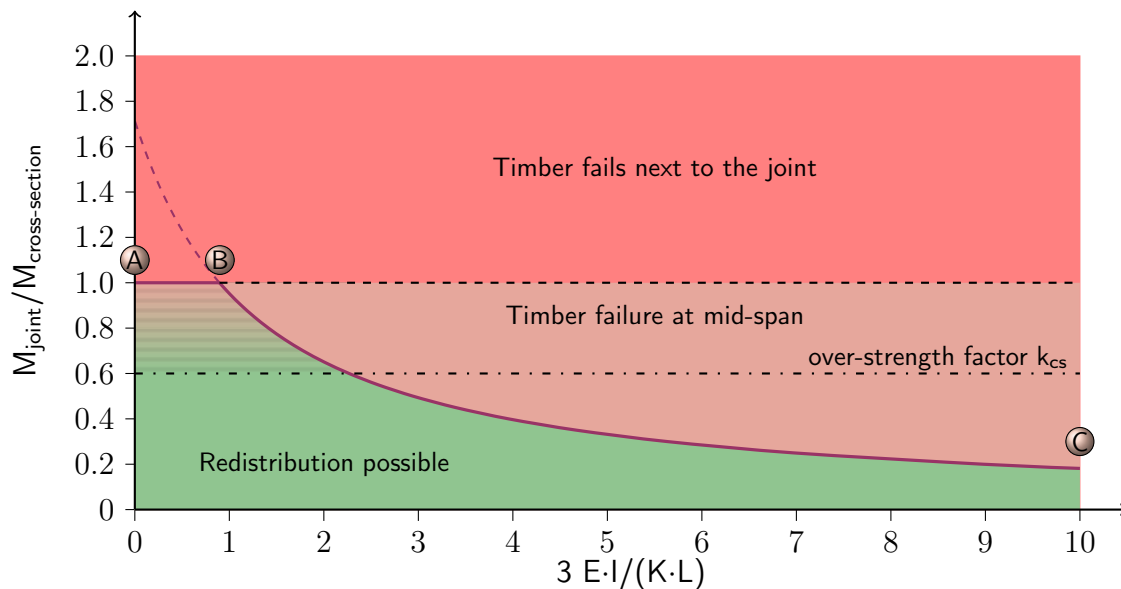


Figure 8.6: Minimum required joint stiffness at the mid supports of a multi span beam in order to activate the joint ductility [51]

8.4 Summary

The stiffness of the joint is a decisive value for the design of a structure. It is important to consider not only the stiffness of certain structural members, but also the stiffness of the joint.

Within this section attention was given to the joint stiffness on a two span beam and on

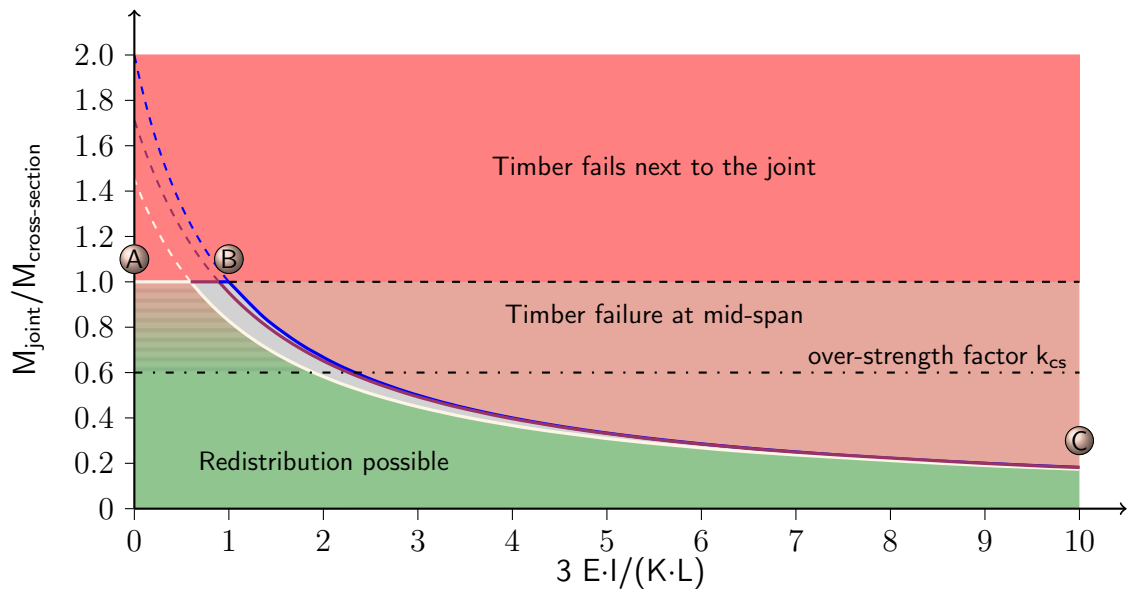


Figure 8.7: Summary of certain minimum joint stiffnesses in order to activate the ductile behavior

a multiple span beam, displayed as a beam consisting of five equal spans. Taking an over-strength factor into account a ratio of M_{joint} to $M_{\text{cross-section}}$ of 0.6 is given in each figure. Minimum joint stiffnesses have been determined in order to activate the ductile behavior of the joint and thus to gain a benefit from the ductile behavior of the joint.

Figure 8.7 shows the summary of the investigated minimum stiffnesses. It is obvious that the minimum required stiffness at the mid support of a two span beam (blue line) and the minimum required stiffness at middle support of the multi-span beam (purple line) does not differ much. On the other hand, the second and second last support of a multiple span beam (light grey) needs a higher stiffness compared to a two span beam.

The lower boundary is described by the behavior of the second support of a multi span beam, whereas the upper boundary is given by the mid support of a two span beam. Hence, if the required stiffness at the mid support of a two span beam is considered, a redistribution of internal actions is possible for all structural systems with equal structural lengths.

9 Conclusions and Outlook

9.1 General remarks

The present thesis addressed *Ductility in timber structures - possibilities and requirements with regard to dowel type fasteners* is focusing on the potentiality of mainly doweled connections for activating the desired ductile behavior of fasteners in timber structures. Within this focus, special attention was given to bridge the gap of the current possibility to use the ductile behavior of fasteners to the unknown behavior and constraints given by the code. Critical discussions are given on state of the art on corresponding findings of the conducted experiments within this research work. A brief summary of the main outcomes and recommendations for future research work is also given.

9.2 Conclusions

Preliminary investigations

A thorough study on experiments known from literature has been conducted to gain knowledge of the ductile behavior of certain types of fasteners. Not only dowel type fasteners have been investigated, but also split rings, nail plates and tube connections. No attention was given to self-drilling fully threaded screws loaded in tension, since this type of fastener behaves currently rather brittle.

No tangible indicators are given by the code to evaluate the ductile behavior of fasteners in timber structures. Therefore, criteria to evaluate the ductile behavior have been developed in a further step. It constitutes the discussion of available methods with the view of a representative result and the applicability.

Some of the methods give a point of yielding, although the behavior is rather brittle. However, the method based on EN 12512 [102] and SIA 265:2012 [114] gives a reliable point of yielding. A certain decrease of the stiffness is requested in the approach in dependence on the initial stiffness. Hence, no point of yielding is found if this criteria is not accomplished. This method has been modified by the approach given by Yasumura and Kawai [80]. Therefore, the displacement at yielding corresponds to the actual load displacement behavior of the fastener and not to an artificial given point next to the graph.

A further issue is set to the basis of the evaluation of the ductile performance. Previous discussion has shown that it is an open question if the basis is set to the displacement at ultimate load or at failure. A solution is given by defining the basis as 98 % of the ultimate load. Therefore only a comprehensible loss of the ductile displacement is given for fasteners with a pronounced ductile behavior.

The classification of the ductility is currently only related to a relative ratio. The relative ratio represents certain correlations of the point of yielding to the point at ultimate load. Hence, fasteners with a small displacement at yielding and a rather small displacement at ultimate load may be classified as ductile, although the ductile performance is not suitable. The evaluation has been extended by the consideration of absolute deformation values to pay attention to the plastic deformability of the connection.

The evaluation of the previously studied experiments on different fasteners with respect to the developed classification model shows that fasteners in timber structures perform with a low to moderate ductility. This is mainly caused due to the inherent brittle material behavior of timber. However, within the introduced classification of fasteners, reinforced doweled connections are classified with a high ductile behavior within the absolute and relative consideration.

Experimental study

Based on the evaluation of conducted experiments further experimental studies on reinforced doweled connections were performed. The experiments were in general divided into two test series. The first series was focused on connections loaded in tension. The second series comprised a joint loaded under a bending moment as a further step. Hence, the connections tested in tension were implemented to a semi-rigid joint. The previously tested dowel arrangement was placed in the tension zone of the joint. The arrangement and the number of dowels remained the same to gain knowledge of the mechanical behavior of such joints.

Neither the dowel diameter nor the dowel arrangement had an influence on the load - displacement and the ultimate load. Hence the findings of Bejtka [82] could be confirmed. The primary experiments were conducted with a dowel diameter of 12 mm. All of the experiments showed a significant ductile behavior based on the introduced classification which is based on Smith et al. [69] and extended by an absolute required yield displacement. The performed experiments on self-drilling dowels of a diameter of 7 mm showed a desired load-displacement behavior. After a level of plasticity the connection gained a solidification with a desired load increase.

Experiments on a dowel diameter with 16 mm were designed with a rather low slenderness ratio to achieve a lower boundary of the ductility. The connections failed brittle due to a tension-bending failure of the timber at the slotting and not at the connection itself.

Four point bending tests were performed to prove the ductile behavior of joints designed with a dowel type connection in the tension zone. It has been shown that the dowel arrange-

ment has an influence on the moment-rotation behavior. Stretched arrangements showed a decrease of the moment resistance with an increase of the rotation. On the other hand, a rather constant level of ductility was accomplished with wide dowel arrangements. An interesting observation was made concerning the experiments with a dowel diameter of 16 mm. The moment-rotation behavior showed a high ductile behavior, although the connection with dowel-type fasteners was designed with a rather small slenderness ratio.

In addition to the main test series, experiments perpendicular to the grain and under a cyclic loading were performed. The connections were also reinforced with fully threaded screws. The experiments perpendicular to the grain showed also a highly ductile behavior. However, the experiments under a cycling loading could be classified as low to a moderate ductile behavior.

To draw a conclusion, the main experiments showed consistently a ductile behavior. Therefore, a model was developed in a further step to describe the load-deflection behavior in a reliable manner. Reliable not only in view of the ultimate load, but also with respect to the stiffness of certain deformation stages.

Requirements

It is generally necessary to describe the load - displacement behavior of different types of fasteners, in order to implement their application in the codes. The presented idea follows the conception of EN 1993-1-8 [107]. Based on the approach it was possible to describe the load - deflection behavior of dowel type fasteners as a trilinear graph. Not only the stiffness and the ultimate load are well displayed, but also the plastic deformability of the connection. Besides the knowledge of the behavior of a single fastener, it is also necessary to gain knowledge of a complete joint. A first model was developed for semi-rigid joints, accomplished with dowel type fasteners in the tension zone, based on the so called component model. Certain objects were analyzed and assembled based on a mechanical model. The different objects are considered individually and discussed.

With regard to the experiments conducted in bending, the developed model is proven to obtain reliable and conclusive results.

The scattering of the material properties has a large influence on the bearing resistance. Therefore, it is indispensable to ensure, that no brittle failure of a timber element occurs before the joint is in the stage of yielding. To meet this requirement, a Monte-Carlo simulation has been performed to gain knowledge of a required over-strength factor, if the ductile behavior is regularly applied. Numerous application possibilities of the ductile behavior are classified in different safety categories. Therefore, the target reliability index varies as well. Within the scientific view, a reliability line was developed to meet this requirement.

The inherent material scattering of timber has also an impact on the end-rotation of a certain beam under loading. The beam end-rotation has subsequently an influence on the required rotation capacity of the joint. The required increase of the necessary joint rotation capacity

was developed for certain load configurations. It could be shown that the beam end-rotation varies by approximately 10 %, compared to a homogenous consideration. Therefore, the required joint rotation has to be increased by the ascertained value as well.

A further requirement is set to the stiffness of the joint. If the ductile behavior is set with the focus on a possible redistribution of internal actions, it is necessary that the joint has a certain stiffness. If the stiffness of the joint is too low, a brittle failure at mid-span may occur due to an already constituted redistribution although the joint is in the elastic range. Certain structural systems have been discussed to gain knowledge of the minimum required joint stiffness in order to apply the ductile behavior with view on the redistribution of internal actions.

9.3 Limitation

The presented findings are based on conducted experiments with dowel-type fasteners. All of the experiments require reinforced dowel connections with self tapping screws to prevent a possible brittle failure mode due to splitting.

The introduced model is investigated on a dowel diameter with 12 mm and compared with the results of the experiments with a diameter of 7 mm and 16 mm. Therefore, the application is limited and further investigations are required.

Furthermore, the investigations are conducted on joints loaded in bending without an additional shear force. Therefore, the presented model is verified on a dowel diameter with 12 mm and a pure loading in bending. The bending moment is divided to a compression and a tension force. Hence a possible application is limited to such joint designs.

9.4 Recommendations for future research

During the conducted research work, the following clarifications became apparent besides the already mentioned topics. The listed recommendations should show indications to continue and intensify this research field:

- Further evaluations on conducted experiments should be evaluated with view on the ductile behavior to extend the database of the ductile behavior given in this work.
- A discussion has been conducted on different methods to evaluate the point of yielding as an indication of the ductile behavior. A principle has to be adopted to give a general rule of the evaluation.
- The model was based on conducted experiments and is concurrently valid for connections with dowel-type fasteners. Therefore, it is necessary to verify the model for different types of fasteners and various types of joints.

- The driving parameter of the developed model to describe the ductile behavior is the initial stiffness. Therefore, it is necessary to have reliable information to take care of the stiffness given by the code, reliable not only for a single fastener, but also for a group of fasteners. Hence it is necessary to develop a coefficient, which takes care of the group effect which was already suggested by Jorissen [84] with the factor k_{bolt} . It is suggested that the tolerances of the borehole and the diameter of the fastener give different hole tolerances for a group of fasteners at the beginning of loading. Therefore, a loosening of the joint stiffness arises compared to a single fastener (see Fig. 9.1).

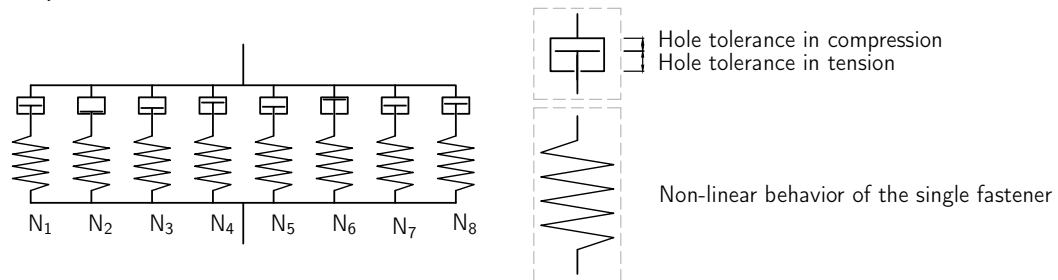


Figure 9.1: Joint model consisting of six dowel type fasteners (N_1 to N_6), showing a different starting point of each fastener at the load-bearing capacity due to an initial slip

- A doubling of the stiffness given in EN 1995-1-1 [109] & SIA 265:2012 [114] is strongly questioned at this point. A suggestion for upcoming experiments is the performance of tests with self-drilling dowels as single fasteners and a group of fasteners with various numbers of fasteners. Self-drilling dowels should not possess any hole tolerance at the beginning of loading, therefore an existence of a group effect based on the initial hole tolerance can be proven.
- Assessing the stiffness of joints within a structural system, it must be considered if it is reasonable to decrease the joint stiffness at ultimate limit state by:

$$K_u = \frac{2}{3} \cdot K_{ser} \quad (9.1)$$

Within this consideration the ultimate load (F_u) is not reached, and only a small plastic deformation is taken into account, (see Fig. 9.2).

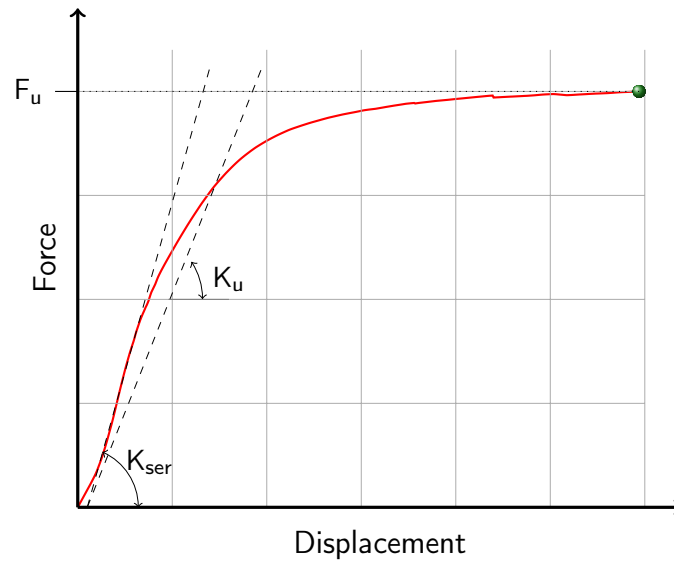


Figure 9.2: Slightly plastic deformation taken into account by K_u

Within an indeterminate structure it is necessary to assess the single stiffnesses of the structural parts to the best possible rate. Otherwise premature failures might occur.

- Only one test setup could be used to reproduce the strain distribution within the compression zone. Since the lever arm is a further important element of the developed model, it would be useful to make a parametrical study based on finite element analysis to gain knowledge of the stress-strain relations and therefore about the inner lever arm in a joint with dowel type fasteners.

To draw a general conclusion, it can be stated that it is possible to introduce the ductile behavior on connections with dowel-type fasteners. The ductile behavior of joints can also be assessed. The gained knowledge was applied on a practical example to show the possibility (see Annex A).

Bibliography

- [1] AF & PA: *Design Specification (NDS) for Wood Construction - Commentary*. American Forest & Paper Association. Washington, DC, USA, 2005
- [2] ALDI, P. ; KUHLMANN, U.: Fatigue strength of timber-concrete composite bridges: Determination of a S-N-line for the grooved connection and the X-connector. In: *World Conference on Timber Engineering*. Riva del Garda, Italy, June 2010
- [3] BATHO, C. ; ROWAN, H.C.: The analysis of the moments in the members having rigid or semi-rigid connections. In: *Second report of the Steel Structures Research Committee (1934)*, pp. 177 – 199
- [4] BENJAMIN, J. ; LIND, N.C.: A Probabilistic Basis for a Deterministic Code. In: *Journal of the American Concrete Institute*, Vol. 66, No. 11, Nov., 1969, pp. 857 – 865
- [5] BIJLAARD, F.S.K. ; NETHERCOT, S.A. ; STARK, J.W.B. ; TSCHEMMERNEGG, F. ; ZOETEMEIJER, P.: Structural properties of semi-rigid joints in steel frames / IABSE surveys, 1989, p. 42/89
- [6] BLAß, H.-J.: Untersuchungen über die Variation des Last-Verschiebungsverhalten in Nagelverbindungen - Variation in Faserrichtung. In: *Holz als Roh- und Werkstoff* 48 (1990), No. 9, pp. 327–332
- [7] BLAß, H.-J.: Untersuchungen über die Variation des Last-Verschiebungsverhalten in Nagelverbindungen - Variation rechtwinklig zur Faserrichtung. In: *Holz als Roh- und Werkstoff* 48 (1990), No. 12, pp. 449–452
- [8] BLAß, H.-J.: Untersuchungen zur Lastverteilung in Nagelverbindungen. In: *Holz als Roh- und Werkstoff* 49 (1991), No. 1, pp. 21–26
- [9] BLAß, H.-J. ; BEJTKA, I. ; UIBEL, T.: Tragfähigkeit von Verbindungen mit selbstbohrenden Holzschrauben / Lehrstuhl für Ingenieurholzbau und Baukonstruktionen, Universität Karlsruhe (TH). Universitätsverlag Karlsruhe, 2006. – Karlsruher Berichte zum Ingenieurholzbau, Band 4
- [10] BLAß, H.-J. ; BIENHAUS, A. ; KRÄMER, V.: Effective bending capacity of dowel-type fasteners. In: *Proceedings of the meeting No. 33 of Working Commission W18 - Timber Structures, CIB*, Delft, The Netherlands, 2000 (paper N° 33-7-5)

- [11] BLAß, H.-J. ; EHLBECK, J. ; KRÄMER, V. ; WERNER, H.: Sicherheitsrelevante Untersuchungen zum Trag- und Verformungsverhalten von mehreren in Kraftrichtung hintereinander liegenden Dübeln besonderer Bauart / Universität Karlsruhe, Versuchsanstalt für Stahl, Holz und Steine, Abteilung Ingenieurholzbau, 1997.
- [12] BLAß, H.-J. ; SCHMID, M.: Self-tapping screws as reinforcement perpendicular to the grain in timber connections. In: *RILEM Symposium: Joints in Timber Structures* (2001), pp. 163–172
- [13] BLAß, H.J. ; FRESE, M. ; GLOS, P. ; DENZLER, J.K. ; LINSENMANN, P. ; RANTAMAUNUS, A.: Zuverlässigkeit von Fichten-Brettschichtholz mit modifiziertem Aufbau / Lehrstuhl für Ingenieurholzbau und Baukonstruktionen, Universität Karlsruhe (TH). Universitätsverlag Karlsruhe, 2008. – Karlsruher Berichte zum Ingenieurholzbau, Band 11
- [14] BOUDREAU, F.A. ; BLAIS, C. ; ROGERS, C.A.: Seismic force modification factors for light-gauge steel-frame-wood structural panel shear walls. In: *Canadian Journal of Civil Engineering* 34 (2007), pp. 56–65
- [15] BRÜHL, F.: *Design of timber structures considering the plastic behaviour of steel fasteners*, University of Canterbury, NZ & Universität Stuttgart, GER, Institute of Structural Design No. 2005-12X, Diploma thesis, July 2005
- [16] BRÜHL, F. ; JORISSEN, A.: *Investigations on conducted experiments with regard to the ductility evaluation of dowel type fasteners*, Scientific Report to COST-STSM-E55-06186 Dec. 2010
- [17] BRÜHL, F. ; SCHÄNZLIN, J. ; KUHLMANN, U.: Ductility in timber structures - investigations on an over-strength factor. In: AICHER, S. (Hrsg.) ; REINHARDT, H.W. (Hrsg.) ; GARRECHT, H. (Hrsg.): *Materials and Joints in Timber Structures - Recent Advancement of Technology*, Springer Verlag, October 2013, pp. 181 – 190
- [18] COLLING, F. ; SCHERBERGER, M.: Die Streuung des Elastizitätsmoduls in Brettschichtholz. In: *Holz als Roh- und Werkstoff* 45 (1987), pp. 95–99
- [19] COMMONWEALTH SCIENTIFIC AND INDUSTRIAL RESEARCH ORGANIZATION (CSIRO): Timber evaluation of mechanical joint systems / CSIRO, Melbourne, Australia. 1996 (Part 3, Earthquake loading)
- [20] DEUTSCHER AUSSCHUSS FÜR STAHLBETON: *Heft 525. Erläuterungen zu DIN 1045-1*. Vol. 2. Berlin : Beuth Verlag GmbH Berlin · Wien · Zürich, 2010
- [21] DIN DEUTSCHES INSTITUT FÜR NORMUNG E.V.: *Grundlagen zur Festlegung von Sicherheitsanforderungen für bauliche Anlagen*. Beuth-Verlag GmbH, 1981

- [22] DITLEVSEN, O. ; MADSEN, H.O.: *Structural reliability methods*. John Wiley & Sons Ltd., 1996 (ISBN 0 471 96086 1)
- [23] EHLBECK, J. ; COLLING, F. ; GÖRLACHER, R.: Einfluss keilgezinkter Lamellen auf die Biegefestigkeit von Brettschichtholzträgern Teil 1: Entwicklung eines Rechenmodells. In: *Holz als Rohstoff* 43 (1985), pp. 333–337
- [24] EHLBECK, J. ; WERNER, H.: Untersuchungen über die Tragfähigkeit von Stabdübelverbindungen. In: *Holz als Roh- und Werkstoff* 46 (1988), No. 8, pp. 281 – 288
- [25] FISCHER, L.: *Das neue Sicherheitskonzept im Bauwesen - Ein Leitfaden für Bauingenieure, Architekten und Studenten*. Bautechnik Spezial. Ernst & Sohn, Berlin, 2001 (ISSN 0932-8351)
- [26] FRESE, M. ; BLAß, H.-J.: System effects in glued laminated timber in tension and bending. In: *Proceedings of the meeting No. 43 of Working Commission W18 - Timber Structures, CIB*, Nelson, New Zealand, 2010 (paper N° 43-12-3)
- [27] FRESE, M. ; HUNGER, F. ; BLAß, H.-J. ; GLOS, P.: Verifikation von Festigkeitsmodellen für die Brettschichtholz-Biegefestigkeit. In: *European Journal of Wood and Wood Products* 68 (2010), pp. 99–108
- [28] GEHRI, E.: Entwurfskriterien. In: *Entwurf und Bemessung von Schnittholzkonstruktionen mit neuzeitlichen Verbindungen*. Arbeitsgemeinschaft für Holzforschung, Lignum, Zürich, 1979
- [29] GEHRI, E.: Grundlagen der Verbindungstechnik. In: *Holzwerkstoffe auf Furnierbasis*. Arbeitsgemeinschaft für Holzforschung, Lignum, Zürich, 1993
- [30] GEHRI, E. ; FONTANA, M.: Betrachtungen zum Tragverhalten von Passbolzen in Holz-Holz-Verbindungen / Publikation Nr 83-1, ETH Zürich. 1983
- [31] GHALI, A. ; NEVILLE, A. M.: *Structural analysis, a unified classical and matrix approach*. 4th edition. E & FN Spon, 1997
- [32] GLOS, P.: Zur Modellierung des Festigkeitsverhaltens von Bauholz bei Druck-, Zug und Biegebeanspruchung / Laboratorium für den konstruktiven Ingenieurbau (LKI), Technische Universität München. 1981 (Heft 61)
- [33] GLOS, P. ; HEIMESHOF, B. ; KELLETSCHOFER, W.: Einfluß der Belastungsdauer auf die Zug- und Druckfestigkeit von Fichten-Brettlamellen / Holz als Roh- und Werkstoff. Springer-Verlag, 1987, pp. 243–249
- [34] HENGARTNER, W. ; THEODORESCU, R.: *Einführung in die Monte-Carlo-Methode*. Carl Hanser Verlag München, Wien, 1978 (ISBN 3-446-12331-8)

- [35] JASPART, J.P. ; MAQUOI, R.: Prediction of the semi-rigid and partial-strength properties of structural joints. In: *Proceedings of the SSRC Annual technical Session and Meeting, Lehigh, USA (1994)*, June 20, pp. 177–192
- [36] JASPART, J.P. ; PIETRAPERTOSA, C. ; WEYNAND, K. ; BUSSE, E. ; KLINKHAMMER, R.: Development of a full consistent design approach for bolted and welded joints in building frames and trusses between steel members made of hollow and/or open sections - Application of the component method, Volume 1- practical guidelines / CIDECT Report: 5BP-4/05. 2005
- [37] JOHANSEN, K. W.: Theory of timber connections. In: *IABSE-International Association for Bridge and Structural Engineering 9 (1949)*, pp. 249–262
- [38] JOINT COMMITTEE ON STRUCTURAL SAFETY (JCSS): *Probabilistic Model Code*. Part 1: Basis of design. March 2001
- [39] JOINT COMMITTEE ON STRUCTURAL SAFETY (JCSS): *Probabilistic Model Code*. Part 3.10: Resistance Models - Dimensions. March 2001
- [40] JOINT COMMITTEE ON STRUCTURAL SAFETY (JCSS): *Probabilistic Model Code*. Part 3.2: Resistance Models - Structural steel. March 2001
- [41] JOINT COMMITTEE ON STRUCTURAL SAFETY (JCSS): *Probabilistic Model Code*. Part 3.5: Resistance Models - Timber. August 2006
- [42] JORISSEN, A. ; FRAGIACOMO, M.: Ductility in timber structures. In: *Proceedings of the meeting No. 43 of Working Commission W18 - Timber Structures, CIB, Nelson, New Zealand, August 2010 (paper N° 43-7-2)*
- [43] KARACABEYLI, E. ; CECCOTTI, A.: Nailed wood-frame shear walls for seismic loads: test results and design considerations. In: *Structural Engineering World Wide, Proceedings of the Structural Engineering Congress, San Fransisco, USA, ISBN 0-08-042845-2*. Paper ref. T207-6, 19-23 July 1998
- [44] KAZINCZY, G.v.: Experiments with clamped beams (in Hungarian). In: *Betonszemele 75 (1914)*, No. 2, pp. 68 – 71 & pp. 101–104
- [45] KINDMANN, R. ; FRICKEL, J.: *Elastische und plastische Querschnittstragfähigkeit*. Ernst & Sohn, Berlin, 2002
- [46] KUHLMANN, U. ; BRÜHL, F.: Robuste Holztragwerke durch duktile Anschlüsse mit stiftförmigen Verbindungsmitteln / Institute of Structural Design. 2011. – Research work supported and financed by Deutschen Instituts für Bautechnik DIBt, DIBt ZP 52-5-13-13.181 1319/09

- [47] KUHLMANN, U. ; BRÜHL, F.: Vorteilhafte Bemessung von Holztragwerken durch duktile, plastische Anschlüsse / Institute of Structural Design. 2012. – Research work (16184N) within the International Association for Technical Issues related to Wood (iVTH e.V.), was supported in the program of “Industrielle Gemeinschaftsforschung (IGF)” and financed by the German Federation of Industrial Research Association (AiF).
- [48] KUHLMANN, U. ; RÖLLE, L.: Verbundanschlüsse nach Eurocode. In: *U. Kuhlmann (eds.): Stahlbaukalender 2010*. Ernst & Sohn, Berlin, 2010, chapter 5, pp. 577 – 642
- [49] KUHLMANN, U. ; SCHÄNZLIN, J. ; F.BRÜHL: *Auswertung der Versuche zur Bestimmung der Tragfähigkeit eines Fachwerkknotens mit selbstbohrenden Holzschrauben*. 2008. – unpublished
- [50] KURRER, K.-E. ; HUERTA, S.: Beitrag zur Geschichte plastischer Berechnungsmethoden im Stahlbau. In: *Stahlbau* 75 (2006), No. 4, pp. 317 – 330
- [51] MAGER, M.: *Untersuchungen zur Verbindungsmittelduktilität rechtwinklig zur Faserichtung und deren Einfluss auf Koppelpfettensysteme*, Universität Stuttgart, Institute of Structural Design, Mitteilung Nr. 2012-1X, Diploma thesis, Jan. 2012
- [52] MAIER-LEIBNITZ, H.: Beitrag zur Frage der tatsächlichen Tragfähigkeit einfacher und durchlaufender Balkenträger aus St 37 und Holz. In: *Die Bautechnik* 6 (1928), Issue 1, pp. 11–14
- [53] MAIER-LEIBNITZ, H.: Beitrag zur Frage der tatsächlichen Tragfähigkeit einfacher und durchlaufender Balkenträger aus St 37 und Holz. In: *Die Bautechnik* 6 (1928), Issue 2, pp. 27–31
- [54] METROPOLIS, N. ; ULAM, S.: The Monte Carlo method. In: *Journal of the American Statistical Association* 44 (1949), September, No. 247, pp. 335 – 341
- [55] MEYER, A.: Die Tragfähigkeit von Nagelverbindungen bei statischer Belastung. In: *Holz als Roh- und Werkstoff* 15 (1957), No. 2, pp. 96–109
- [56] MISCHLER, A.: *Untersuchungen zum Tragverhalten des SFS WS-Verbindungssystem / Eidgenössische Technische Hochschule Zürich*. 2001
- [57] MUÑOZ, W. ; MOHAMMAD, M. ; SALENIKOVICH, A. ; QUENNEVILLE, P.: Need for a harmonized approach for calculations of ductility of timber assemblies. In: *Proceedings of the meeting No. 41 of Working Commission W18 - Timber Structures, CIB*, St. Andrews, Canada, August 2008 (paper N° 41-15-1)
- [58] NOVÁK, B. ; KUHLMANN, U. ; EULER, M.: *Einwirkung-Widerstand-Tragwerk*. Ernst & Sohn, Berlin, 2012 (ISBN: 978-3-433-02917-6)

- [59] PAULAY, T. ; PRIESTLEY, M.J.N.: *Seismic design of reinforced concrete and masonry buildings*. John Wiley & Sons, Inc., 1992
- [60] P.HALLER: *Timber joints in joint research*. Cost C1-Semi-rigid timber joints - structural behaviour modelling and new technologies, 1992-1999, pp. 11–21
- [61] PÖRSCHMANN, H.: Tragwerke aus Holz, nach TGL 112-0730 (Feb. 1963). In: *H. Pörschmann (eds.): Bautechnische Berechnungstabeln für Ingenieure*. BSB B.G. Teubner Verlagsgesellschaft, Leipzig, 1972, chapter 6, pp. 177–210
- [62] RACHER, P.: Mechanische Holzverbindungen - Allgemeines. In: *STEP 1* (1995), pp. C1/1 – C1/11
- [63] RAVENHORST, G.J.P. ; VAN DE KUILEN, J.W.G.: Relationships between local, global and dynamic modulus of elasticity for soft- and hardwoods. In: *Proceedings of the meeting No. 42 of Working Commission W18 - Timber Structures, CIB*, Zurich, Switzerland, August 2009, (paper N° 42-10-1)
- [64] REYER, E. ; BRETTLÄNDER, Th. ; LINZNER, P.: Untersuchungen über die mögliche Übertragung von Scher- und Lochleibungskräften durch die Gewindebereiche von Passbolzen bzw. Gewindestangen / Lehrstuhl für Baukonstruktionen, Ingenieurholzbau und Bauphysik, Ruhr-Universität Bochum. 1993
- [65] RUBINSTEIN, R.Y. ; KROESE, D.P.: *Simulation and the Monte Carlo Method*. Vol. 2. John Wiley & Sons, Inc., 2007
- [66] SCHÄNZLIN, J. ; BRÜHL, F. ; DEAM, B.: Design of timber structures considering the plastic behavior of steel fasteners. In: *World Conference on Timber Engineering*. Portland, OR, USA, August 2006, Vol., pp. 187–194
- [67] SCHEER, J. ; PEIL, U. ; NÖLLE, H.: *Schrauben mit planmäßiger Biegebeanspruchung*. IRB-Verl., 1987 (Bericht 6079. Institut für Stahlbau der Technischen Universität Braunschweig)
- [68] SCHICKHOFER, G. ; AUGUSTIN, M. ; JEITLER, G.: Einführung in die Verbindungstechnik mit Stabdübeln, Schrauben und eingeklebten Stahlstangen. In: *6. Grazer Holzbau-Fachtagung*, 2007, Vol. 6, pp. A1–A66
- [69] SMITH, I. ; ASIZ, A. ; SNOW, M. ; CHUI, I.H.: Possible Canadian/ISO approach to deriving design values from test data. In: *Proceedings of the Meeting No. 39 of Working Commission W18 - Timber Structures, CIB*, Florence, Italy, August 2006 (paper N° 39-17-1)
- [70] SPAETHE, G.: *Die Sicherheit tragender Baukonstruktionen*. Springer Verlag, Wien, 1992

- [71] STAPEL, P.: Auswirkung der Herkunft auf die Festigkeit bei verschiedenen Sortierverfahren. In: *Doktorandenkolloquium - Holzbau Forschung und Praxis*, Stuttgart, 2010, pp. 43–48
- [72] STEHN, L. ; BJÖRNFOOT, A.: Comparison of different ductility measurements for a nailed steel-to-timber connection. In: *Proceedings of the 7th World Conference on Timber Engineering WCTE 2002*, Shah Alam, Malaysia, August 2002, Vol. 2, pp. 155–162
- [73] STEPHAN, K.: *Untersuchungen zur Verbindungsmittelduktilität im Holzbau und deren Einfluss auf die Erdbebenbemessung*, Universität Stuttgart, Institute of Structural Design No. 2011-5X, Diploma thesis, Feb. 2011
- [74] STÜSSI, F.: Fehler und Mängel des Traglastverfahrens. Mitteilung der Technischen Kommission des Schweizer Stahlbauverband, Zürich. 1963 (Issue 25)
- [75] STÜSSI, F. ; KOLLBRUNNER, C. F.: Beitrag zum Traglastverfahren. In: *Bautechnik* 13 (1935), Issue 21, pp. 264–267
- [76] SYMONDS, P. S. ; NEAL, B.G.: The Interpretation of Failure Loads in the Plastic Theory of Continuous Beams and Frames. In: *Journal of the Aeronautical Sciences* 19 (1952), January, No. 1, pp. 15 – 22
- [77] TECHNICAL COMMITTEE 1 - STRUCTURAL SAFETY AND LOADINGS, TECHNICAL WORKING GROUP 1.3 - SEISMIC DESIGN: Study on design of steel building in earthquake zones. In: *ECCS European Convention for Constructional Steelwork* No. 47 (1986), pp. 3/12 – 3/24
- [78] TSCHEMMERNEGG, F.: Zur Entwicklung der steifenlosen Stahlbauweise. In: *Der Stahlbau* 51 (1982), pp. 201–206
- [79] TSCHEMMERNEGG, F. ; ANGERER, T. ; FRISCHHUT, M.: Bemessungshilfen für nachgiebige Stahlknoten mit Stirnplatten. In: *U. Kuhlmann (Hrsg.): Stahlbaukalender 1999*. Verlag Ernst & Sohn, Berlin, 1999, chapter 5, pp. 457–514
- [80] YASUMURA, M. ; KAWAI, N.: Estimating seismic performance of wood-framed structures. In: *Proceedings of I.W.E.C. Switzerland* Bd. 2, 1998, pp. 564–571
- [81] ZILCH, K. ; ZEHETMAIER, G.: *Bemessung im konstruktiven Betonbau*. 2. Springer Verlag, 2009

Dissertations

- [82] BEJTKA, I.: *Verstärkungen von Bauteilen aus Holz mit Vollgewindeschrauben*, Universität Karlsruhe, Lehrstuhl für Ingenieurholzbau und Baukonstruktionen, Dissertation, 2005
- [83] GLOS, P.: *Zur Bestimmung des Festigkeitsverhaltens von Brettschichtholz bei Druckbeanspruchung aus Werkstoff- und Einwirkungskenngrößen*, Laboratorium für den konstruktiven Ingenieurbau, Technische Universität München, Dissertation, December 1978
- [84] JORISSEN, A.: *Double shear timber connections with dowel type fasteners*, Delft University of Technology, The Netherlands, Dissertation, 1998
- [85] KEVARINMAKI, A.: *Semi-rigid behaviour of nail plate joints*, Helsinki University of Technology, Dissertation, March 2000
- [86] KÖHLER, J.: *Reliability of timber structures*, Swiss Federal Institute of Technology, Zürich, Dissertation, April 2006
- [87] KÜHNEMUND, F.: *Zum Rotationsnachweis nachgiebiger Knoten im Stahlbau*, Institut für Konstruktion und Entwurf, Universität Stuttgart, Mitteilung Nr. 2003-1, Dissertation, 2003
- [88] LEIJTEN, A.J.M.: *Densified veneer wood reinforced timber joints with expanded tube fasteners*, Delft University of Technology, The Netherlands, Dissertation, 1998
- [89] MISCHLER, A.: *Bedeutung der Duktilität für das Tragverhalten von Stahl-Holz-Verbindungen*, Swiss Federal Institute of Technology, Zurich, Dissertation, April 1998
- [90] RÖLLE, L.: *Das Trag- und Verformungsverhalten geschraubter Stahl- und Verbundknoten bei vollplastischer Bemessung und in außergewöhnlichen Bemessungssituationen*, Mitteilungen des Instituts für Konstruktion und Entwurf, Nr. 2013-1, Dissertation, June 2013
- [91] SANDHAAS, C.: *Mechanical behaviour of timber joints with slotted-in steel plates*, Delft University of Technology, The Netherlands, Dissertation, 2012
- [92] SCHÄFER, M.: *Zum Rotationsnachweis teiltragfähiger Verbundknoten in verschieblichen Verbundrahmen*, Institut für Konstruktion und Entwurf, Universität Stuttgart, Mitteilung Nr.2005-1, Dissertation, 2005

- [93] WERNER, H.: *Tragfähigkeit von Holz-Verbindungen mit stiftförmigen Verbindungsmitteln unter Berücksichtigung streuender Einflussgrößen*, Universität Friedericiana zu Karlsruhe, Dissertation, Dezember 1993

Standards

- [94] DIN 1052:1944: *Bestimmungen für die Ausführung von Bauwerken aus Holz im Hochbau*. Verlagsgesellschaft Rudolf Müller, Eberswalde, Berlin, Leipzig, 1944
- [95] DIN 1052:2008-12: *Entwurf, Berechnung und Bemessung von Holzbauwerken – Allgemeine Bemessungsregeln und Bemessungsregeln für den Hochbau*. DIN-Deutsches Institut für Normung e.V., 2008
- [96] DIN 1052:1988: *Holzbauwerke T.1. Berechnung und Ausführung & T.2. Mechanische Verbindungsmittel mit Ergänzungen A1 und A2 (1996)*. DIN-Deutsches Institut für Normung e.V., 1988
- [97] DIN 18203-3:2008-08: *Toleranzen im Hochbau - Teil 3: Bauteile aus Holz und Holzwerkstoffen*. DIN-Deutsches Institut für Normung e.V., 2008
- [98] DIN EN 1992-1-1/NA: *National Annex - Design of concrete structures - Part 1-1: General rules and rules for buildings*. DIN-Deutsches Institut für Normung e.V., 2013
- [99] DIN EN 1995-1-1/NA: *National Annex - Design of timber structures - Part 1-1: General rules and rules for buildings*. DIN-Deutsches Institut für Normung e.V., 2013
- [100] EN 10025-2: *Hot rolled products of structural steels. Technical delivery conditions for - non-alloy structural steels*. European Committee for Standardization (CEN), Bruxelles, 2004
- [101] EN 1194: *Timber structures - Glued laminated timber - Strength classes and determination of characteristic values*. European Committee for Standardization (CEN), Bruxelles, 1999
- [102] EN 12512: *Timber structures - Test methods - Cyclic testing of joints made with mechanical fasteners*. European Committee for Standardization (CEN), Bruxelles
- [103] EN 14080:2013-09: *Timber structures - Glued laminated timber and glued solid timber - Requirements*. European Committee for Standardization (CEN), Brussels, 2011
- [104] EN 1990:2010-12: *Eurocode: Basis of structural design, EN 1990:2002 + A1:2005 + A1:2005/AC:2010*. European Committee for Standardization (CEN), Brussels, 2010

- [105] EN 1992-1-1: *Design of concrete structures - Part 1-1: General rules and rules for buildings, EN 1992-1-1:2004 + AC:2010*. European Committee for Standardization (CEN), Brussels, 2010
- [106] EN 1993-1-1: *Eurocode 3: Design of steel structures - Part 1-1 General rules and rules for buildings, EN 1993-1-1:2005 + AC:2009*. European Committee for Standardization (CEN), Brussels, 2005
- [107] EN 1993-1-8: *Eurocode 3: Design of steel structures - Part 1-8: Design of joints, EN 1993-1-8:2005 + AC:2009*. European Committee for Standardization (CEN), Brussels, 2005
- [108] EN 1994-1-1: *Eurocode 4: Design of composite steel and concrete structures - Part 1-1: General rules and rules for buildings, EN 1994-1-1:2004 + AC:2009*. European Committee for Standardization (CEN), Brussels, 2004
- [109] EN 1995-1-1: *Eurocode 5: Design of timber structures - Part 1-1: General - Common rules and rules for buildings, EN 1995-1-1:2004 + AC:2006 + A1:2008*. European Committee for Standardization (CEN), Brussels, 2004
- [110] EN 26891: *Timber structures; Joints made with mechanical fasteners; General principles for the determination of strength and deformation characteristics*. European Committee for Standardization (CEN), Brussels, 1991
- [111] EN 409: *Timber structures - Test methods - Determination of the yield moment of dowel type fasteners*. European Committee for Standardization (CEN), Bruxelles, 2009
- [112] ENV 1995-1-1: *Eurocode 5: Design of timber structures - Part 1-1: General - Common rules and rules for buildings*. European Committee for Standardization (CEN), Bruxelles, 1994
- [113] ISO 6891: *Timber structures; Joints made with mechanical fasteners; General principles for the determination of strength and deformation characteristics*. International Organization of Standardization, 1983
- [114] SIA 265:2012: *Holzbau*. Schweizerischer Ingenieur- und Architektenverein, 2012

A Example of the application of the findings on the ductile behavior

A.1 General

Within this section, an exemplary application of the ductile behavior is given. The structure is a two-bay hall with fish-belly beams as the main roof structure. The example analysis the possibility of the strengthening of an existing building, using a plastic hinge as a connection between two single span beams.



Figure A.1: Fish-belly beams in the state of construction (Source: WiEHAG)

The shape of the fish-belly beam follows the moment distribution within the structural element and is therefore an economical solution in the building sector (see Fig. A.1). The lamella at the bottom of the beam is continuous within the production of such beams. On the other hand, the upper lamellae are cut to achieve the shape of the beam. This enables a continuous flow of forces within the tension zone and no danger due to cut edges at the bottom.

A.2 Introduction of the structure

A.2.1 General

The structure is located in Germany in the snow area II at a height of 422 m above sea level. The center distance of each bay is 24 m. The resulting span of each beam is therefore 23.84 m (see Fig. A.2). The dead load of the structure was assumed as 0.3 kg/m².

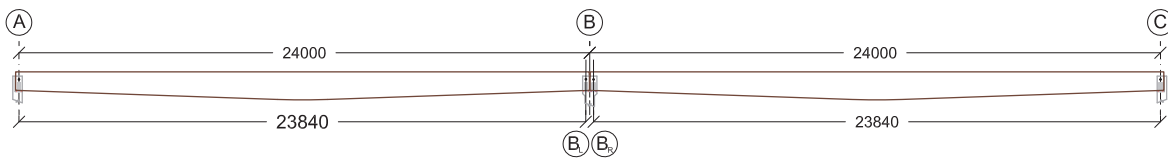


Figure A.2: Cross section of the hall

The distance of each fish belly beam is 5 m, hence a resulting load of

$$q_d = 5 \text{ m} \cdot (1.35 \cdot 0.3 \text{ kN/m} + 1.5 \cdot 0.8 \cdot 1.295 \text{ kN/m}) = 9,79 \text{ kN/m} \quad (\text{A.1})$$

is considered.

The beam width is chosen as 180 mm with respect to the experiments with a glulam grade of GL28c. Such beams are in general produced with a combined layout. Since the height of the beam is below 10 times the beam width, lateral torsional buckling can be determined based on the existing rules given in the code [109]. Due to the chosen grade of GL28c it can be ensured that the experiments conducted with GL24h can be projected. The dowels are embedded in lamellae with a grade of T14 in both examples [103]. The angle between the force and grain direction is not considered within this example

A.2.2 Elastic beam design

Table A.1 shows the geometrical properties of the designed fish belly beam.

The beams are reinforced with fully threaded screws (10x350) at the supports to increase the resistance perpendicular to the grain (see Fig. A.3). To guarantee the rotation of the

Table A.1: Geometrical properties of the fish belly beam

Height at the beam ends:	77.7 cm	Inclination of the lower belt:	2°
Height at the supports:	78.1 cm	Radius:	30 m
Height at the center of the beam:	117.9 cm	Thickness of the lamellae:	41 mm
Beam length:	23.84 m		

A.3 Design considering the plastic behavior

A.3.1 General

The aim of the consideration of the plastic behavior is to achieve a load increase within the structure. Hence a plastic hinge is located at grid-line B (see Fig. A.2). The installation of a solar system, the need for refrigeration units or further loads within the hall (lights, advertisement, etc.), might be reasons for the desired load increase.

A.3.2 Design of the joint

The most important demand within the design of the joint is the required over-strength factor with respect to the reliability index β . A reliability index of 4.2 has been chosen for the design of the joint (comp. Sec. 7.2.2.2). Based on the investigations on the over-strength factor (comp. Sec. 7.2.5), a k_{cs} factor of 0.45 is determined.

The characteristic values are used within the determination of both, the bearing resistance of the beam (M_{cs}) and the ultimate resistance of the dowel connection (M_{joint}). The cut edge and the net cross-section (taking account of the drilling area of the dowels and milling of the flitch plate) were considered in the determination of the bearing resistance of the joint. A maximum bending moment at the joint of **391.69 kNm** was determined. The ultimate load of the doweled connection was calculated based on a steel grade of S355 and the characteristic density [109]. Hence, the ultimate load for a dowel with a diameter of 12 mm and two shear planes turns out at (comp. Eq. (6.13))

$$R_{v,g,k} = 22.70 \text{ kN} \quad (\text{A.2})$$

The determined factor ξ of 0.55 was chosen to calculate the lever arm within the compression zone (see Fig. 6.12), with respect to the assumption of the Monte-Carlo simulation. With respect to the assumption given in the Monte-Carlo simulation, a triangular stress distribution was chosen to model the moment rotation behavior of the joint. The joint consists of 12 dowels in the tension zone and a compression zone with a height of 150 mm. Therefore, the ultimate bending moment is calculated at

$$M_{joint} = 22.70 \text{ kN} \cdot 12 \text{ dowels} \cdot 60.95 \text{ cm} = 166.03 \text{ kNm} \quad (\text{A.3})$$

Hence, an over-strength factor is given as

$$k_{cs} = \frac{M_{joint}}{M_{cs}} = \frac{166.03 \text{ kNm}}{391.69 \text{ kNm}} = 0.424 < 0.45 \checkmark \quad (\text{A.4})$$

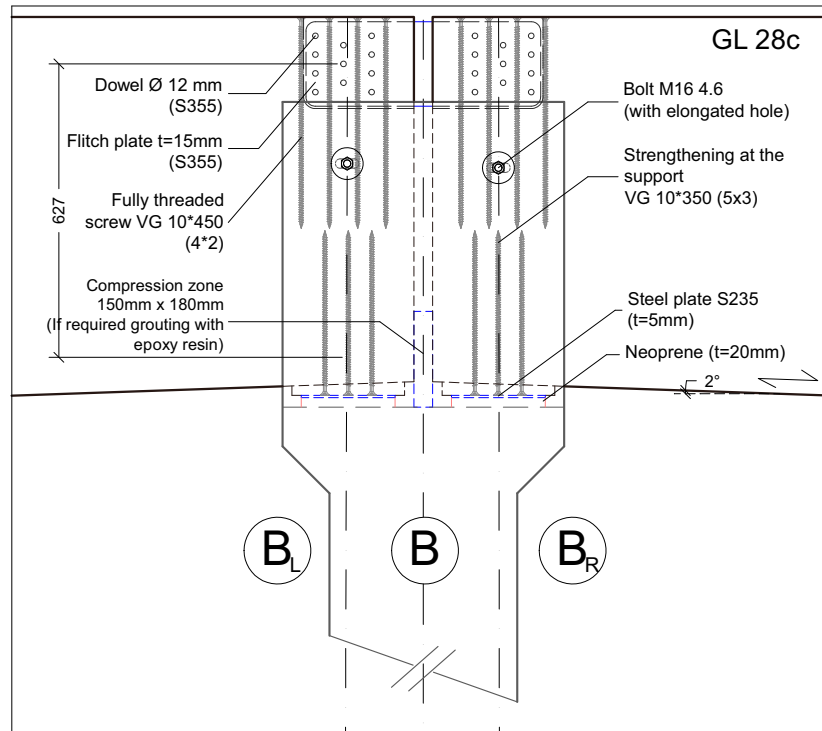


Figure A.4: Design of the plastic hinge in grid-line B

The compliance of the k_{CS} value ensures that no brittle failure occurs with a certain probability next to the joint.

The doweled connection is also reinforced with fully threaded screws (10x450) in order to gain a ductile behavior. Thus, no reduction of the ultimate load has to be considered.

Determination of the moment-rotation behavior

The moment - rotation behavior of either side of the joint is determined based on the simplified procedure presented in Section 6.5. The load - deflection behavior is found in a first step (see Fig. A.5(a)). This result forms the basis for the moment - rotation behavior, which is found by applying the simplified method as described in Section 6.5.3 (see Fig. A.5(b)).

The decrease of the inner lever arm was considered in every three points of the behavior by applying the factor $k_{\phi,e}$. Therefore, a slight decrease of the plastic plateau takes place in the plastic stage. The determination of the factor $k_{\phi,e}$ is exemplary determined.

$$r = \sqrt{a_{\text{end}}^2 + a_{\text{top}}^2} = \sqrt{160 \text{ mm}^2 + 677 \text{ mm}^2} = 693.4 \text{ mm} \quad (\text{A.5})$$

$$b = 2 \cdot r \cdot \sin\left(\frac{\phi}{2}\right) = 2 \cdot 693.4 \text{ mm} \cdot \sin\left(\frac{46.4 \text{ mrad}}{2}\right) = 32.2 \text{ mm} \quad (\text{A.6})$$

$$\Delta_{\text{lever arm}} = \sqrt{u_i^2 - b^2} = \sqrt{28.2 \text{ mm}^2 - 32.2 \text{ mm}^2} = 15.56 \text{ mm} \quad (\text{A.7})$$

$$k_{\phi,3} = \frac{\text{inner lever arm} - \Delta_{\text{lever arm}}}{\text{inner lever arm}} = \frac{609.5 \text{ mm} - 15.56 \text{ mm}}{627 \text{ mm}} = 0.978 \quad (\text{A.8})$$

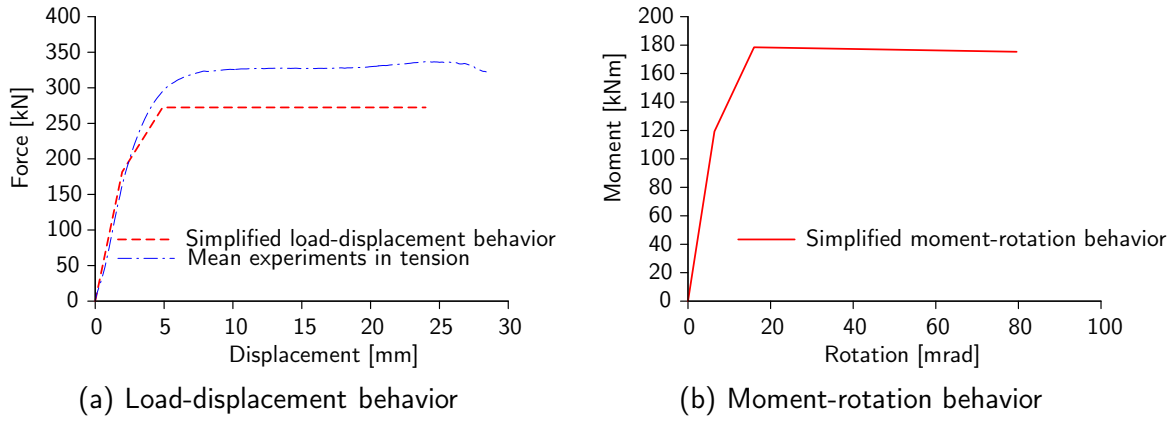


Figure A.5: Determination of the joint behavior based on the simplified model

Due to the rotational stiffness a slight increase of the actual bending moment capacity at each point is applied by a generalized factor $k_{\phi,M}$, which is estimated by 8% (comp. Sec. 6.5.3).

Verification of the joint stiffness

It is important to prove the minimum required stiffness within the application of a ductile behavior in timber structures. If a minimum required stiffness is not achieved, a brittle timber failure occurs at mid-span before the joint is in the plastic stage (comp. Chap. 8). Figure A.6 shows the minimum required stiffness depending on the rotational stiffness of a beam element ($3EI/L$) and the corresponding factor k_{CS} .

The stiffness of a beam element refers to a constant second moment of inertia, whereas a fish belly beam has a varying second moment of area. Hence, the following equation was applied in order to find a parallel beam with the same rotational stiffness as the fish belly beam.

$$\int_0^l \bar{M} \cdot \frac{M}{E \cdot I_{\text{Fish belly beam}}} dx = \varphi = \int_0^l \bar{M} \cdot \frac{M}{E \cdot I_{\text{Parallel beam}}} dx \quad (\text{A.9})$$

An effective geometrical moment of inertia of

$$I_{\text{Parallel beam}} = 12128612129 \text{ mm}^4 \quad (\text{A.10})$$

reflects the stiffness of the analyzed fish belly beam.

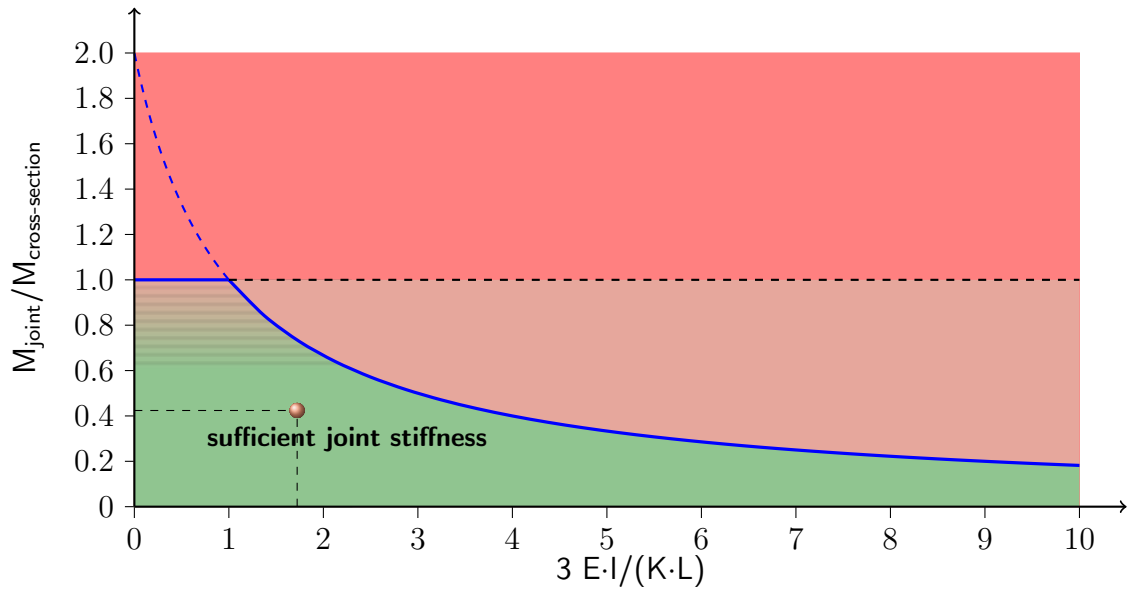


Figure A.6: Representation of the present joint stiffness

The stiffness of the designed joint shows a sufficient rotational stiffness for an over-strength factor $k_{cs} = 0.424$ (see Fig. A.6). Therefore, a plastic hinge is formed at mid support before the maximum stresses are reached at the center of the beam and a brittle failure may occur.

Verification of the rotational capacity

In order to ensure that a redistribution of internal actions can take place, it is important that the joint has a sufficient rotational capacity.

Within this study, a factor k_{mat} has been introduced which considers the scattering of the modulus of elasticity for the beam end-rotation (comp. Sec. 7.3).

The following conditional equation has been developed:

$$k_{mat} \cdot \varphi_{req} \geq \varphi_{exist} \quad (\text{A.11})$$

with

$$k_{mat} = 1.10 \quad (\text{comp. Eq. (7.57)})$$

The structural calculation gives a required rotation (φ_{req}) of **21.47** mrad on either side of the joint to allow stress redistributions in the structural system. The existing rotation (φ_{exist}) is found with the application of the component model (see Fig. A.7).

Therefore, the verification of the joint rotation is :

$$\begin{aligned} 2 \cdot k_{mat} \cdot \varphi_{req} &= \varphi_{exist} & (\text{A.12}) \\ 2 \cdot 1.10 \cdot 21.47 \text{ mrad} &= 47.23 \text{ mrad} \end{aligned}$$

Within Section 6.4.3 two ultimate displacements are presented, the mean value and the 2% percentile if the displacement of the connection of a diameter of 12 mm is considered. In order to show the difference of both magnitudes, the utilization is given for both values.

$$\begin{aligned} &\underline{\text{2\% percentile}} \\ \eta &= \frac{47.23 \text{ mrad}}{40.24 \text{ mrad}} = 117\% \end{aligned} \quad (\text{A.13})$$

$$\begin{aligned} &\underline{\text{mean value}} \\ \eta &= \frac{47.23 \text{ mrad}}{79.58 \text{ mrad}} = 59\% \checkmark \end{aligned} \quad (\text{A.14})$$

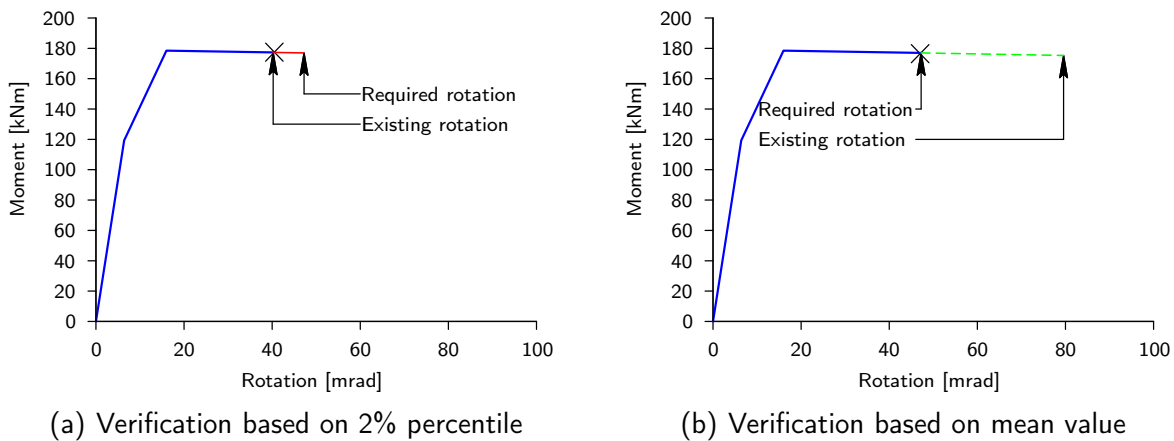


Figure A.7: Comparison of the existing and required rotation

Figure A.7 shows schematically the required and existing rotation of the joint. It can be seen that the 2% percentile is slightly below the required rotation whereas the mean value of the rotation easily reaches the required rotation. Since the simplified model does not account for the stiffness at the compression zone a higher rotation is actually achieved.

It has to be discussed which limit state has to be chosen as a decisive value. An estimation with a 2 percentile is most probably a strict limit, whereas the mean value may be rather uncertain.

A.3.3 Determination of the internal actions under the consideration of a plastic hinge

The previous verifications showed that the designed joint fulfils all the investigated requirements. However, as previously stated, the governing rotation capacity of the different fasteners needs to be specified. Within the last step, the stresses at the fish belly beams have

to be verified with a non-linear joint behavior at mid-support. Furthermore, a possible load increase has to be determined. Figure A.8(a) shows the stresses of the beam considering a

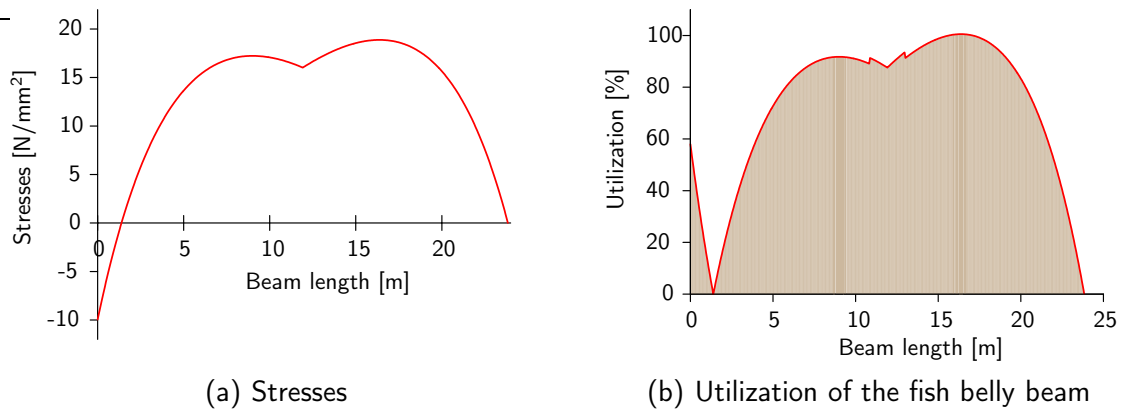


Figure A.8: Stresses and corresponding utilization of the fish belly beam

non-linear behavior of the joint between grid line A-B_L respectively B_R-C. It can be shown, that the structural element is additionally loaded with tension stresses at cut fibers due to the negative bending moment at the support. The governing position is changing due to the change of the moment distribution. However, within the design of the fish belly beam the compression zone (cut fibers) is governing in both cases.

The design showed, that the load could be increased to **10.90 kN/m** considering a plastic hinge. Therefore, a load increase of:

$$\nu = \frac{q_{plastic} - q_{elastic}}{q_{elastic}} = \frac{10.90 \text{ kN/m} - 9.79 \text{ kN/m}}{9.79 \text{ kN/m}} = \mathbf{11\%} \quad (\text{A.15})$$

could be achieved.

Table A.3 shows the utilization of the fish belly beam considering a non-linear joint at the

Table A.3: Utilization of the fish belly beam considering a non-linear joint at the support in grid line B

	η		η
Shear at the support (B):	85 %	Bearing pressure (reinforced):	81 %
Tension at the cut grain	58 %	Compression zone	51 %
<u>governing position x:</u>	16.36 m		
Tensile edge:	97.5 %	Compression edge:	100 %
Curved section:	93.5 %	Compression perp. to the grain:	13 %

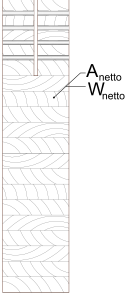
mid-support. Hence, the beam has a higher overall utilization (see Fig. A.8(b)) and is therefore more efficient. On the other hand, it could be shown, that an additional load can be applied if a plastic hinge is introduced at a support.

A.4 Summary & scheduling of the process steps

The application of certain process steps is exemplary displayed within this section. A two-bay hall with fish belly girders served as an example for the plastic design. It has been shown, that the plastic design is in general possible. The joint showed a sufficient rotation capacity and stiffness. It was possible to increase the load by 11 % of its initial load, due to the consideration of the connection ductility.

The example of a fish belly beam gives a low, conservative estimation, since the moment at the support is limited due to the conical cross section. The result of a parallel girder would increase since the possible bearing resistance is higher and therefore the moment at the support due to the connection. However, a fish belly girder was chosen, since this is a widely used beam for such an application.

Table A.4: Summary of the process steps

Process step	Note
<p>1.) <u>Determination of the moment load capacity</u></p> <ul style="list-style-type: none"> • Determination of the bearing resistance of the net cross section • Determination maximum bending moment (net cross-section) at the joint (comp. Sec. A.3.2) • Determination of the inner lever arm (comp. Sec. 6.2). • Specification of a reliability index β • Determination of the maximum permitted bending moment of the joint considering the k_{cs} value • Verification of the tension and compression component considering the inner lever arm 	 <p>Center of the dowel arrangement → third-point of the compression zone</p> $k_{cs} = 1 - \frac{\beta(k_{cs})}{7,65}$
<p>2.) <u>Determination of the moment rotation behavior of the plastic hinge</u></p> <ul style="list-style-type: none"> • Determination of the initial stiffness • Determination of the load bearing resistance of the dowel arrangement • Determination of the simplified load-deflection behavior (comp. Sec. 6.5.2) • Determination of the simplified moment-rotation behavior (comp. Sec. 6.5.3). 	<p>K_{ser} [109] and ρ_k [103]</p> <p>failure mode (g) or (h)</p> <p>lever arm see 1.) $K_{Comp} = \infty$</p>

Process step	Note
<ul style="list-style-type: none"> Determination of $k_{\phi,e}$ to determine the decrease of the inner lever arm 	$k_{\phi,e} = \frac{e - \Delta_{\text{lever arm}}}{e}$
<ul style="list-style-type: none"> Application of $k_{\phi,M}$ to consider the increase of the bending moment (comp. Sec. 6.2.4) 	$k_{\phi,M} = 1.08$
3.) <u>Verification of the sufficient joint stiffness</u>	
<ul style="list-style-type: none"> The minimum stiffness is given on a two-span beam as: 	$K_{ser,min} = \frac{3 \cdot EI \cdot M_{joint}}{l \cdot (2 \cdot M_{cs} - M_{joint})}$
4.) <u>Verification of the sufficient rotation capacity</u>	
<ul style="list-style-type: none"> Application of k_{mat} to consider the scattering of the material properties (comp. Sec. 7.3.2) 	$k_{mat} = 1,10$
5.) <u>Verification of the internal action on the structural system</u>	
<ul style="list-style-type: none"> The structural elements need to be checked based on the stresses due to the nonlinear behavior of the joint 	

B Load-deflection graphs

B.1 Nailed connections

Experiments performed by Blaß [6]

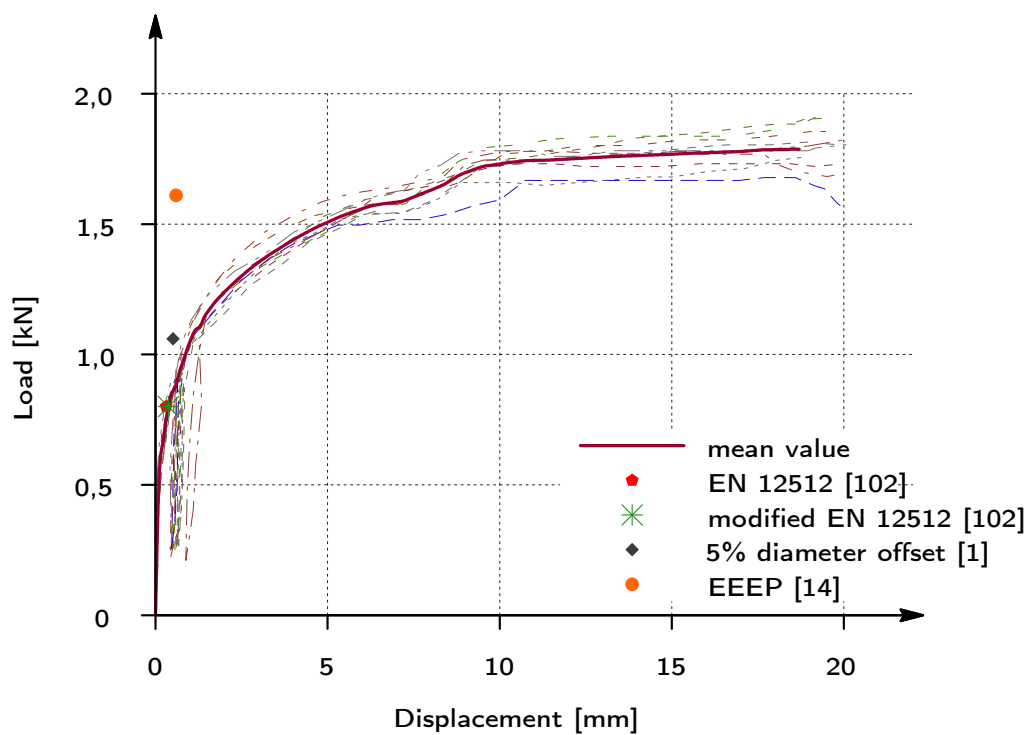


Figure B.1: Variation in grain direction, experiments 1A19A

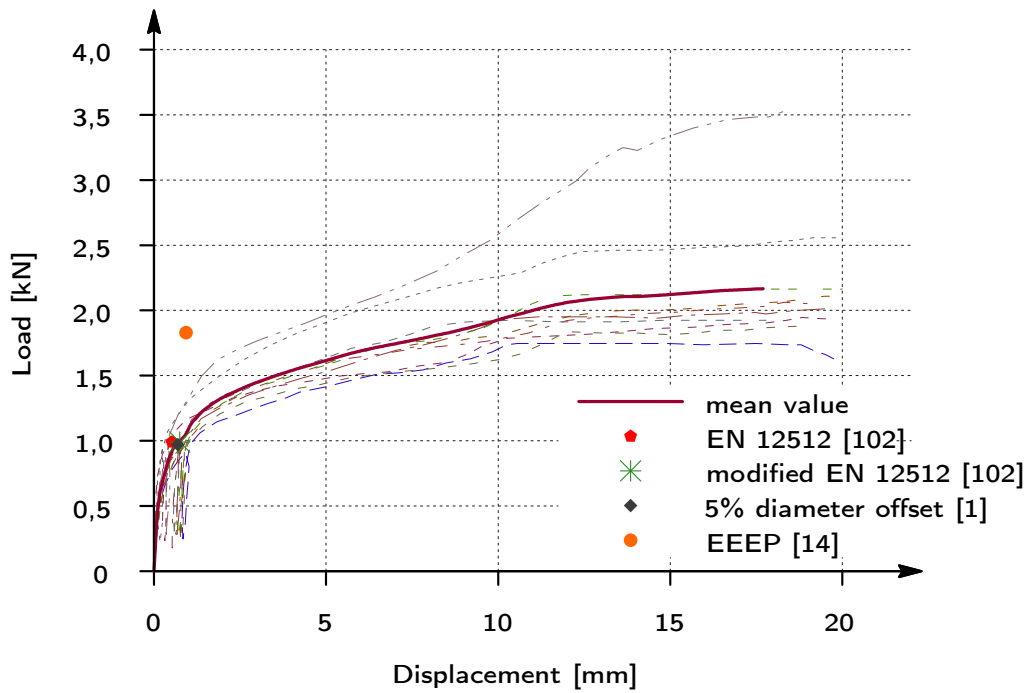


Figure B.2: Variation in grain direction, experiments 23C3A

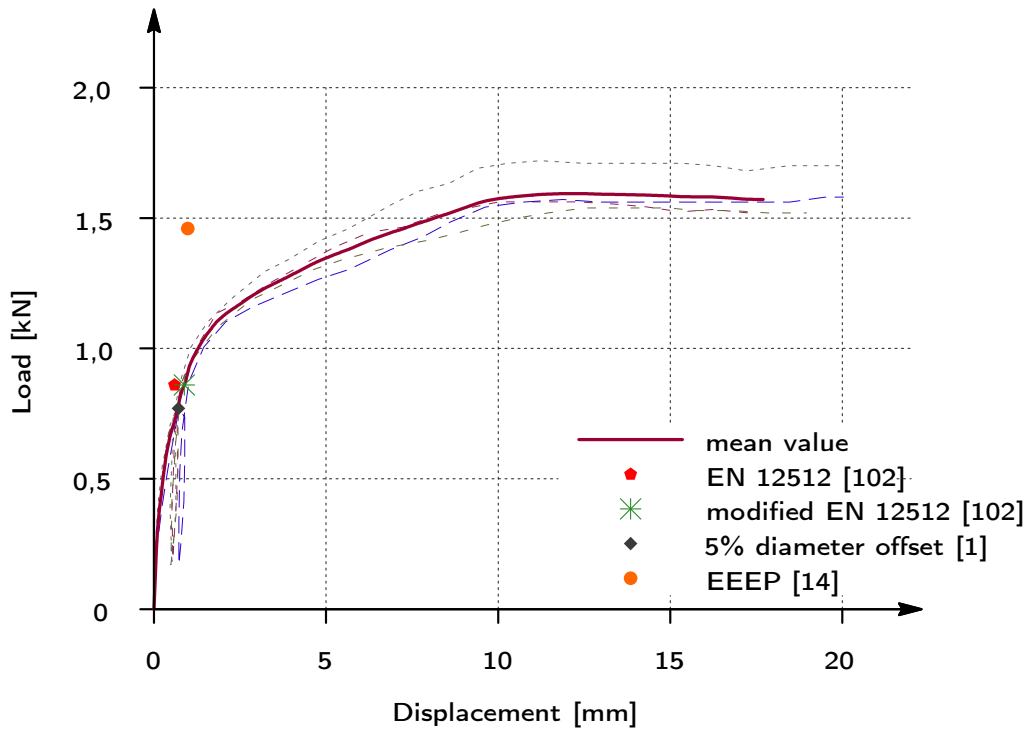


Figure B.3: Variation parallel to grain direction, experiments 30A-30D

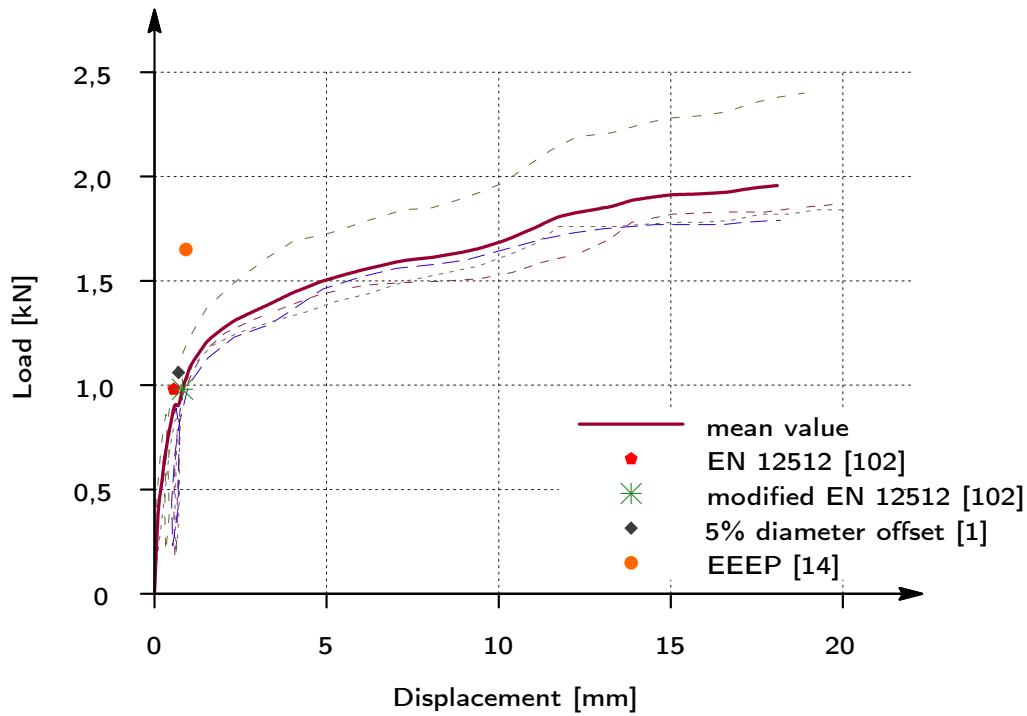


Figure B.4: Variation parallel to grain direction, experiments 40-44

B.2 Timber-steel-timber doweled connections

B.2.1 Experiments on BSB-connections performed by Mischler [88]

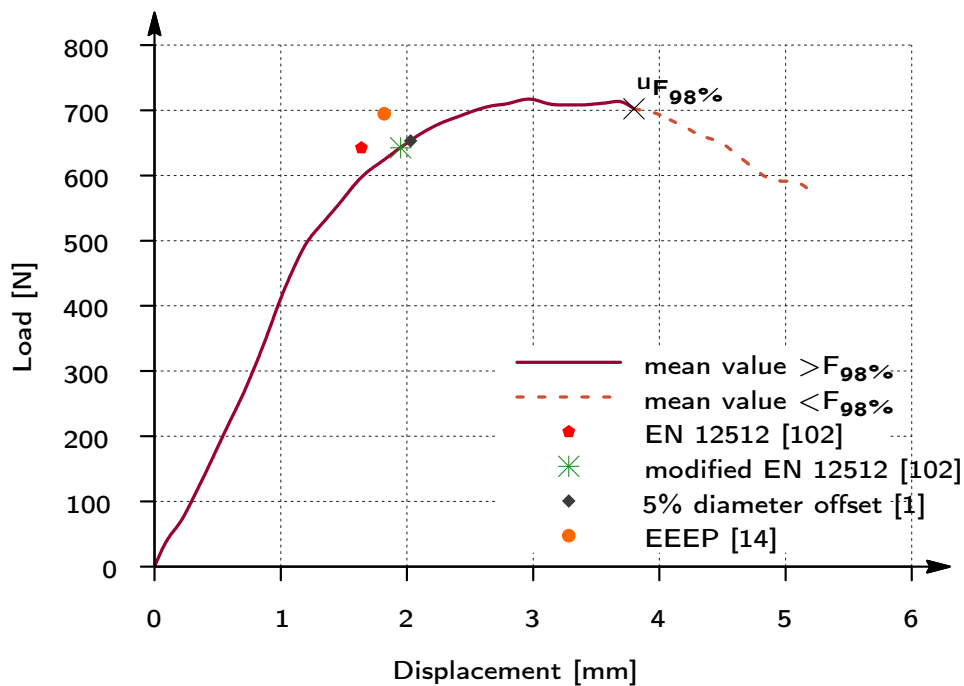


Figure B.5: Investigations on the timber thickness, $t_2=67\text{mm}$

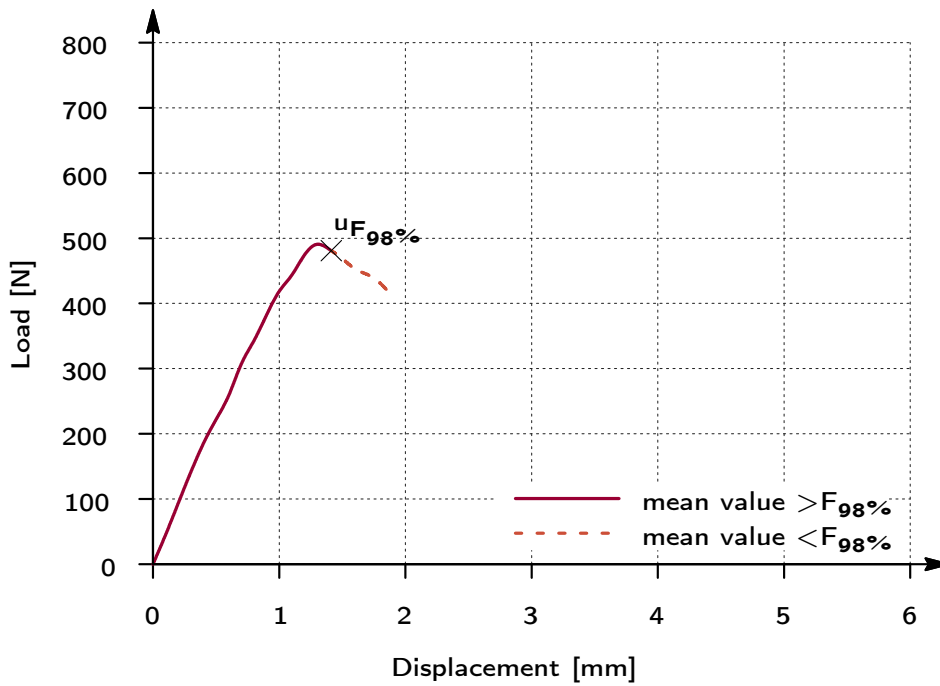


Figure B.6: Investigations on the timber thickness, $t_2=50\text{mm}$

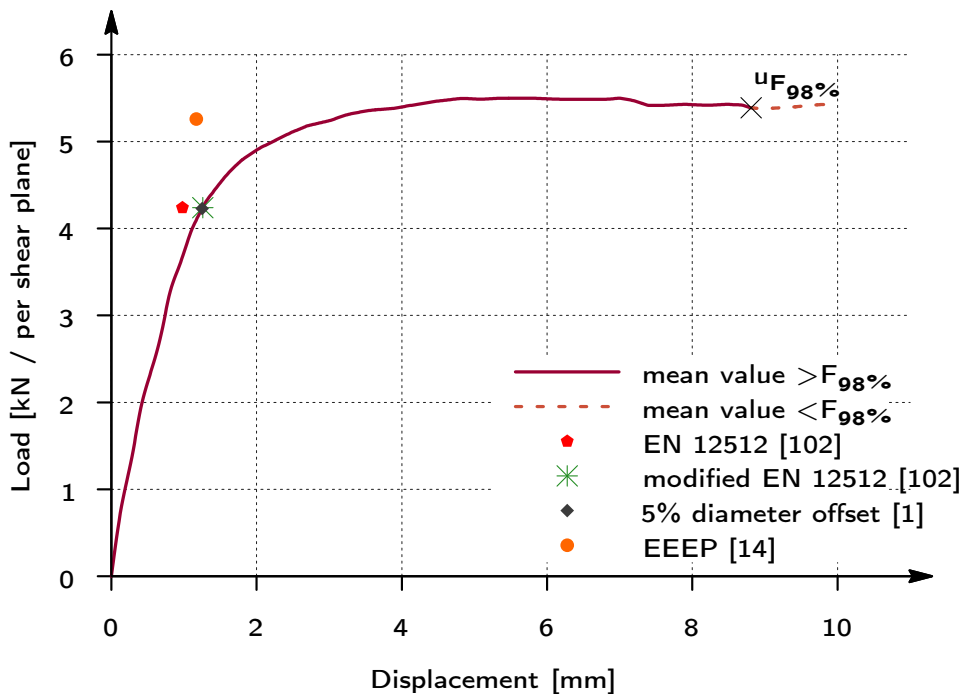


Figure B.7: One bolt in grain direction

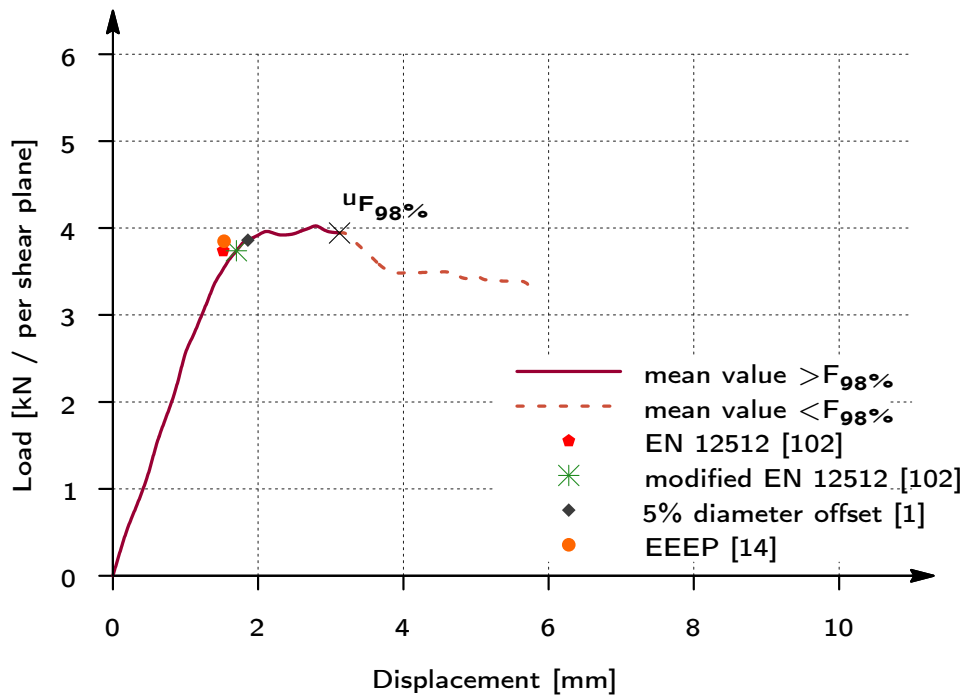


Figure B.8: Three bolts in grain direction

B.2.2 Experiments on self-drilling dowels performed by Mischler [56]

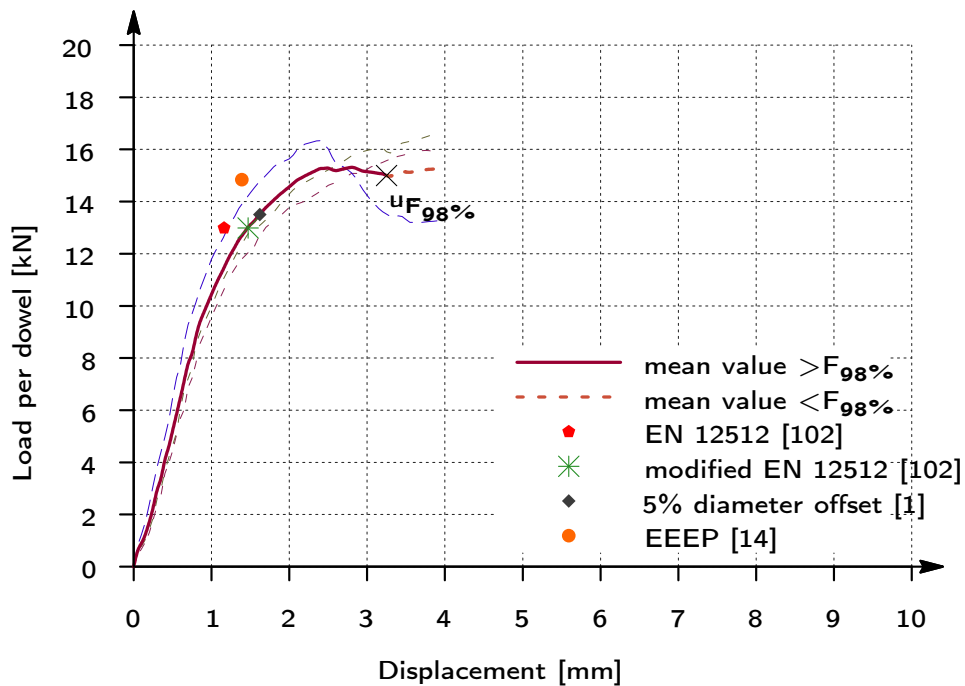


Figure B.9: Load-slip behavior of experiment 3E

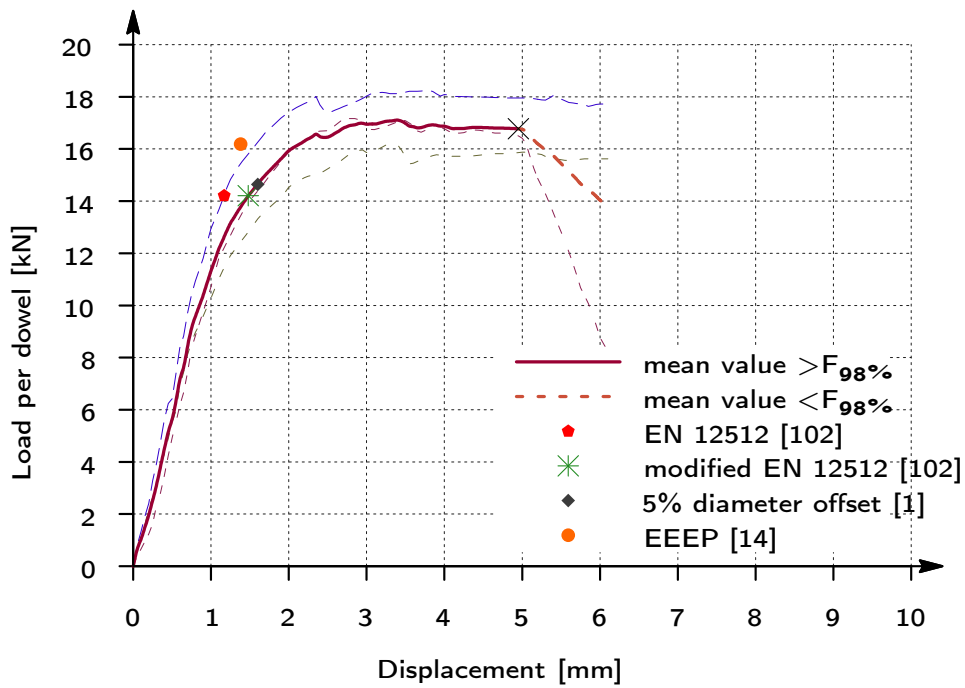


Figure B.10: Load-slip behavior of experiment 3F

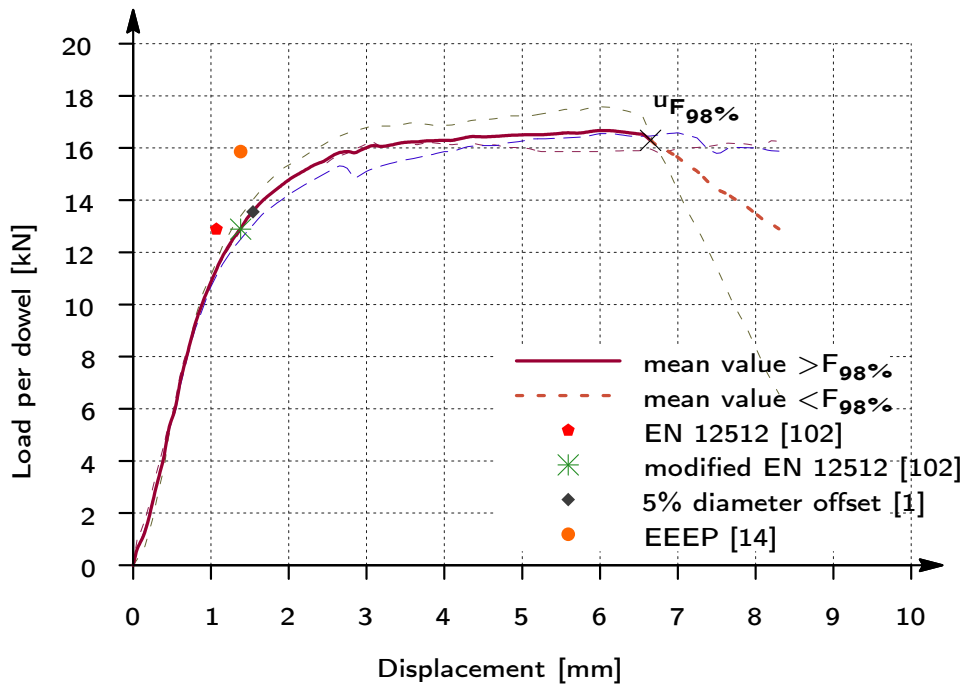


Figure B.11: Load-slip behavior of experiment 3G

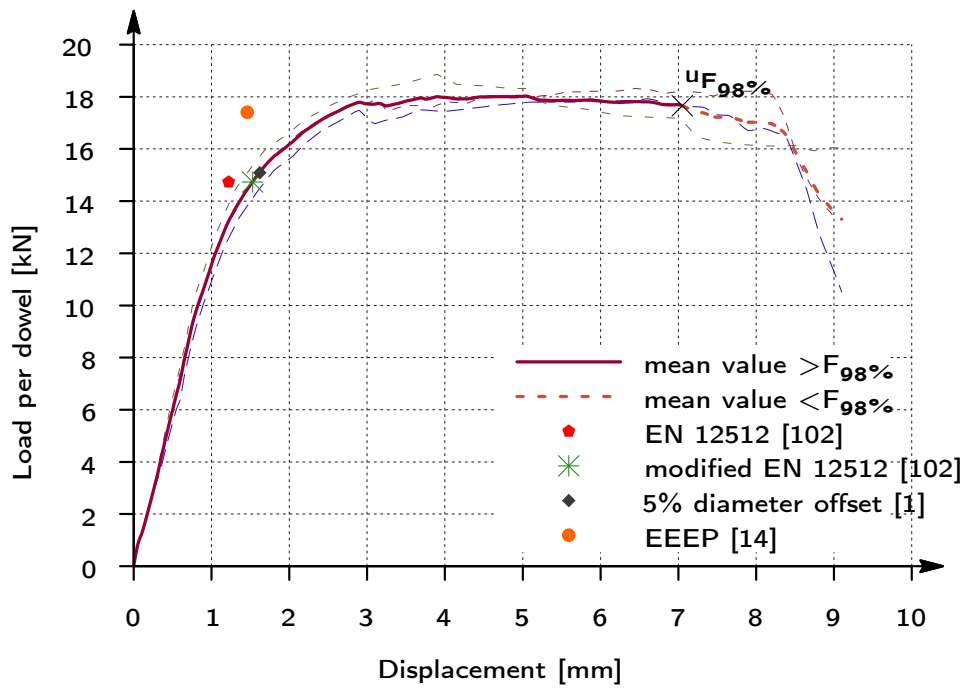


Figure B.12: Load-slip behavior of experiment 3H

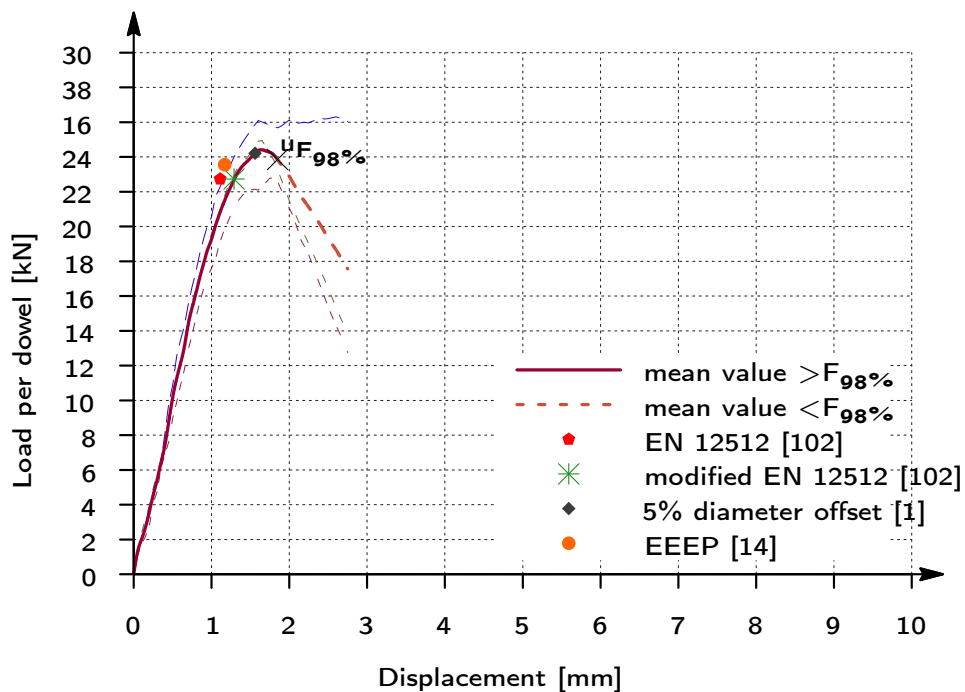


Figure B.13: Load-slip behavior of experiment 4F

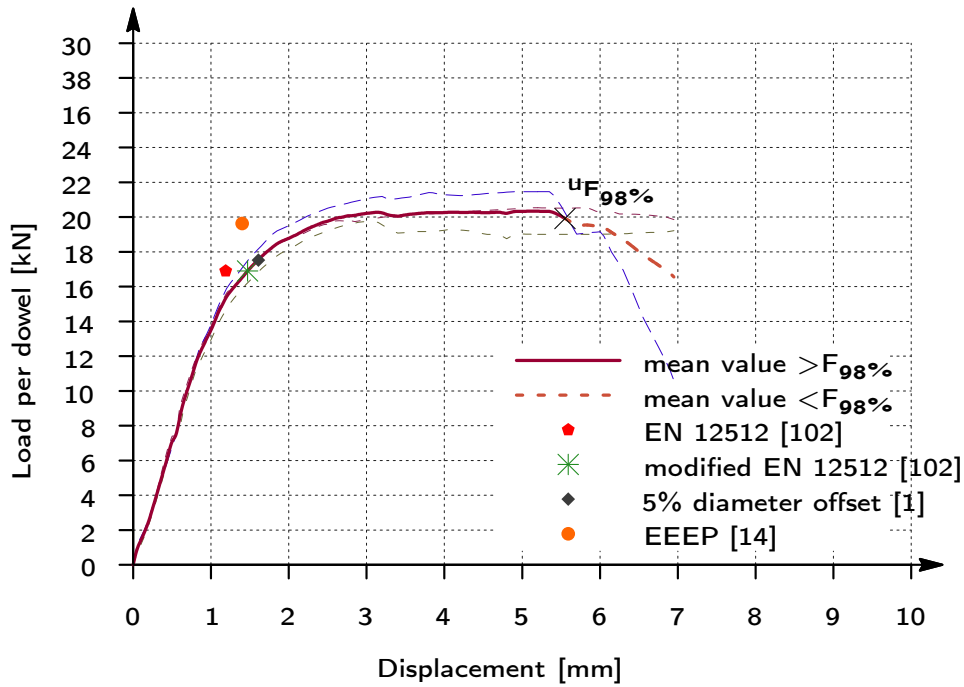


Figure B.14: Load-slip behavior of experiment 4G

B.2.3 Experiments on ordinary dowels performed by Sandhaas [90]

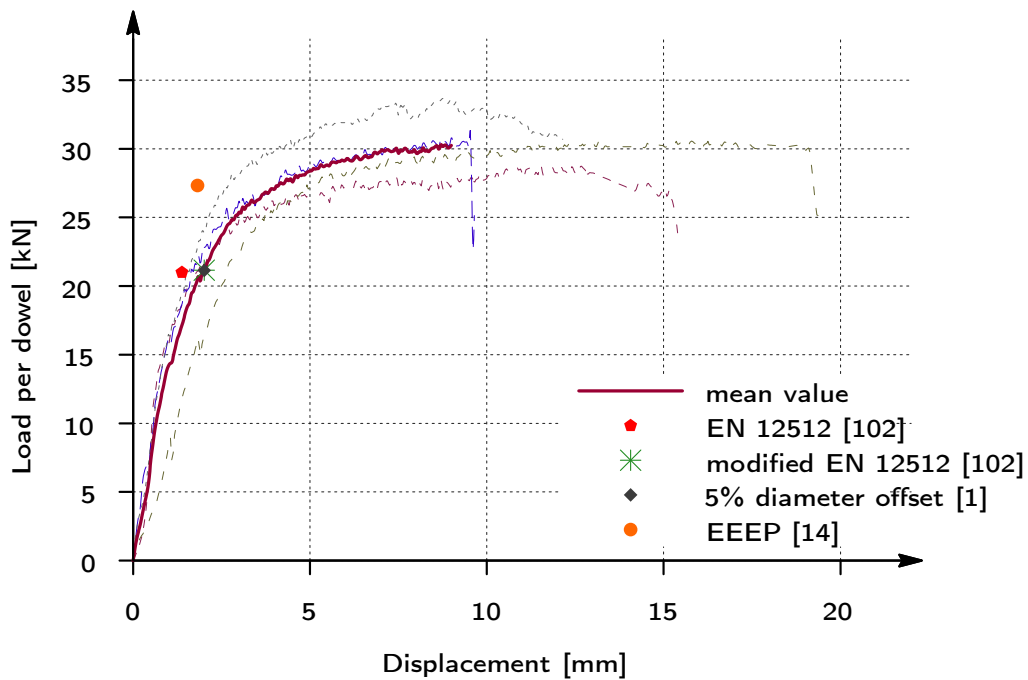


Figure B.15: Load-slip behavior of experiment S12C_1

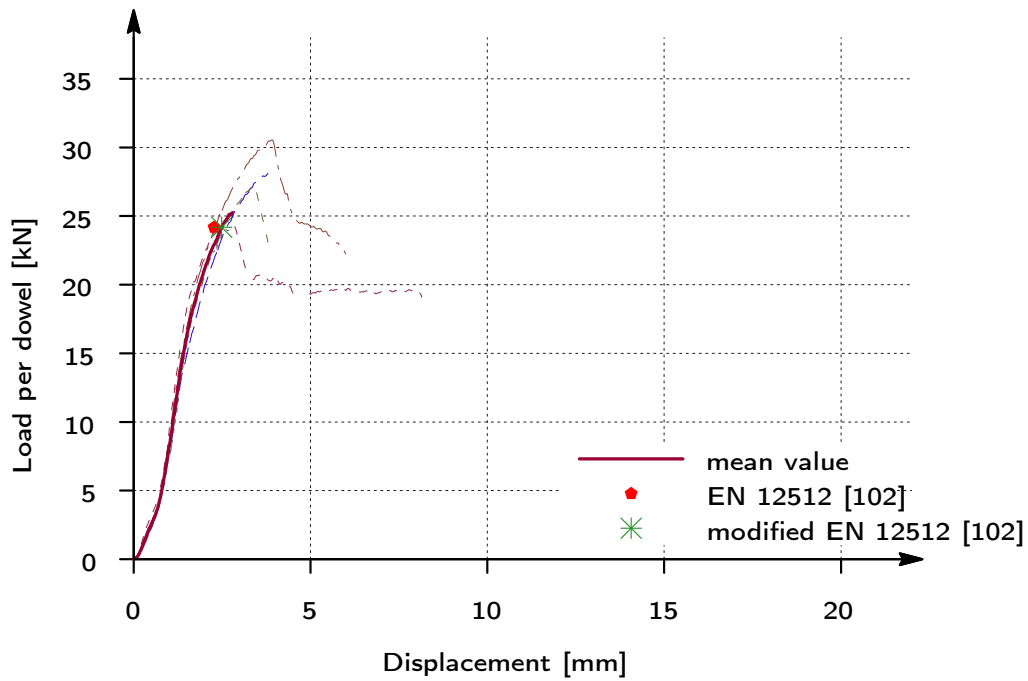


Figure B.16: Load-slip behavior of experiment S12C_5

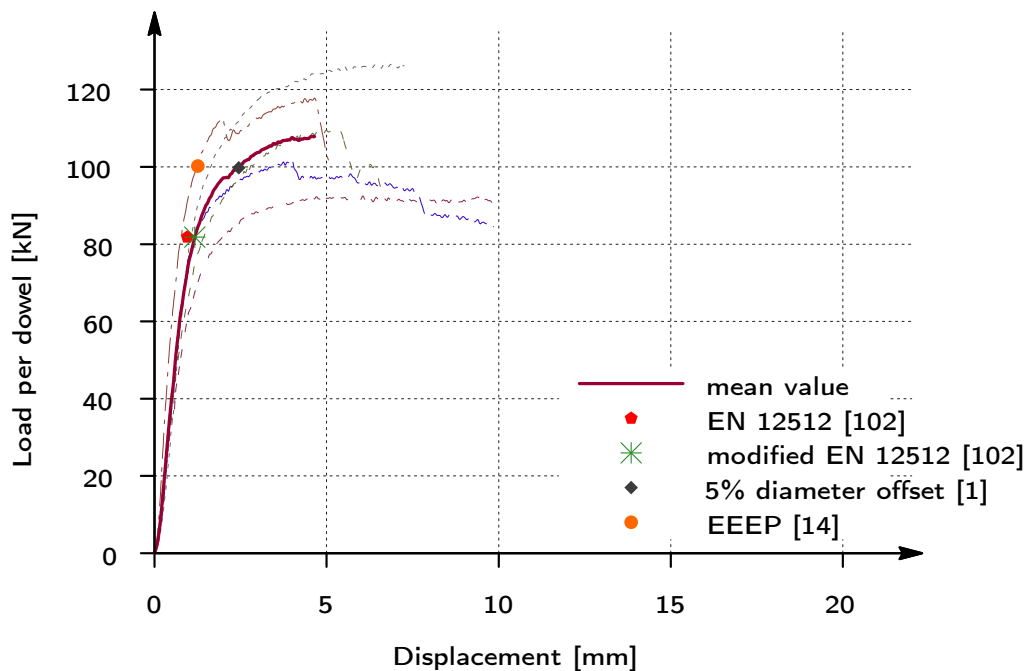


Figure B.17: Load-slip behavior of experiment S24C_1

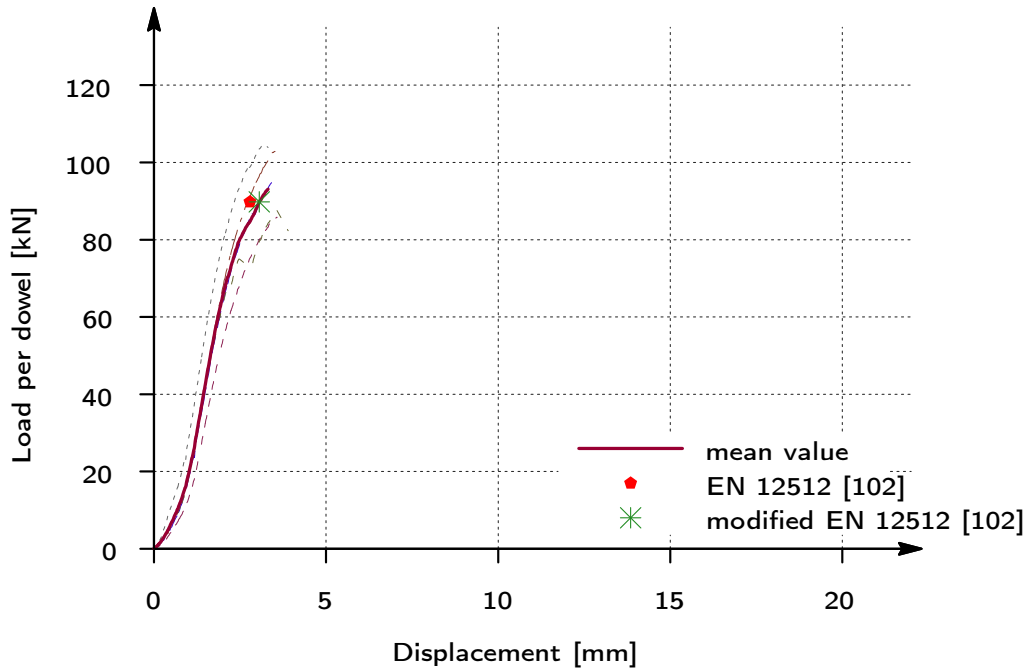


Figure B.18: Load-slip behavior of experiment S24C_5

B.3 Timber-timber doweled connections

Experiments performed by Jorissen [84]

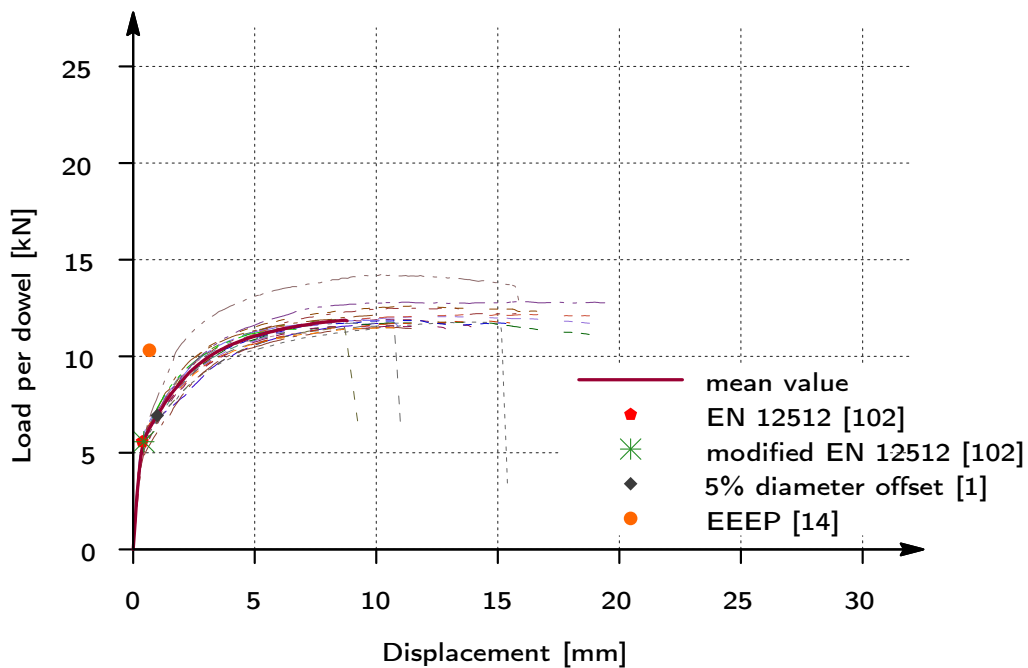


Figure B.19: Load-slip behavior of experiment 31107

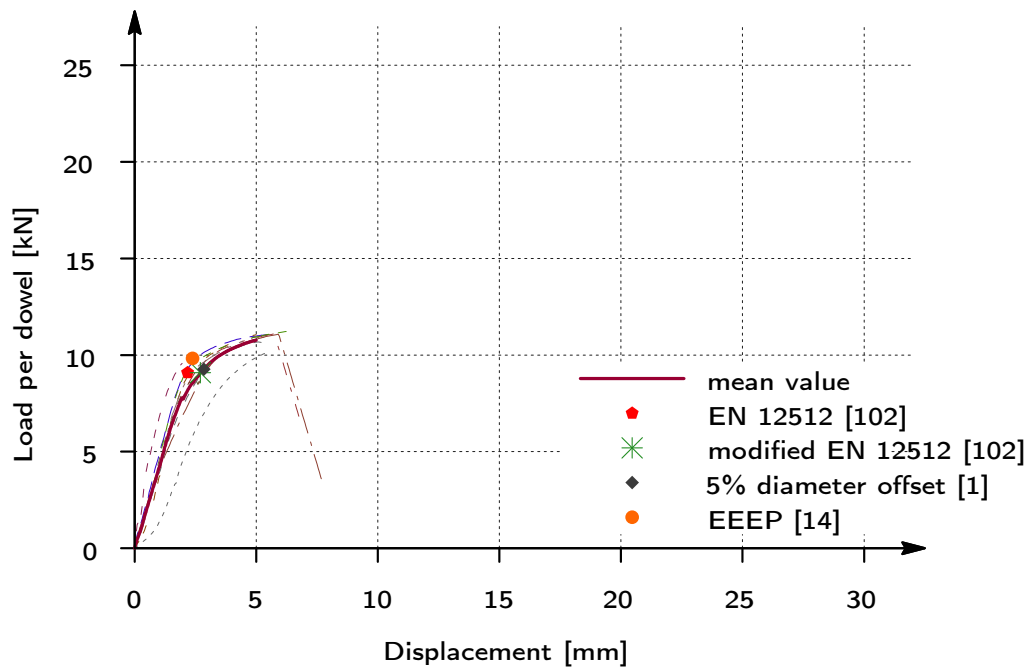


Figure B.20: Load-slip behavior of experiment 39127

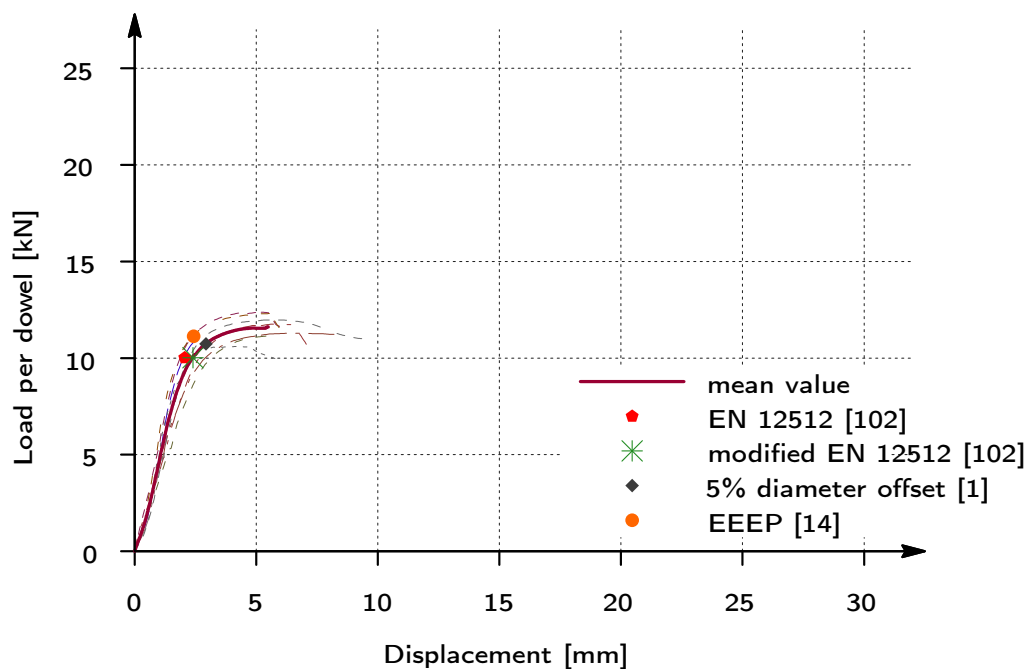


Figure B.21: Load-slip behavior of experiment 39157

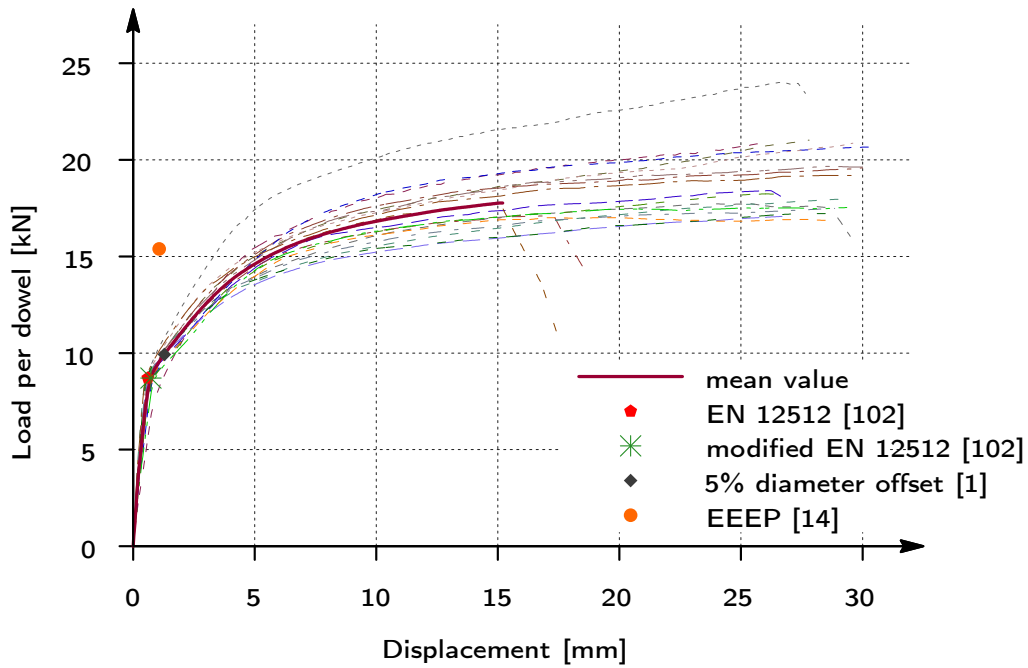


Figure B.22: Load-slip behavior of experiment 81107

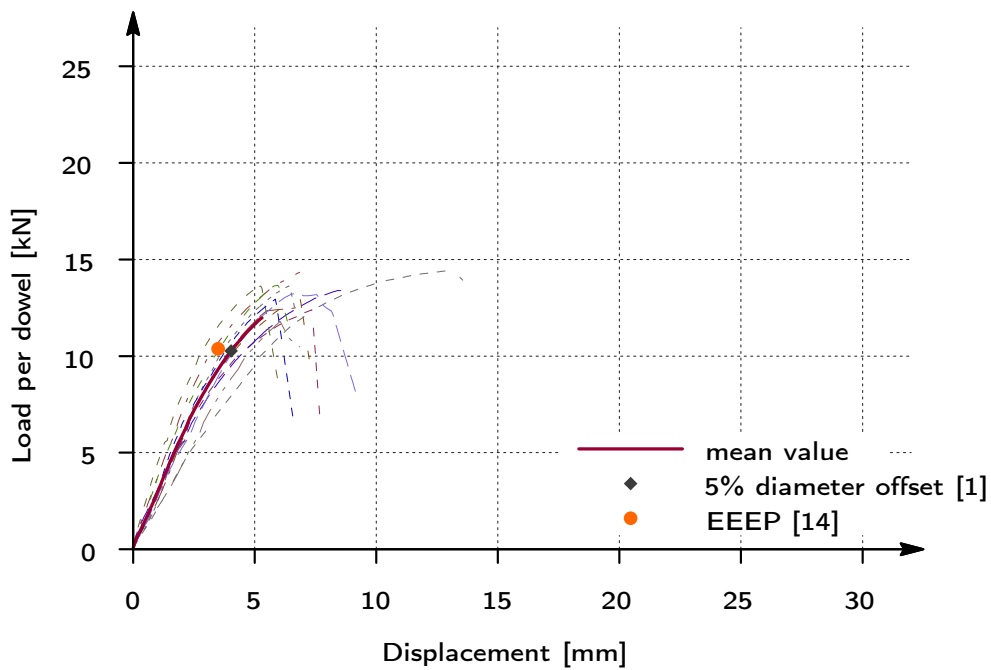


Figure B.23: Load-slip behavior of experiment 89127

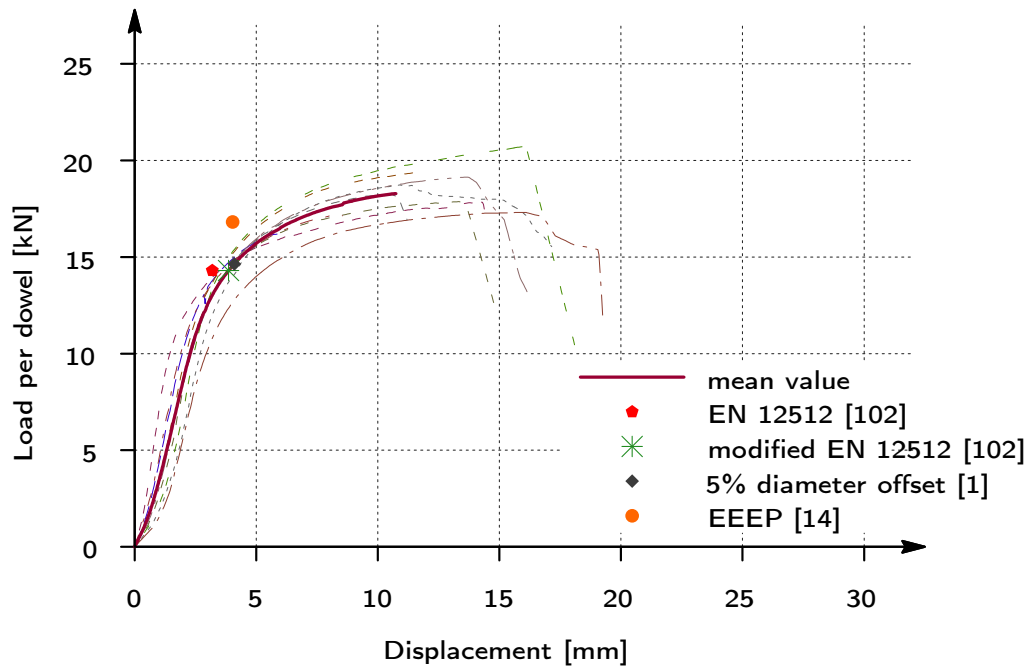


Figure B.24: Load-slip behavior of experiment 89157

B.4 Reinforced timber-steel-timber connections

Experiments performed by Bejtka [82]

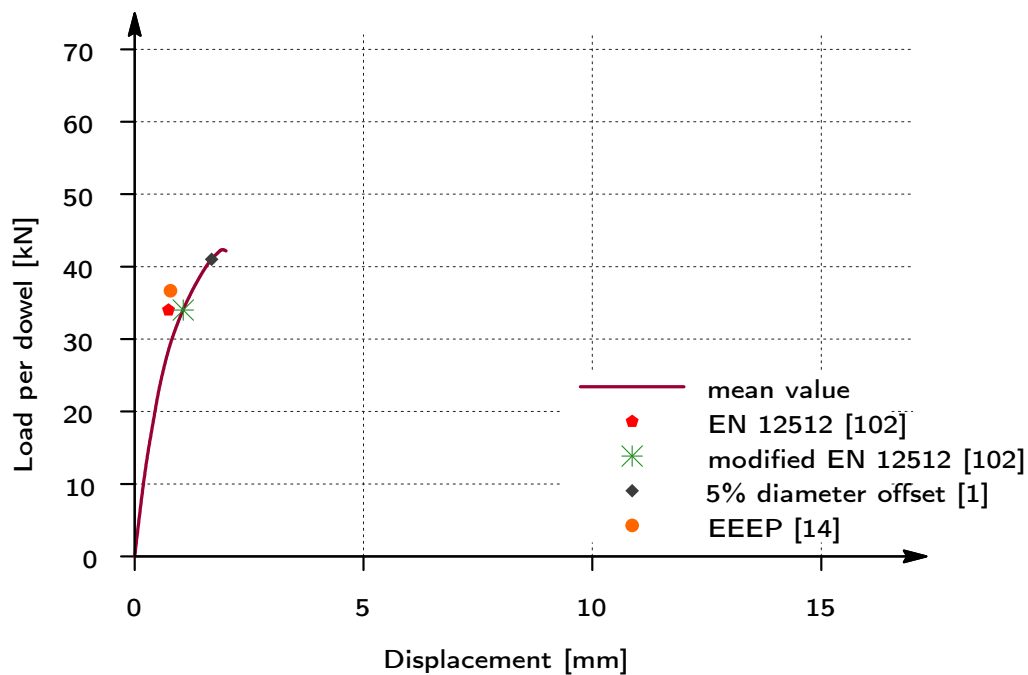


Figure B.25: Load-slip behavior of experiment V30

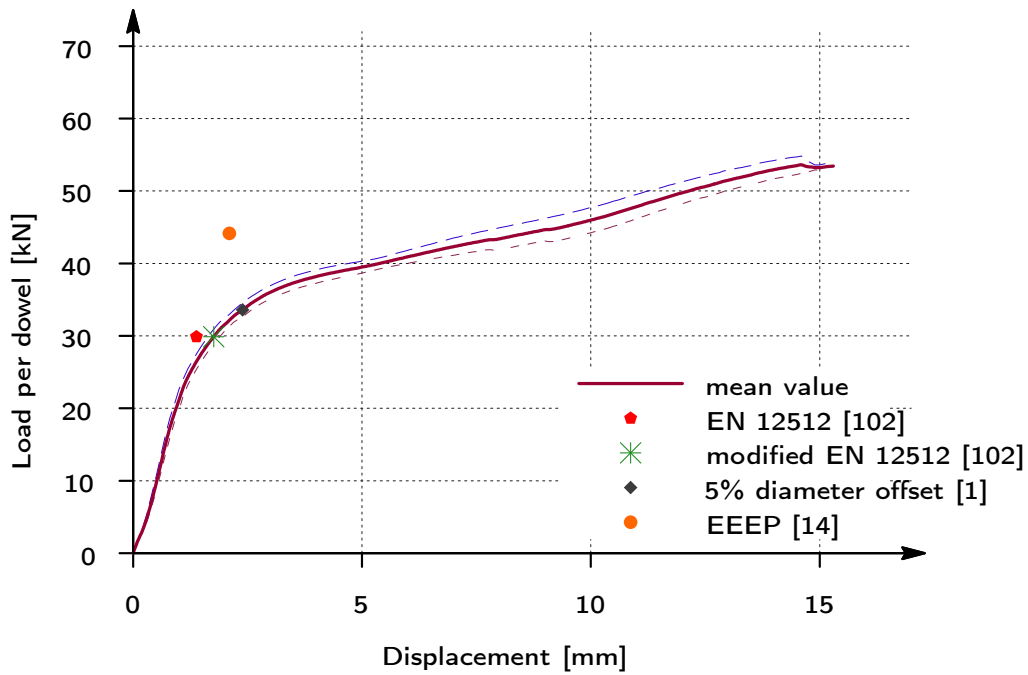


Figure B.26: Load-slip behavior of experiment V36 & V37

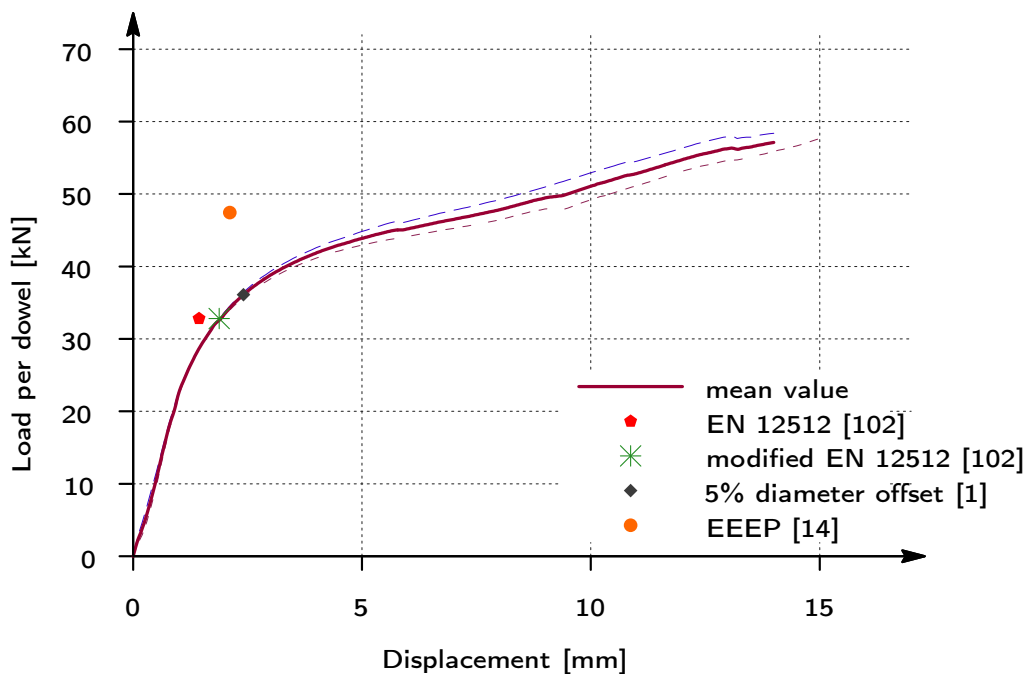


Figure B.27: Load-slip behavior of experiment V38 & V39

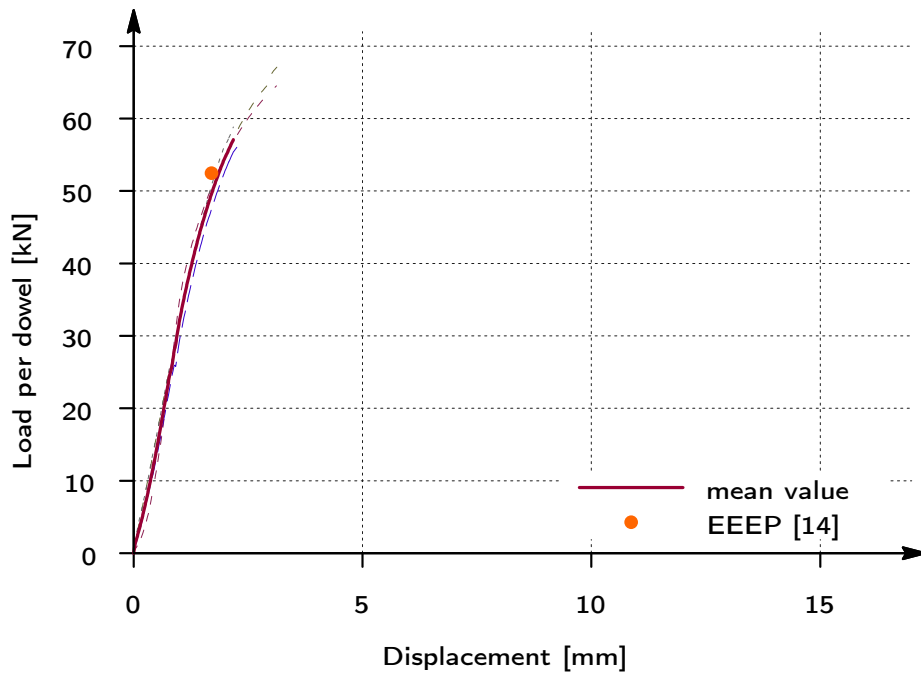


Figure B.28: Load-slip behavior of experiment M1 - M4

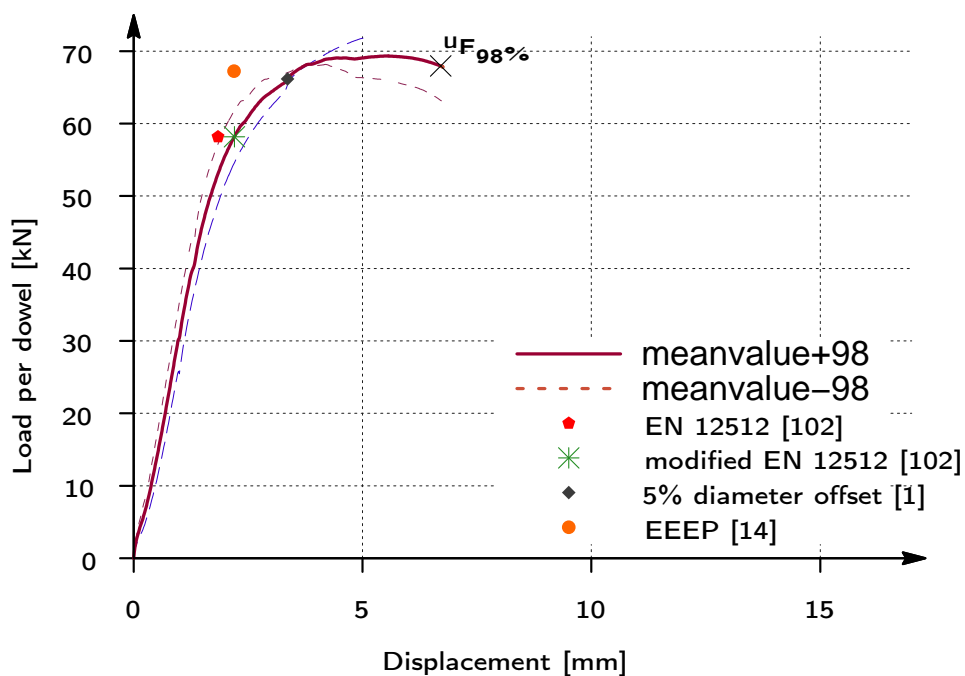


Figure B.29: Load-slip behavior of experiment M5 & M6

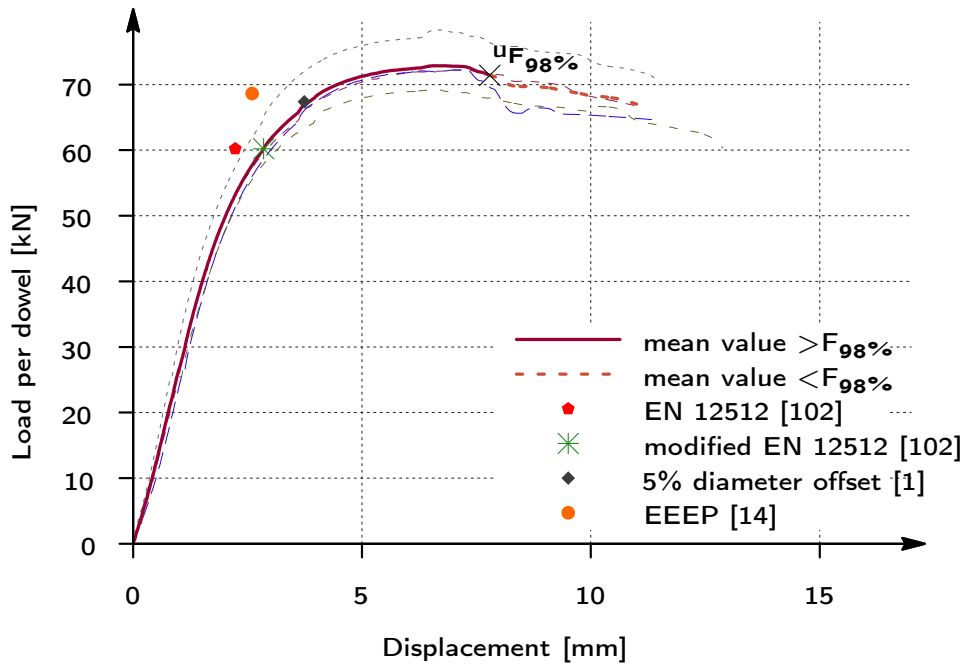


Figure B.30: Load-slip behavior of experiment M7 - M10

B.5 Miscellaneous connections

B.5.1 Experiments on tube connections performed by Leijten [87]

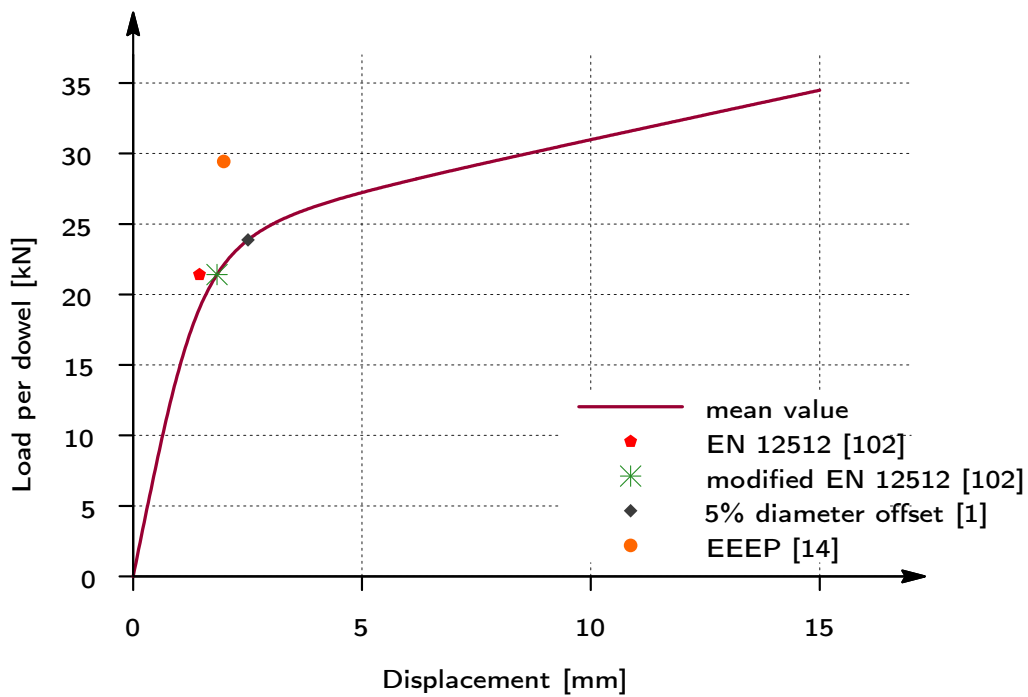


Figure B.31: Load-slip behavior of 18 mm tube connections

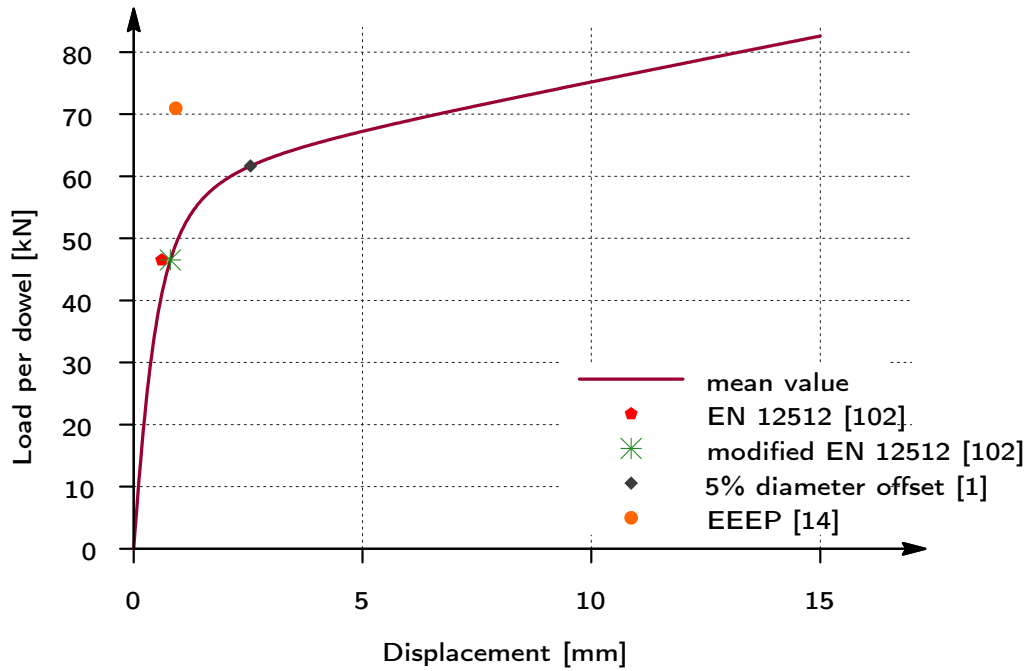


Figure B.32: Load-slip behavior of 35 mm tube connections

B.5.2 Experiments on split rings performed by Blaß et al. [11]

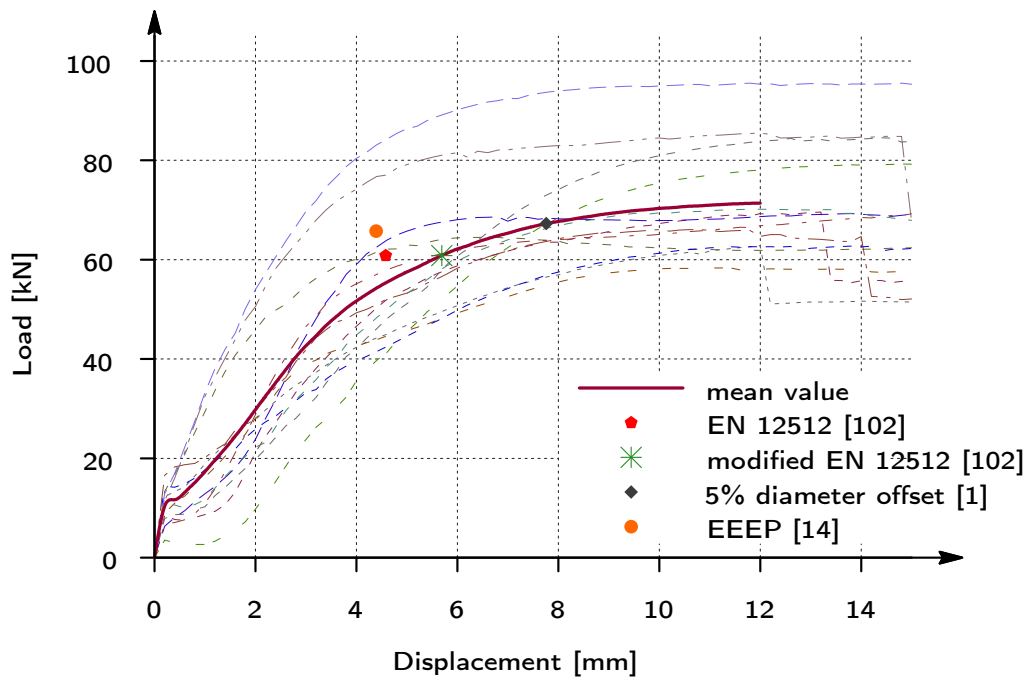


Figure B.33: Load-slip behavior of experiment A65N

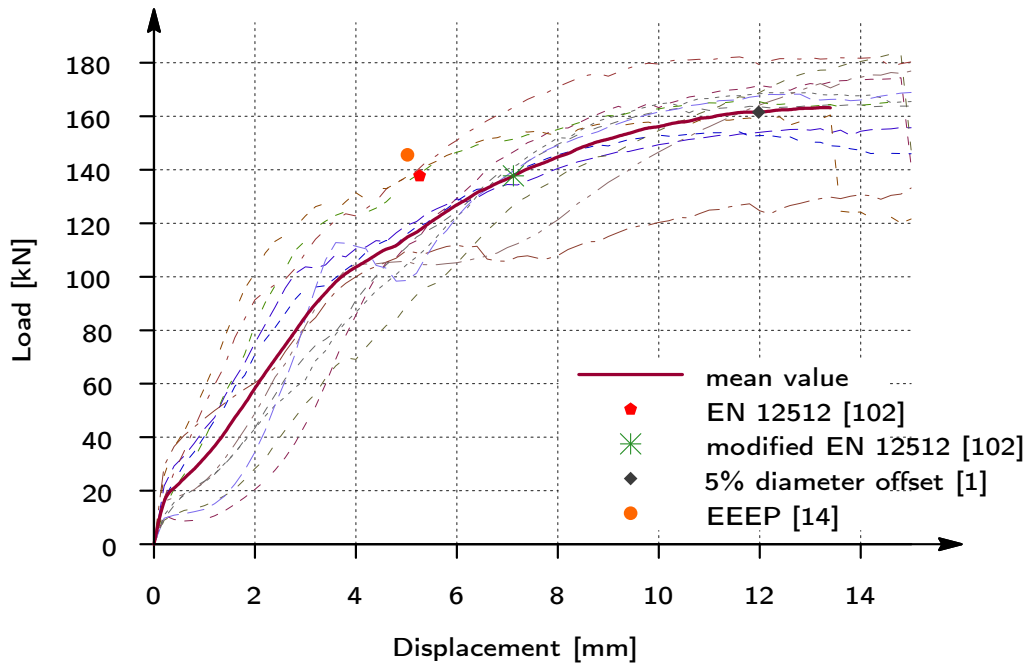


Figure B.34: Load-slip behavior of experiment A128N

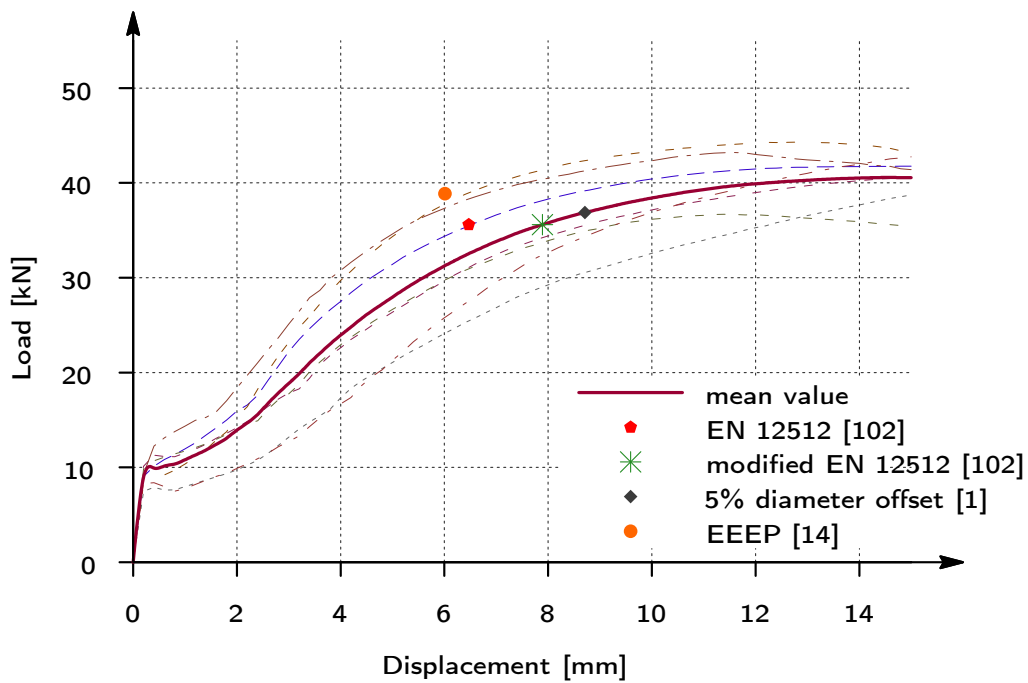


Figure B.35: Load-slip behavior of experiment D50N

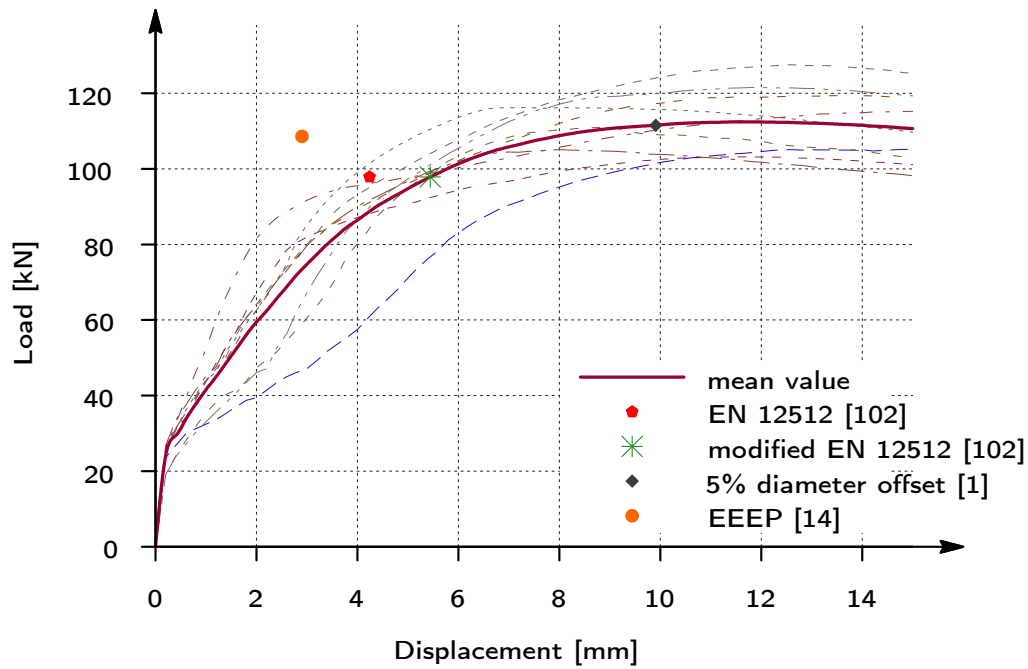


Figure B.36: Load-slip behavior of experiment D115N

B.5.3 Experiments on split rings performed by Reyer et al. [64]

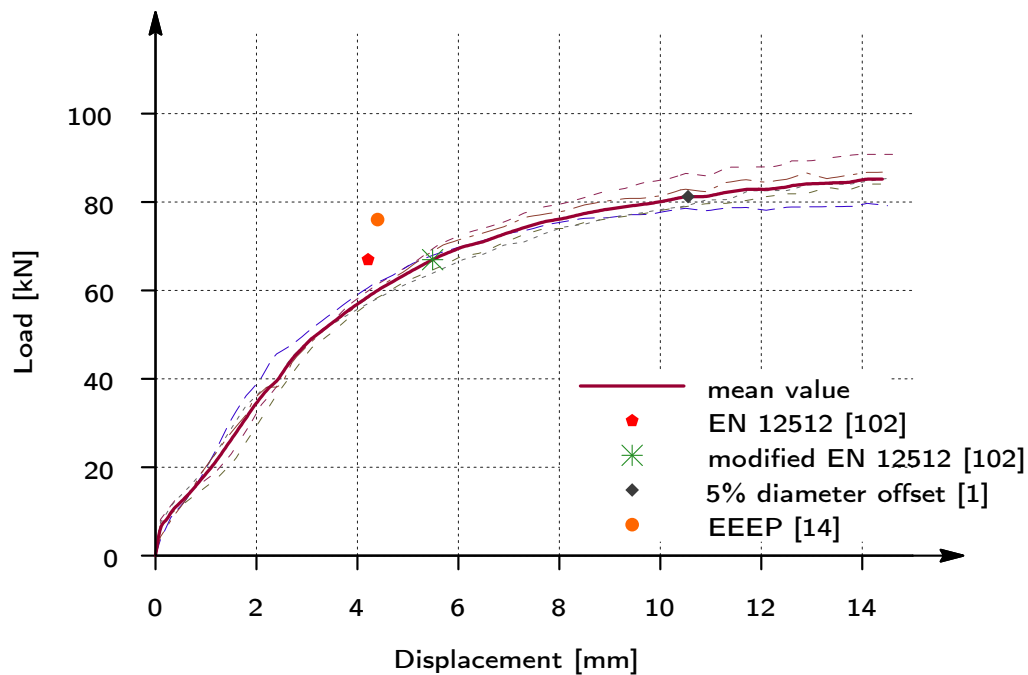


Figure B.37: Load-slip behavior of experiment AC117HH

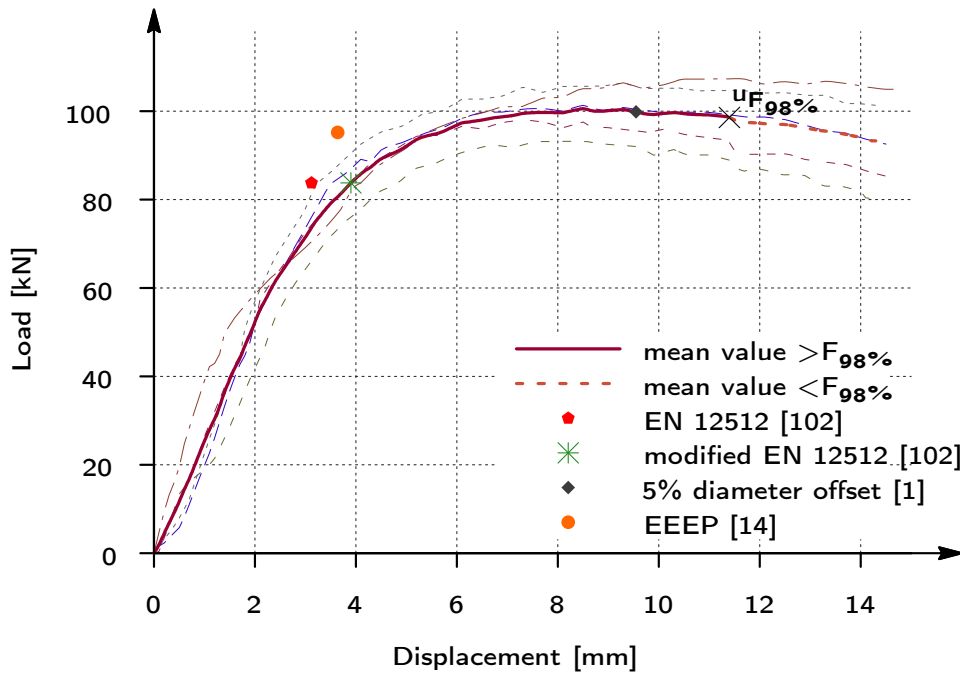


Figure B.38: Load-slip behavior of experiment D115HH

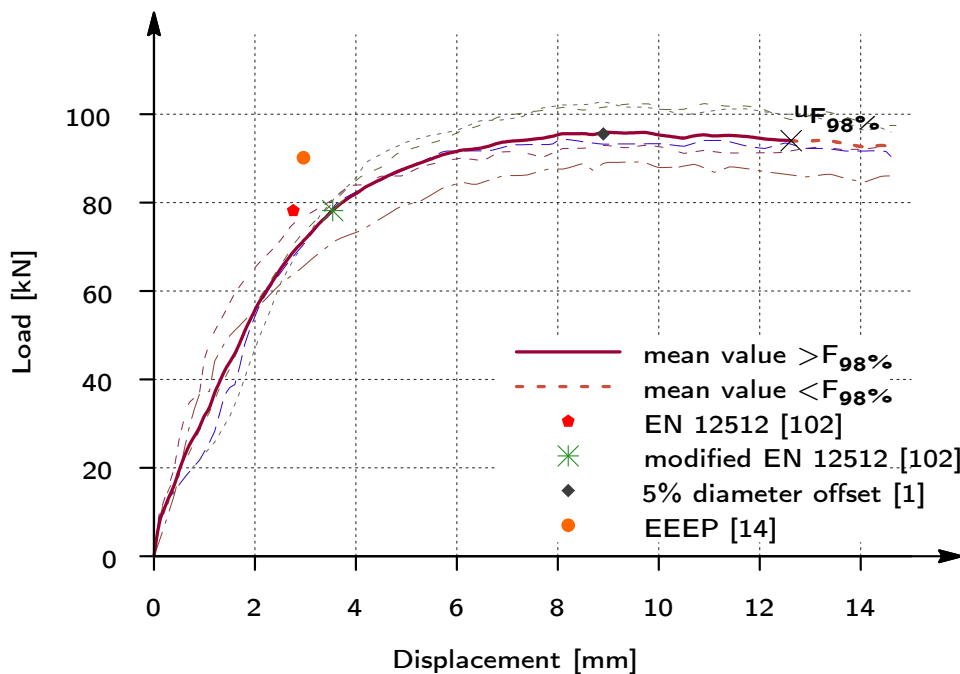


Figure B.39: Load-slip behavior of experiment C117SH

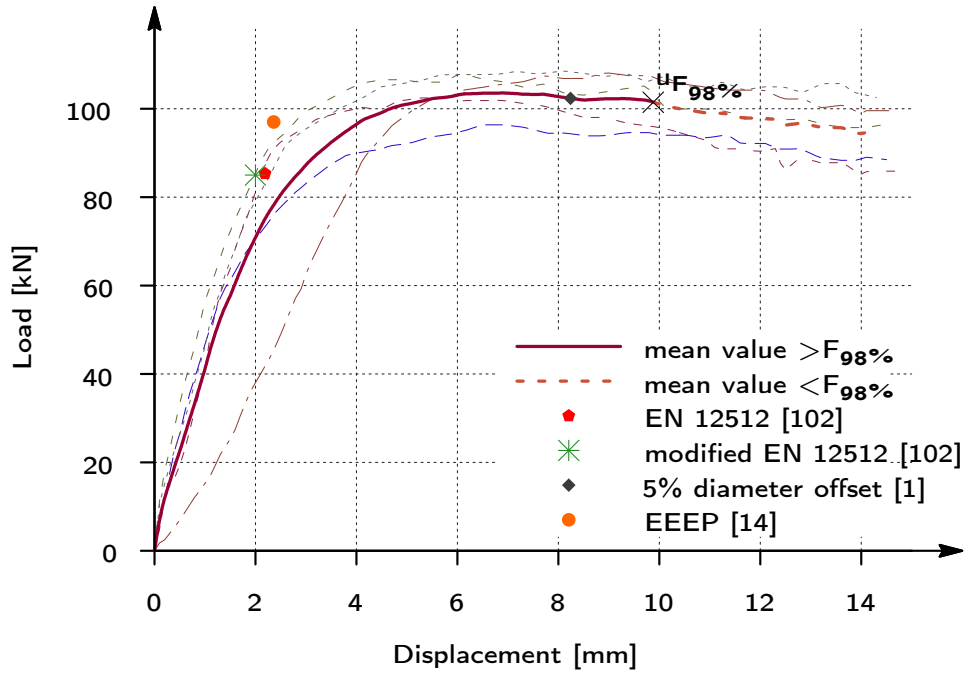


Figure B.40: Load-slip behavior of experiment D115SH

B.5.4 Experiments on nail plates performed by Kevarinmaki [84]

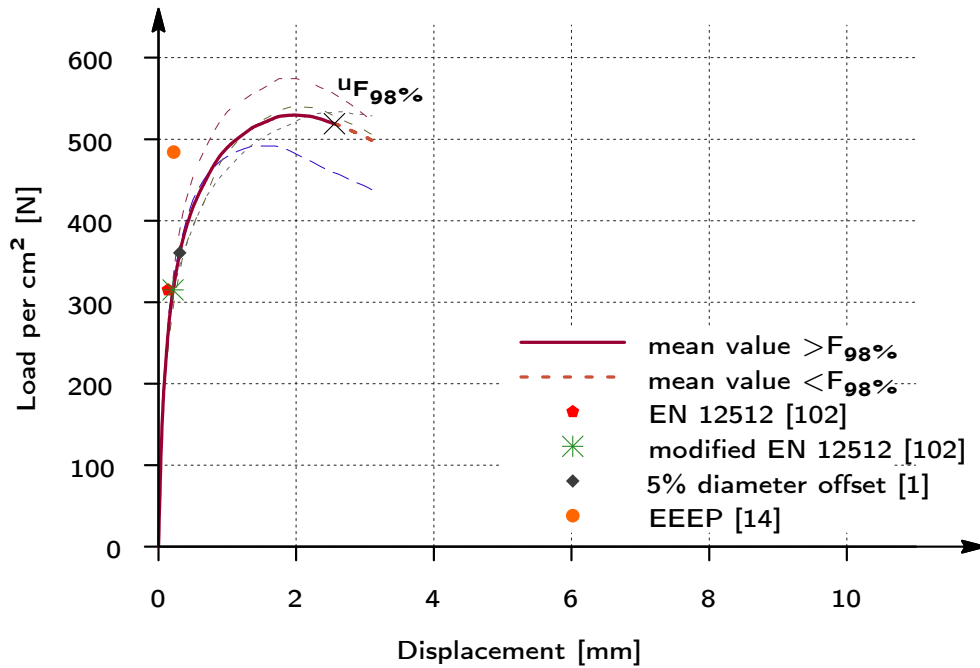


Figure B.41: Load-slip behavior of experiment with nail plate type Fix

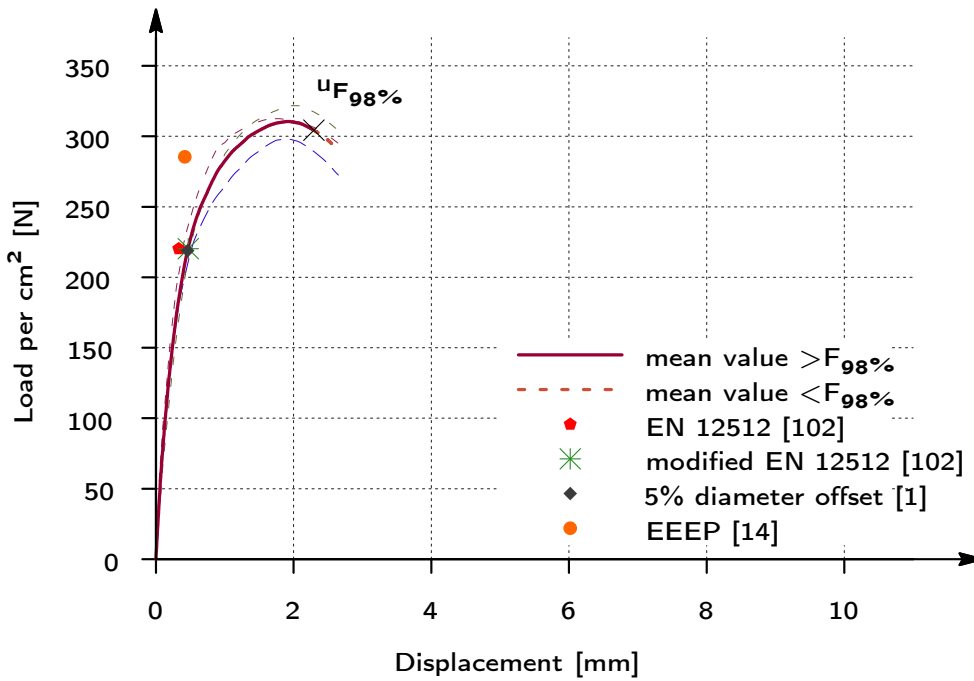


Figure B.42: Load-slip behavior of experiment with nail plate type TOP 91

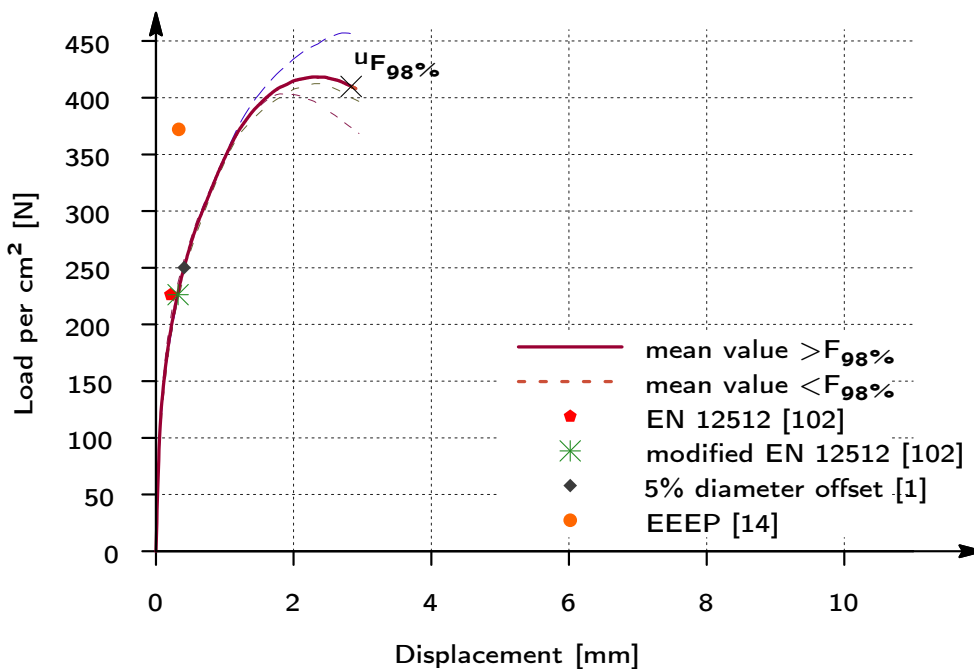


Figure B.43: Load-slip behavior of experiment with nail plate type W

C Material properties

C.1 Timber properties

C.1.1 Overview of all lamellae

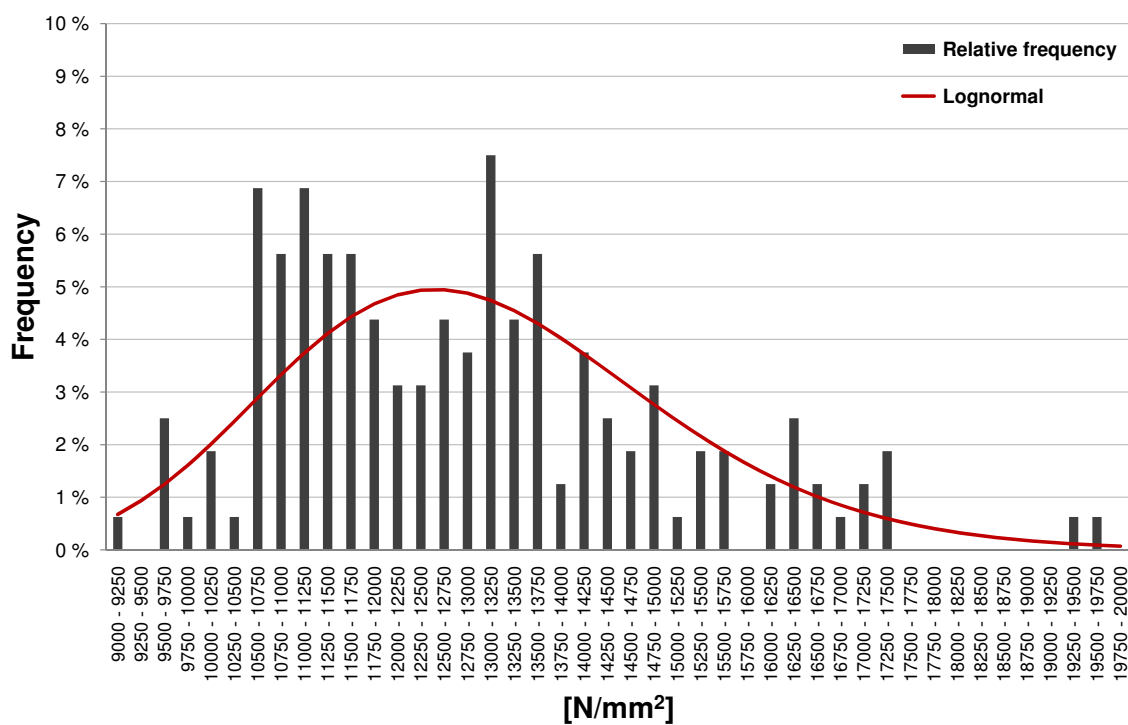


Figure C.1: Distribution of the modulus of elasticity of all lamellae

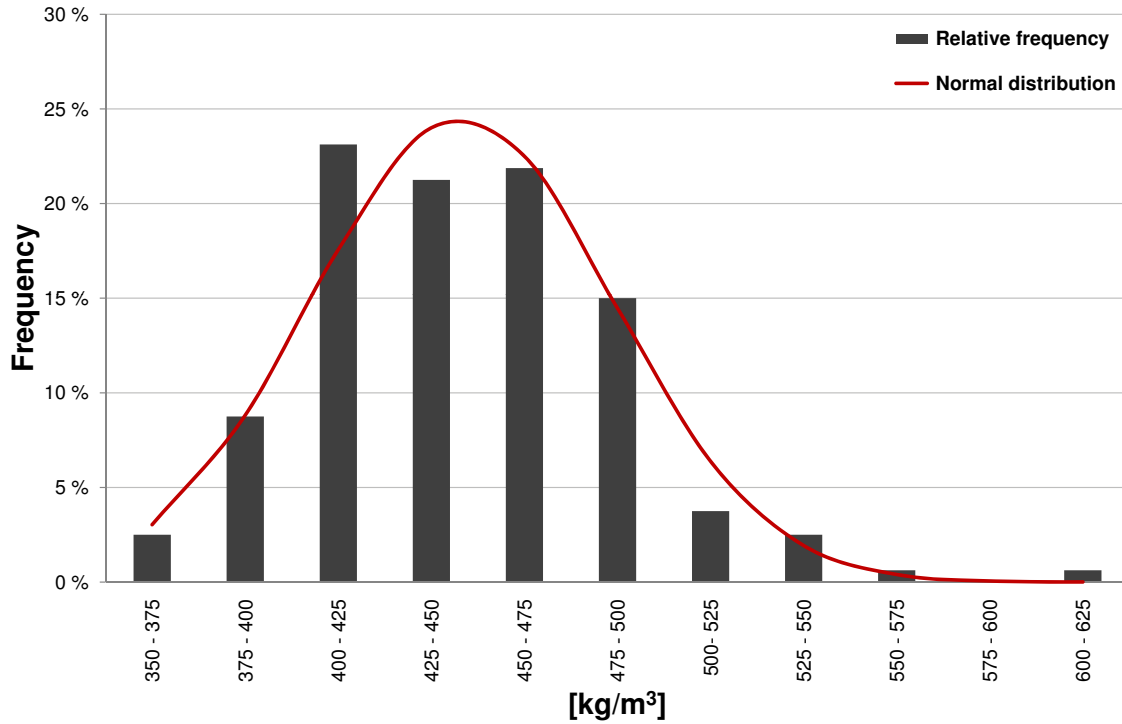


Figure C.2: Distribution of the density of all lamellae

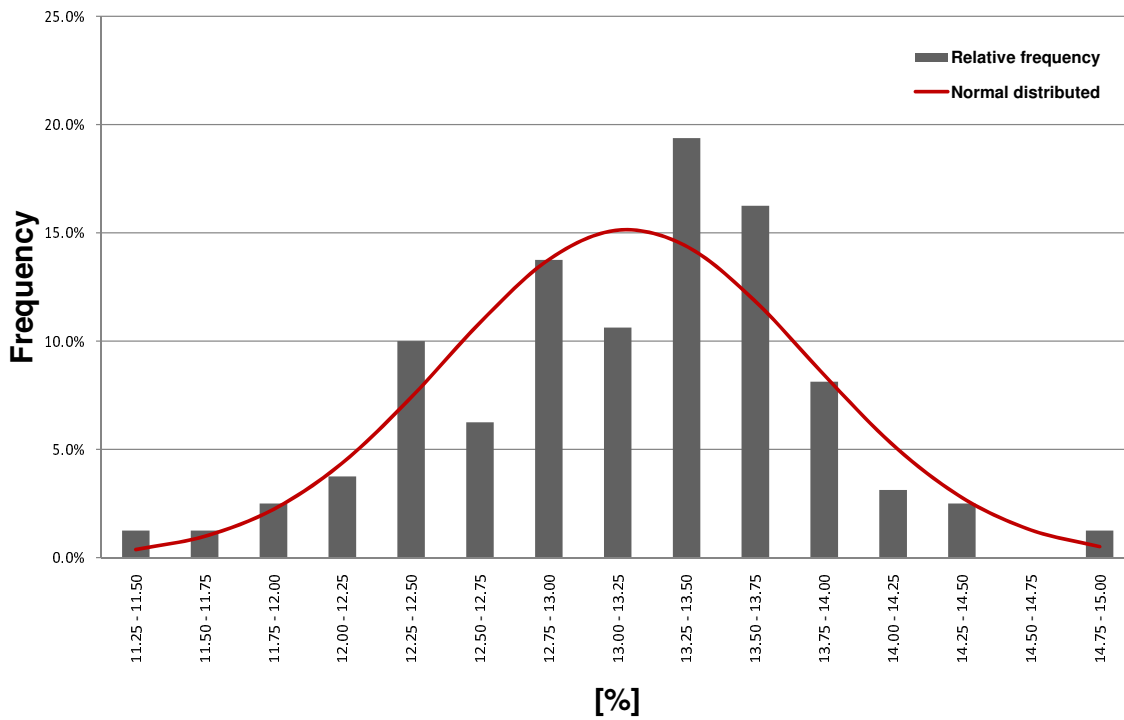


Figure C.3: Distribution of the moisture content of all lamellae

C.1.2 Density of the tension specimens

The density of the timber specimens was determined based on the lamellae, which were laminated within the section of the beam.

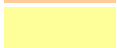
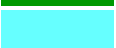
Ø7 mm		Ø12 mm		Ø16 mm	
Specimen	Density [kg/m ³]	Specimen	Density [kg/m ³]	Specimen	Density [kg/m ³]
2×3_1	468.9	4×2_1	437.0	3×2_1	421.8
2×3_2	476.0	4×2_2	420.6	3×2_2	437.0
2×3_3	479.2	4×2_3	442.4	3×2_3	449.0
3×2_4	415.2	4×2_4	-	3×2_4	453.0
4×2_1	463.2	3×3_1	458.6		
4×2_2	410.2	3×3_2	443.2		
4×2_3	437.8	3×3_3	448.6		
4×2_4	450.8	3×3_4	439.4		
		5×2_1	431.2		
		5×2_2	431.8		
		5×2_3	431.8		
		5×2_4	426.4		

C.1.3 Density of the joints of the bending specimens

In order to gain knowledge of the timber density at the connection, the mean value was determined of the lamellae within the connection. Table C.1 gives the settings for the different density ranges.

Certain specimens with its laminate structure are described below.

Table C.1: Classification of the color settings for different densities ranges

kg/m ³		kg/m ³		kg/m ³		kg/m ³	
	330 - 340		340 - 350		350 - 360		360 - 370
	370 - 380		380 - 390		390 - 400		400 - 410
	410 - 420		420 - 430		430 - 440		440 - 450
	450 - 460		460 - 470		470 - 480		480 - 490
	490 - 500		500 - 510		510 - 520		520 - 530
	530 - 540		540 - 540		550 - 560		560 - 570
	570 - 580		580 - 590		590 - 600		600 - 610

Specimen 1 (18 cm × 32 cm)



Experiment left side : Ø12 mm 3×3_1
 Experiment right side : Ø12 mm 2×4_3
 Mean density left connection : 457.1 [kg/m³]
 Mean density right connection : 460.8 [kg/m³]

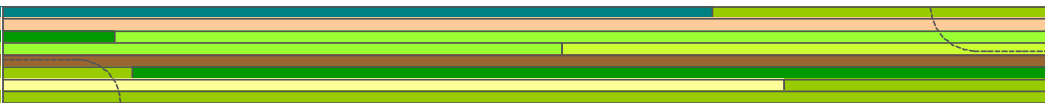
Specimen 2 (18 cm × 32 cm)



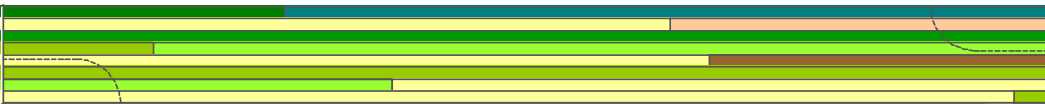
Experiment left side : Ø16 mm 3×2_1
 Experiment right side : Ø12 mm 5×2_3
 Mean density left connection : 442.8 [kg/m³]
 Mean density right connection : 449.3 [kg/m³]

Specimen 3 (18 cm × 32 cm)

Experiment left side	: Ø12 mm 5×2_3
Experiment right side	: Ø16 mm 3×2_1
Mean density left connection	: 454.5 [kg/m ³]
Mean density right connection	: 480.8 [kg/m ³]

Specimen 4 (18 cm × 32 cm)

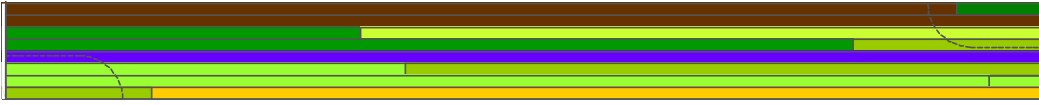
Experiment left side	: Ø12 mm 2×4_2
Experiment right side	: Ø12 mm 2×4_1
Mean density left connection	: 428.8 [kg/m ³]
Mean density right connection	: 430.3 [kg/m ³]

Specimen 5 (18 cm × 32 cm)

Experiment left side	: Ø12 mm 2×4_1
Experiment right side	: Ø12 mm 2×4_2
Mean density left connection	: 448.3 [kg/m ³]
Mean density right connection	: 433.3 [kg/m ³]

Specimen 6 (18 cm × 32 cm)

Experiment left side	: Ø16 mm 3×2_2
Experiment right side	: Ø16 mm 3×2_3
Mean density left connection	: 472.3 [kg/m ³]
Mean density right connection	: 458.0 [kg/m ³]

Specimen 7 (18 cm × 32 cm)

Experiment left side	: Ø16 mm 3×2_3
Experiment right side	: Ø16 mm 3×2_2
Mean density left connection	: 434.4 [kg/m ³]
Mean density right connection	: 476.0 [kg/m ³]

Specimen 8 (18 cm × 32 cm)

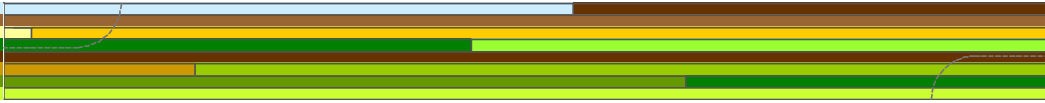
Experiment left side	: Ø12 mm 2×4_3
Experiment right side	: Ø12 mm 3×3_1
Mean density left connection	: 448.8 [kg/m ³]
Mean density right connection	: 458.8 [kg/m ³]

Specimen 9 (18 cm × 32 cm)

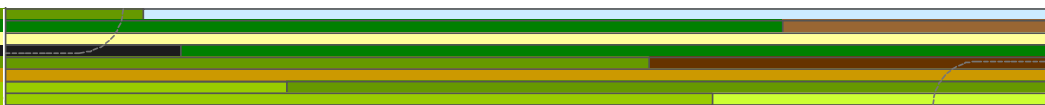
Experiment left side	: Ø7 mm 2×3_3
Experiment right side	: Ø7 mm 4×2_3
Mean density left connection	: 429.0 [kg/m ³]
Mean density right connection	: 444.8 [kg/m ³]

Specimen 10 (18 cm × 32 cm)

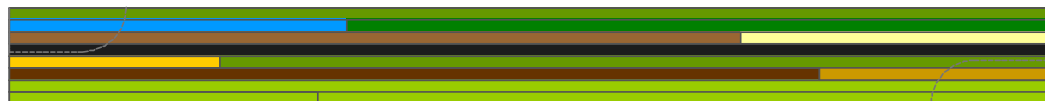
Experiment left side	: Ø12 mm 3×3_3
Experiment right side	: Ø12 mm 3×3_2
Mean density left connection	: 418.0 [kg/m ³]
Mean density right connection	: 466.5 [kg/m ³]

Specimen 11 (18 cm × 32 cm)

Experiment left side	: Ø12 mm 3×3 _2
Experiment right side	: Ø12 mm 3×3 _3
Mean density left connection	: 445.0 [kg/m ³]
Mean density right connection	: 452.5 [kg/m ³]

Specimen 12 (18 cm × 32 cm)

Experiment left side	: Ø12 mm 5×2 _2
Experiment right side	: Ø12 mm 5×2 _1
Mean density left connection	: 431.0 [kg/m ³]
Mean density right connection	: 424.0 [kg/m ³]

Specimen 13 (18 cm × 32 cm)

Experiment left side	: Ø12 mm 5×2 _1
Experiment right side	: Ø12 mm 5×2 _2
Mean density left connection	: 444.8 [kg/m ³]
Mean density right connection	: 438.3 [kg/m ³]

Specimen 14 (18 cm × 32 cm)

Experiment left side	: Ø7 mm 2×3 _1
Experiment right side	: Ø7 mm 2×3 _2
Mean density left connection	: 424.0 [kg/m ³]
Mean density right connection	: 456.5 [kg/m ³]

Specimen 15 (18 cm × 32 cm)

Experiment left side : Ø7 mm 2×3_2
 Experiment right side : Ø7 mm 2×3_1
 Mean density left connection : 445.3 [kg/m³]
 Mean density right connection : 431.0 [kg/m³]

Specimen 16 (18 cm × 32 cm)

Experiment left side : Ø7 mm 4×2_2
 Experiment right side : Ø7 mm 4×2_1
 Mean density left connection : 418.8 [kg/m³]
 Mean density right connection : 446.3 [kg/m³]

Specimen 17 (18 cm × 32 cm)

Experiment left side : Ø7 mm 4×2_1
 Experiment right side : Ø7 mm 4×2_2
 Mean density left connection : 433.0 [kg/m³]
 Mean density right connection : 441.6 [kg/m³]

Specimen 18 (18 cm × 32 cm)

Experiment left side : Ø7 mm 4×2_3
 Experiment right side : Ø7 mm 2×3_3
 Mean density left connection : 410.8 [kg/m³]
 Mean density right connection : 432.5 [kg/m³]

Summary

Ø7 mm			Ø12 mm			Ø16 mm		
Specimen	Density [kg/m ³]		Specimen	Density [kg/m ³]		Specimen	Density [kg/m ³]	
	left	right		left	right		left	right
2×3_1	424.0	431.0	2×4_1	448.3	430.3	3×2_1	480.8	442.8
2×3_2	445.3	456.5	2×4_2	428.8	433.3	3×2_2	472.3	476.0
2×3_3	429.0	432.5	2×4_3	448.8	460.8	3×2_3	434.4	458.0
4×2_1	433.0	446.3	3×3_1	457.0	458.8			
4×2_2	418.8	441.6	3×3_2	445.0	466.5			
4×2_3	410.8	444.8	3×3_3	418.0	452.5			
			5×2_1	444.8	424.0			
			5×2_2	431.0	438.3			
			5×2_3	454.5	449.3			

D Experimental results

D.1 Experiments on connections in tension

Experiments with a dowel diameter of 7 mm

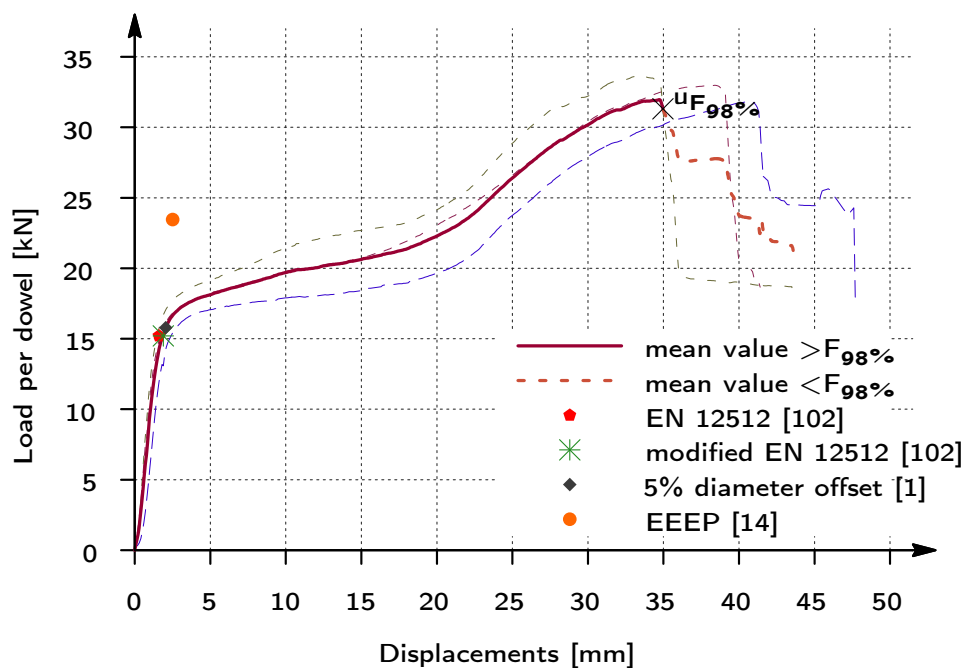


Figure D.1: Load-displacement behavior of a dowel arrangement 2x3

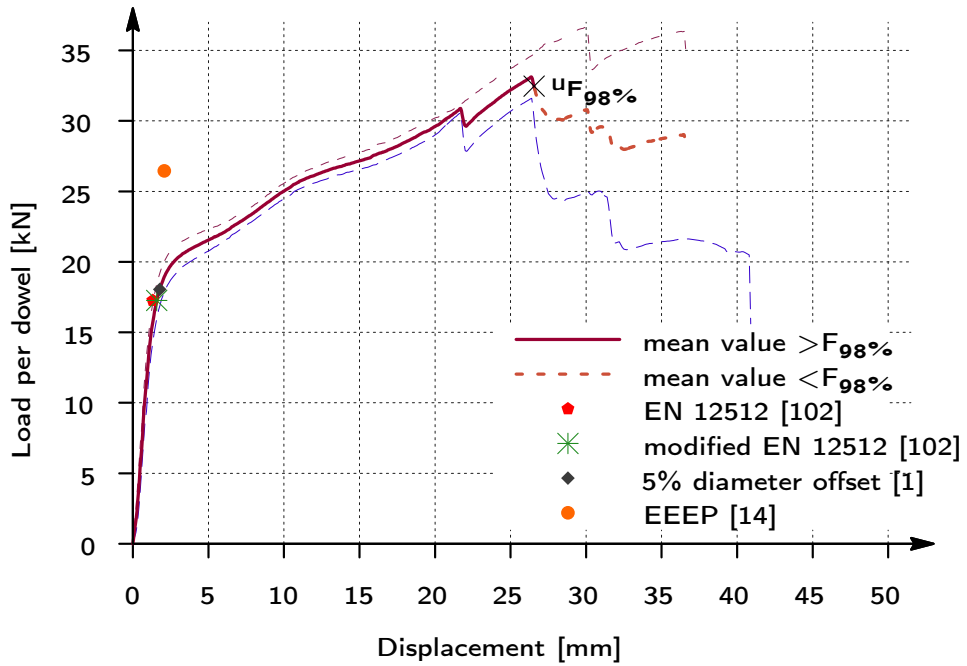


Figure D.2: Load-displacement behavior of a dowel arrangement 4x2
Type a: Decrease of the stiffness after yielding

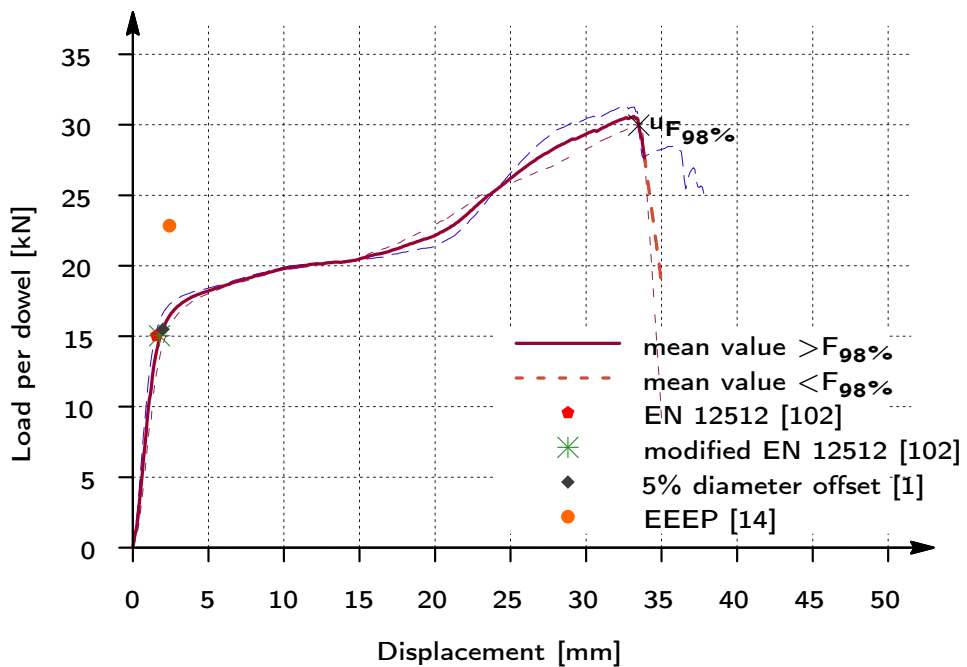


Figure D.3: Load-displacement behavior of a dowel arrangement 4x2
Type b: Pronounced plastic plateau followed by a load increase

Experiments with a dowel diameter of 12 mm

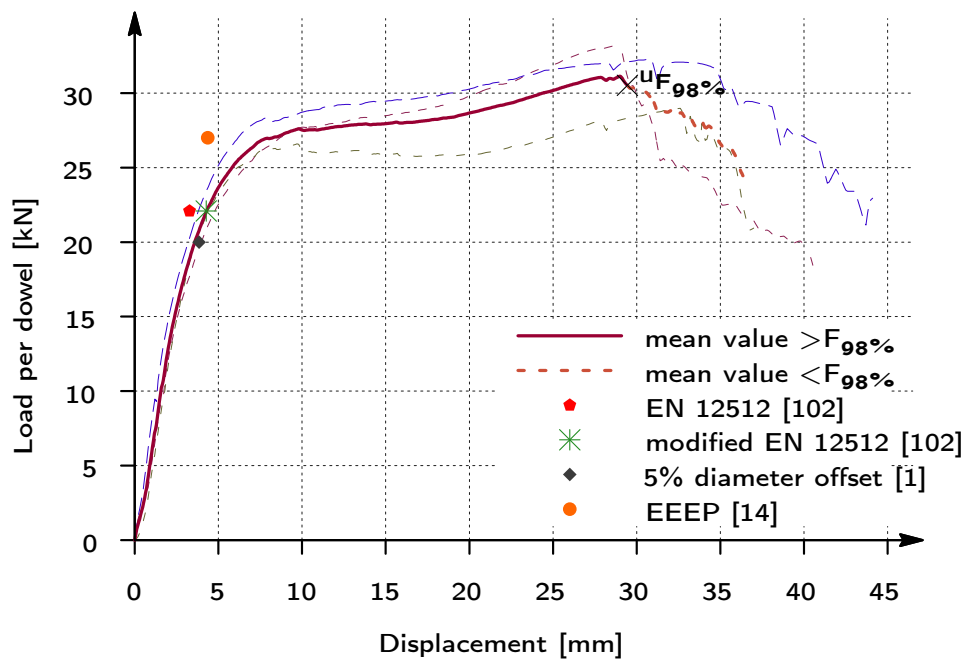


Figure D.4: Load-displacement behavior of a dowel arrangement 2x4

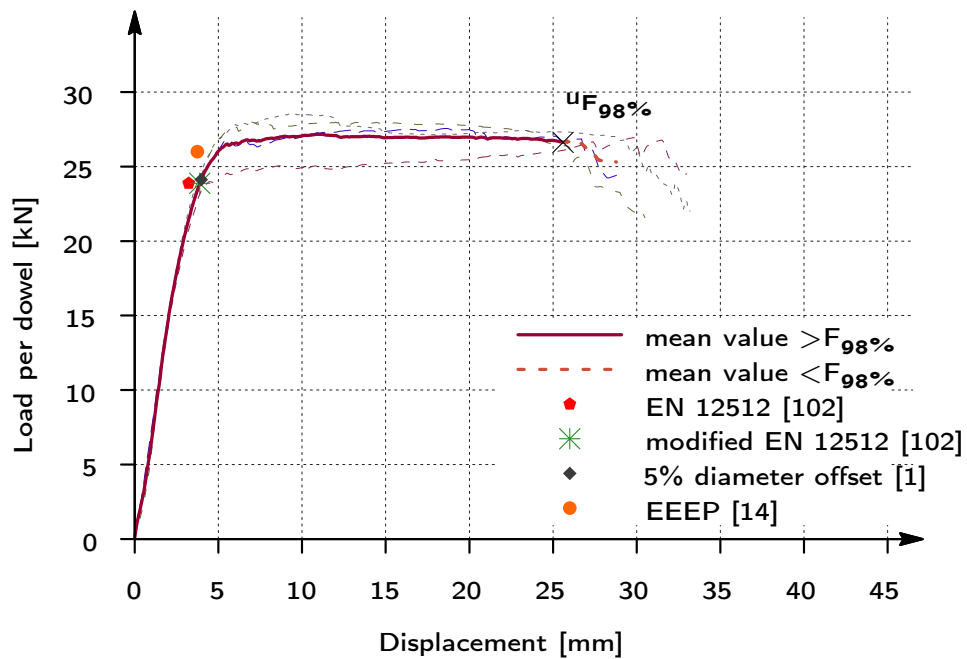


Figure D.5: Load-displacement behavior of a dowel arrangement 3x3

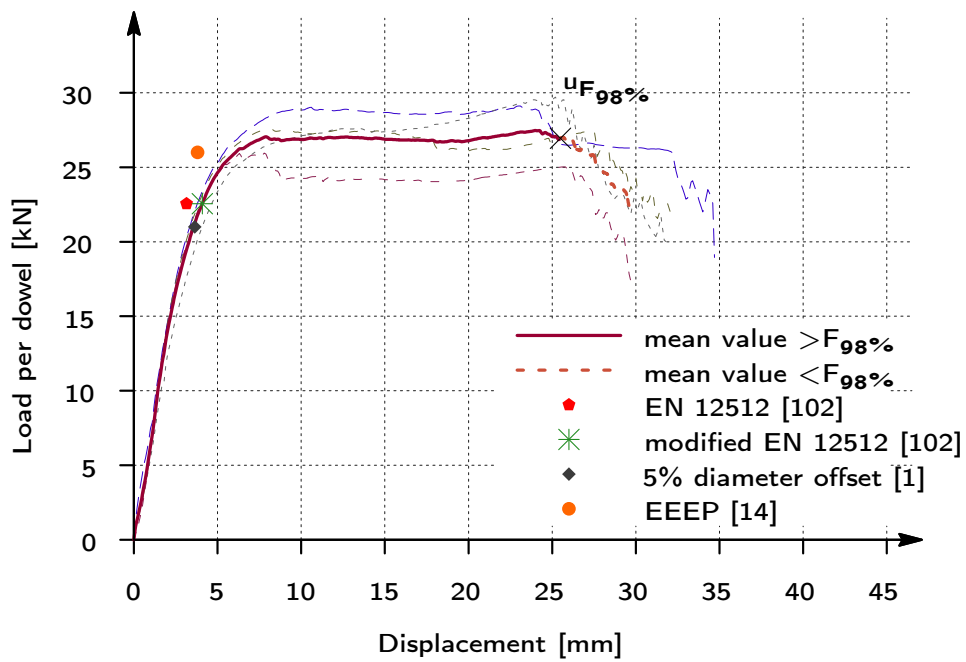


Figure D.6: Load-displacement behavior of a dowel arrangement 5x2

Experiments with a dowel diameter of 16 mm

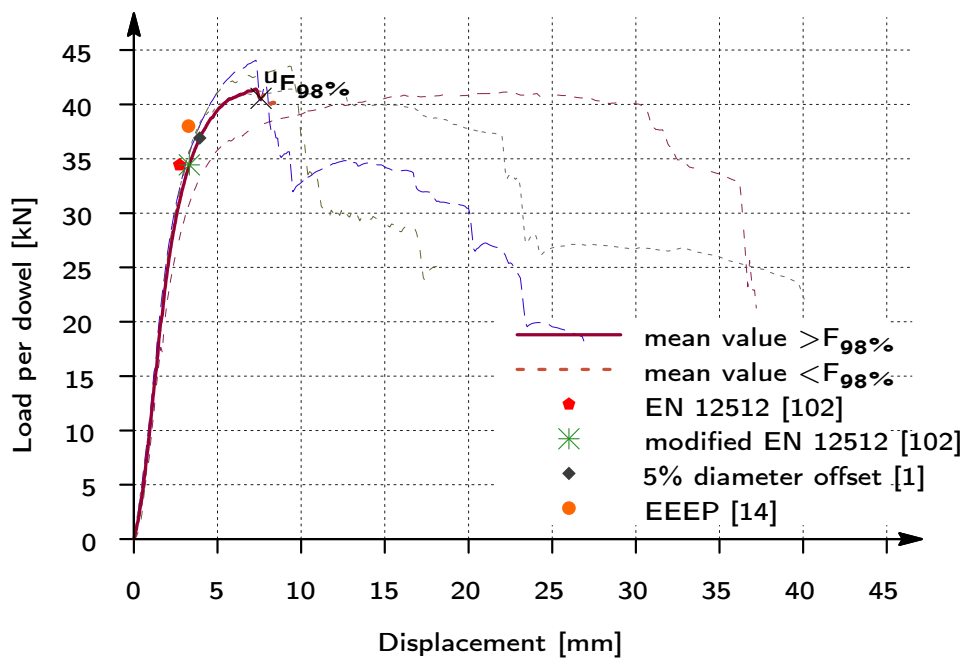


Figure D.7: Load-displacement behavior of a dowel arrangement 3x2

D.2 Experiments on joints in bending

Experiments with a dowel diameter of 7 mm

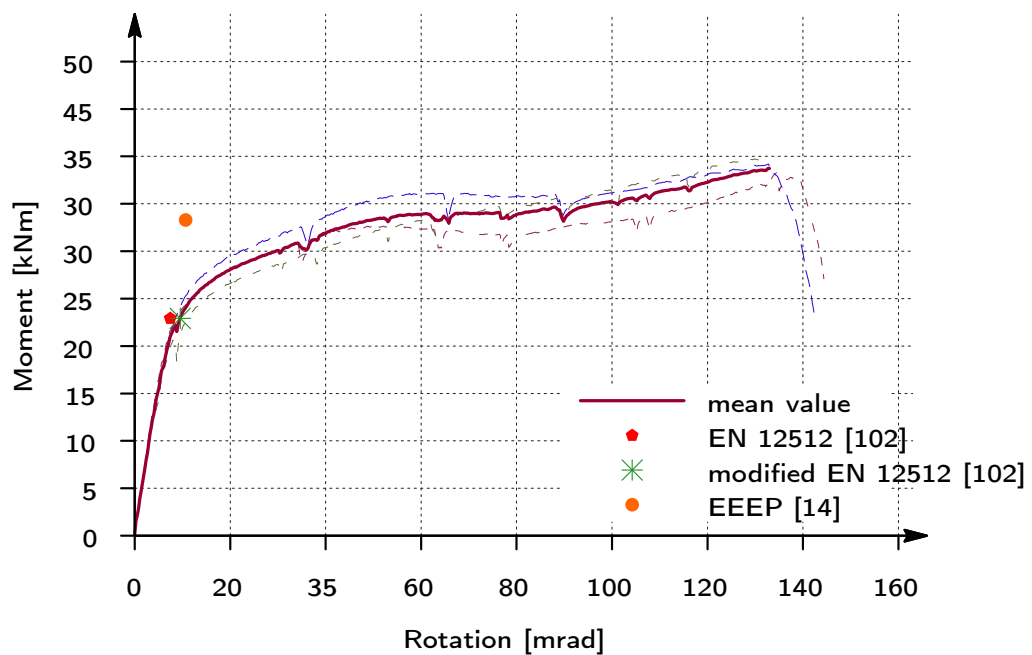


Figure D.8: Moment-rotation behavior of a dowel arrangement 2x3

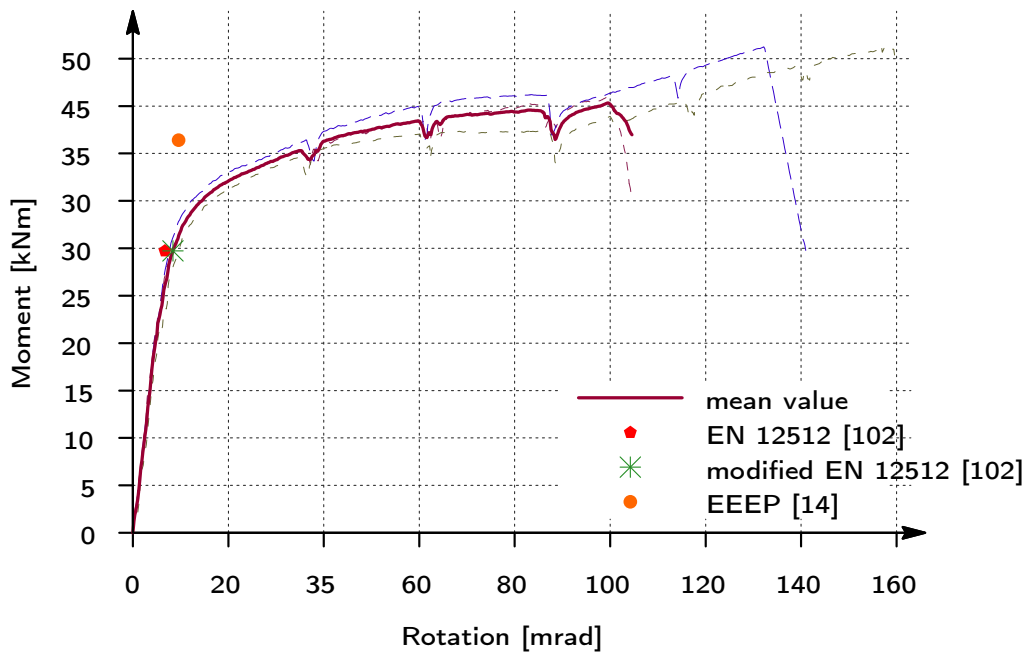


Figure D.9: Moment-rotation behavior of a dowel arrangement 4x2

Experiments with a dowel diameter of 12 mm

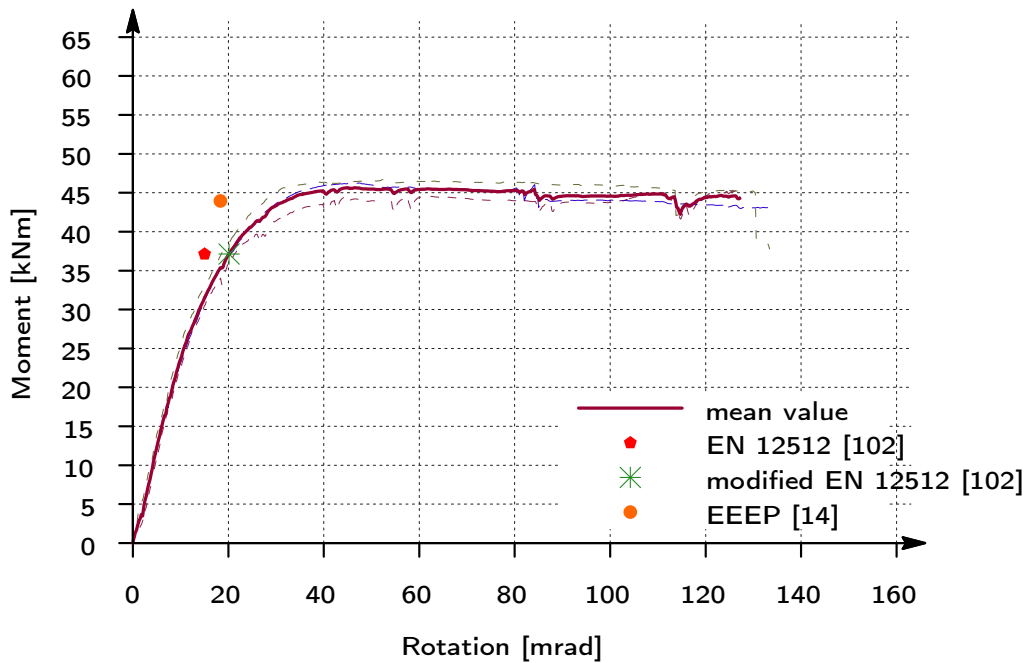


Figure D.10: Moment-rotation behavior of a dowel arrangement 2x4

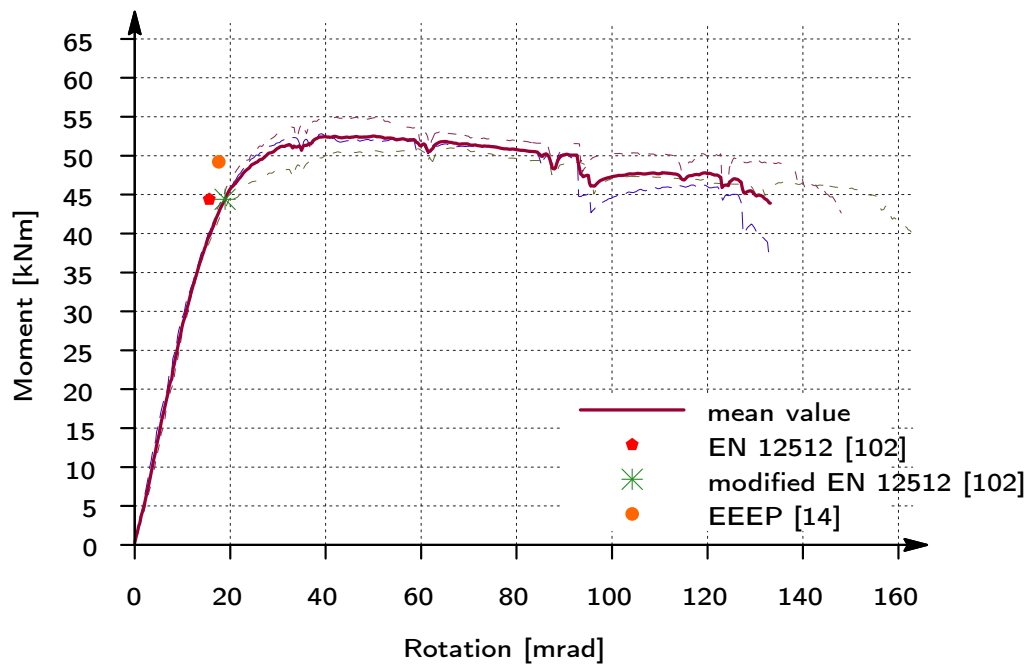


Figure D.11: Moment-rotation behavior of a dowel arrangement 3x3

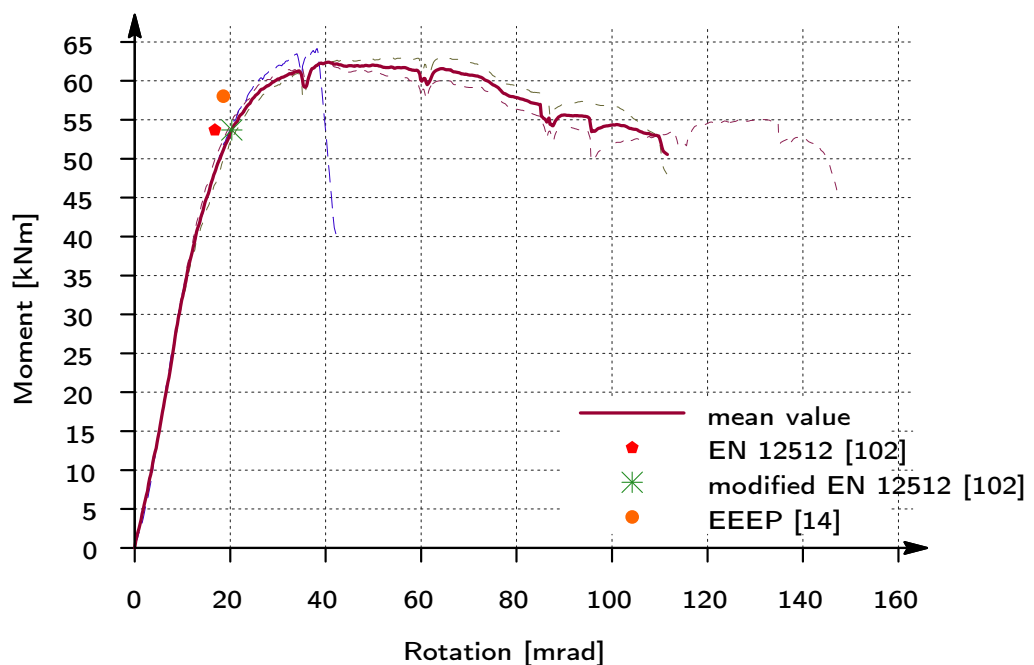


Figure D.12: Moment-rotation behavior of a dowel arrangement 5x2

Experiments with a dowel diameter of 16 mm

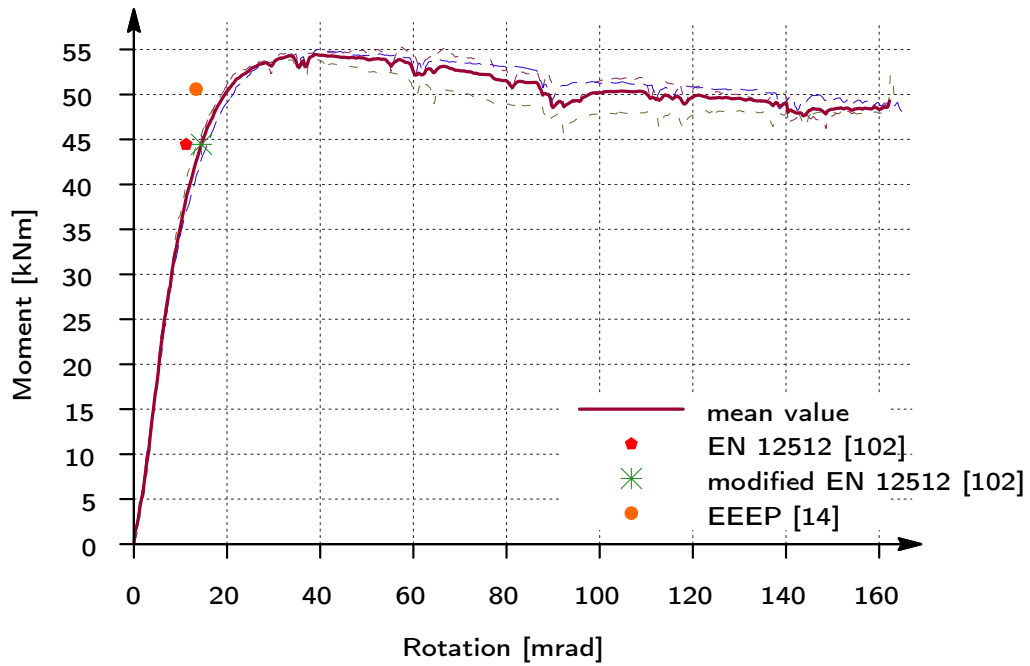


Figure D.13: Moment-rotation behavior of a dowel arrangement 3x2

D.3 Miscellaneous experiments

Experiments in tension perpendicular to the grain [51]

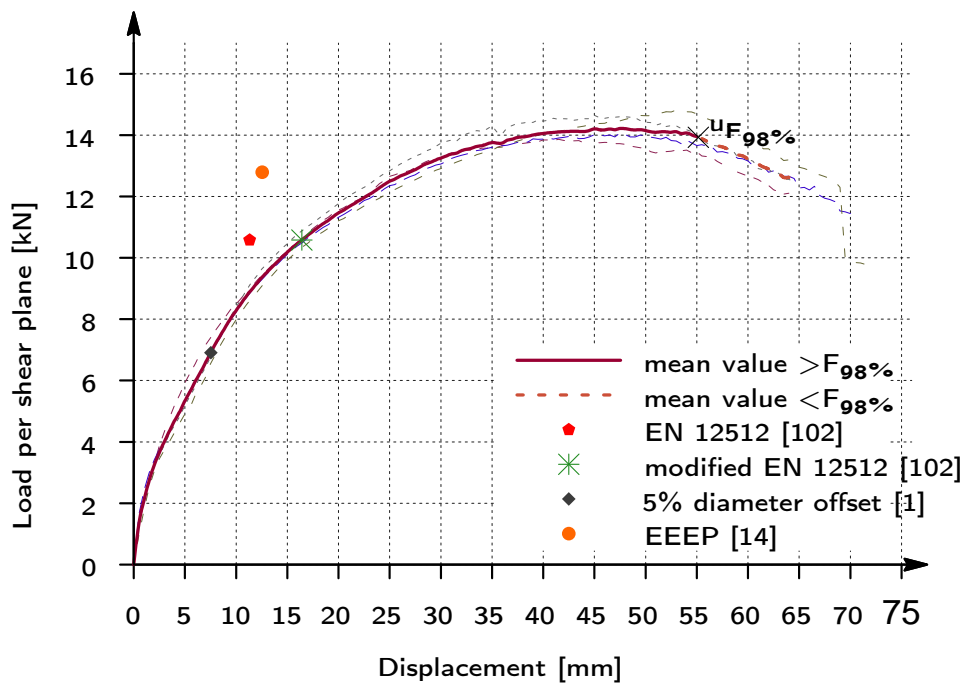


Figure D.14: Load-displacement behavior with eight (four) dowels

Experiments under a cyclic loading [73]

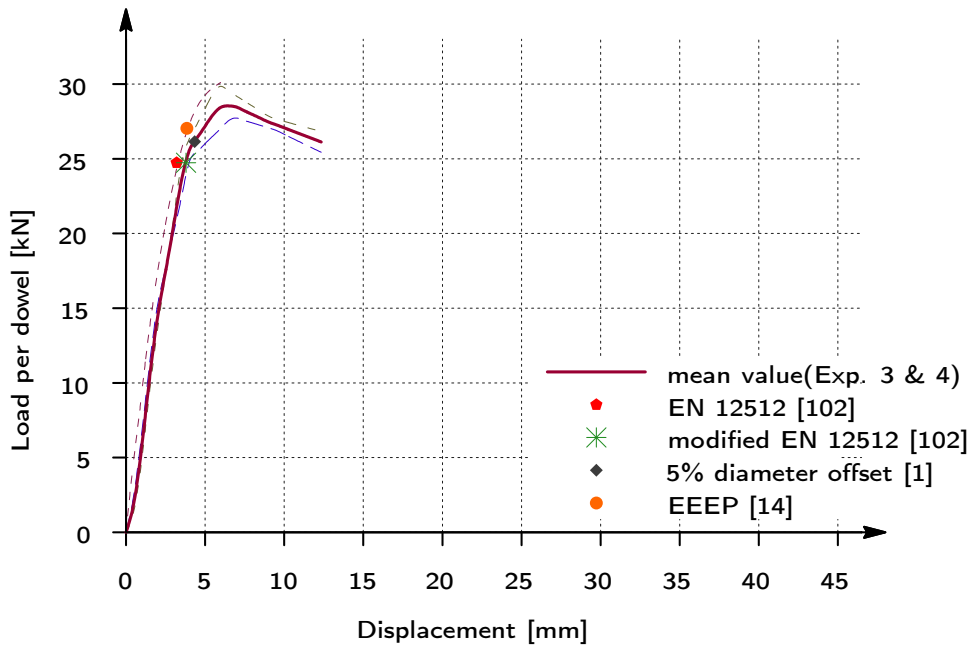


Figure D.15: Load-displacement behavior of a dowel arrangement 3x3

Single experiments with a dowel diameter of 12 mm

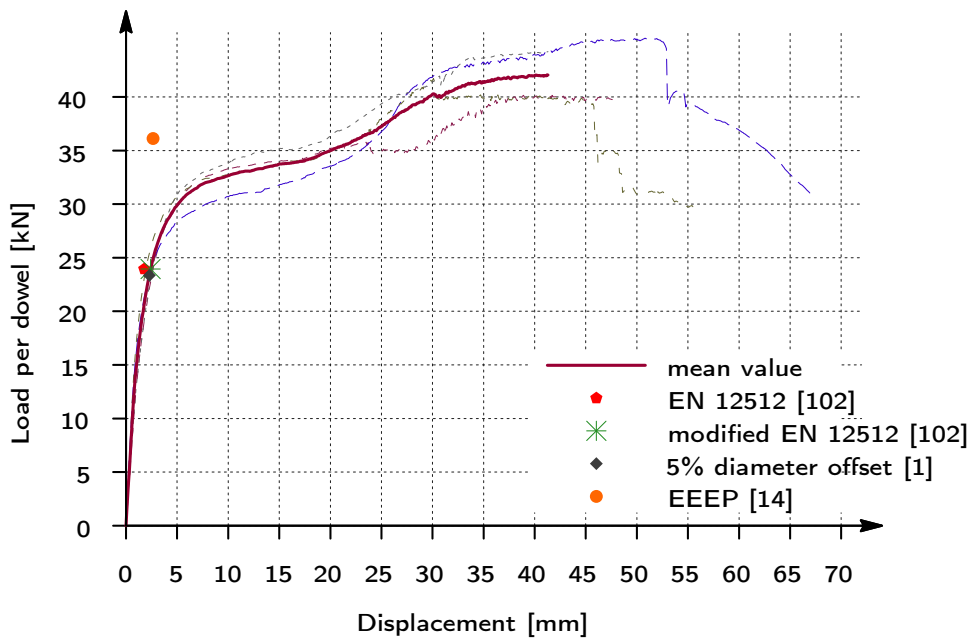


Figure D.16: Load-displacement behavior of a dowel arrangement 1x1

E X-ray scans

E.1 Introduction

All of the experiments were x-ray scanned to gain knowledge of the actual bending angle of the dowels and to detect uncertainties in the timber.



(a) Tension specimen

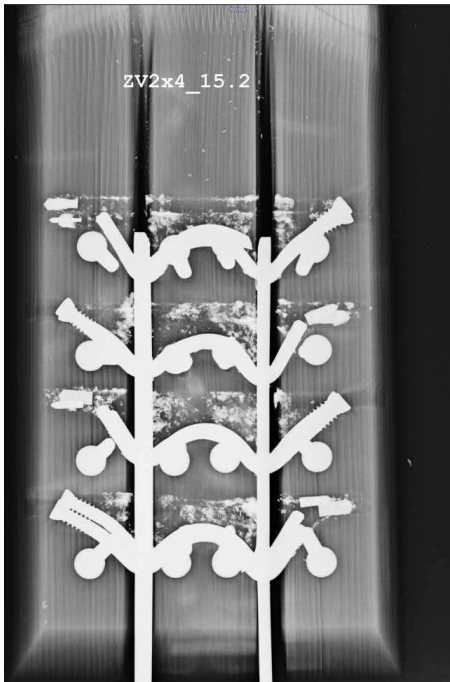


(b) bending specimen

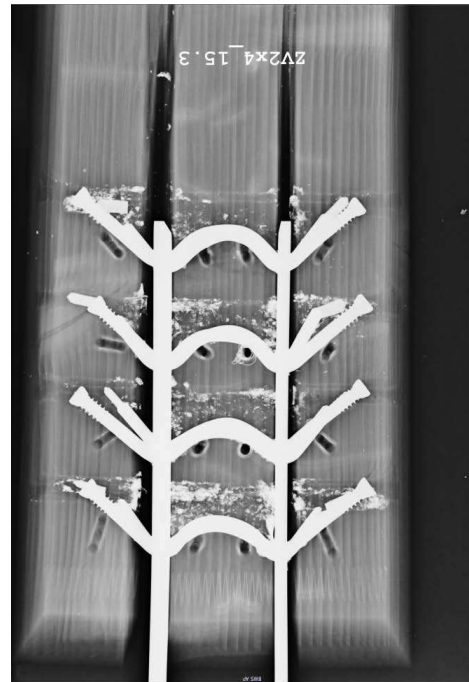
Figure E.1: X-ray scanning of already examined connections

Hence a hospital was visited to x-ray scan all the timber elements.

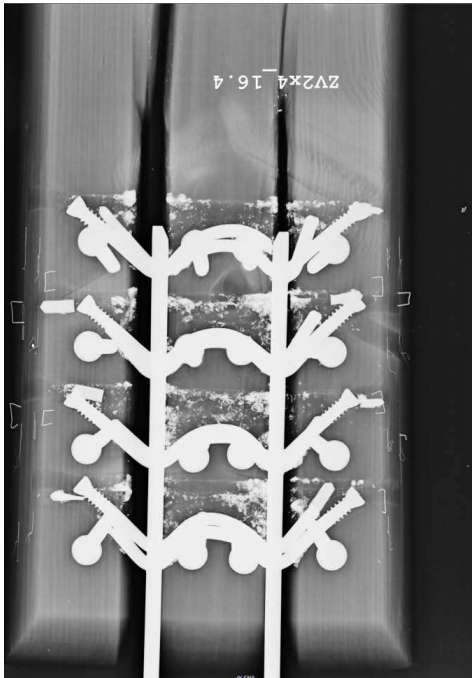
E.2 Tension specimens



(a) Experiment 1



(b) Experiment 3

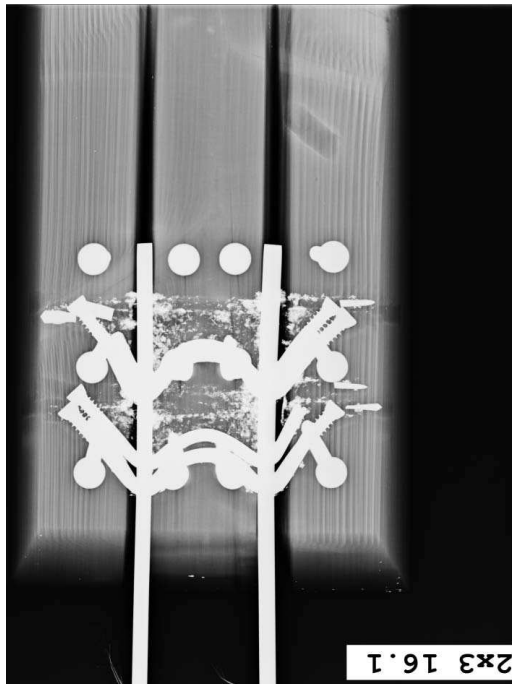


(c) Experiment 4

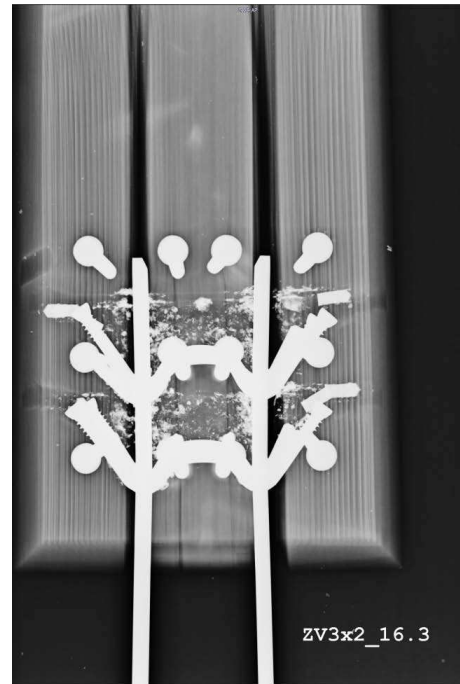


(d) Experiment 5

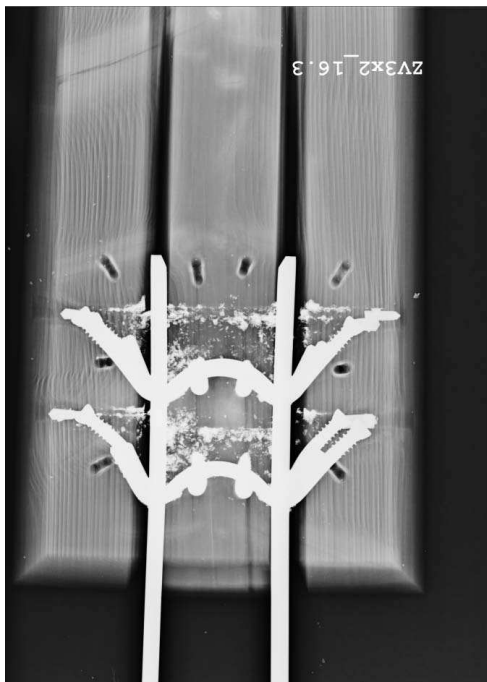
Figure E.2: Specimens with a dowel configuration of 4×2 dowels with a diameter of 7 mm



(a) Experiment 1



(b) Experiment 2

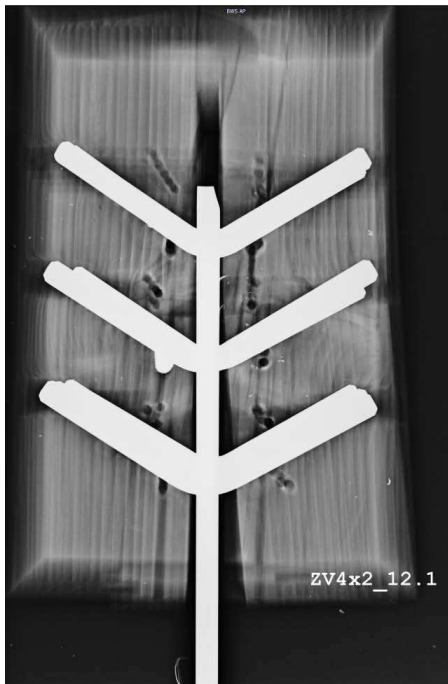


(c) Experiment 3



(d) Change to 3×2 dowels within the test series of 4×2

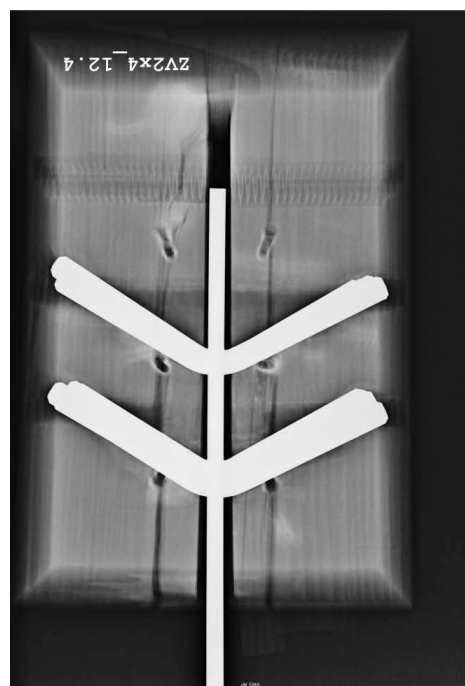
Figure E.3: Specimens with a dowel configuration of 2×3 dowels with a diameter of 7 mm



(a) Experiment 1

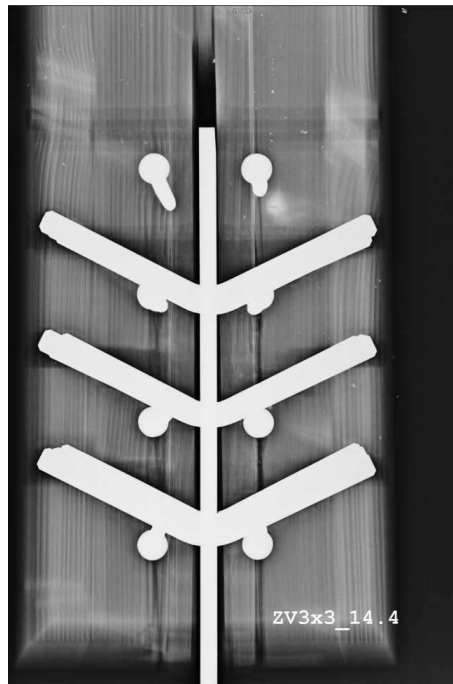


(b) Experiment 2

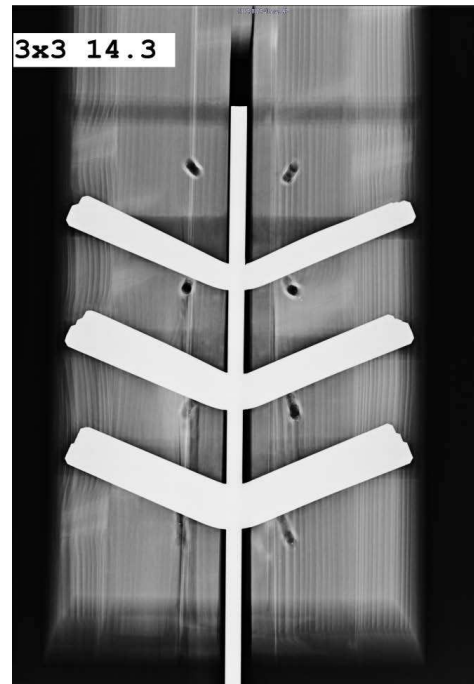


(c) Experiment 4

Figure E.4: Specimens with a dowel configuration of 2×4 dowels with a diameter of 12 mm



(a) Experiment 1



(b) Experiment 2



(c) Experiment 3



(d) Experiment 4

Figure E.5: Specimens with a dowel configuration of 3×3 dowels with a diameter of 12 mm



(a) Experiment 1



(b) Experiment 2

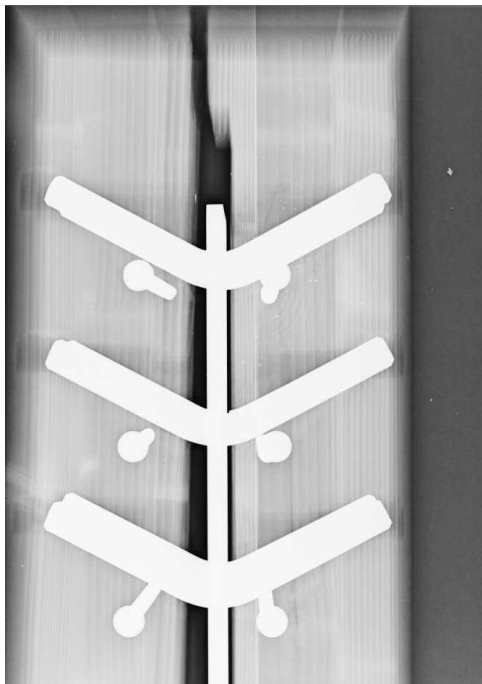


(c) Experiment 3



(d) Experiment 4

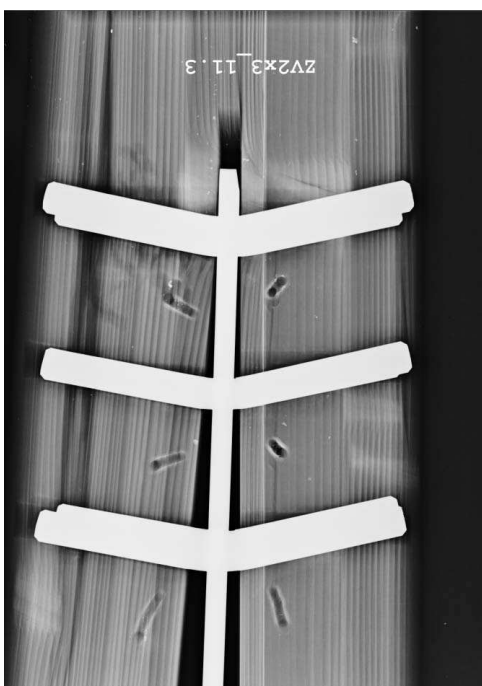
Figure E.6: Specimens with a dowel configuration of 5×2 dowels with a diameter of 12 mm



(a) Experiment 1



(b) Experiment 2



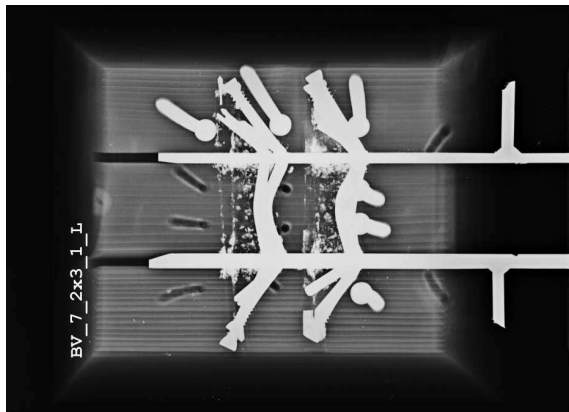
(c) Experiment 3



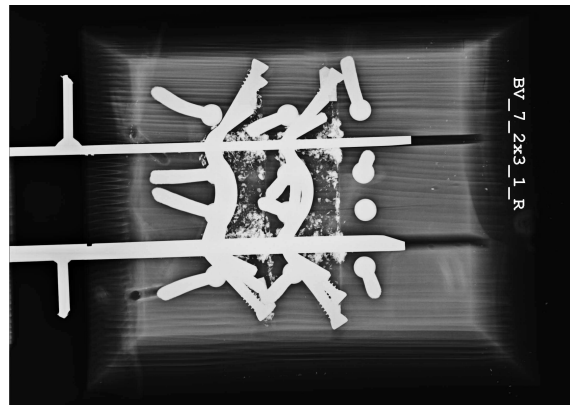
(d) Experiment 4

Figure E.7: Specimens with a dowel configuration of 3×2 dowels with a diameter of 16 mm

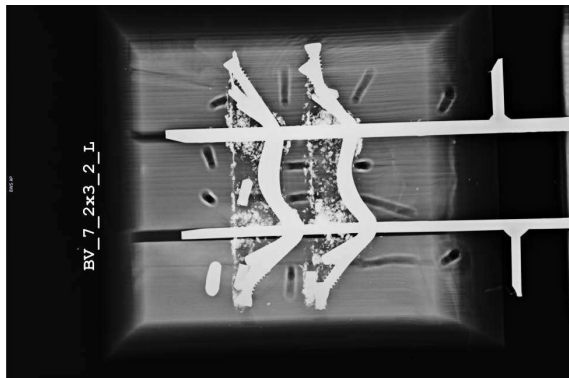
E.3 Bending specimens



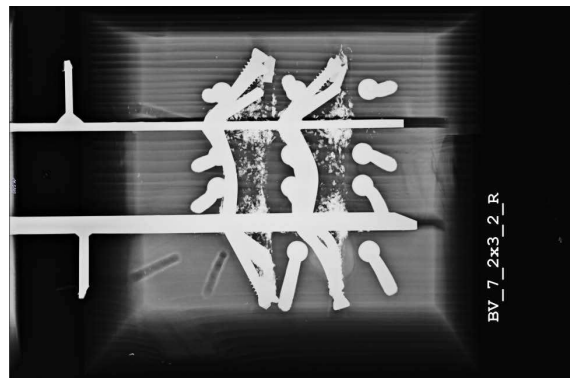
(a) Experiment 1, left hand side



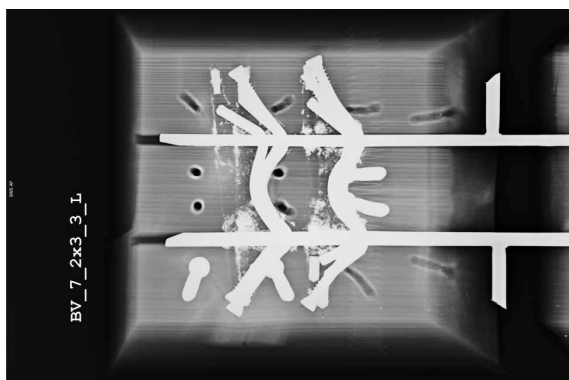
(b) Experiment 1, right hand side



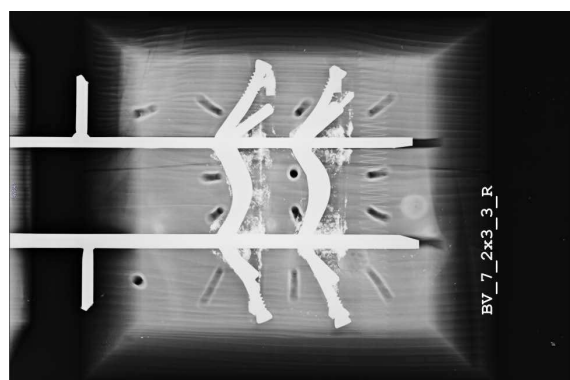
(c) Experiment 2, left hand side



(d) Experiment 2, right hand side



(e) Experiment 3, left hand side



(f) Experiment 3, right hand side

Figure E.8: Bending specimens with a dowel configuration of 2×3 dowels with a diameter of 7 mm

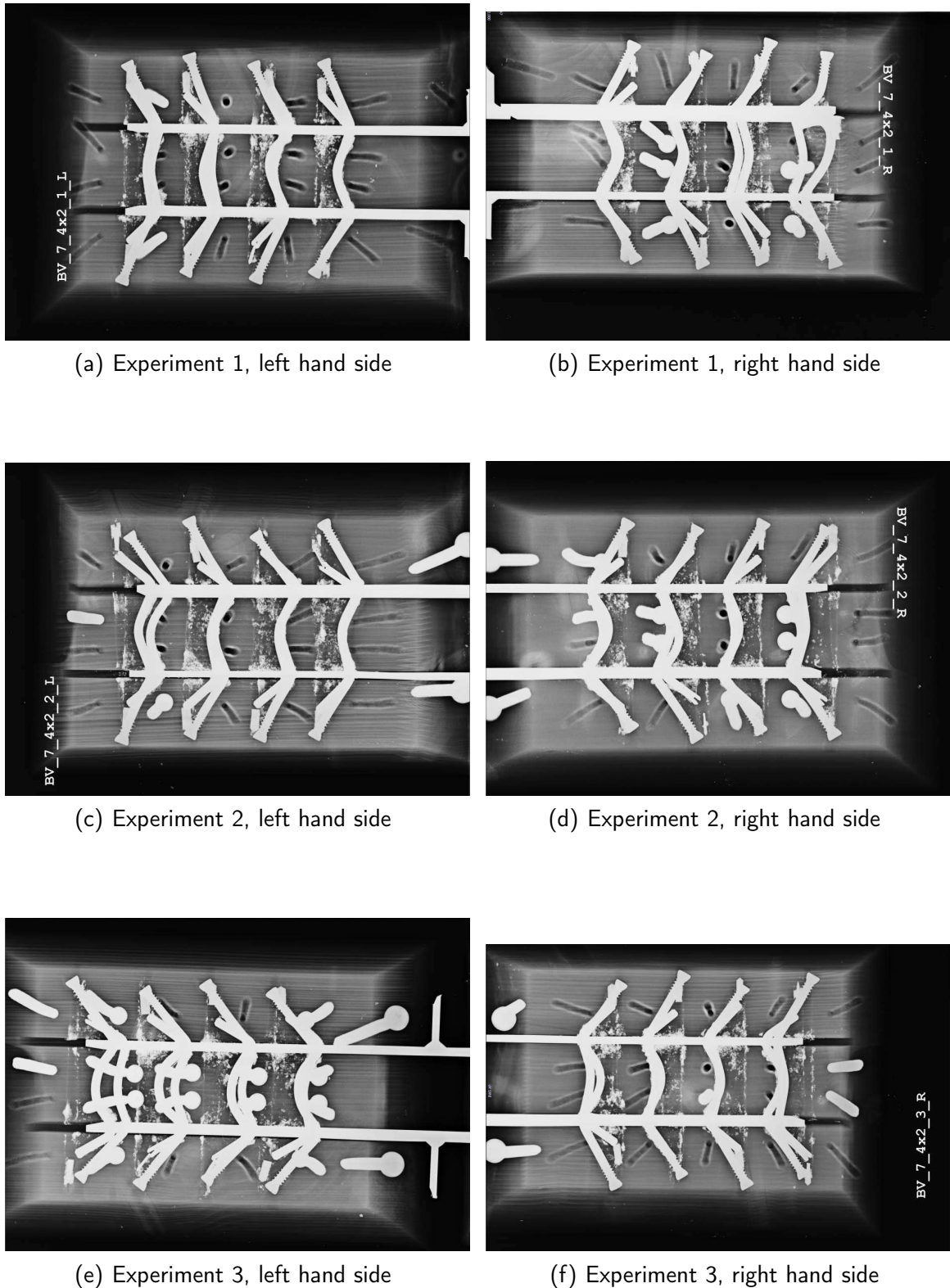


Figure E.9: Bending specimens with a dowel configuration of 4×2 dowels with a diameter of 7 mm

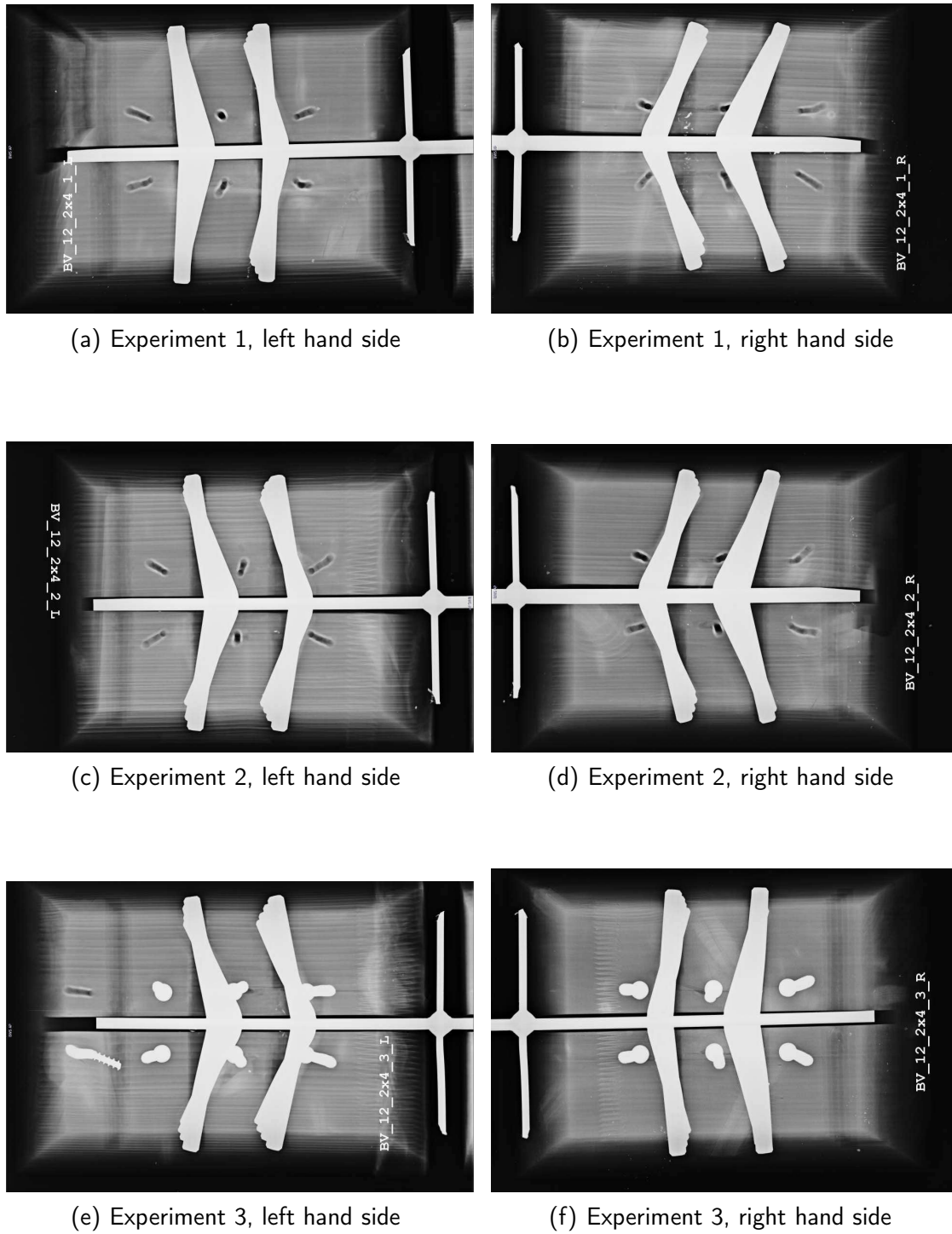


Figure E.10: Bending specimens with a dowel configuration of 2×4 dowels with a diameter of 12 mm

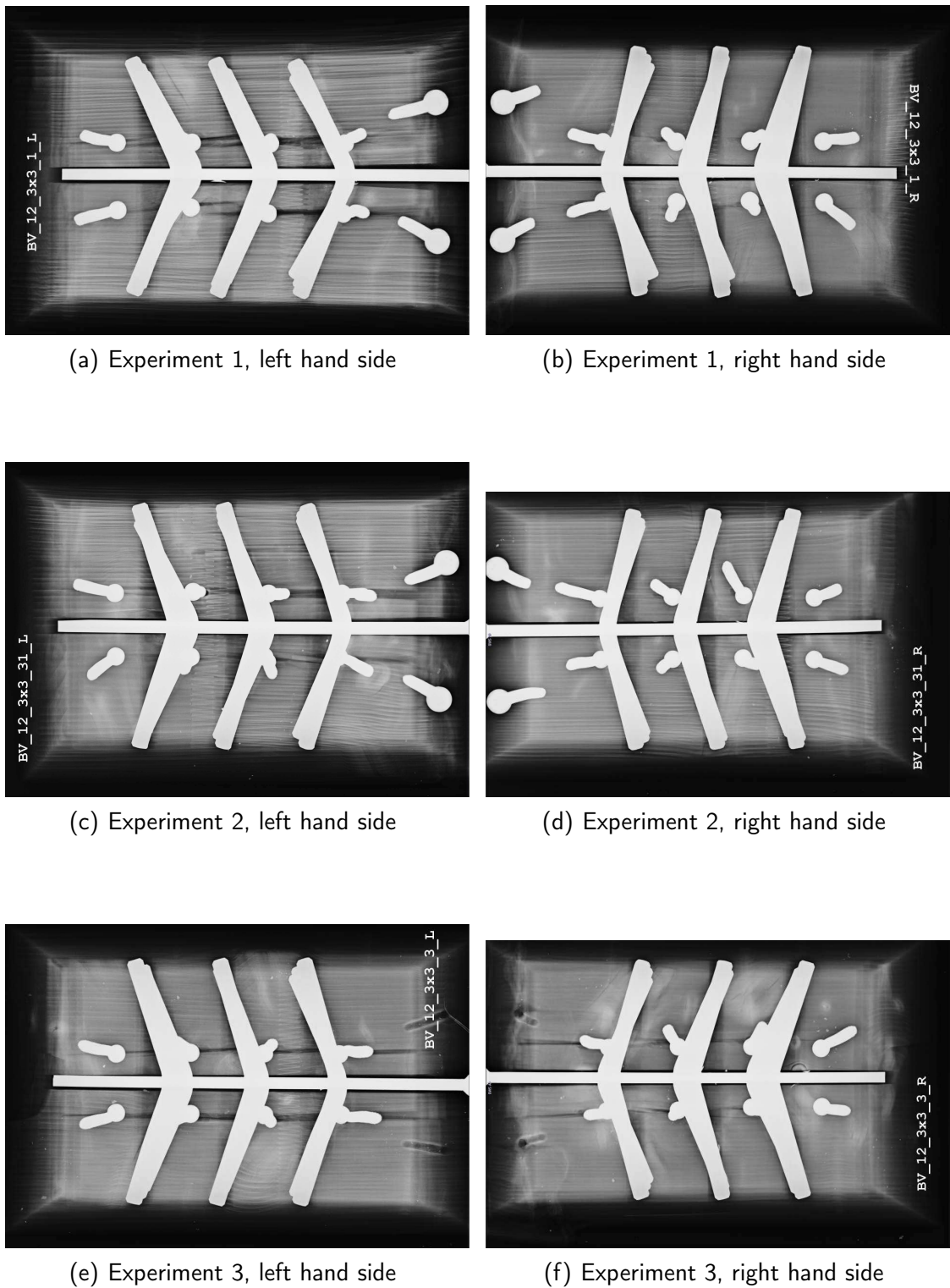
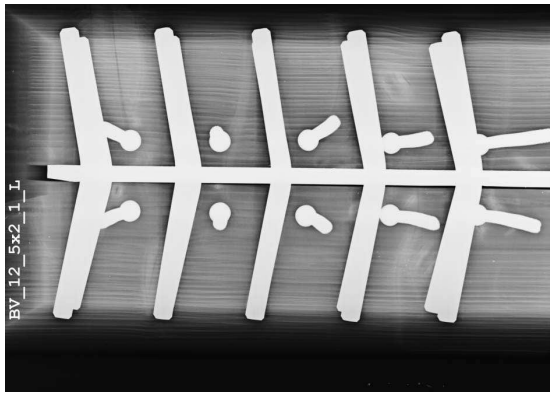
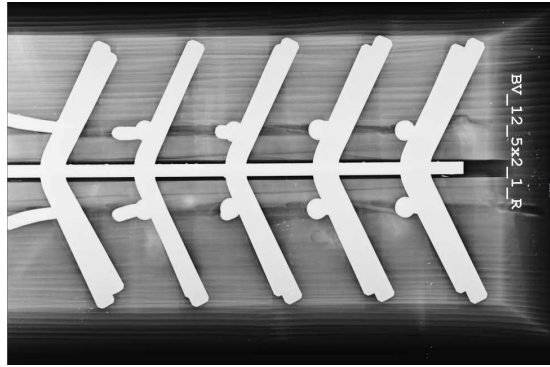


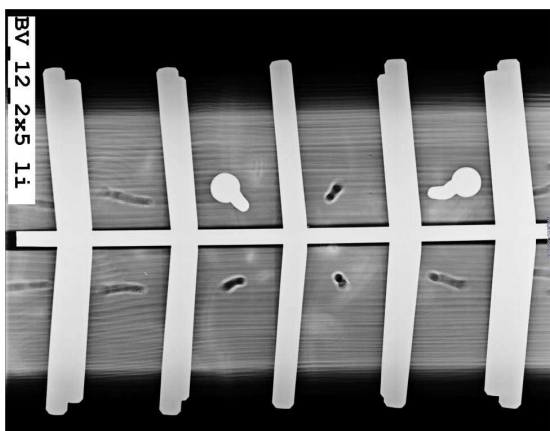
Figure E.11: Bending specimens with a dowel configuration of 3×3 dowels with a diameter of 12 mm



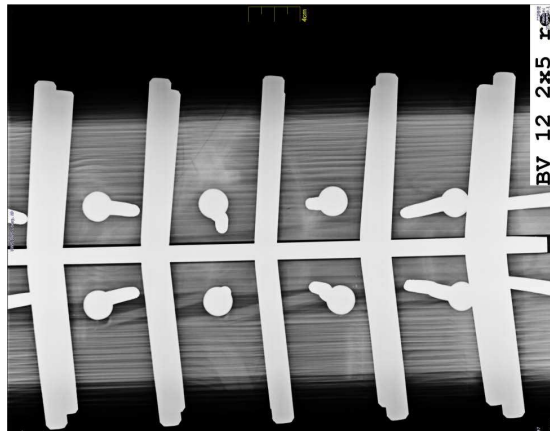
(a) Experiment 1, left hand side



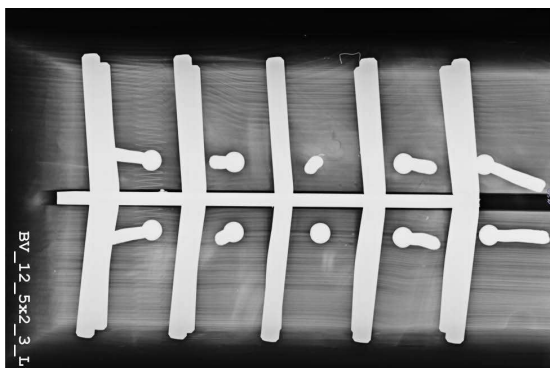
(b) Experiment 1, right hand side



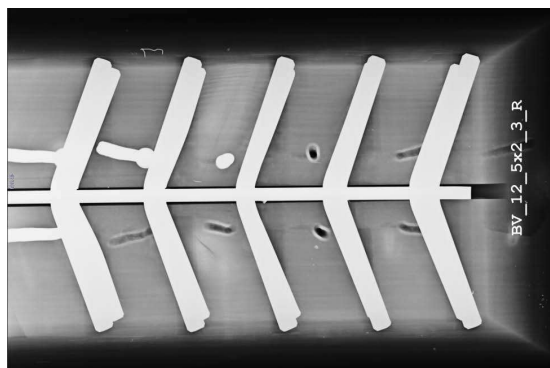
(c) Experiment 2, left hand side



(d) Experiment 2, right hand side



(e) Experiment 3, left hand side



(f) Experiment 3, right hand side

Figure E.12: Bending specimens with a dowel configuration of 5×2 dowels with a diameter of 12 mm

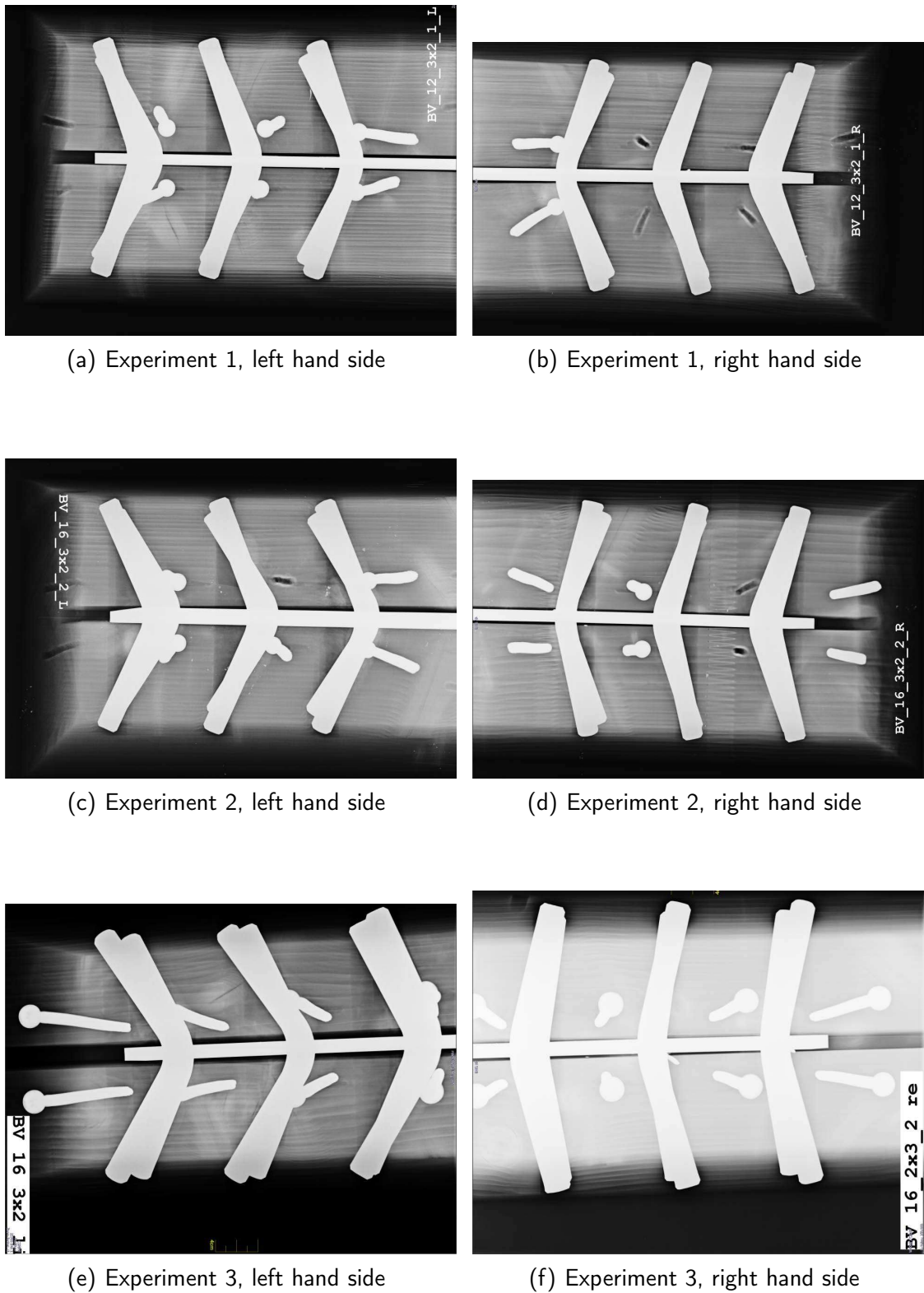


Figure E.13: Bending specimens with a dowel configuration of 3×2 dowels with a diameter of 16 mm

F.1.2 Steel Elements

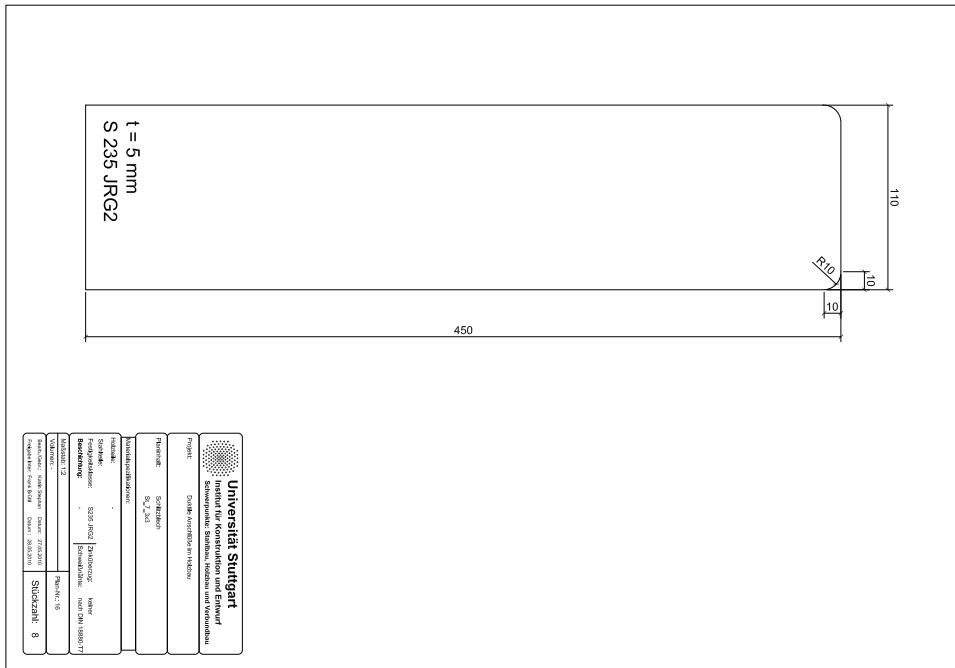


Figure F.2: Connection 7_3x2 (planned 7_3x3)

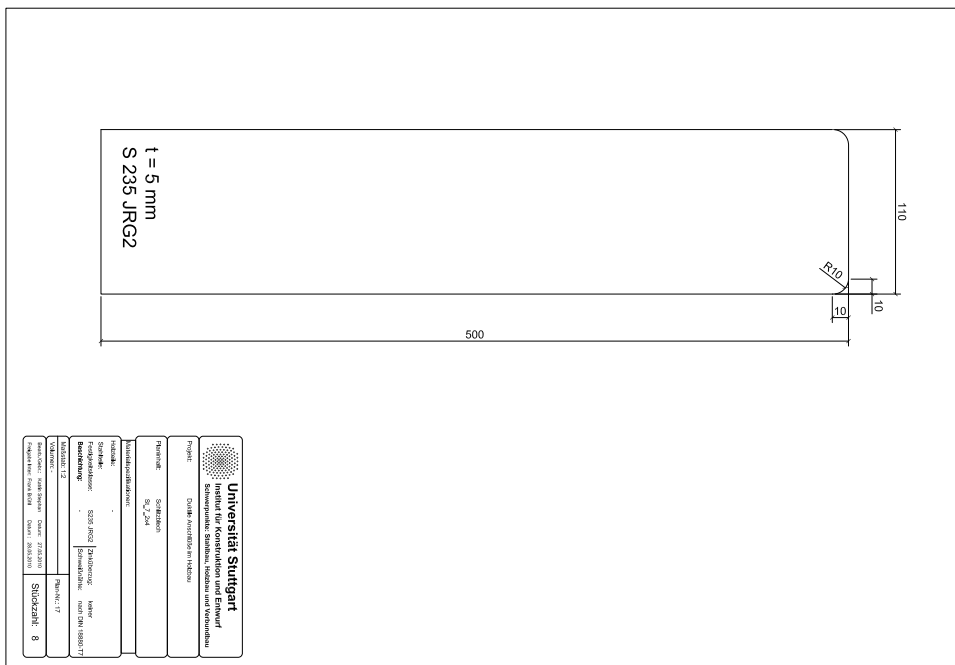


Figure F.3: Connection 7_2x4

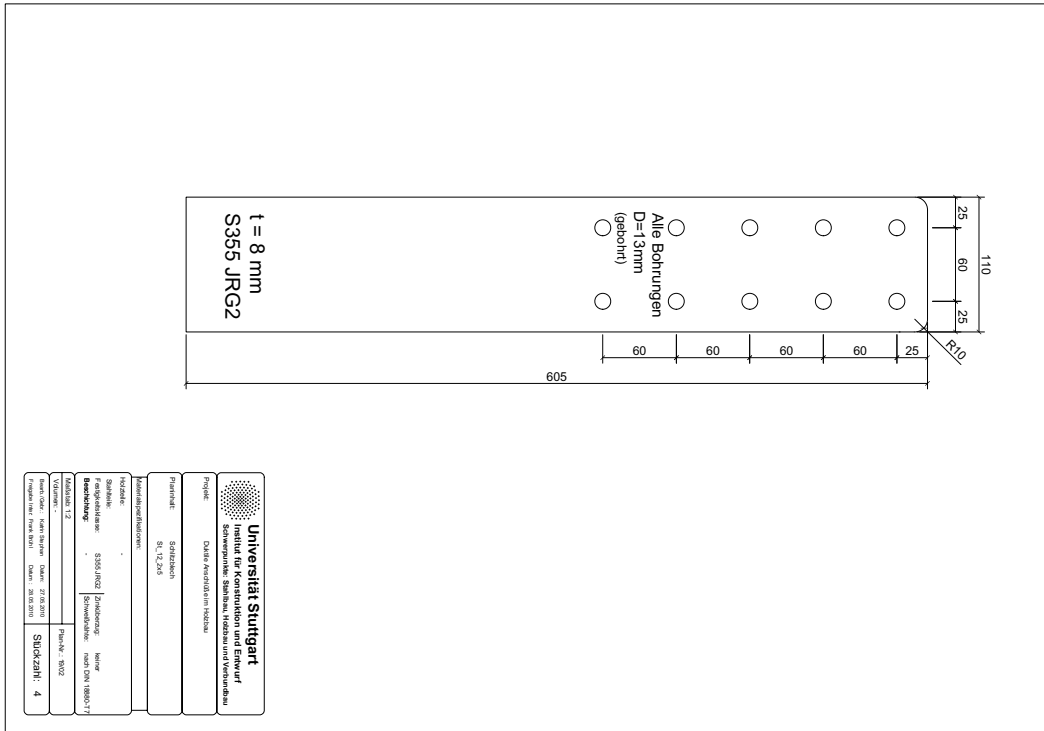


Figure F.6: Connection 12_2x5

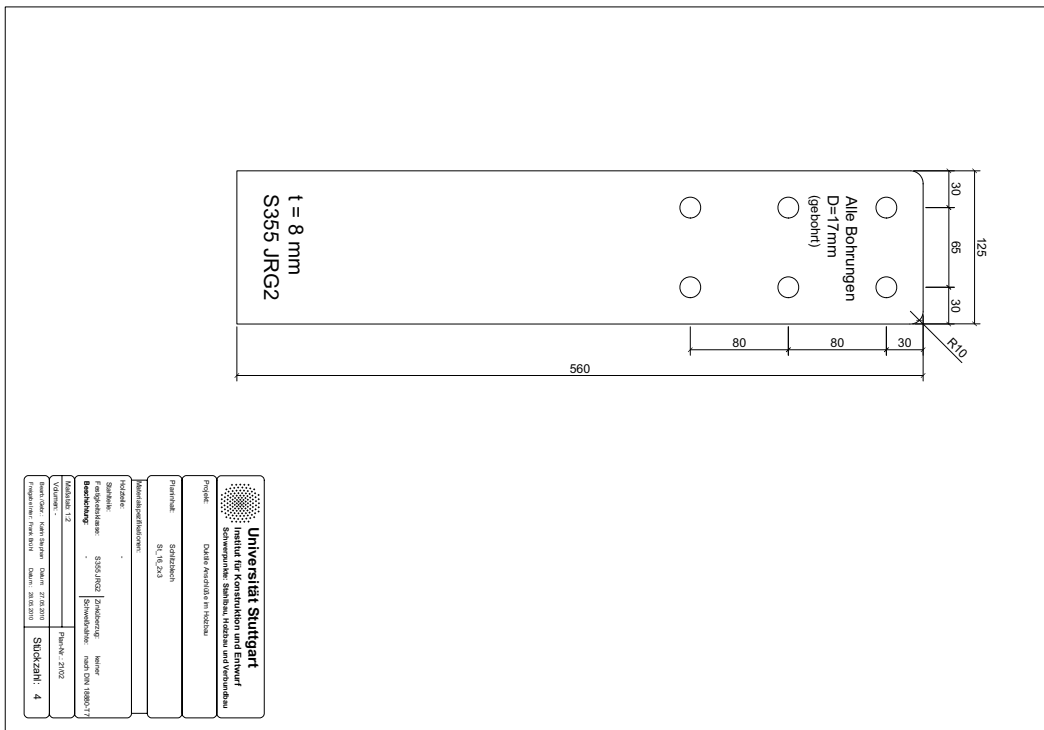


Figure F.7: Connection 16_2x3

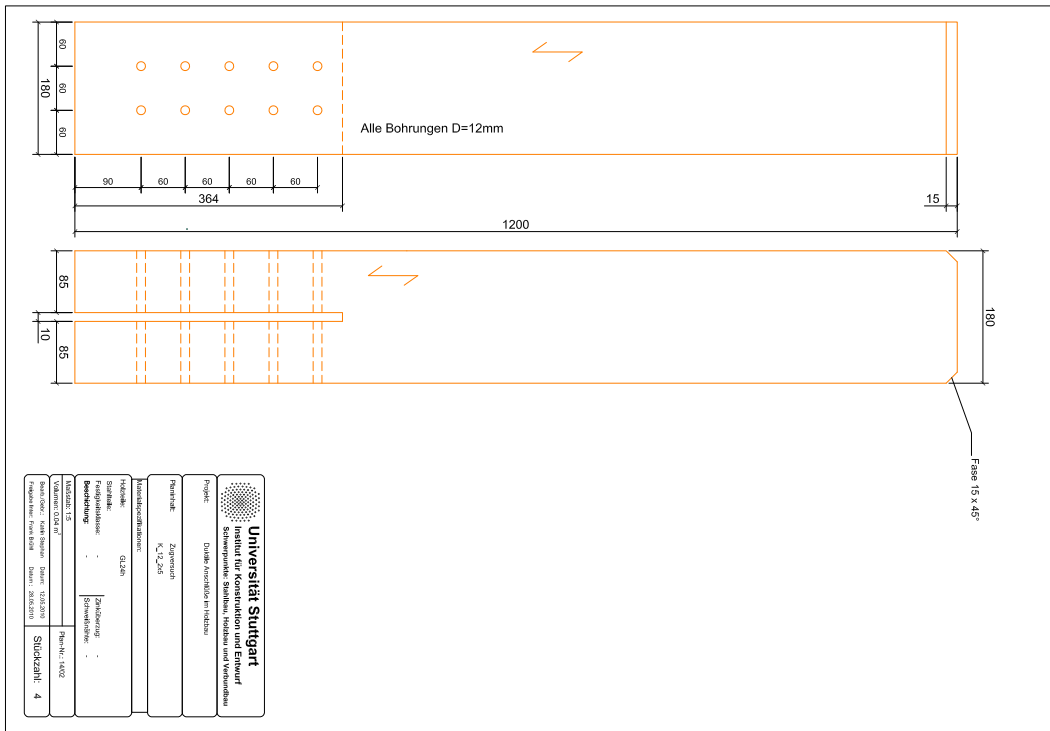


Figure F.12: Connection 12_2x5

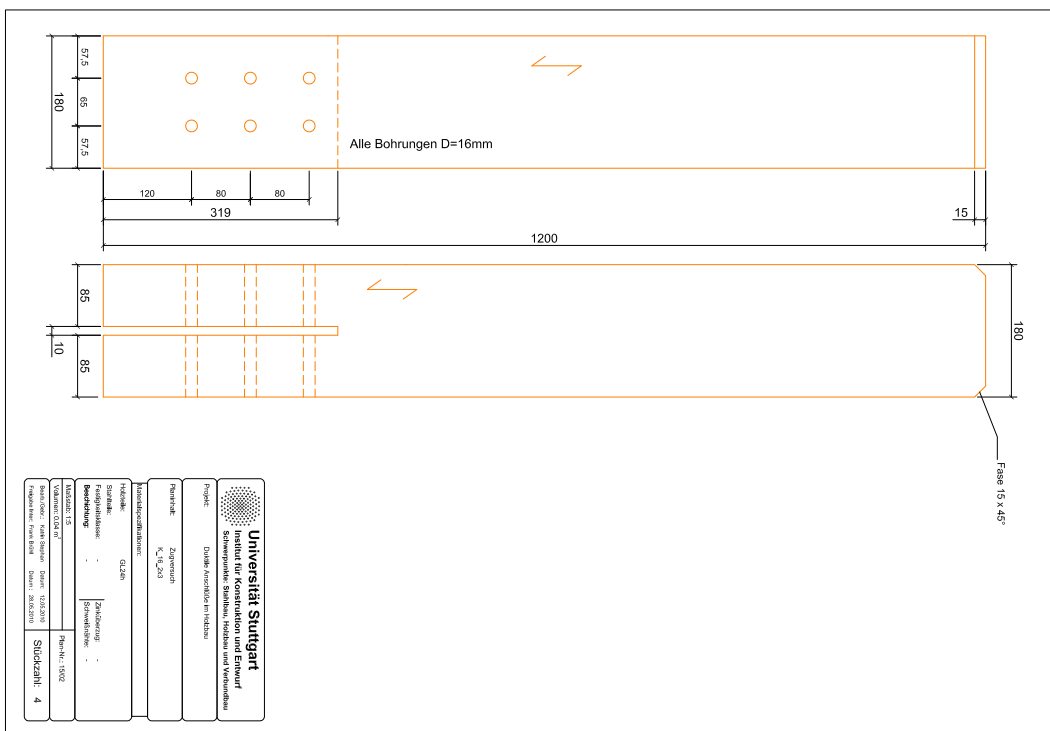


Figure F.13: Connection 16_2x3

F.2 Experiments on joints in bending

F.2.1 Steel Parts

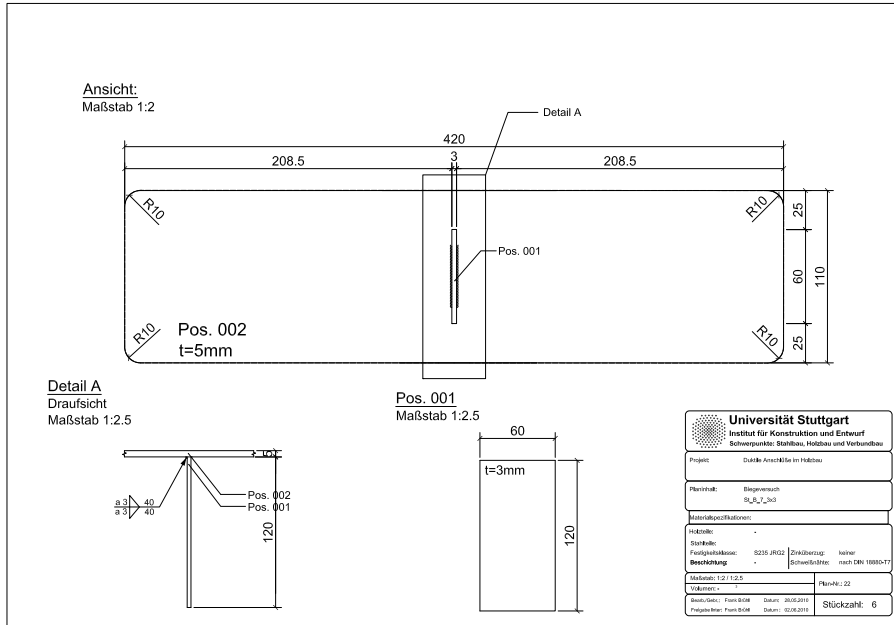


Figure F.14: Connection 7_3x2 (planned 7_3x3)

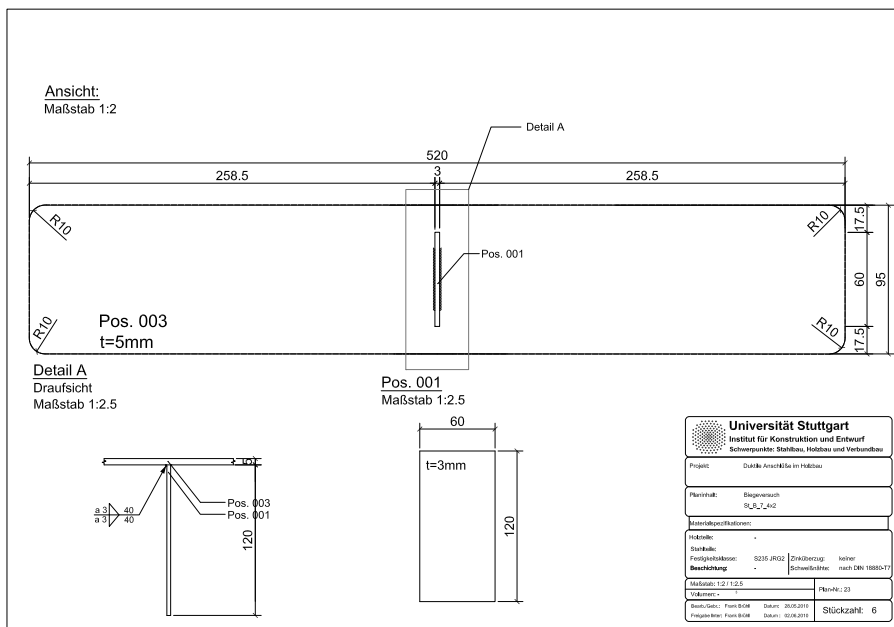


Figure F.15: Connection 7_2x4

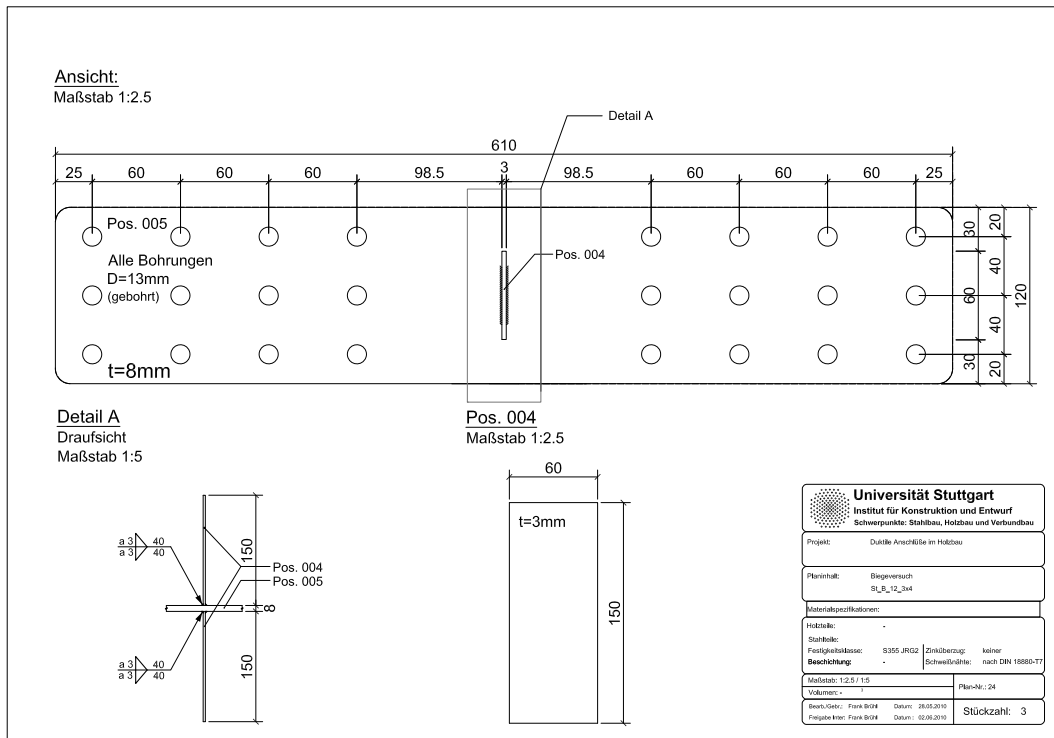


Figure F.16: Connection 12_3x3 (planned 12_3x4)

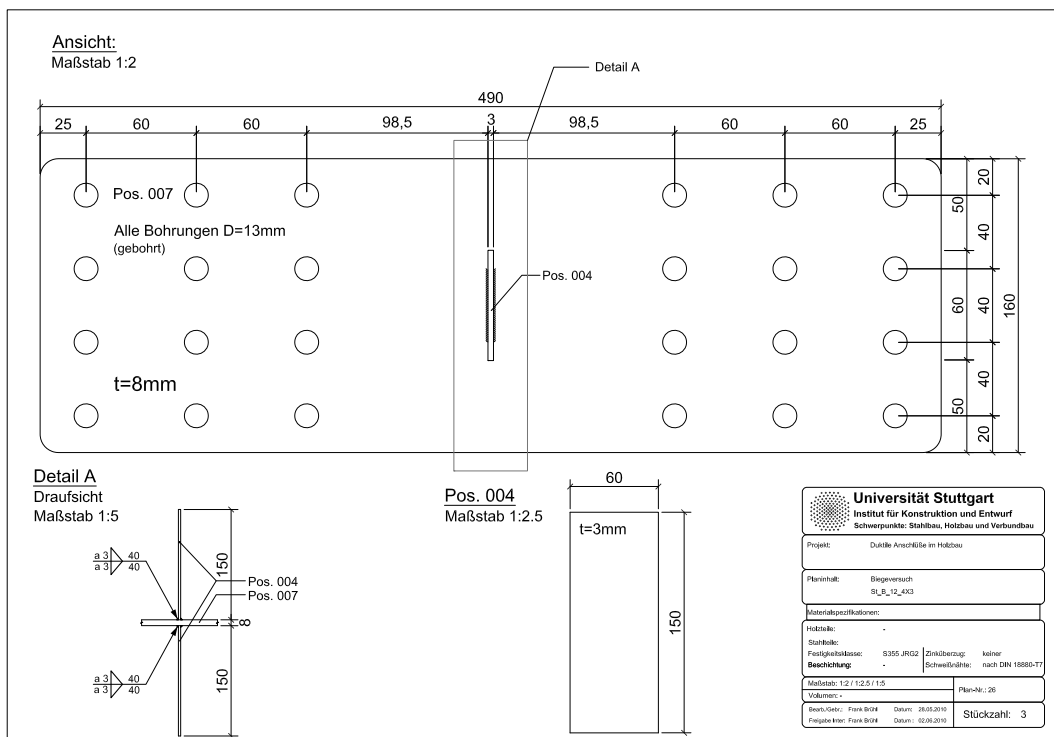


Figure F.17: Connection 12_4x3

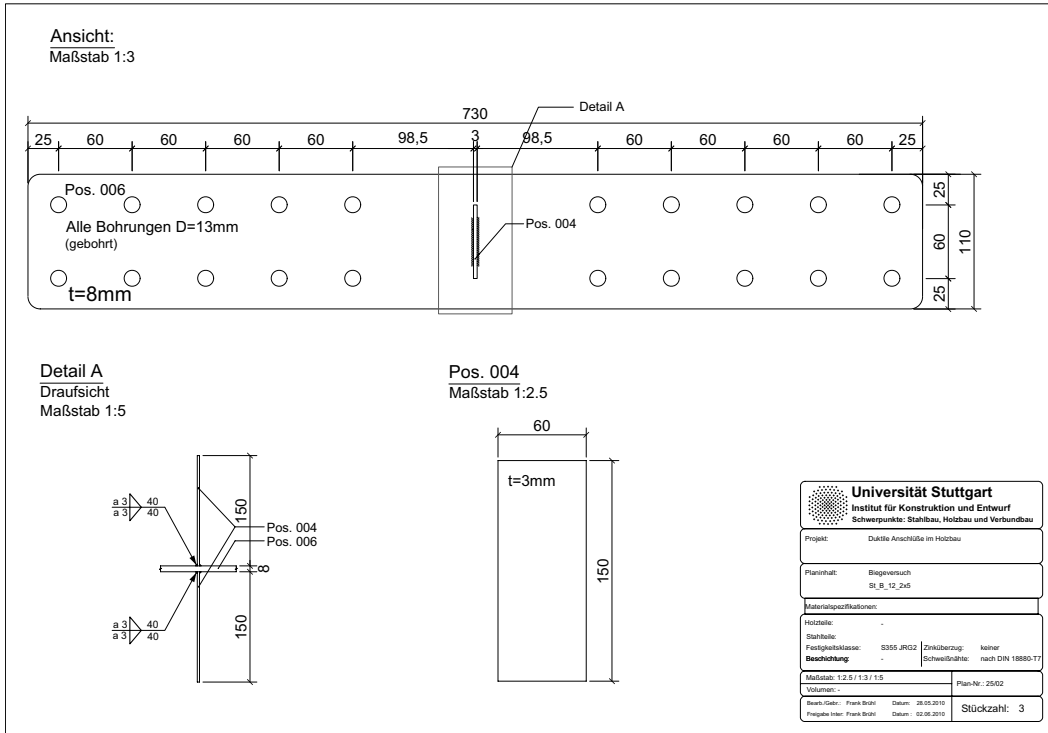


Figure F.18: Connection 12_2x5

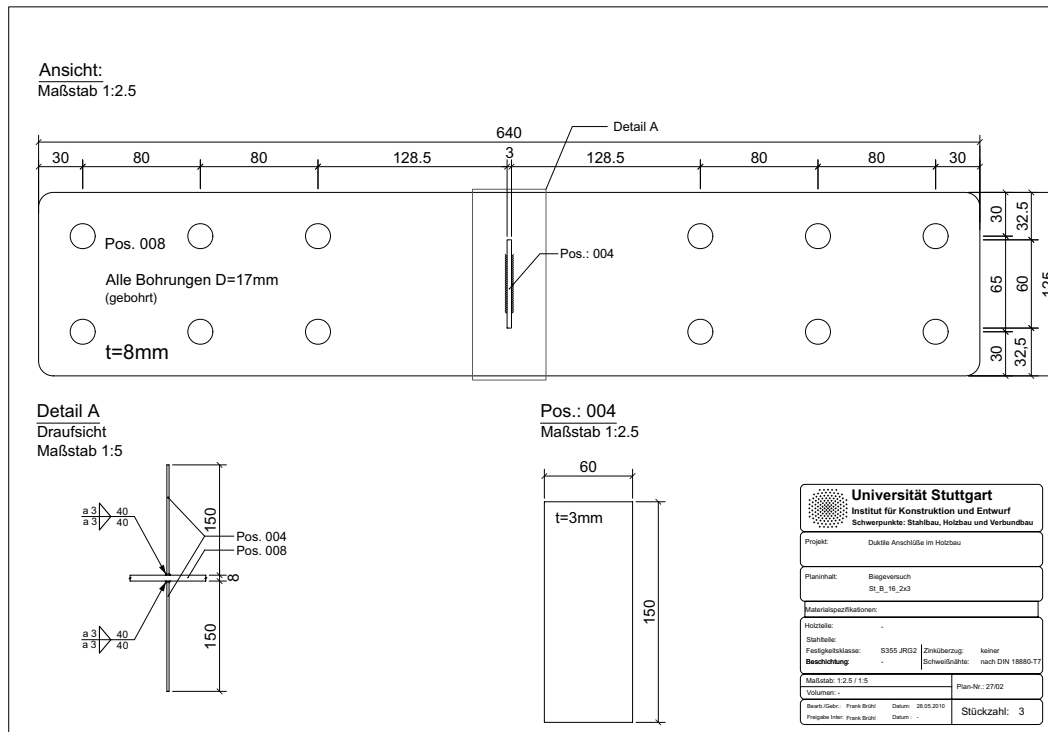


Figure F.19: Connection 16_2x3

F.2.2 Timber Parts

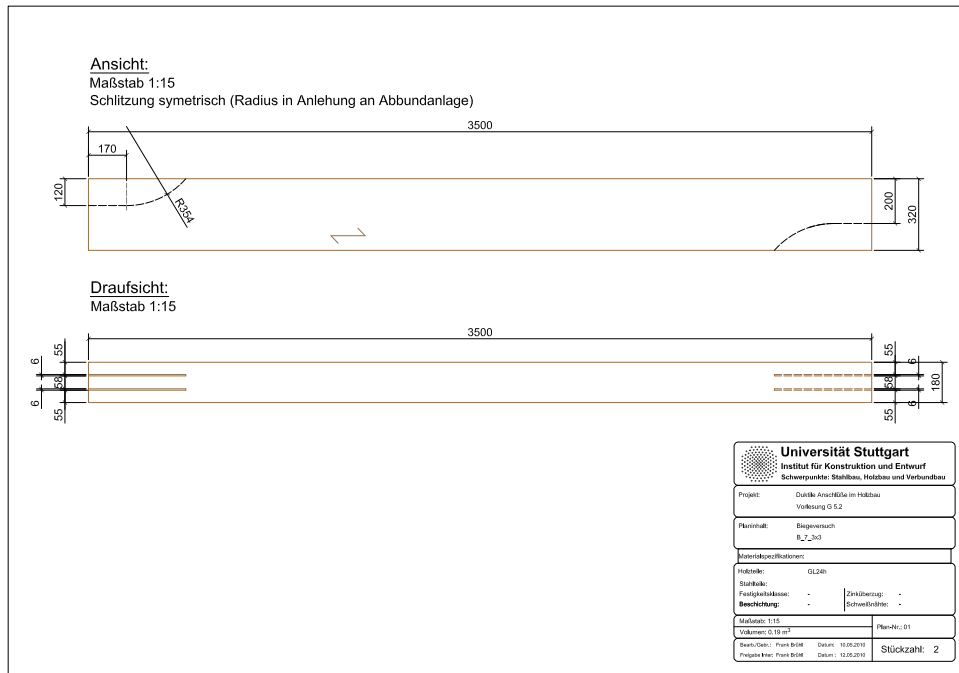


Figure F.20: Connection 7_3x2 (planned 7_3x3)

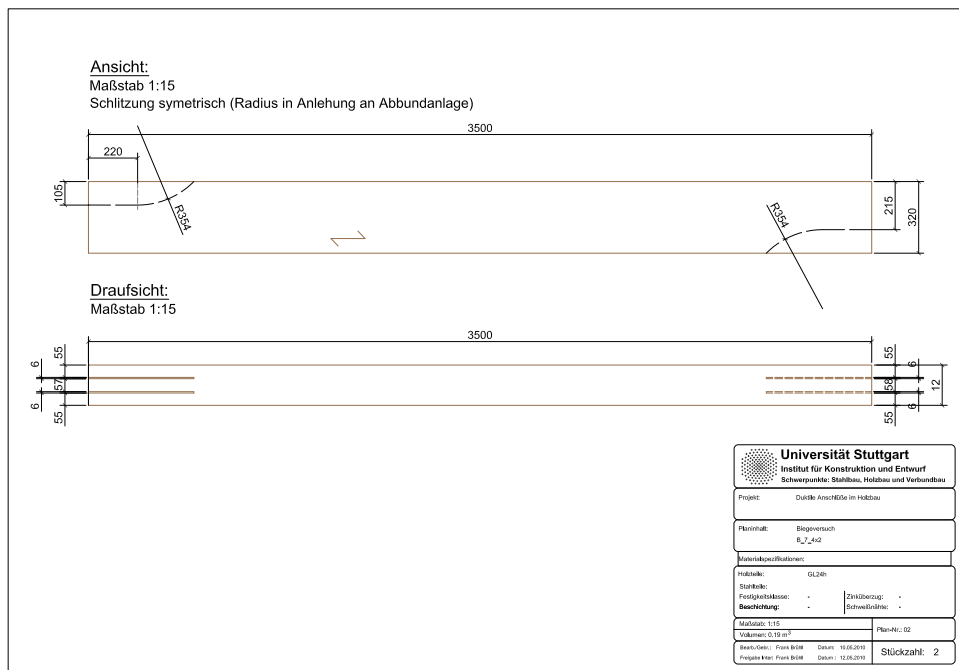


Figure F.21: Connection 7_2x4

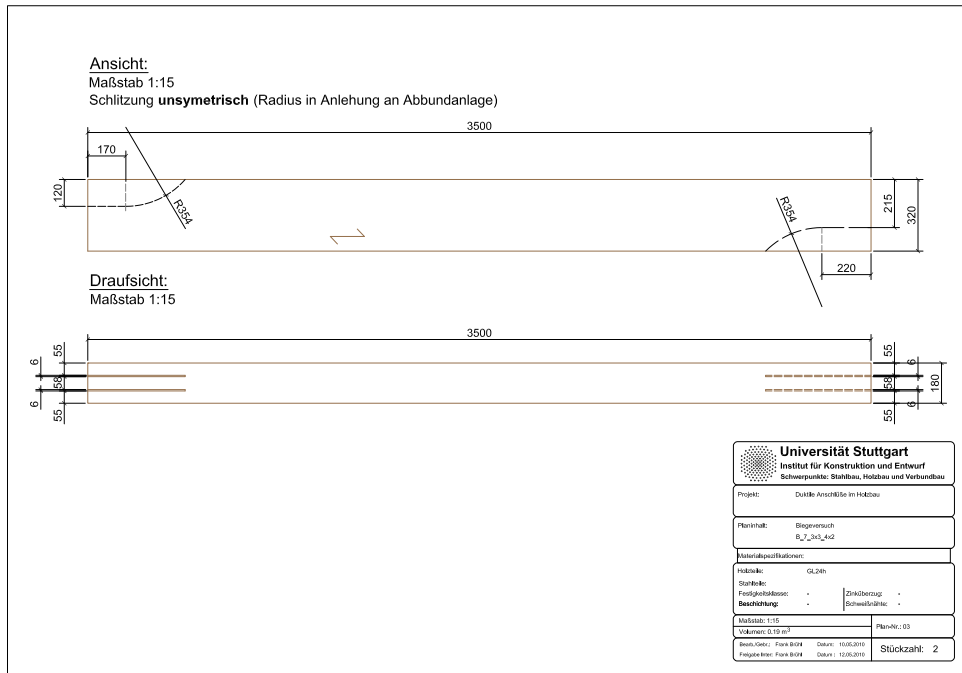


Figure F.22: Connection 7_2x4 & 7_3x3

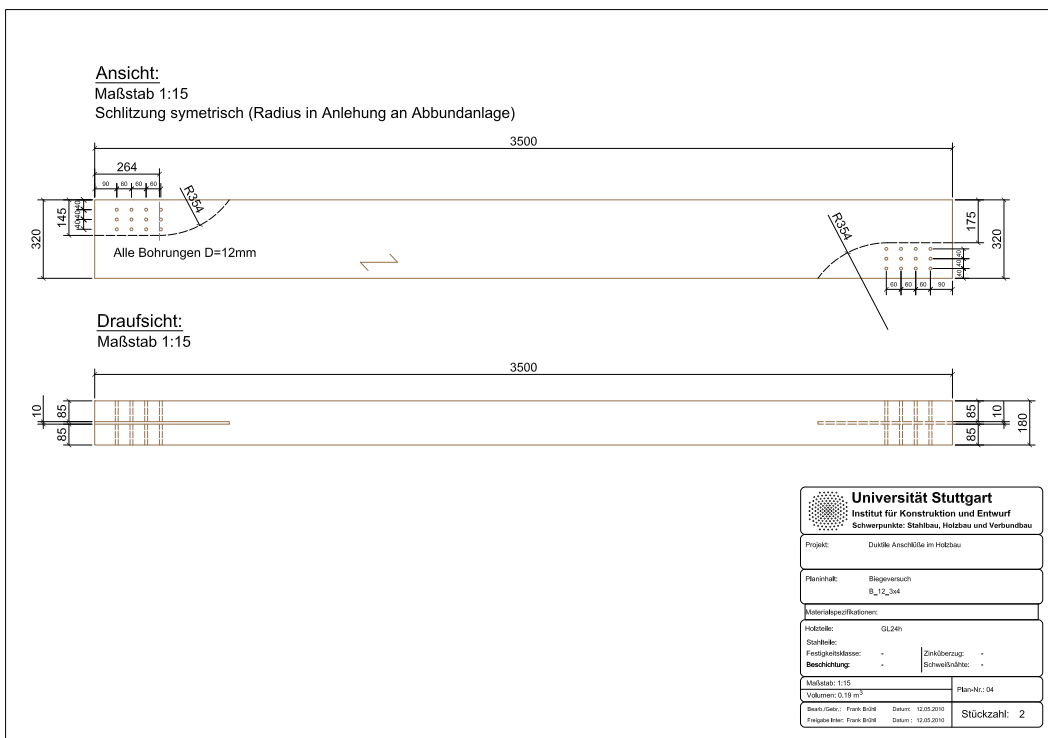


Figure F.23: Connection 12_3x3 (planned 12_3x4)

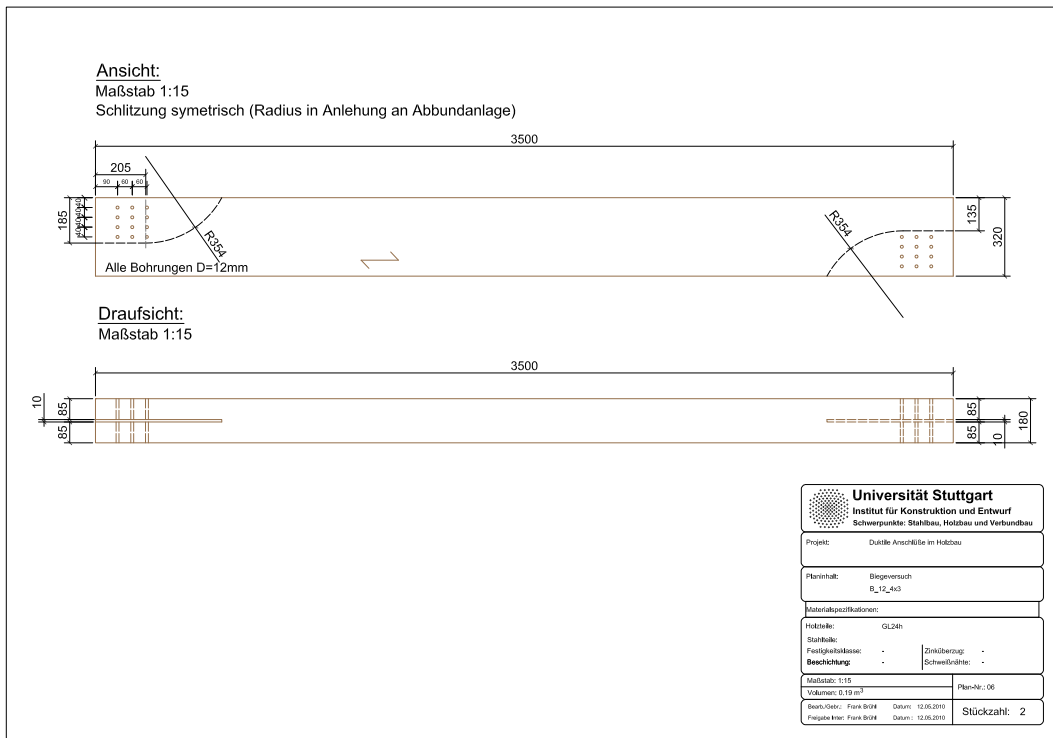


Figure F.24: Connection 12_4x3

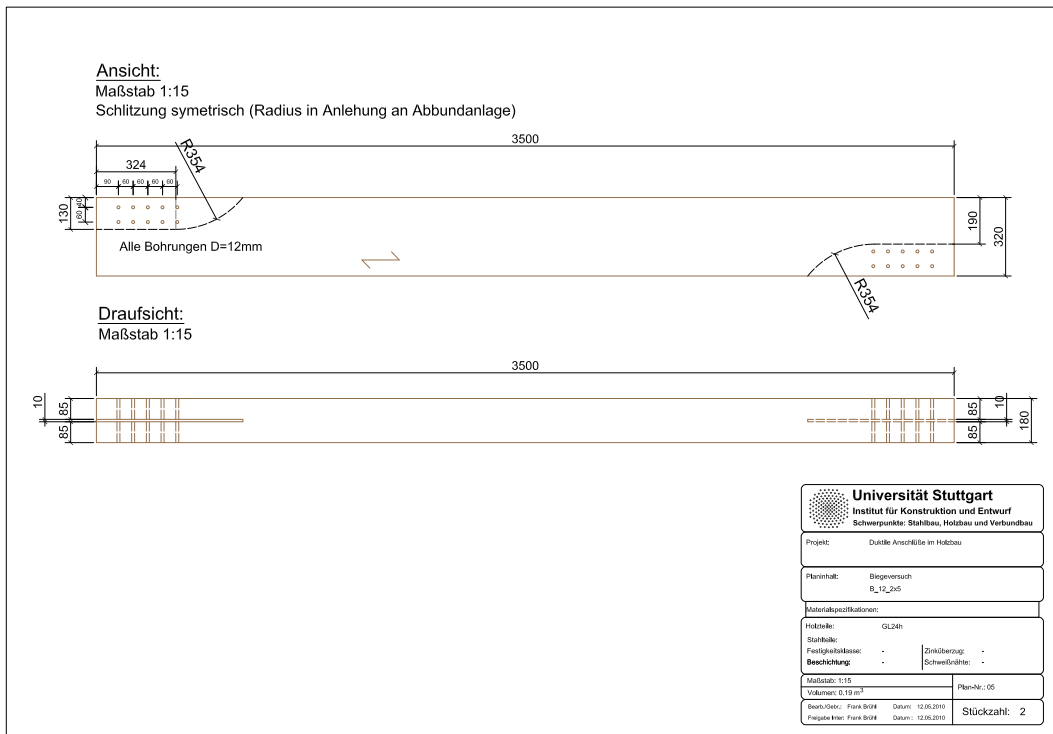


Figure F.25: Connection 12_2x5

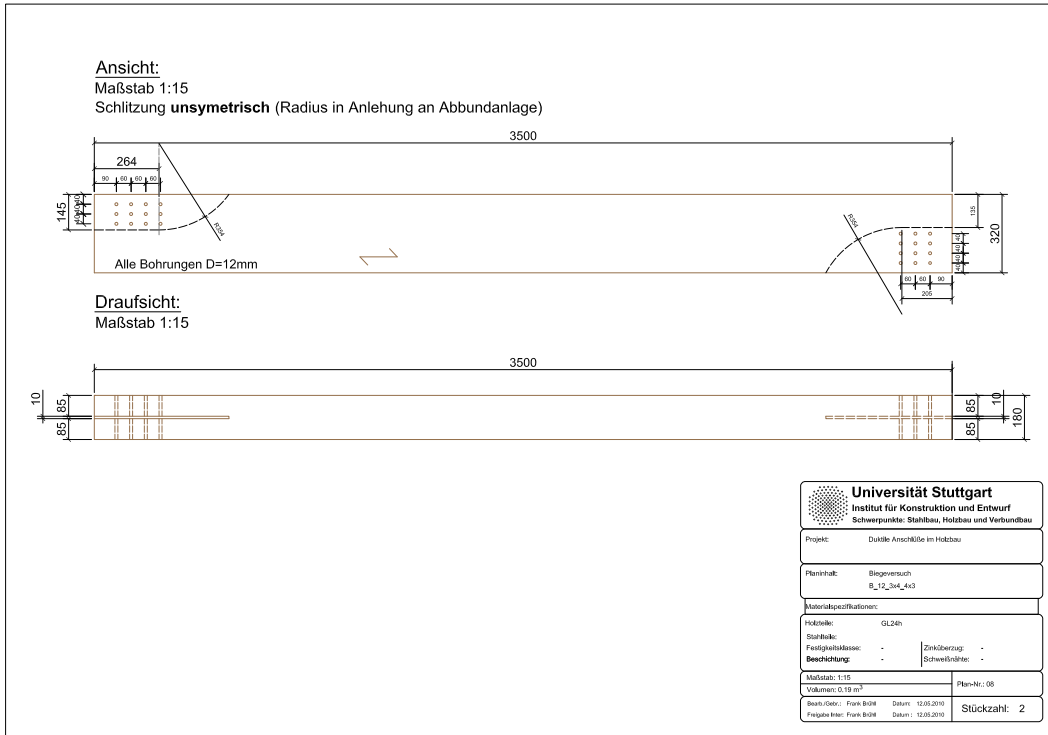


Figure F.26: Connection 12_4x3 & 3x4

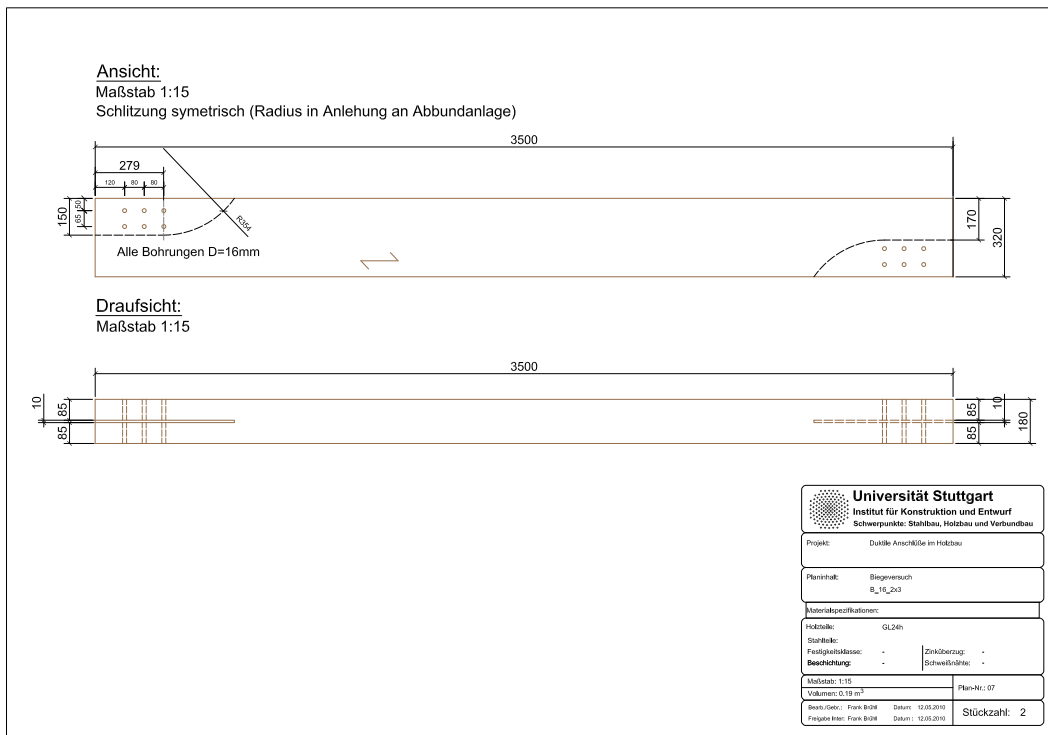


Figure F.27: Connection 16_2x3

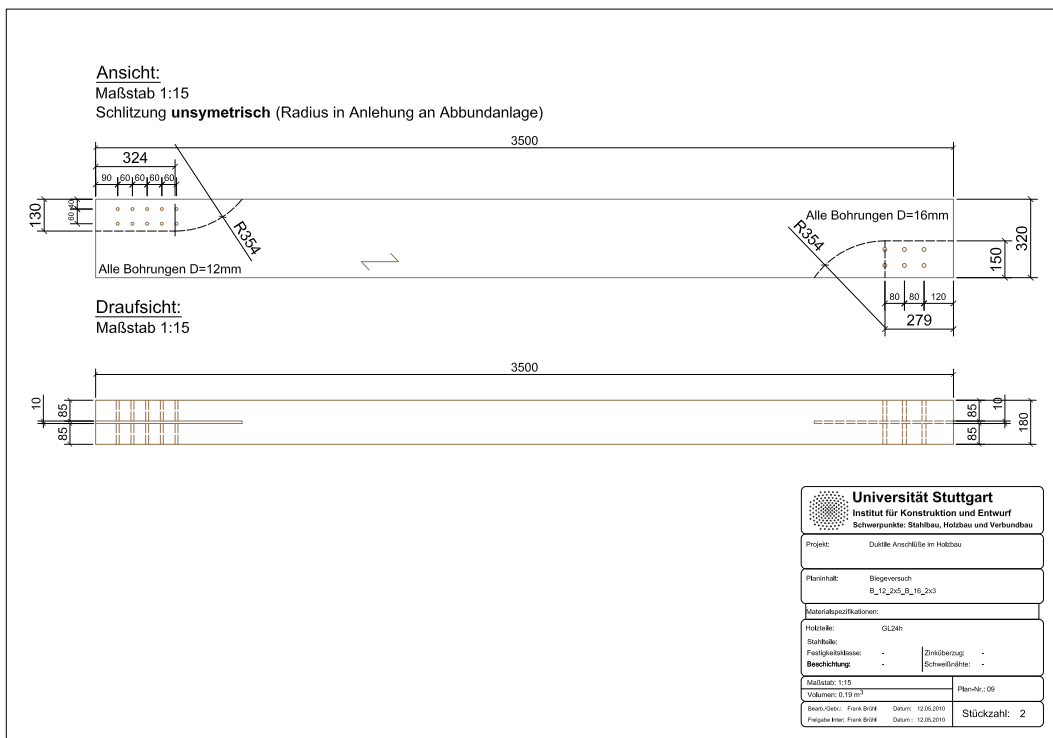


Figure F.28: Connection 12_2x5 & 16_2x3